Vol. 284, No. 2, December 30, 1993 ISSN 0003-2670

ANALYTICA CHIMICA ACTA

An international journal devoted to all branches of analytical chemistry

ELSEVIER

ANALYTICA CHIMICA ACTA

Scope. *Analytica Chimica Acta* publishes original papers, rapid publication letters and reviews dealing with every aspect of modern analytical chemistry. Reviews are normally written by invitation of the editors, who welcome suggestions for subjects. Letters can be published within **four months** of submission. For information on the Letters section, see inside back cover.

Submission of Papers

Americas

Prof. Harry L. Pardue
Department of Chemistry
1393 BRWN Bldg, Purdue University
West Lafayette, IN 47907-1393
USA

Tel:(+1-317) 494 5320
Fax:(+1-317) 496 1200

Computer Techniques

Prof. J.T. Clerc
Universität Bern
Pharmazeutisches Institut
Baltzerstrasse 5, CH-3012 Bern
Switzerland

Tel:(+41-31) 654171
Fax:(+41-31) 654198

Prof. Sarah C. Rutan
Department of Chemistry
Virginia Commonwealth University
P.O. Box 2006
Richmond, VA 23284-2006
USA
Tel:(+1-804) 367 1298
Fax:(+1-804) 367 7517

Other Papers

Prof. Alan Townshend
Department of Chemistry
The University
Hull HU6 7RX
Great Britain

Tel:(+44-482) 465027
Fax:(+44-482) 466410

Prof. Willem E. van der Linden
Laboratory for Chemical Analysis
Department of Chemical Technology
Twente University of Technology
P.O. Box 217, 7500 AE Enschede
The Netherlands
Tel:(+31-53) 892629
Fax:(+31-53) 356024

Prof. Paul Worsfold
Dept. of Environmental Sciences
University of Plymouth
Plymouth PL4 8AA
Great Britain

Tel:(+44-752) 233006
Fax:(+44-752) 233009

Submission of an article is understood to imply that the article is original and unpublished and is not being considered for publication elsewhere. *Anal. Chim. Acta* accepts papers in English only. There are no page charges. Manuscripts should conform in layout and style to the papers published in this issue. See inside back cover for "Information for Authors".

Publication. *Analytica Chimica Acta* appears in 16 volumes in 1994 (Vols. 281-296). *Vibrational Spectroscopy* appears in 2 volumes in 1994 (Vols. 6 and 7). Subscriptions are accepted on a prepaid basis only, unless different terms have been previously agreed upon. It is possible to order a combined subscription (*Anal. Chim. Acta* **and** *Vib. Spectrosc.*).
Our p.p.h. (postage, packing and handling) charge includes surface delivery of all issues, except to subscribers in the U.S.A., Canada, Australia, New Zealand, China, India, Israel, South Africa, Malaysia, Thailand, Singapore, South Korea, Taiwan, Pakistan, Hong Kong, Brazil, Argentina and Mexico, who receive all issues by air delivery (S.A.L.-Surface Air Lifted) at no extra cost. For Japan, air delivery requires 25% additional charge of the normal postage and handling charge; for all other countries airmail and S.A.L. charges are available upon request.

Subscription orders. Subscription prices are available upon request from the publisher. Subscription orders can be entered only by calendar year and should be sent to: Elsevier Science Publishers B.V., Journals Department, P.O. Box 211, 1000 AE Amsterdam, The Netherlands. Tel: (+31-20) 5803 642, Telex: 18582, Telefax: (+31-20) 5803598, to which requests for sample copies can also be sent. Claims for issues not received should be made within six months of publication of the issues. If not they cannot be honoured free of charge. Readers in the U.S.A. and Canada can contact the following address: Elsevier Science Publishing Co. Inc., Journal Information Center, 655 Avenue of the Americas, New York, NY 10010, U.S.A. Tel: (+1-212) 6333750, Telefax: (+1-212) 6333990, for further information, or a free sample copy of this or any other Elsevier Science Publishers journal.
Advertisements. Advertisement rates are available from the publisher on request.

US mailing notice - Analytica Chimica Acta (ISSN 0003-2670) is published biweekly by Elsevier Science Publishers (Molenwerf 1, Postbus 211, 1000 AE Amsterdam). Annual subscription price in the USA US$ 3035.75 (valid in North, Central and South America), including air speed delivery. Second class postage paid at Jamaica, NY 11431. *USA Postmasters*: Send address changes to Anal. Chim. Acta, Publications Expediting, Inc., 200 Meacham Av., Elmont, NY 11003. Airfreight and mailing in the USA by Publication Expediting.

ANALYTICA CHIMICA ACTA

An international journal devoted to all branches of analytical chemistry

(Full texts are incorporated in CJELSEVIER, a file in the Chemical Journals Online database available on STN International; Abstracted, indexed in: Aluminum Abstracts; Anal. Abstr.; Biol. Abstr.; BIOSIS; Chem. Abstr.; Curr. Contents Phys. Chem. Earth Sci.; Engineered Materials Abstracts; Excerpta Medica; Index Med.; Life Sci.; Mass Spectrom. Bull.; Material Business Alerts; Metals Abstracts; Sci. Citation Index)

VOL. 284 NO. 2 CONTENTS DECEMBER 30, 1993

(Continued overleaf)

Analytica Chimica Acta, 284 (1993) 249–255
Elsevier Science Publishers B.V., Amsterdam

An integrated reduction method for the determination of urea as ammonia in fresh water samples

Andre Schmitt, Louise Buttle and Roger Uglow

Department of Applied Biology, University of Hull, Hull HU6 7RX (UK)

Kathleen Williams and Stephen Haswell

School of Chemistry, University of Hull, Hull HU6 7RX (UK)

(Received 4th June 1993; revised manuscript received 2nd August 1993)

Abstract

A flow-injection system for the on-line microwave preparation of natural water samples with determination of urea as ammonia by colorimetric detection is described. Urea present in the samples is reduced on line to ammonium ions which on reaction with NaOH release gaseous ammonia which passes through a gas permeable membrane causing a pH change in a Bromothymol Blue (BTB) indicator stream which is colorimetrically determined at 635 nm. Signals from the flow through detector were recorded as peak height measurements on a chart recorder. Calibration proved to be linear up to 45 μmol l^{-1} urea with an LOD of 2.40 μmol l^{-1} urea (R.S.D. < 4%, $n = 10$). Samples were analysed at a rate of 14 min per sample and proved to show superior results when compared to a conventional batch preparation methodology.

Keywords: Flow injection; Environmental analysis; Microwave enhanced reduction; On-line reduction; Urea; Waters

Most aquatic species of animal excrete ammonia and urea, the rate of excretion and levels of efflux being dependent upon the individual physiological status of the animals and the modifying influences of their environment [1].

Ammonia is more toxic and water soluble than urea and this has important implications for successful husbandry of commercially-important, cultured aquatic animals – or any that are held in fixed volumes of water. The quantitative determination of the principal metabolic endproducts excreted to the external medium are thus important analytical procedures.

Several works have previously been published which succesfully report the direct analysis of ammonia [2–4] in water samples by flow-injection analysis (FIA). The determination of urea however, requires reduction to ammonia prior to analysis. A modification of a Kjeldahl method was described by Yang [5] that enabled the analysis of urea as ammonia to be achieved. However, this modified method involved a tedious and time consuming batch sample preparation step which was susceptible to contamination and volatile analyte loss.

The development of microwave sample dissolution techniques [6] and more recently on-line microwave digestion [7,8] has proved to be advantageous as it offers a dramatic reduction in sample preparation time, reduces atmospheric contamination and volatile analyte loss.

The method described in this paper utilises a further modification of the Yang method to suc-

Correspondence to: S. Haswell, School of Chemistry, University of Hull, Hull HU6 7RX (UK).

SSDI 0003-2670(93)E0475-M

cessfully determine levels of urea, as ammonia in natural water samples by means of a continuous flow methodology involving on-line sample preparation and colorimetric detection. It should be stressed that the presence of any easily reduced nitrogen species will be detected by either of the systems but as the levels of such species are insignificantly low in the samples studied here, there effect can be in this case considered to be a negligible contribution to the nitrogen budget.

EXPERIMENTAL

All chemicals were of analytical reagent grade, and distilled, deionized water was used throughout.

Reagents

Sodium hydroxide (1.5 M) (Merck, Poole) in distilled water and BTB (Bromothymol Blue) (0.3 g/l) (Merck) were used as reagents. Ammonia stock standard solution (0.5 mM NH_4^+ l^{-1}) prepared from ammonium sulphate (Merck) and urea (Merck) (40 μmol l^{-1}) were made up to volume in ammonia free distilled water (Nanopure II, Barnstead). A reducing agent containing 2 g mercury sulphate ($HgSO_4$) (Fisons, Loughborough), 134 g potassium sulphate (Merck) and 200 ml of 96% sulphuric acid (Prolabo, Manchester) was used.

Apparatus

The on-line system is illustrated in Fig. 1 and consisted of the folowing: a water carrier stream in 0.5 mm i.d. polytetrafluoroethylene (PTFE) tubing; an Ismatec MV-Z pump (Glottbrugg, Zürich); a Rheodyne injection valve (Anachem 5020), (Anachem, Luton) with a 0.8 ml sample loop; a CEM, MDS81 microwave oven (CEM, Buckingham) containing 0.5 mm i.d. PTFE tubing wrapped around a PTFE box; a 7 m cooling coil in an antifreeze bath cooled by Peltier devices (MI1069T-03AC, Marlow Industries, Tadworth); a CEM pressure sensor; and a 516.75 kPa (75 p.s.i.) back-pressure regulator (Anachem P736).

The outlet from the back-pressure regulator was coupled to a colorimetric detection system

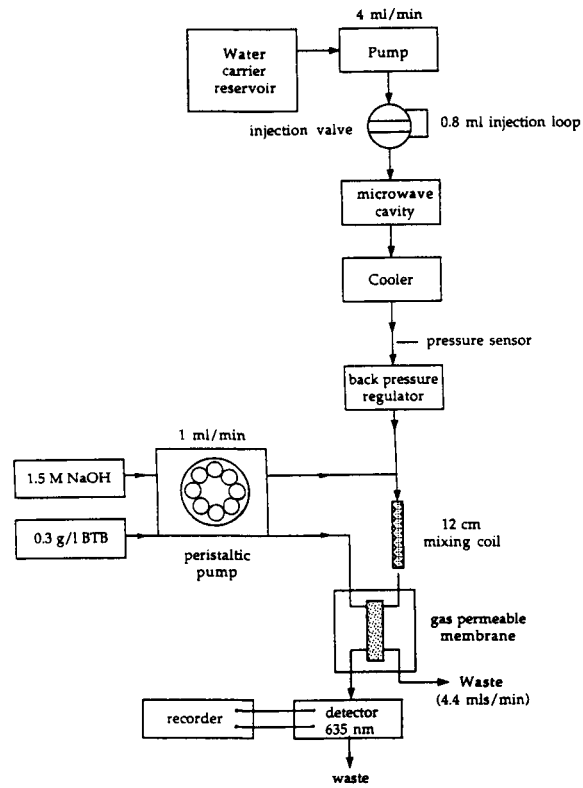

Fig. 1. Schematic diagram of the on-line digestion FI system.

consisting of: two reagent streams, one for BTB and the other sodium hydroxide reagents; a Gilson Minipuls 2 peristaltic pump (Anachem), a 12 cm mixing coil; an in house built gas diffusion cell with PTFE membrane (diffusion path length = 240 mm × 1.5 mm); a photometric detector (in house built); and a Chessell BD 4040 chart recorder (Kipp and Zonen).

PTFE tubing of 0.5 mm i.d. was used throughout the whole system.

Procedure

Preparation of reducing agent. A reducing agent was prepared by taking 200 ml of 96% H_2SO_4, 134 g K_2SO_4, 2 g $HgSO_4$ and making up to volume (1 l) with distilled water.

Standards. Standards covering a range of 0–45 μmol l^{-1} urea were prepared by taking appropriate dilutions of a stock urea solution (0.1 M) and

making up to volume in ammonia free distilled water. Ammonia standards (20, 30, 40 and 60 μmol l^{-1}) were prepared by taking appropriate dilutions of a stock ammonium sulphate solution (0.5 mM $NH_4^+ l^{-1}$) and making up to volume in the same way.

Samples. Water samples were obtained from 0.5-l water tanks which had held prawns in their environment for 2 h.

Spikes. Spiked samples were prepare by taking a 10-ml aliquot of sample and adding to it 0.4 ml of ammonium sulphate (0.001 M) or 0.2 ml urea (0.001 M). The spiked samples were otherwise treated with the reducing agent in the usual way (see below).

Sample preparation. (a) On-line microwave method: 1 ml of reducing agent was added to 10 ml of standard or sample resulting in a 10% solution. Standards, samples and spiked solutions were analysed by injecting 0.8 ml aliquots into the system. Absorbance signals were recorded on a chart recorder and peak height measurements taken. Total analysis time for each sample was approximately 14 min (including sample preparation). Replicate measurements of standards, samples and spiked solutions were taken.

(b) Conventional method: 1 ml of sample was placed in a test tube with 0.1 ml of reducing agent resulting in a 10% solution. The test tube was then heated in a heating block for 12 h at 110°C and upon cooling, a 0.5-ml aliquot taken and injected into a conventional FI system for ammonia determination [2]. Absorbance signals were recorded on a chart recorder and peak height measurements taken. Total analysis time for a batch of (up to) 40 samples was approximately 15 h (including sample preparation).

RESULTS AND DISCUSSION

Optimisation of ammonia detection by FI

During the optimisation of the FI detection system sensitivity was evaluated by the absorbance response (peak height) at 635 nm. The variables most effecting signal response were carrier flow-rate, injection volume, reagent flow-rate and concentration and reaction coil length.

A sodium hydroxide reagent is required for the production of gaseous ammonia, upon reaction with ammonium ions present in the acidic carrier stream. The concentration of NaOH used is therefore dependent upon the acid concentration in the reducing agent. A higher acid concentration would result in a more rapid reduction of sample but would require a stronger NaOH concentration in the FI detector system to neutralise the solution. However, a strong NaOH solution rapidly reduced the lifetime of the gas-permeable membrane and so compromise conditions were required to reconcile these two competitive effects.

Signal response was evaluated during the optimisation process by comparing the absorbance response (peak height) for ammonium sulphate standard solutions of known concentration (20, 30, 40 and 60 μmol l^{-1}). Ammonia standards were used here because as it is ammonia that is being detected after phase separation a direct measurement of the optimised conditions for ammonia could be made, without the added complication of a sample reduction step.

Figure 2 shows a plot of absorbance as a function of carrier flow-rate through the FIA system. At lower flow-rates, dispersion effects increased resulting in a broad peak being observed. As the flow-rate was increased, an increase in peak height is observed.

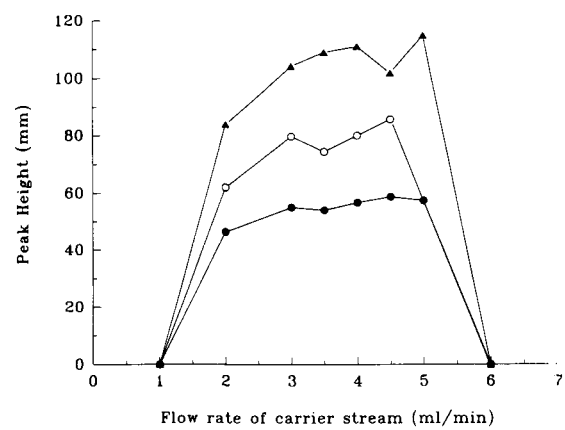

Fig. 2. Effect of carrier flow-rate on signal response using 20 (●), 40 (○) and 60 (▲) μmol/l solutions of ammonium sulphate.

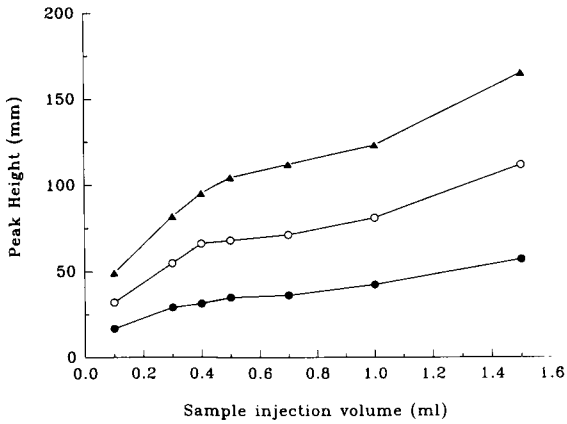

Fig. 3. Effect of sample injection volume on signal response using 20 (●), 40 (○) and 60 (▲) μmol/l solutions of ammonium sulphate.

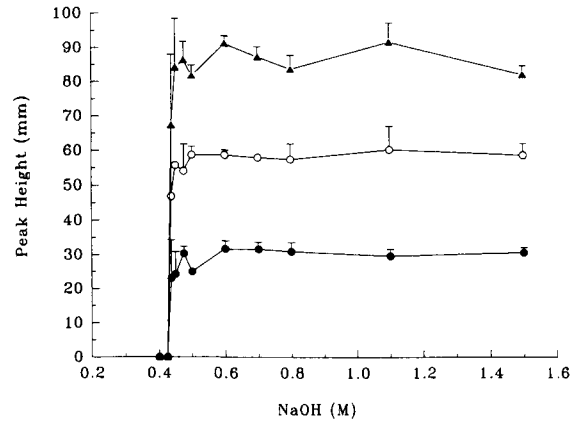

Fig. 4. Effect of sodium hydroxide concentration on signal response using 20 (●), 40 (○) and 60 (▲) μmol/l solutions of ammonium sulphate.

At higher flow-rates insufficient time for the complete transfer of gaseous ammonia through the membrane occurred and accordingly reduced colour development, signal response was seen to gradually decrease as the flow-rate increased.

An optimum flow rate of 4 ml/min was selected since this value gave a response within the maximum range.

The effect of sample volume on signal response is shown in Fig. 3. This illustrates a steady increase in signal response as the injection volume increased. It is expected that the peak height will eventually reach an optimum plateau if the injection volume is increased further. However, due to low availability of samples the maximum injection volume allowed was set at 0.8 ml.

Figure 4 illustrates the effect of sodium hydroxide concentration on signal response. It can be seen that fluctuations in peak height occur when sodium hydroxide concentration is below 0.6 M. These fluctuations cannot be attributed to dispersion since they are not reproducible. It is thought therefore that these fluctuations result from a combination of two factors, firstly an incomplete reaction taking place due to insufficient NaOH present to neutralise the acidic solution and hence free the ammonia, and secondly, since the fluctuations are small, they could be attributed to noise in the system associated with gaseous product formation (see Fig. 9).

As the concentration of NaOH is increased, the rate of production of gaseous ammonia tends to level out to give an optimum plateau. This indicates that the production of gaseous ammonia is increased as pH increases. Thus an optimum signal response is obtained when NaOH concentration is at 0.8 M or greater. The concentration selected was 1.5 M as this represented the minimum concentration required to fully neutralise the acidic stream whilst minimising degradation of the PTFE membrane. A study of the effect of NaOH flow-rate on peak height was carried out

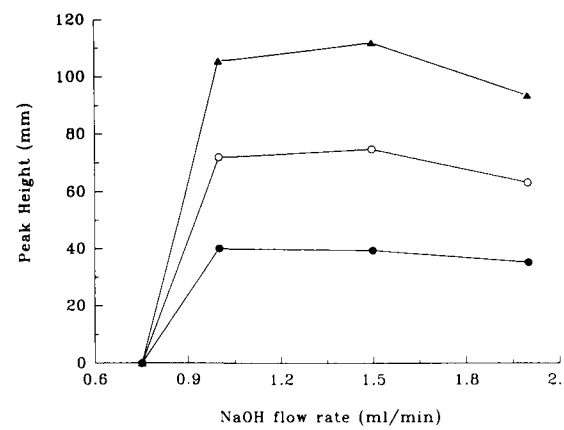

Fig. 5. Effect of sodium hydroxide flow-rate on signal response using 20 (●), 40 (○) and 60 (▲) μmol/l solutions of ammonium sulphate.

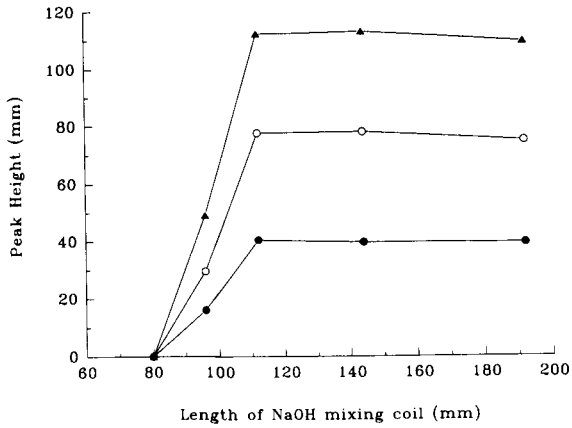

Fig. 6. Effect of sodium hydroxide mixing coil length on signal response using 20 (●), 40 (○) and 60 (▲) μmol/l solutions of ammonium sulphate.

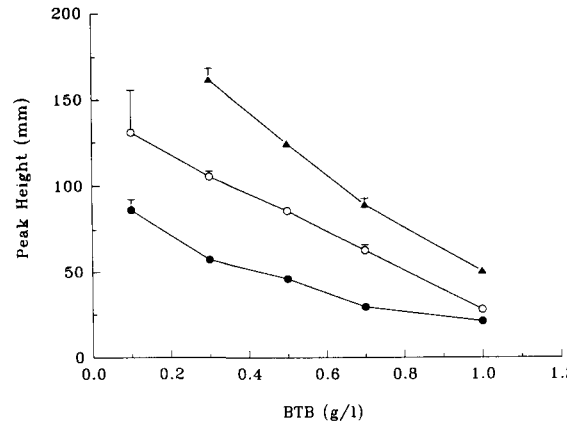

Fig. 7. Effect of BTB concentration on signal response using 20 (●), 40 (○) and 60 (▲) μmol/l solutions of ammonium sulphate.

and the results shown in Figure 5. As the flow-rate increases, an increase in signal response is observed due to a reduced dispersion effect, whilst still maintaining sufficient reaction time for ammonia to be produced. An optimum signal response was reached at flow rates covering the range 1–1.5 ml/min. At flow-rates greater than 1.5 ml/min, insufficient reaction time and hence pH shift reduced the production of gaseous ammonia and thus reduced transfer of ammonia through the membrane resulted in a decrease in peak height.

Figure 6 illustrates what the effect of changing the NaOH reaction coil length has on signal response. The reaction involves the production of gaseous ammonia through an increase in pH from NH_4^+ held in acidic solution. The use of too small a reaction coil results in an incomplete reaction and hence low signal response. As the coil length is increased, an increase in signal response is observed as the reaction approaches completion, an optimum reaction time being achieved when the coil length was found to be greater than 12 cm.

The detector system is based upon the colorimetric detection of a pH change in the BTB (Bromothymol Blue) reagent, which is induced by the diffused ammonia mixing with the reagent stream. The detected pH change, i.e., signal response can be effected by both the concentration and flow-rate of the indicator solution, therefore, these variables were investigated and the results shown in Figs. 7 and 8.

Figure 7 indicates that as the concentration of BTB is increased, a decrease in signal response is observed. This decrease is caused by an increased masking effect of BTB at the detector and consequently results in deviations from Beer's Law. Thus a BTB concentration of 0.3 g/l was selected for this work since the peak response at this concentration resulted in a smaller standard error

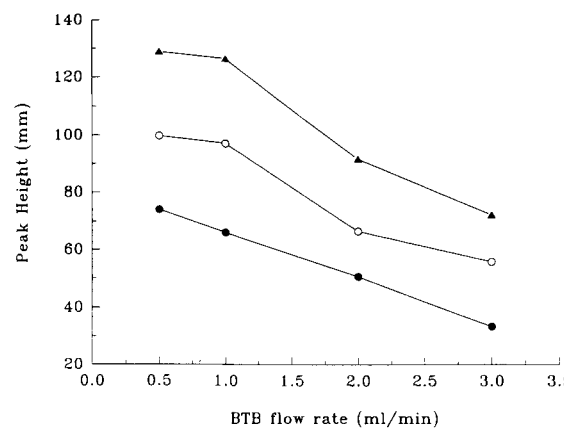

Fig. 8. Effect of changing the BTB flow-rate on signal response using 20 (●), 30 (○) and 40 (▲) μmol/l solutions of ammonium sulphate.

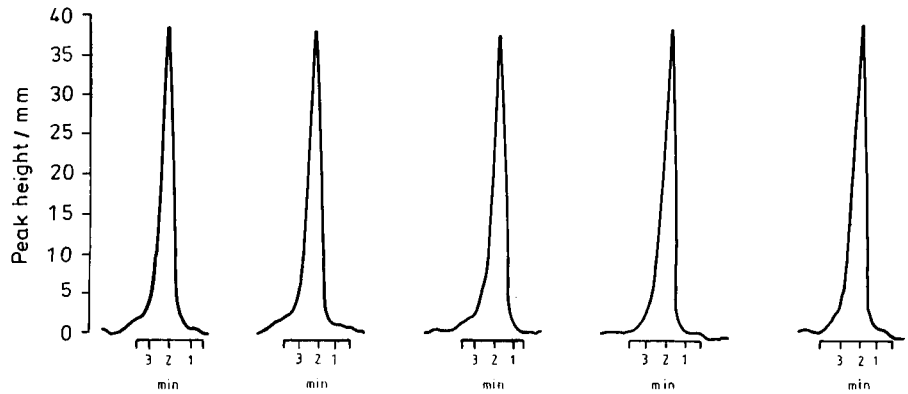

Fig. 9. Flow signals for a standard 40 μmol/l urea solution.

(Fig. 7) compared to the response at 0.1 g/l concentration.

The effect of BTB flow-rate on signal response is shown in Fig. 8. It can be seen that as the flow-rate increased, a decrease in peak height resulted. This was due to insufficient time for the chromophore to develop from the BTB–ammonia reaction. An overall increase in flow-rate resulted in a reduction in time allowed for passage of ammonia through the membrane and hence the smaller response. The optimum signal can be seen to occur at 0.5 ml/min, however, the chosen flow-rate for the system was 1 ml/min for experimental convenience.

From the experiments described above, it can be concluded that the optimum conditions for the detector system were chosen to be: carrier flow-rate 4 ml/min, sample injection volume 0.8 ml, NaOH concentration 1.5 M at a flow-rate of 1 ml/min, a reaction coil length of 12 cm, a BTB concentration of 0.3 g/l and a BTB flow-rate of 1 ml/min.

Optimisation of reduction conditions

The reaction of a sample in the microwave cavity is essentially a function of microwave power, sample residence time and the strength of the reducing agent used. Previous experiments have shown an optimum microwave power of 90% (485 W) [7,8] is ideal for such applications and the strength of the reducing agent and carrier flow-rate are governed by the detection system, and are therefore not considered as variables in this optimisation procedure. Thus the only remaining variable of importance for the reduction of urea to ammonia is residence time, which can be related to tube length. The use of a 30 m coil was found to give a recovery for urea of 99.6 ± 2.01% for the given flow-rate of 4 ml/min and injection volume of 0.8 ml. Shorter lengths of

TABLE 1

Results obtained for 'real' and spiked samples using the described FI methology

	On line MW method			Conventional method		
	[Ammonia]	R.S.D.(%) ($n = 4$)	%Recovery	[Ammonia]	R.S.D.(%) ($n = 6$)	%Recovery
Sample	76	1.5	–	61	5.5	–
Sample + amm. spike (40 μmol l^{-1})	116.5	3.7	101	101	4.5	99
Sample + urea spike (20 μmol l^{-1})	114	2.1	95	96	4.7	87.6

reduction coil were found to give lower recoveries and poorer precision, and were therefore not considered suitable for the present application.

Calibration

Calibration of a series of standards over the range 5–45 μmol l^{-1} urea was carried out and proved to be linear to 45 μmol l^{-1}, with a relative standard deviation (R.S.D.) for a 40 μmol l^{-1} urea standard of 3.53% ($n = 10$) (Fig. 9). The equation for the linear calibration was: $y = 1.7284x + 39.2231$ ($r = 0.9980$) where y = peak height and x = urea concentration. A limit of detection of 2.40 μmol l^{-1} urea was obtained with a sample throughput time of 14 minutes (including sample preparation).

Analysis of samples

Table 1 summarises the results obtained for 'real' and spiked samples using the described FI methodology. A comparison is made of these results with the conventional batch method. The results in general were higher than the conventional method, suggesting a reduction in analyte loss, and better recoveries of spiked samples indicated an increase in extraction efficiency.

Precision data for the proposed FI methodology (R.S.D. < 4%, $n = 4$) was also found to be superior to the conventional method (R.S.D. < 6%, $n = 6$) at a concentration of 40 μmol l^{-1}. This was to be expected since the FI method utilises minimum manual procedures and hence a decrease in operator and experimental error occurs. The sampling rate of the on-line system was approximately 14 min per sample (including sample preparation). Although the batch method used can prepare up to 40 samples at once, the time taken to heat, cool, transfer and analyse these samples would be approximately 15 h. The FI methodology would take less than 10 h to do the same number of analyses and would be expected to give improved results. It could be argued that the time scale for the FI method is still quite large, however, the system has potential for automation.

Conclusion

The proposed on-line sample preparation methodology with colorimetric detection was found to have a limit of detection of 2.4 μmol l^{-1} urea, a precision (R.S.D.) of < 4% ($n = 4$) and a sampling rate of 14 min per sample (including sample preparation). Results for analysis of 'real' and spiked samples proved to be superior to the conventional 'block' batch preparation method described. However, many samples can be prepared at once in the conventional method (40 in 12 h), but total analysis time can take up to 15 h. This would be comparable to the analysis of 60 samples with the on-line method. Although a poorer sensitivity is obtained with the proposed FI system (2.4 μmol l^{-1} urea, compared to 0.263 μmol l^{-1} urea for the conventional method), there are still several advantages over the conventional methodology namely, greater precision and recoveries, a more rapid analysis time and the facility for instrumental automation.

REFERENCES

1 M.J. Dagg, Int. Rev. Gesamt. Hydrobiol., 61 (1976) 297.
2 J. Ruzicka and E.H. Hansen, Flow Injection Analysis, Wiley, New York, 1981.
3 J.R. Clinch, PhD. Thesis, University of Hull, 1988.
4 J.R. Clinch, P.J. Worsfold and F.W. Sweeting, Anal. Chim. Acta, 214 (1988) 401.
5 T.A.B. Yang, PhD. Thesis, University of Hull, 1993.
6 A. Abu-Sumara, J.S. Morris and S.P. Koirtyohann, Anal. Chem., 47 (1975) 1475.
7 S.J. Haswell and D.A. Barclay, Analyst, 117 (1992) 117.
8 K.E. Williams, S.J. Haswell, D.A. Barclay and G. Preston, Analyst, 118 (1993) 245.

Analytica Chimica Acta, 284 (1993) 257–263
Elsevier Science Publishers B.V., Amsterdam

Flow-injection analysis with a linear pH gradient and diode-array detection applied to organic dyes

Ch.-H. Fischer and J.G. Rabe

Hahn-Meitner-Institut Berlin, Abt. Photochemie, P.O. Box 390128, D-14091 Berlin (Germany)

(Received 5th May 1993; revised manuscript received 24th August 1993)

Abstract

Organic dyes were identified using flow-injection analysis with a linear pH gradient and diode-array detection. The identification is based on three independently determined parameters, the two optical absorption spectra measured in acidic and alkaline solution and the pH range of their conversion near the pK values. Binary mixtures can also be analysed. The detection limit of the method was found to be 100 ng for 4-nitrophenol as an example. The possibility of quantitative analyses is discussed.

Keywords: Flow injection; UV–Visible spectrophotometry; Dyes; Nitrophenol

Various methods are used for dye analysis [1]: IR spectrometry, UV–visible spectrophotometry, thin-layer chromatography (TLC) and, more recently, liquid chromatography (LC), especially in combination with diode-array detection [2]. Flow-injection analysis (FIA) is a method for fast and easy routine analyses [3]. Most dyes exhibit different colours in either acidic or alkaline solutions and the pH at which the change in colour occurs differs from one dye to another. Based on these properties, an FIA method has been developed that provides absorption spectra of a dye in acidic and alkaline solutions and also the pK value, thus allowing identification of the dye.

In essence, the method consists of establishing a linear pH gradient in the solution of the dye and the measurement of the UV–visible spectra by means of a diode-array detector. When a steady stream of an acidic solution of a sample is mixed with an alkaline the flow of which increases, a pH gradient may be established. Provided that the analyte is either an acid or a base, the optical properties change when the pH value of the mixture reaches the pK value. This spectral change is continuously monitored with a diode-array spectrophotometer. A simple linear flow gradient of the alkaline stream would produce a typical pH titration curve with a steep jump over many pH units, but a linear pH gradient is needed to identify dyestuffs on the basis of their pK values. Therefore, a very accurate multi-linear flow gradient is necessary. Modern LC pumps fulfil these demands.

Correspondence to: Ch.-H. Fischer, Hahn-Meitner-Institut Berlin, Abt. Photochemie, P.O. Box 390128, D-14091 Berlin (Germany).

EXPERIMENTAL

Apparatus and chemicals

Two Merck–Hitachi HPLC pumps were used: type L6000 as pump P_1 and type L6200 as P_2. The sample was introduced by a Knauer electrically driven injection valve with a 1000-μl sample loop. A Waters Model 990 diode-array detector was

SSDI 0003-2670(93)E0486-Q

used. All devices were connected via Peek capillaries of 0.25 mm i.d. A Knauer Lab-Timer FR-10 actuated all processes. Dyes were obtained from Aldrich and phosphoric acid and sodium hydroxide of analytical-reagent grade from Merck.

Procedure

To realize a linear increase in pH with time, the titration of a multibasic acid seemed to be easier than that of a monobasic acid, as in the former instance the pH changes relatively smoothly in several smaller steps whereas in the latter there is one step with broad flat regions on both sides. Weak organic acids have the disadvantage that they absorb light up to about 300 nm, a region which is important for the analysis of dyes. Therefore, phosphoric acid, which does not show any significant absorbance above 210 nm was chosen. This tribasic acid has values of $pK_1 = 2.12$, $pK_2 = 7.21$ and $pK_3 = 12.67$ [4].

The scheme of the experimental set-up is shown in Fig. 1. The method requires two pumps, P_1 and P_2. P_1 delivers 0.1 M phosphoric acid at a constant flow-rate of 0.25 ml min^{-1}, which was found to be sufficiently high to give a reliable flow. P_2 delivers 0.1 M NaOH at a variable rate. Both streams are combined in a T-shaped junction and passed into the diode-array spectrophotometer via a 0.25 mm i.d. peek capillary with a length of 30 cm.

The pH values of the resulting mixture were measured with a glass electrode for different flow-rates of the alkaline solution. The result is shown in Fig. 2a. A linear pH gradient could easily be constructed from this plot by reading the NaOH flow-rate corresponding to the desired pH value at a certain time. In this work, a linear gradient between pH 1.5 and 11.5 in 3.7 min was attempted. For this purpose the flow-rate of P_2 was programmed. The pump allowed only linear gradients. Therefore, the calculated flow-rate vs. time curve had to be approximated by several linear parts. The flow rates and pH values as a function of time are shown in Fig. 2b. This procedure has to be repeated for each pair of new stock solutions, as the pH is very sensitive around

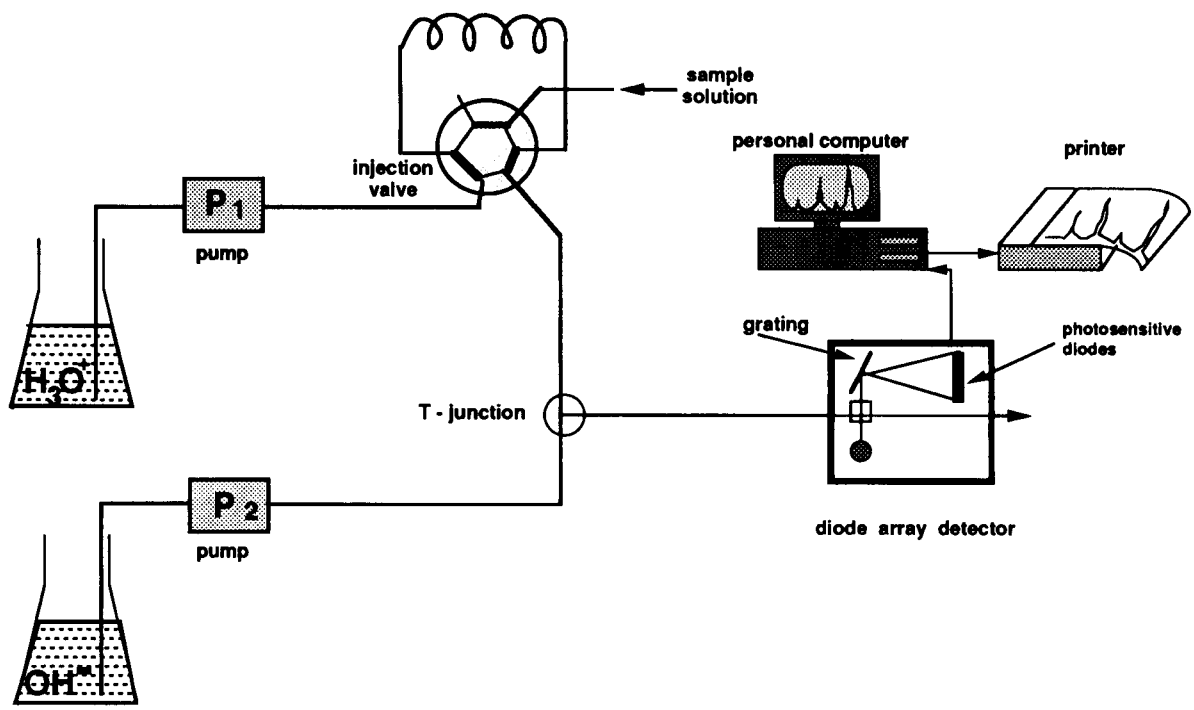

Fig. 1. Scheme of the experimental set-up.

the pK to minute changes in the acid or alkali concentrations.

For an analysis the sample is dissolved in the stock solution of phosphoric acid. To keep the influence of the sample on the pH negligible, its concentration must be low. With a syringe the solution is transferred into a 1000-μl sample loop (Fig. 1) of an automatically driven valve. With a flow-rate of 0.25 ml min^{-1} it would take 4 min to flush the sample from the loop. During this time the flow gradient had to be accomplished by operating pump P_2. A programmed timer was used to coordinate all devices. The sequence of all functions was as follows: (1) start of P_1 in order to equilibrate the detector; (2) start of the detector to obtain a reference spectrum of the solvent, which is automatically subtracted from all following spectra; (3) the sample valve is switched to the inject position and the spectrum is measured in strongly acidic medium; (4) 0.25 min after switching the valve, the flow programme for pump P_2 (NaOH solution) is started and a spectrum is measured every 1 s.

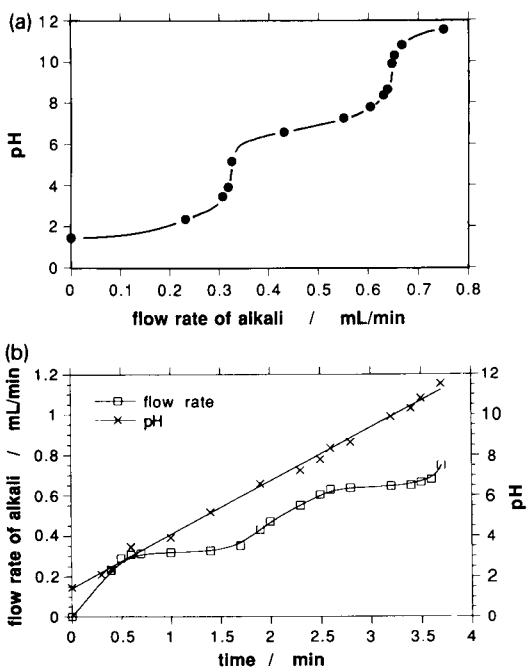

Fig. 2. (a) pH values measured in mixtures of phosphoric acid and a solution of sodium hydroxide. 0.1 M phosphoric acid with a constant flow-rate of 0.25 ml min^{-1} and 0.1 M sodium hydroxide with flow-rates between 0 and 0.75 ml min^{-1}. (b) Flow-rates of 0.1 M sodium hydroxide at different times to establish a linear pH gradient in the mixture with 0.1 M phosphoric acid (flow-rate 0.25 ml min^{-1}). The straight line represents the linear increase in pH with time.

RESULTS AND DISCUSSION

Single substances

4-Nitrophenol is used to demonstrate the method. The measurements are presented in Fig. 3. In Fig. 3a the absorption spectra as a function of time are shown in a three-dimensional plot. It should be remembered that within the time of the measurements a linear pH gradient was established. During this period the time scale represents the pH scale in accordance with Fig. 2b. For the sake of clarity this pH scale is also used in subsequent figures. The appearance of an absorption spectrum after approximately 1 min indicates that the analyte has entered the detector cell. The spectrum is in its acidic form with maxima at $\lambda_{ac} = 320$ and 225 nm. The absorption decreases slightly but the spectrum remains unchanged. Although this effect can be reproduced with a few substances, it is unimportant for the main result and is probably due to adsorption-desorption on the wall of the capillaries.

The peak at $\lambda_{ac} = 320$ nm then decreases while a new peak at $\lambda_{alk} = 400$ nm grows to almost the same extent. This effect is better demonstrated in Fig. 3b which shows a two-dimensional contour plot resulting from a view down on to the mountain-like shapes of the spectra in Fig. 3a. The connected lines represent identical absorbances. From Fig. 3b it is easy to find the maxima of absorption λ_{ac} and λ_{alk} and the pH where the change takes place. In Fig. 3c four spectra in the pH range 3.9–5.9 are shown. The distinct isosbestic point is proof that the direct transition from one compound to another is observed.

Evaluating the date in Fig. 3a–c eventually leads to Fig. 3d, which demonstrates the transformation of one species absorbing at 320 nm into one absorbing at 400 nm while the pH value is increased from about 5.5 to about 7.5. This is in

good agreement with the literature [5], where a pH range of 5.4–7.5 is given. This type of plot is termed a chromagram. Similarly to a polarogram from which the half-wave potential is taken to identify a compound, in the present instance the point of inflection, i.e., $pH_{1/2}$, may be used. At this point both the acidic and the alkaline form are present at the same concentration. $pH_{1/2} = 6.8$ was found for 4-nitrophenol.

Of further interest is the first appearance of the less acidic and the complete disappearance of the more acidic spectrum at pH_1 and pH_2, because the region pH_2–pH_1 in which the conversion takes place is characteristic for the compound. The match of all the parameters, λ_{ac}, λ_{alk}, $pH_{1/2}$, pH_1, pH_2 of the sample with those of a test dye guarantees high reliability of its identification. As such reference data are often available in the literature (many dyes are used as pH indicators), identification of a substance is possible even without a suitable test dye. It should also be mentioned that the absence of columns eliminates the calibration of columns necessary in LC.

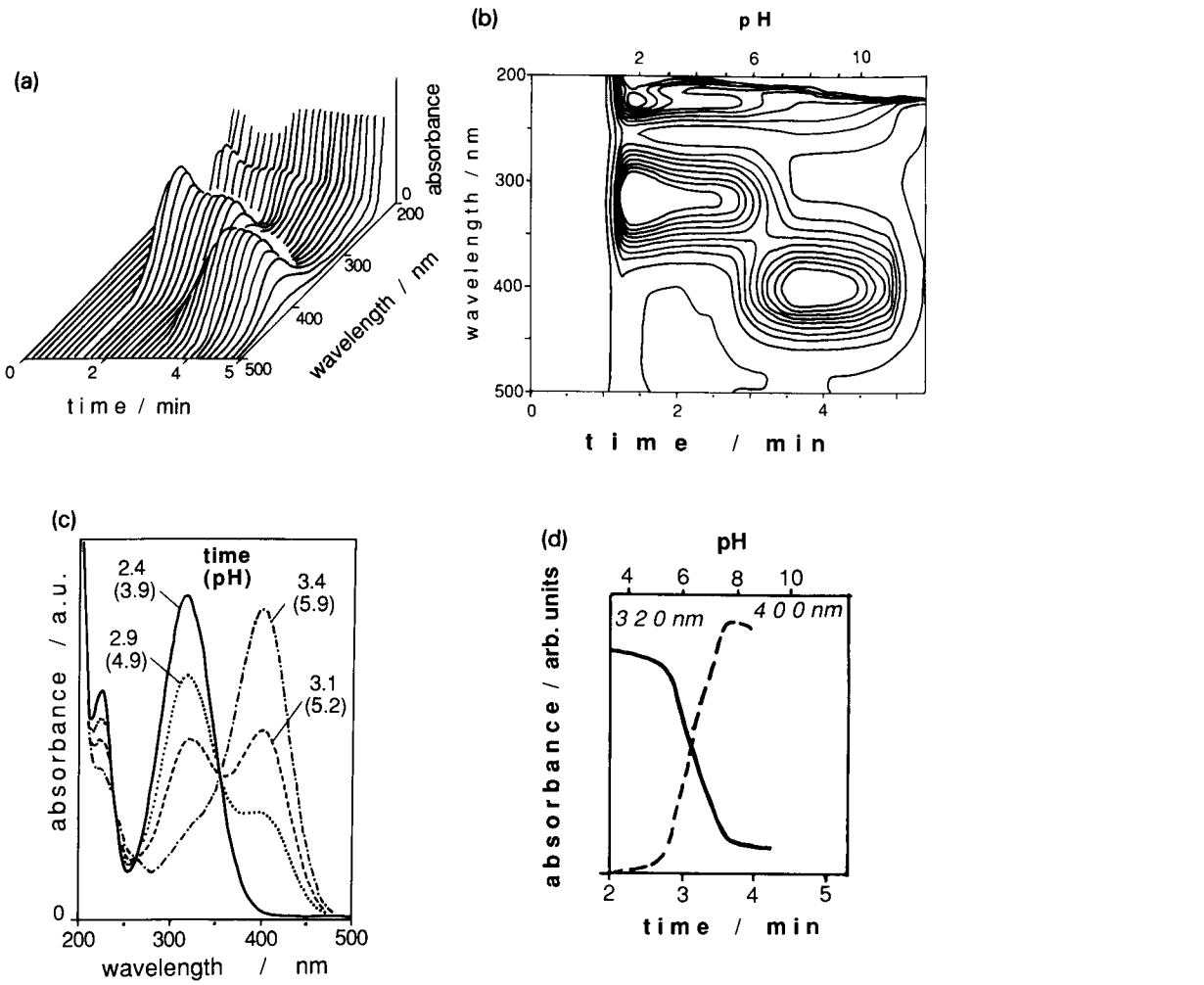

Fig. 3. Flow-injection analysis of 4-nitrophenol. (a) Three-dimensional plot of the absorption spectra as a function of time (pH); (b) two-dimensional contour plot of the absorbance; (c) absorption spectra at selected pH values; (d) chromagrams: the decrease in the absorbance at 320 nm and the simultaneous increase at 400 nm as the pH increases.

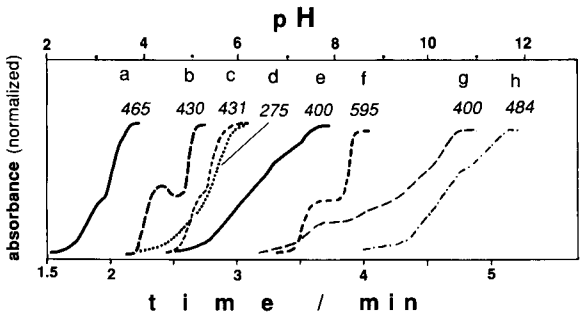

Fig. 4. Change in the absorbance at the absorption maxima (chromagram) of a number of dyes as a function of the pH or time. (a) Methyl orange; (b) methyl red; (c) tropaeolin; (d) brilliant green; (e) 4-nitrophenol; (f) thymol blue; (g) Meldola blue; (h) Victoria blue.

Even if no test substance or suitable data are available, certain rules in colour chemistry with respect to the red or blue shift in a pH gradient offer clues as to the identity of the chemical class of the dye in question [5]. A plot similar to Fig. 3d, where the increasing absorption at 400 nm indicates the transformation of the spectrum in a more acidic medium into one in a less acidic medium, is shown in Fig. 4 for a number of dyestuffs. Curve e is that of 4-nitrophenol (approximately the section between pH_1 and pH_2 in Fig. 3d). All curves were measured at different characteristic wavelengths. Some of them differ from the ideal shape. This is due to very small deviations from the ideal linear pH gradient and occurs mainly when the pK of a dyestuff is similar to a pK of phosphoric acid, because at the pK an equilibrium is very sensitive to minute changes in concentration. All the relevant data are collected in Fig. 5.

Dye mixtures

The identification of dyes in a binary mixture is demonstrated with 4-nitrophenol–methyl orange as an example. As before, the contour plot was examined (Fig. 6a) and two main spectral changes were recognized: a shift of the peak at 510 nm to a weaker peak at 470 nm and at higher pH a shift of the peak at 320 nm to 400 nm. The change of the latter was accompanied by bleaching at 470 nm. The corresponding chromagrams are shown in Fig. 6b. $pH_{1/2}$, pH_1 and pH_2 are

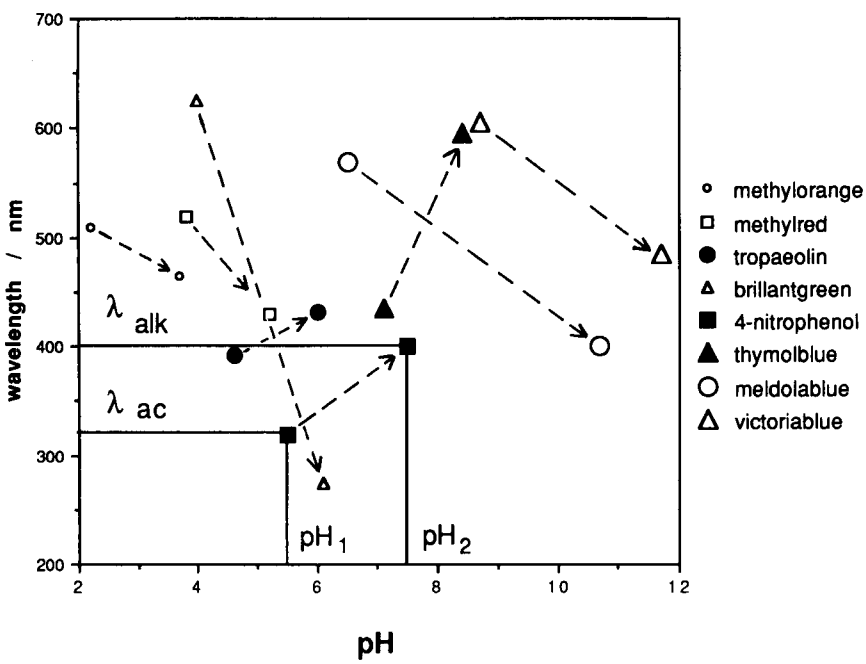

Fig. 5. Correlation of pH_1 and pH_2 with λ_{ac} and λ_{alk}. pH_1 and pH_2 indicate the beginning and the end of the conversion, respectively, from the more acidic form (absorption maximum at λ_{ac}) to the more alkaline form (absorption maximum at λ_{alk}).

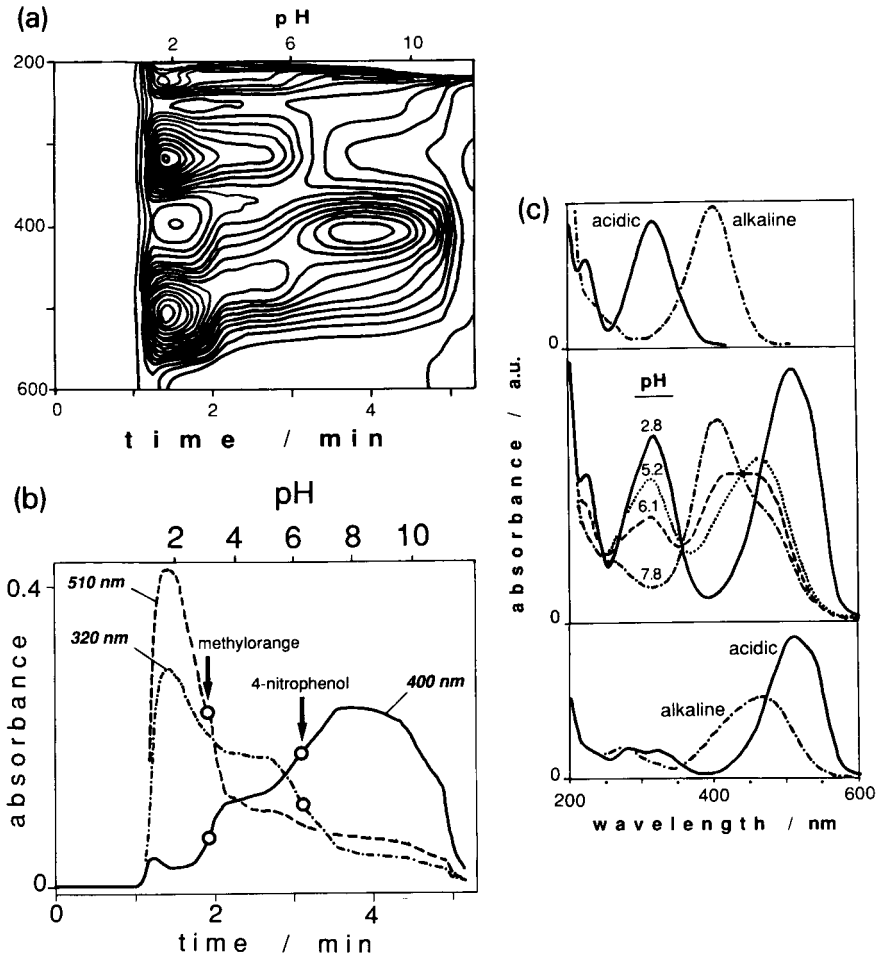

Fig. 6. Flow-injection analysis of a mixture of 4-nitrophenol and methyl orange. (a) Two-dimensional contour plot of the absorbance; (b) chromagrams observed at 510, 400 and 320 nm; (c) absorption spectra at different pH values (centre) and spectra of pure 4-nitrophenol (top) and of pure methyl orange (bottom).

obtained from this plot. It is seen that these values are in good agreement with those presented in Fig. 5 for 4-nitrophenol and methyl orange. The spectra of the mixture at various pH values are shown in Fig. 6c (centre). Comparison with the spectra of the pure compounds, 4-nitrophenol [Fig. 6c (top)] and methyl orange [Fig. 6c (bottom)] shows the presence of all relevant absorption maxima in the mixture. It can also be seen that at pH 2.8 the two absorption peaks of the mixture originate from the single peaks of 4-nitrophenol and methyl orange obtained in an acidic medium. Because in an alkaline solution the absorption maxima of both compounds occur close to each other (at 400 and 470 nm), the spectrum of the mixture at pH 7.8 consists of two overlapping peaks.

Quantitative analysis

The loss and gain in absorbance, ΔE, in a chromagram equals the difference between the absorbances E_{ac} and E_{alk} of the acidic and alkaline forms, respectively. According to the Lambert–Beer law, both the absorbances are proportional to concentration. Therefore, the difference in absorption, ΔE, is also proportional to concen-

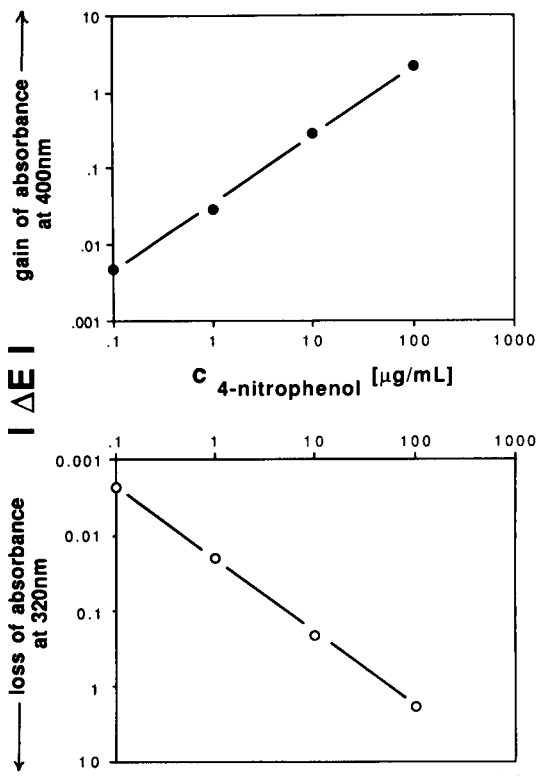

Fig. 7. Increase in absorption at $\lambda_{alk} = 400$ nm and loss at $\lambda_{ac} = 320$ nm for 4-nitrophenol as a function of its concentration (double logarithmic plot).

tration (Eqn. 1), as long as this law is valid, i.e., as long as the concentration is not too high and the conversion time is short enough that the dilution caused by the flow gradient is negligible (Eqn. 2):

$$\Delta E = E_{ac} - E_{alk} = \epsilon_{ac} c_{ac} d - \epsilon_{alk} c_{alk} d \quad (1)$$

For $c_{ac} = c_{alk} = c$:

$$\Delta E = (\epsilon_{ac} d - \epsilon_{alk} d) c = \text{constant} \times c \quad (2)$$

where E_{ac} = absorbance of the acidic form, E_{alk} = absorbance of the alkaline form, ϵ_{ac} = molar absorptivity of the acidic form, ϵ_{alk} = molar absorptivity of the alkaline form and d = optical path length.

It follows that chromagrams can be calibrated and therefore be used for quantitative analysis. This is demonstrated in Fig. 7 for 4-nitrophenol. The change in absorbance, ΔE, i.e., the loss of absorbance at 320 nm and the gain of absorbance at 400 nm when the pH is increased from pH_1 to pH_2, is shown in a double logarithmic plot as a function of concentration. It is linear over four decades of concentration. The detection limit for 4-nitrophenol was found to be less than 100 ng, corresponding to a concentration of 100 ng ml^{-1}.

Conclusion

The FIA method with a pH gradient and diode-array detection is a powerful technique for the identification of those organic acids (including phenols) and bases whose optical absorption spectrum changes at the pH of their pK value. The identification is very reliable as it is based on three independent parameters: the acidic and alkaline spectra and the pH range for their conversion. The method is well suited for the determination of pK values and is easy and rapid. The sensitivity of the method depends on the smallest measurable change in absorbance. For 4-nitrophenol a limit of 100 $\mu g\ l^{-1}$ was observed. For some of the non-polar natural dyes mixed organic–aqueous solvents can be used to dissolve them.

Although LC pumps were applied in this work, other pumps may be used if they pump reproducibly and if their flow-rates can be programmed. If the pumps cannot withstand strong acids or alkalis, water can be used as the transport medium, i.e., the acidic solution of the analyte can be located in the loop of one valve and the aqueous alkali in the loop of a second valve.

REFERENCES

1 K. Venkataraman (Ed.), The Analytical Chemistry of Synthetic Dyes, Wiley, New York, 1977.
2 Ch.-H. Fischer, M. Bischof and J.G. Rabe, J. Liq. Chromatogr., 13 (1990) 319.
3 J. Ruzicka and E.H. Hansen, Flow Injection Analysis, Wiley, New York, 2nd edn., 1988.
4 Handbook of Chemistry and Physics, Chemical Rubber Company, Boca Raton, FL, 73rd edn., 1992.
5 W. Kratzert and R. Peichert, Farbstoffe, Quelle und Meyer, Heidelberg, 1981.

Analytica Chimica Acta, 284 (1993) 265–273
Elsevier Science Publishers B.V., Amsterdam

On-line monitoring of flowing samples using solid phase microextraction-gas chromatography

Safa Motlagh and Janusz Pawliszyn

Waterloo Center for Groundwater Research and Department of Chemistry, University of Waterloo, Waterloo, Ontario N2L 3G1 (Canada)

(Received 4th June 1993; revised manuscript received 23rd August 1993)

Abstract

The rapid sampling and concentration response of solid phase microextraction (SPME) facilitate the monitoring of organic analytes present in a flowing stream. It was determined that in addition to convection introduced by flow in the system, an efficient means of agitation is required to achieve rapid extractions. Three agitation techniques; magnetic mixing, intrusive mixing and sonication were tested. While magnetic stirring is inexpensive and easy to automate, it exhibited low mixing efficiency. Intrusive mixing allows efficient agitation but caused sample heating and is not easily amenable to on-line analysis. Sonication proved to be the most efficient and the most convenient means of agitation for sampling from flowing streams. For example, toluene equilibrates in less then 1 min, which is very close to theoretical predictions assuming perfect agitation conditions. The on-line SPME-GC technique allows gas chromatography to be incorporated into a flow-injection analysis system.

Keywords: Flow systems; Gas chromatography; On-line monitoring; Solid phase microextraction

Current methods of analysis for organic compounds in water are often slow, labour intensive, expensive and use large quantities of toxic solvents. Volatiles are usually analyzed by the purge and trap technique which is U.S. Environmental Protection Agency (EPA) approved [1,2], or by headspace analysis. These methods either require expensive instrumentation or are not sufficiently sensitive. Semivolatiles are usually analyzed by the use of liquid–liquid extraction (LLE), which is EPA approved [1,2], or by solid phase extraction (SPE). These methods are time consuming, difficult to automate and use toxic, expensive, high purity solvents.

A recent technique called solid phase microextraction (SPME) solves most of the problems associated with the more traditional methods. SPME involves coating a thin fiber (usually made of fused silica) with a cross-linked polymeric organic liquid such as poly(dimethylsiloxane). This coated fiber is placed into the contaminated aqueous sample. The analytes partition into the stationary phase and are then thermally desorbed in the injector of a gas chromatograph. Thus, the extraction is, in effect, a non-exhaustive liquid–liquid extraction. It is also convenient since the organic phase is permanently attached to the fiber. This fiber is contained in a syringe needle which protects it during sample introduction into the gas chromatograph injector. The total time taken for the extraction is usually a few minutes. Coated optical fibers have been used thus far because they are inexpensive and are commercially available from a number of suppliers with a variety of coating materials and thicknesses. These fibers also have a small diameter which allows

Correspondence to: J. Pawliszyn, Waterloo Center for Groundwater Research and Department of Chemistry, University of Waterloo, Waterloo, Ontario N2L 3G1 (Canada).

SSDI 0003-2670(93)E0497-U

them to be contained in a syringe needle and thus be introduced into the injector of a gas chromatograph [3]. SPME has been used in conjunction with gas chromatography–mass spectrometry for the part-per-trillion (ppt) level detection of organic compounds such as benzene, toluene, ethylbenzene, the xylene isomer [4], many of the more common polychlorinated biphenyls (PCBs) and polyaromatic hydrocarbons (PAHs), phenols and the compounds in the EPA method 624 [5]. SPME has also been used in the isotope dilution analysis of caffeine in tea and cola beverages [6]. The technique has been fully automated and matrix effects such as organic interferences, ionic strength, pH and solution temperature have been investigated [7]. Solid phase microextraction is an equilibrium method and therefore the amount of analytes extracted into the given volume of coating is proportional to the analyte concentration [8] and is independent of sample volume for large amounts of sample.

The continuous monitoring of levels of organics present in process streams and waste water effluents are of particular importance to industry. This can be accomplished by using specific sensors. However this approach is difficult to implement practically because of the complexity of real samples. In this paper we propose an alternative scheme which interfaces gas chromatography to the analytical system through a simple SPME device.

EXPERIMENTAL

Apparatus

The assembly of the SPME device involved replacing the metal wire plunger assembly of a Hamilton 7105-N syringe (Supelco, Oakville) with a modified optical fiber which was modified as follows. A 6 cm length of optical fiber was cut from a spool of the fiber. 5 cm of the polymer coating was removed by soaking a section of the fiber for 1 min in concentrated sulfuric acid. A 1 cm length of this uncoated section was inserted into a 15 cm long metal sheath cut from 1 foot of 30 gauge stainless-steel tubing (Chromatographic Specialties, Brockville) and glued in place using epoxy glue. The fiber was then "conditioned" in the injector of a gas chromatograph by heating it at the maximum injector temperature being used in the gas chromatograph program for a few minutes. This treatment removed impurities present in the coating introduced during the manufacturing, shipping and preparation of the fiber. During the desorption step, the fiber is exposed in the injector such that the bottom of the fiber is as close as possible to the top of the column.

Poly(dimethylsiloxane) coated fibers with silica cores o.d. of 141 ± 5 μm and a total o.d. of 253 ± 8 μm (i.e., a 56 μm thick coating) were used in all experiments.

A Varian 6000 gas chromatograph (Varian, Mississauga) equipped with a 1075 split/splitless injector used in splitless mode and a flame ionization detector was used for the desorption and analysis of analytes from the fiber. The gas chromatograph was equipped for sub-ambient analysis using dry ice as coolant. 11 mm o.d. LB-2 septa (Supelco, Oakville) were used in the injector. Septum coring was initially a problem because of the rather thick needle used. A variety of septa were tested and the LB-2 exhibited the least coring. A 15 m long SPB-1 column (Supelco) with a 0.53 mm i.d. and a 0.5 μm thick stationary phase was used.

The sonication experiments were done using a TSD-600 Sonic Disruptor (Tekmar, Cincinnati, OH) equipped with a $\frac{1}{2}''$ stepped horn, a $\frac{1}{8}''$ stepped microtip and a 5 gallon/h stainless-steel continuous flow cell (Fig. 1). Note that the figure does not show the water jacket of the continuous flow cell. The cell was used in an inverted position and the hole normally used for the exit of waste was blocked off with a Microsep F-138 PTFE-backed silicone septum (Supelco). The hole used for analyte sampling was used as the waste exit. This was done in order to reduce vaporization loss by decreasing the surface area of analyte exposed to the atmosphere. This was done by raising the level of analyte solution such that its surface of is in the narrow part of the cell. The steel-to-glass connection needed in the continuous flow cell was made using Masterflex Viton™ tubing (Cole-Parmer, Chicago, IL) which absorbs negligible amounts of aromatic hydrocarbons. The

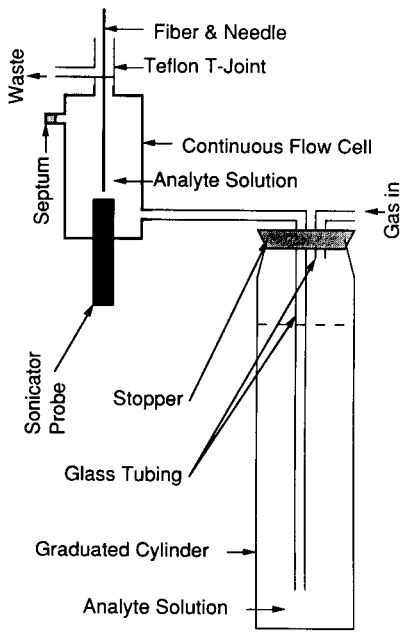

Fig. 1. Experimental set-up for continuous-flow sonication experiments. Cooling jacket of cell and gas flow controller is not shown.

flow-rate of the analyte was controlled by a 0–0.5 p.s.i. compressed inert gas regulator (InterCity Welding, Kitchener).

The sonication experiments using the $\frac{1}{2}''$ horn were performed using a custom-made water-jacketed container (Fig. 2). The stopper was made of silicone and covered with heat-resistant glass fiber tape. This prevented absorption of analytes by the stopper and also prevented the stopper

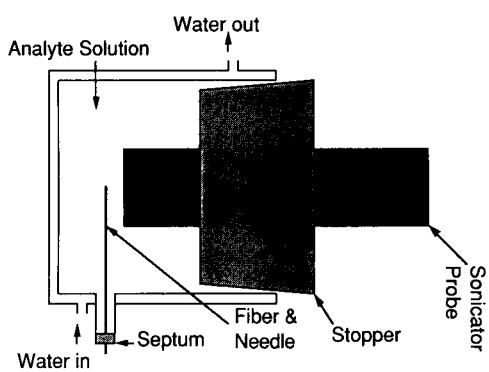

Fig. 2. Experimental set-up for high powered static sonication experiments.

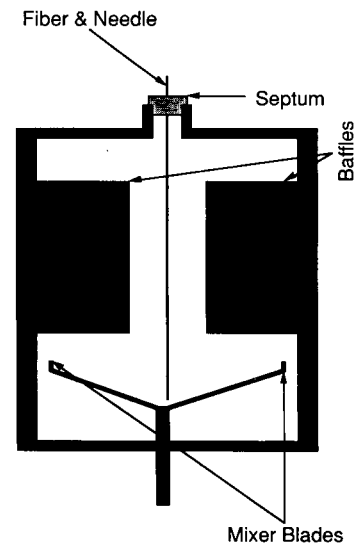

Fig. 3. Experimental set-up for intrusive mixing. One of the baffles is not shown and neither is one of the mixer blades.

from being burned or melted by the hot sonicator probe. The container was equipped with a screw-top hole cap which accommodated a PTFE-backed silicone septum.

The stirring rate experiments were done using a VWR Dylastir magnetic stirrer (Canadawide Scientific, Ottawa). The star-shaped starburst stirring head (Cole-Parmer) was $\frac{3}{8}'' \times \frac{3}{8}''$ in size and the cylinder shaped micro-stir bar (Cole-Parmer) was 7 mm in size. The disc-shaped star-head stir bar (Canadawide Scientific, Ottawa) was $\frac{5}{16}'' \times \frac{5}{16}''$ in size. The mixing rate experiments were done using an Osterizer 8 blender by Sunbeam (Canadian Tire, Waterloo).

All experiments were done using 7.4-ml screw-cap vials with a hole cap and PTFE-backed silicone septa (Supelco) Sonication experiments using the stepped microtip probe were performed using a 50 mL hypo vial with a teflon-backed silicone septa (Supelco, Oakville).

The mixing rate experiments were done using a custom-made stainless-steel container with removable baffles (Fig. 3) and equipped with a screw-top hole cap which accommodated a PTFE-backed silicone septum. This was designed to fit onto the Osterizer mixer.

Reagents

Deionized water was used for all experiments. All organic reagents used were ACS grade (BDH, Toronto). All gases (Inter City Welding, Kitchener) were of ultra-high purity grade (Linde standard) except for the dry ice which was syphon grade.

Procedure

All extractions were performed using a 0.1 ppm solution of benzene, toluene and *p*-xylene in water. However, since all three analytes gave similar results, only the data for toluene are presented in this paper.

Magnetic stirring. 1 μl ml^{-1} analyte standards were prepared in methanol and diluted in water on the day of the analysis since it had been observed that the concentration of analyte in the vials decreased measurably after 24 h. Vials were filled to the brim with the aqueous solution to prevent loss of analyte to the headspace. A stirbar (cylindrical or cross-shaped) was placed into the vial, and 0.05 ml (about 1 drop) of the solution was removed (to prevent the solution wicking up the needle). The septum of the vial was pierced with the syringe needle and 1 cm of the fiber was exposed to the solution by pushing down on the syringe plunger. After the lapse of a specific known time, the plunger was retracted, and the needle was removed from the septum of the vial. It was then immediately inserted in the injector of the gas chromatograph. The time lapse between removal of the fiber from solution to the start of the gas chromatograph run was always less than 30 s. Experiments have shown that this time can be as long as 5 min (for the most volatile compounds being analyzed, i.e., benzene) without loss of analyte to the atmosphere [9]. A mark was made on the syringe needle such that the fiber would be reproducibly exposed in the injector insert just above the column inlet. The fiber was left inside the GC injector for the duration of the run. The vial of analyte was discarded after single use so as not to deplete the solution.

The calibration to obtain the actual mass of analyte desorbed from the fiber was done by injecting 0.2 μl of 100 ppm analyte in dichloromethane.

Sonication with $\frac{1}{8}$" horn. The microtip was exposed to the analyte solution through a hole made in the septum of a 50-ml hypo vial. The syringe needle pierced this septum at a 45° angle, thereby allowing the coated portion of the fiber to be held immediately below the tip of the probe. No significant heating of the sample was observed because of the large volume of water and the low power setting on the sonicator.

Sonication with $\frac{1}{2}$" horn. Due to the extremely rapid temperature rise in analyte temperature during sonication at higher powers, a special glass water-cooled cell was designed (Fig. 2) which allowed for longer sonication times. The silicone stopper was taped with heat resistant glass tape to prevent contact with the analyte solution. The sampling was performed by piercing a septum at the bottom of the container and exposing the fiber about a millimeter below the tip of the probe.

Continuous flow sonication. The set-up shown in Fig. 1 was used. The flow-rate of the analyte was determined by the flow-rate of the gas which was set at about 16 ml min^{-1}. Note that the continuous flow cell is jacketed by a water bath which is not shown in Fig. 1.

Intrusive mixing. The set-up shown in Fig. 3 was used. The large glass jar on the mixer was replaced by a stainless-steel container with a screw-top equipped with a hole cap which held a PTFE-backed silicone septum. The baffles were mounted on a removable sleeve which was snug with the inner wall of the container. The bottom of the metal container was threaded so it fitted onto the plastic bottom that held the mixer blades.

The gas chromatograph program which was used for both fiber and syringe injections was as follows. The column was started at 0°C and immediately ramped at 25°C min^{-1} to 211°C, where it was held for 1.25 min. The injector temperature was held at 211°C and the detector temperature was held at 300°C with its sensitivity set at range 12. A Varian 4270 integrator was used for peak area integration. The split valve was turned on at 0.5 min and turned off at the end of the run. The helium carrier gas flow-rate was set at 4.2 ml min^{-1}, the air flow-rate was set at 300 ml min^{-1}, the hydrogen flow-rate was set at 30 ml

min^{-1} and the helium make-up flow-rate was set at 30 ml min^{-1}.

Cryogenic focusing was used to cool the gas chromatograph column below room temperature to trap the volatiles at the head of the column in a narrow band. Prior to analysis, the linearity of the detector was determined over the range of concentrations encountered in the experiments. 0.2 μl of a 100 ppm mixture of benzene, toluene and *p*-xylene was injected every day and the detector response tabulated to ensure proper instrumental performance. Fiber blanks were run immediately after the longest exposure of the fiber to the analyte to check for carryover.

RESULTS AND DISCUSSION

The theoretical investigations [8] predict that the time required to complete extractions from well-agitated solutions is proportional to the thickness of the polymer coating; and inversely proportional to the diffusion coefficient of the analyte in the coating. However, if the agitation is not efficient, the rate of diffusion through the static aqueous layer adjacent to the fibre surface becomes the major factor in determining the time required to reach equilibrium in the system.

An extraction done from a flowing sample (Fig. 4) shows that while the flowing stream does provide some agitation and reduces extraction times noticeably when compared with an extraction done from a static solution (ca. 20 min vs. ca. 1 h), equilibration times are still unacceptably high. The extraction times can be further reduced by using higher flows, but the optimum solution would be to use an appropriate agitation technique, so that the results will be independent of flow conditions. Below, three commonly used techniques of agitation (magnetic stirring, intrusive mixing and sonication) were evaluated for this application.

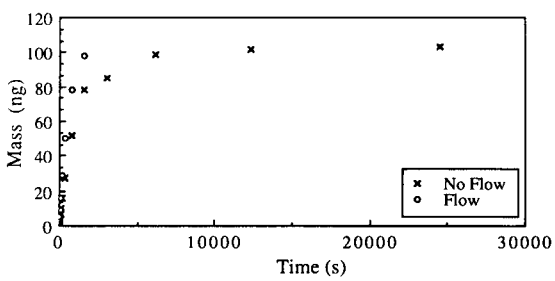

Fig. 4. Time taken for an unagitated extraction from a flowing stream of 0.1 ppm toluene. The flow-rate of analyte was set at 16 ml min^{-1}.

Magnetic stirring

Magnetic stirring is the least expensive, cleanest, most convenient and the most common method of agitation used in chemical laboratories. Since inert PTFE-coated stir bars are the only part of the setup that comes into direct contact with the analyte, cross-contamination is minimized while maximum speeds of up to about 3300 rpm are attainable with magnetic stirring. Higher rotational speeds can be reached only by using stronger magnets which can withstand the frictional forces acting on the stir-bar. These forces can also be reduced by using smaller stir-bars with less surface area exposed to the water. Lighter stir-bars also spin faster due to the reduced frictional forces between the bottom of the vial and the stir-bar.

It was noticed that as the speed setting on the stir-plate was increased, the rotational speed of the cylindrical stir-bar also increased up to a point where the speed of the stir-bar was very unstable and the stir-bar would either vibrate in one place or move about the vial in a random fashion. To overcome this problem, the agitation efficiency of stir-bars with other shapes were tested. The small size of the stir-bars precluded the use of a tachometer to measure the speed of rotation and so the stirring efficiency of the three stir-bars was tested by comparing the extraction times of benzene, toluene and *p*-xylene using each stir-bar at a constant stir-plate setting. The star-shaped stir-bar was in fact X-shaped (i.e., two cylinders of similar dimensions fused at the center) while the disc-shaped stir-bar was in fact O-shaped with X-shaped ridges on both the flat surfaces. The star-shaped stir-bar gave the shortest extraction times, followed by the disc shaped stir-bar; the cylinder-shaped stir-bar was the least effective. The depth of the vortex formed by the three stir-bars followed the same order. As a

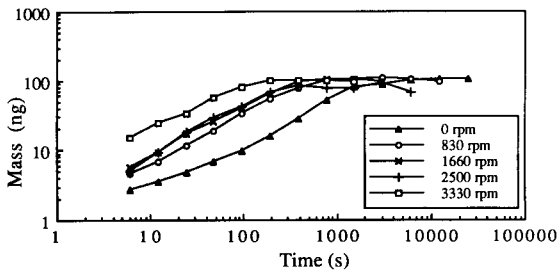

Fig. 5. Effect of stirring rate on extraction time of toluene using star-shaped stir-bar. A 56 μm thick poly(dimethylsiloxane) coating was used to analyze 7.4 ml of a 0.1 ppm solution of toluene.

result of these experiments, the star-shaped stir-bar was used in all further experiments. The shape and size of the bottom of the vial also affected the stability of the stir-bar. 50-ml hypovials have a convex bottom that prevent higher speeds from being attained. Vials with flat bottoms (7.4 ml) were superior and were used in all experiments. The diameter of the stir-bar also had to be very close to that of the bottom of the vial. When this was not the case, the stir-bar did not spin evenly but moved about the bottom of the vial randomly colliding with the sides. The smallest commercially available star-shaped stir-bar fit the bottom of the 7.4-ml vial quite well. A wide-necked vial must be used in order to allow the stir-bar to be inserted into it. Again, the 7.4-ml vial fit this requirement.

Using the 7.4-ml vial and the small star-shaped stir-bar, the effect of stirring rate on the extraction time of benzene, toluene and *p*-xylene was investigated. Figure 5 shows the effect of stirring rate on the extraction time of toluene. The equilibration time is about 2 min for the fastest rotational speed of 3330 rpm and slowly increases with decrease of agitation. The rotational speed of the stir-bar was not constant at the lower speeds between 830 rpm and 2500 rpm and over a few minutes, the speeds varied by several hundred rpm. It was initially thought that this was due to line voltage fluctuation; however, a voltage regulator was ineffective. The result of this wide variation in the set speed is that the extraction times for speeds between 830 and 2500 rpm are very similar. There are no problems such as sample heating, etc., associated with running the stir-plate at its maximum speed, however, and the speed is very stable, so extractions should be performed at this high speed whenever possible in order to decrease extraction times and to improve precision.

Intrusive mixing

Intrusive mixers can attain speeds of up to 20 000 rpm which is almost an order of magnitude higher than with magnetic stirring. However, with such high speeds, sample heating is significant due to the vigorous agitation. The temperature rise of the solution was monitored over time at two speeds. The effect of baffles on the temperature rise was also tested. It was seen that at high speeds of about 20 500 rpm, the 170 ml of water in the container began to boil in about 10 min. At low speeds of about 13 100 rpm, the temperature of the water only rose from 25 to 45°C in 10 min. Hence, without cooling, the higher mixing speeds will result in significant loss of analyte thus adversely affecting the precision and accuracy of the technique. The presence of baffles did not significantly affect the rate of temperature increase in the solution.

The effect of mixing rate on the speed of extraction was also investigated. As can be seen in Fig. 6, the faster the rate of mixing, the faster the extraction. For 20 500 rpm the extraction time is below 100 s. However, the higher mixing rates cause an rise in solution temperature and consequently a significant loss of analyte at longer mixing times.

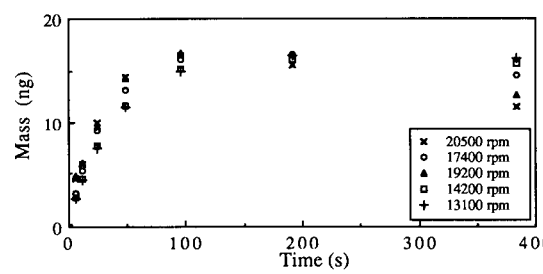

Fig. 6. Effect of mixing rate with intrusive mixing on extraction time and mass absorbed from 170 ml of 0.1 ppm toluene.

Sonication

Sonication is commonly used to homogenize biological samples in order to facilitate the extraction of inorganic analytes. It is a very powerful means of agitation and the high flux of power entering the solution from the sonicator probe causes a substantial increase in solution temperature. Therefore, all extractions performed using this method of agitation must involve one of three techniques; using low sonication power, cooling the vial, or using a larger volume of solution to prevent temperature increases. A large increase in solution temperature will result in increased vaporization of the more volatile analytes and consequently increased headspace losses and a loss of precision and accuracy. The temperature increase of a sonicated solution was monitored over time using a relatively low power setting of about 45 W; the temperature of the 60-ml solution rose by almost 20° from room temperature in 10 min. This moderate temperature increase should not affect experimental results significantly [7].

The temperature increase of a sonicated solution was monitored over time using a high power setting of about 170 W and a smaller volume of solution (17 ml). It was observed that in the absence of a cooling jacket, the temperature of the solution rises close to the boiling point of benzene (80°C) after only about a minute of sonication at this power. With water-cooling, however, the temperature reaches a steady state of about 60°C after 2 min. In order to minimize the effect of this temperature increase, the system must be airtight to prevent loss of analyte to the headspace. Thus cooling is indispensable when sonicating small volumes of analyte at high power settings.

The effect of probe diameter on the extraction time was investigated. It was seen that the extraction times of benzene, toluene and *p*-xylene are significantly lower when the wide 19-mm probe is used (see also Fig. 2 for experimental set-up). The extraction time decreased to below 50 s vs. 100 s for the 4-mm probe. This is because when the large probe was used, the whole length of the fiber was held horizontal to the tip of the probe and about 1 mm away from the end. However, this could not be done with the narrower probe and so the fiber was held at a 45° angle to the tip of the probe. Thus the end of the fiber was about 7 mm away from the tip of the probe.

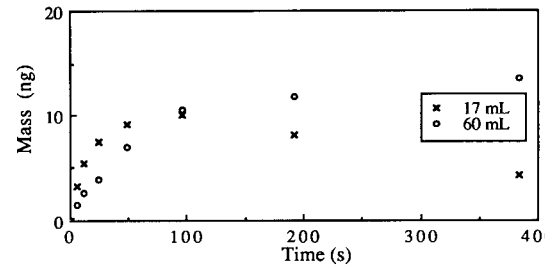

Fig. 7. Sonication induced decomposition of 0.1 ppm toluene.

Figure 7 shows that with prolonged sonication, the mass of analyte extracted decreases. This loss is more apparent when a smaller volume of sample is sonicated. There is a considerable amount of literature available on the affect of ultrasonic waves on aromatic hydrocarbons. The decomposition of benzene, toluene, phenol, etc., has been documented [10–12]. In water, sonication produces hydrogen peroxide and molecular hydrogen via the highly energetic hydrogen and hydroxy radicals, whose reactivity may account for the destruction of organic solutes [13]. The hydrogen and hydroxy radicals are produced by the high temperatures (5000 K) and pressures (1000 atm) produced by the sonic waves in solution. The products of the sonic decomposition of benzene, for example, are toluene, naphthalene, methane, formaldehyde, ethene and phenol. Some evidence of decomposition was found in the chromatograms. It was noticed that as the size of the analyte peaks decreased, the size of two unidentified peaks, both of which eluted after *p*-xylene, increased. These two peaks are probably naphthalenes since the more volatile analytes, i.e., methane, ethene and formaldehyde will not be detected with the chromatographic separation conditions used. It was also observed that the narrow probe does not cause noticeable decomposition.

The literature also indicates that sonication can cause depolymerization of most polymers [11,12]. However, no significant damage to the

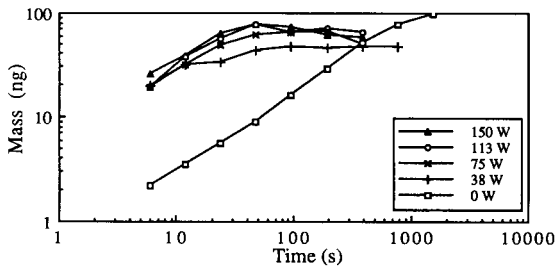

Fig. 8. Effect of sonication power on extraction time of toluene using continuous-flow cell at 16 ml min^{-1}. The 19 mm probe was used to sonicate 0.1 ppm toluene.

coating was observed at the powers and geometric configurations used in the experiments.

Among three agitation techniques tested, the most effective was sonication. The extraction time for toluene with sonication is only about 50 s (see Fig. 7), which is close to theoretical predictions assuming perfect agitation conditions. [8]. The significant drawbacks of sonication are sample heating and decomposition. However, when used in the analysis of a flowing stream, sample heating will be minimal since the sample is constantly being replenished, and the decomposition of target analytes can be eliminated by using the low power sonication.

To simulate extractions from an on-line system using sonication as the primary means of agitation, a continuous-flow set-up was investigated (see Fig. 1 for experimental set-up). The flow-rate of the analyte was kept constant (at 16 ml min^{-1}) while the sonicator was on and the extraction was proceeding. The mass of benzene, toluene and *p*-xylene extracted over time by the fiber was monitored. Figure 8 shows the effect of sonication power on the extraction time from a flowing stream of 0.1 ppm toluene. While the difference between the extraction times obtained using power settings between 38 and 150 W was significant, the most drastic decrease in extraction time was between the unsonicated extractions and the extractions performed at the low power setting of only 38 W. This indicates that low power sonication is sufficiently vigorous for most extractions thus eliminating the need to use high-powered sonication with its accompanying disadvantages of sample decomposition and high-pitched noise. It can also be seen from the Fig. 8 that even at the very high power setting of 150 W, sample decomposition is negligible. This is because the analyte is being constantly replenished and the decomposition by-products are being carried away. In addition, localized sample heating is reduced because the analyte is constantly flowing aqueous stream over the sonicator tip.

Conclusions

SPME extractions using sonication as a means of agitation are very rapid (about 1 min) and therefore can be used to isolate organics present in flowing streams which are changing in analyte composition and concentration. Automated SPME [7] can be used as an effective means of coupling flow-injection analysis with chromatographic separation and quantitation. New developments in the SPME technology, such as headspace approach [14] extend application of this method to analysis of dirty samples. In addition use of ion exchange polymeric phases allows determination of ionic compounds [15] in combination with appropriate chromatographic and/or spectroscopic technique.

This work was financially supported by Supelco Canada and the Natural Sciences and Engineering Research Council of Canada.

REFERENCES

1 I.H. Suffet and M. Malaiyandi (Eds.), Organic Pollutants in Water: Sampling, Analysis, and Toxicity Testing, Advances in Chemistry Series, Vol. 214, American Chemical Society, Washington, DC, 1987.
2 L.S. Clesceri, A.E. Greenberg and R.R. Trussell (Eds.) Standard Methods for the Examination of Water and Wastewater, American Public Health Association, Washington, DC, 17th edn., 1989.
3 C.L. Arthur and J. Pawliszyn, Anal. Chem., 62 (1990) 2145.
4 D.W. Potter and J. Pawliszyn, J. Chromatogr., 625 (1992) 247.
5 C.L. Arthur, K. Pratt, S. Motlagh, J. Pawliszyn and R.G. Belardi, J. High Resolut. Chromatogr., 15 (1992) 741.
6 S.B. Hawthorne, D.J. Miller, J. Pawliszyn and C.L. Arthur, J. Chromatogr., 603 (1992) 185.
7 C.L. Arthur, L.M. Killam, J. Pawliszyn and J.R. Berg, Anal. Chem., 64 (1992) 1960.

8 D. Louch, S. Motlagh and J. Pawliszyn, Anal. Chem., 64 (1992) 1187.
9 C.L. Arthur, L.M. Killam, S. Motlagh, M. Lim, D.W. Potter and J. Pawliszyn, Environ. Sci. Technol., 26 (1992) 979.
10 M.A. Khenokh and E.M. Lapinskaya, J. Gen. Chem., 26 (1956) 2727.
11 I.E. El'piner, Ultrasound: Physical, Chemical and Biological Effects, Consultants Bureau, New York, 1964.
12 K.S. Suslick, Ultrasound: Its Chemical, Physical, and Biological Effects, VCH, New York, 1988.
13 A.P. D'Silva, S.K. Laughlin, S.J. Weeks and W.H. Buttermore, Polycyclic Aromatic Compounds, 1 (1990) 125.
14 Z. Zhang and J. Pawliszyn, Anal. Chem., 65 (1993) 1843.
15 E. Otu and J. Pawliszyn, Microchim. Acta, 112 (1993) 41.

Analytica Chimica Acta, 284 (1993) 275–279
Elsevier Science Publishers B.V., Amsterdam

Determination of paraquat by flow-injection spectrophotometry

Archana Jain [a], Krishna K. Verma [a] and Alan Townshend

School of Chemistry, University of Hull, Hull HU6 7RX (UK)

(Received 18th June 1993; revised manuscript received 27th September 1993)

Abstract

The solution obtained by oxidizing some of the ascorbic acid to dehydroascorbic acid by reaction with potassium iodate is used as a reagent for the reduction of paraquat to a blue radical cation in the flow-injection spectrophotometric determination of paraquat. A rectilinear calibration graph was obtained over the range 0.1–100 μg ml^{-1} paraquat, and the limit of detection was 20 ng ml^{-1} paraquat (signal-to-noise ratio = 3). This reagent has been found superior to ascorbic acid alone or sodium dithionite because of the lower limit of detection, wide linear range of determination, rapid reaction and high stability.

Keywords: Flow system; Spectrophotometry; Paraquat

Paraquat (the 1,1′-dimethyl-4,4′-bipyridylium ion) is one of the most important of a group of bipyridylium herbicides for both terrestrial and aquatic plants [1]. Paraquat has achieved great prominence because of its wide spectrum of activity against grasses as well as most broad-leaved weed species. It is an unselective, quick-acting herbicide and desiccant, and leaves no residues because of its rapid inactivation by irreversible adsorption on contact with soil. Paraquat is structurally related to 1-methyl-4-phenyl-1,2,3,6-tetrahydropyridine, a compound which is known to produce Parkinsonism in man [2], and paraquat has been shown to cause Parkinsonism in the leopard frog when injected peritoneally [3]. Although the field safety record of paraquat is fairly good, there remain several areas of concern [4–6].

Correspondence to: A. Townshend, School of Chemistry, University of Hull, Hull HU6 7RX (UK).

[a] Present address: Department of Chemistry, Loughborough University of Technology, Loughborough, Leicestershire LE11 3TU (UK).

This herbicide is extremely toxic to man and consequently it is often encountered in cases of accidental and intentional ingestion. The toxicity is due to the rapid development of pulmonary fibrosis, caused by major lung retention of the ion [7]. Availability of a rapid and inexpensive analytical method could facilitate collection of data on exposure levels in such situations.

Several methods have been described for the determination of paraquat and related bipyridylium herbicides. For determination by gas chromatography, either fully reduced [8] or mono- and diunsaturated derivatives [9] have been prepared. Much of the chromatographic work on paraquat has concerned clinical samples and natural waters [10,11]. Two independent modes of detection have been used in liquid chromatography, direct UV absorptiometry [12–14] or post-column reaction with sodium dithionite before UV absorptiometry [14].

Paraquat forms a precipitate with tetraiodomercurate(II) [15] and tetraiodobismuthate(III) [16]; however, ethanol, acetone, starch [15] and

SSDI 0003-2670(93)E0552-I

gum arabic [16] inhibit precipitate formation, and what is apparently a solution, orange in colour, is obtained which is suitable for spectrophotometric determination [15,16].

A blue semiquinoid radical cation is formed on reduction of paraquat by sodium dithionite in alkaline medium [17–23], and this technique forms the basis of the most often used spectrophotometric method which allows the determination of 4–12 μg ml^{-1} paraquat [17,18]. The radical is quite unstable owing to its rapid oxidation by atmospheric oxygen which produces fading of colour and difficulties in solution handling in batch experiments. These inconveniences have been minimized by determinations under flow-injection conditions [24], but the dithionite reagent is unstable and should be prepared hourly. Ascorbic acid has been reported to be a more stable reagent than dithionite and has been used for the determination of 1.2–9.8 μg ml^{-1} paraquat by a batch method [25]. If the solution of ascorbic acid is one day or more old, the absorption spectrum of the coloured cation is changed. Therefore only a freshly prepared reagent solution should be used.

In the present work, ascorbic acid partially pre-oxidized to dehydroascorbic acid by reaction with potassium iodate (potassium iodate and ascorbic acid react in a molar ratio of 1:3) has been utilized for the reduction of paraquat to its blue radical cation in a flow-injection system. It was found to be superior to ascorbic acid alone or to dithionite because it was stable for up to 5 days at room temperature, it gave a broad linear range of determination (0.1–100 μg ml^{-1}) and a limit of detection of 20 ng ml^{-1} paraquat. Thus, the present flow injection method has a lower limit of determination [26] of paraquat 12 times less than the ascorbic acid batch method, and 40 times less than the dithionite batch method.

EXPERIMENTAL

Reagents and samples

Ascorbic acid reagent. 2.5 g of ascorbic acid (BDH, Poole), 0.1 g of potassium iodate and 1 g of EDTA, disodium salt (BDH) were dissolved by stirring in about 400 ml of water and the solution was diluted exactly to 1 l with deionized distilled water. This solution, stored at 18°C, did not show any change in paraquat peak absorbance when used up to 5 days after its preparation.

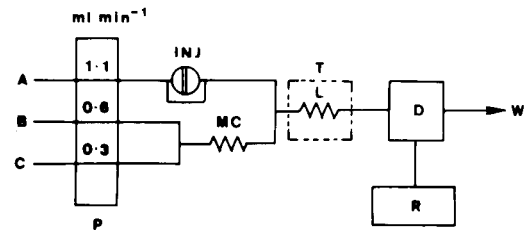

Fig. 1. Schematic diagram of the flow-injection system used for the determination of paraquat. A = deionized water carrier; B = ascorbic acid–iodate–EDTA (1.5×10^{-2} M–5×10^{-4} M–0.1%); and C = 1 M sodium hydroxide. MC = 50 cm mixing coil, L = 75 cm reaction coil; P = peristaltic pump; INJ = injector (75 μl); T = thermostat (60°C); D = detector (600 nm); R = recorder, and W = waste. All flow lines were made from 0.5 mm i.d. PTFE tubing.

Standard paraquat solutions. A 1 mg ml^{-1} stock solution of paraquat was prepared by dissolving paraquat dichloride (Sigma, St. Louis, MO) in deionized distilled water. Less concentrated working standards were prepared by sequential dilution of the stock solution with water.

All other chemicals used were of analytical-reagent grade and deionized distilled water was used for preparing all the solutions.

Apparatus

The flow system (Fig. 1) consisted of a Gilson Minipuls 3 peristaltic pump (Anachem), a 4-way Rheodyne 5020 rotary valve injector (Anachem), an LKB Ultrospec II 4050 spectrophotometer equipped with a flow-through cell (18-μl volume, 1-cm path length) and a Chessel Type BD 40 04 chart recorder. The sample stream was propelled by a separate Ismatec Mini-S 820 pump (Zurich). The manifold and reaction coil tubing was 0.5 mm i.d. PTFE. Flanged end fittings were made using plastic nuts and polypropylene couplers (Anachem). Home-made T-joints of 0.8 mm bore were used.

In the optimized flow-injection system, 1 M sodium hydroxide (flow rate 0.3 ml min^{-1}) and ascorbic acid reagent (0.6 ml min^{-1}) streams were

merged and mixed by passing through a 50 cm coil, and combined with the carrier stream of water (1.1 ml min^{-1}) into which a 75-μl aliquot of paraquat sample was injected. The reaction occurred in a knitted delay coil of 75 cm thermostated at 60°C. Detection was at 600 nm.

RESULTS AND DISCUSSION

Preliminary observations

In the flow-injection manifold used in pilot studies on the determination of paraquat, reagent streams of 0.5 M sodium hydroxide and 0.5% ascorbic acid (flow-rate, 0.5 ml min^{-1} each) were T-merged, passed through a 50-cm coil and combined with a carrier stream of deionized water (1 ml min^{-1}) into which a 50-μl sample was injected. The reaction was allowed to occur in a 100-cm coil and the blue cation formed detected at 600 nm. The detector signal was found to be insensitive to changes in ascorbic acid concentration (over the range 0.1–2%) but, at a fixed ascorbic acid concentration, the signal steadily increased on raising the temperature from 25 to 70°C. The most surprising observation was the effect of the age of the ascorbic acid solution. Injection of a 100 μg ml^{-1} paraquat solution into the above flow system (with the reaction coil thermostated at 60°C), using fresh, 1 day and $\geqslant 2$ days old solutions of 0.5% ascorbic acid, gave peak absorbances of 0.580, 0.900 and 1.321, respectively. This effect was believed to be due to the presence of dehydroascorbic acid, which is formed in solutions of ascorbic acid by air oxidation.

The effect of dehydroascorbic acid, therefore, on the formation of the blue cation was investigated. In a preliminary experiment, 0.5 g of ascorbic acid and 0.05 g of chloramine T or potassium iodate, each dissolved in about 25 ml of water, were mixed together to oxidize some of the ascorbic acid to dehydroascorbic acid. This solution was diluted accurately to 100 ml and used as a reagent. The peak absorbance obtained was 1.330 which confirmed the increased sensitivity.

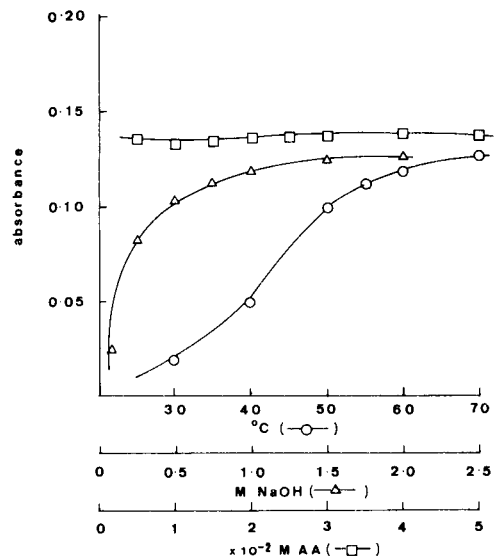

Fig. 2. Effect of ascorbic acid concentration (solution in 5×10^{-4} M iodate); sodium hydroxide concentration; and reaction temperature on the peak absorbance of 10 μg ml^{-1} paraquat. Other flow conditions as described in Fig. 1.

Optimization of the flow system

The formation of the blue radical reduction product of paraquat occurs only in alkaline medium, and since ascorbic acid is unstable in alkaline solution [27], sodium hydroxide and ascorbic acid were mixed on-line before reaction with paraquat. The effect of ascorbic acid concentration was studied over the range 0.5–0.05 M, the solutions being prepared in 5×10^{-4} M potassium iodate. The peak absorbance for 10 μg ml^{-1} paraquat was practically constant over the entire range studied (Fig. 2). In subsequent experiments a 1.5×10^{-2} M solution of ascorbic acid in 5×10^{-4} M potassium iodate was used. This solution can be used immediately after its preparation. The absorbance increased on increasing the sodium hydroxide concentration up to 1 M, which was selected as optimum, then remained constant (Fig. 2). A six-fold increase in signal was obtained by increasing the temperature of the reaction coil from 30 to 60°C; on changing from 60 to 70°C, the increase was only 5% (Fig. 2). During the optimization of other variables the reaction coil was kept thermostated at 60°C.

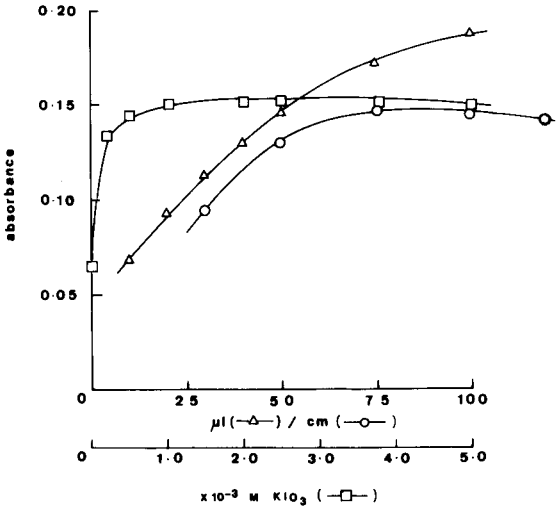

Fig. 3. Effect of iodate concentration (solution in 1.5×10^{-2} M ascorbic acid); sample injection volume; and the length of reaction coil, L, on the peak absorbance of 10 μg ml^{-1} paraquat. Other flow conditions as described in Fig. 1.

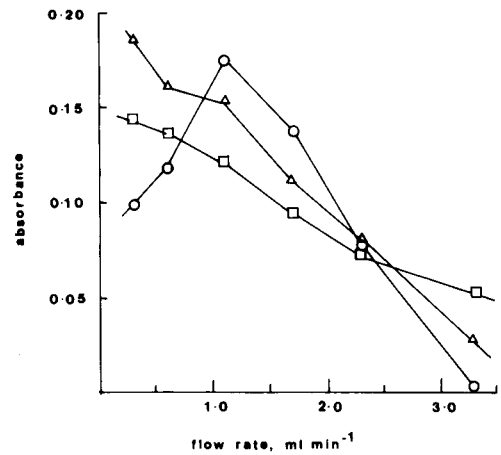

Fig. 4. Effect of flow-rate of water carrier (○); 1 M sodium hydroxide (△); and 1.5×10^{-2} M ascorbic acid (solution in 5×10^{-4} M iodate and 0.1% EDTA; □) streams on the peak absorbance of 10 μg ml^{-1} paraquat. Excepting the parameter under study, all other conditions were the same as described in Fig. 1.

As shown in Fig. 3, the peak absorbance obtained was maximum when a reaction coil of 75 cm (studied 30–120 cm) was used, and showed a constant increasing trend with increasing injection volume in the range 10–100 μl. Using a 75-μl injection volume the sample throughput was 120 h^{-1}, though the peak absorbance was about 8% lower than that obtained for a 100-μl injection. The effect of potassium iodate (and hence the amount of dehydroascorbic acid formed) was studied by varying the potassium iodate concentration in 1.5×10^{-2} M ascorbic acid from 0 to 5×10^{-3} M. The peak absorbance using ascorbic acid reagent which was 5×10^{-4} M in potassium iodate (ascorbic acid–dehydroascorbic acid mole ratio, 9:1) was double that which had no iodate; a further increase in iodate concentration did not significantly affect the absorbance. The use of 5×10^{-3} M iodate oxidized all the ascorbic acid to dehydroascorbic acid, yet the formation of the blue reduction species remained the same. This was a very unexpected observation and seemed to indicate that dehydroascorbic acid was more effective at producing the radical reduction product. The blue reduction species formed by ascorbic acid alone and by ascorbic acid–iodate reagent both absorbed maximally at 600 nm.

The effect of change in the flow-rate of carrier, ascorbic acid and sodium hydroxide streams is shown in Fig. 4; the optimum rates selected are those given in Fig. 1.

Analytical characteristics

The calibration graphs for paraquat were prepared under the optimum conditions, which are given in Fig. 1. For aqueous paraquat solutions, linear plots were obtained for three concentration ranges 2.5–100, 0.5–10 and 0.1–1.2 μg ml^{-1} paraquat (Table 1). The overall (0.1–100 μg ml^{-1}) linear regression had a slope of 0.0178 Abs ml μg^{-1}, an y-intercept of 0.0015 Abs (equivalent to

TABLE 1

Calibration data for the determination of paraquat (Abs = absorbance)

Paraquat range (μg ml^{-1})	n	r	Slope (Abs ml μg^{-1})	Intercept (Abs)
2.5–100	8	0.9993	0.01830	0.0080
0.5–10	7	0.9998	0.01796	−0.0031
0.1–1.2	7	0.9983	0.01714	-0.0003_8

84 ng ml^{-1} paraquat; Abs = absorbance) and a correlation coefficient (r) of 0.9991 ($n = 22$). The detection limit (signal-to-noise ratio = 3) was 20 ng ml^{-1} paraquat.

The relative standard deviations ($n = 6$) were 2.5, 1.0, 1.2 and 1.6% for the determination of 0.1, 5, 20 and 60 $\mu g\ ml^{-1}$ paraquat, respectively.

Interferences

A large variety of other substances was tested as possible interferents in the determination of paraquat by the present method. Not more than $\pm 1\%$ error was produced by up to 500-fold (w/w) excess of chloride, sulphate, borate, carbonate, nitrate and phosphate, and a 250-fold excess of zinc(II), aluminium(III), tin(II), lead(II), magnesium(II), calcium(II) and iron(III). Up to a 1000-fold excess of other pesticides, e.g., 2,4-D, DDT, parathion and benzene hexachloride did not interfere. Diquat (1,1′-ethylene-2,2′-bipyridylium ion) is structurally related to paraquat and interferes in the determination of paraquat by producing a green colour which also absorbs at 600 nm. Treatment with sodium hydroxide of samples containing both paraquat and diquat has been recommended for the removal of diquat; there is no loss of paraquat [15,16]. Diquat interference is not a problem when this method is used as a post-column detection technique in liquid chromatography (LC).

Application

The present method was applied to determine paraquat in spiked potable water. The relationships between the added value, x ($\mu g\ ml^{-1}$) and the observed value, y ($\mu g\ ml^{-1}$) were, $y = 0.989x + 0.012$, $r = 0.998$ for the range 0.1–1 $\mu g\ ml^{-1}$ paraquat ($n = 6$); $y = 0.991x + 0.062$, $r = 0.999$ for the range 1–10 $\mu g\ ml^{-1}$ paraquat ($n = 6$); and $y = 0.992x + 0.348$, $r = 0.999$ for the range 10–100 $\mu g\ ml^{-1}$ paraquat ($n = 6$). The tested levels of paraquat are higher than that permissible by the EC standard of 0.1 $\mu g\ l^{-1}$ for individual pesticides in drinking water. Solid-phase extraction and enrichment on silica appear to improve the limit of detection, as reported in LC methods [14,28].

Sincere thanks are due to the Commission of the European Communities, Brussels, and the Department of Science and Technology, New Delhi, for award of a postdoctoral research fellowship to K.K.V.

REFERENCES

1 G. Zwig, Plant Growth Regulators and Food Additives, Vol. V, Academic Press, New York, 1967, p. 473.
2 J.A. Javitch, R.J. D'Amato, S.M. Strittmatter and S.H. Snyder, Proc. Natl. Acad. Sci., U.S.A., 82 (1985) 2177.
3 A. Barbeau, L. Dallaire, N.T. Buu, J. Poirier and E. Rucinska, Life Sci., 37 (1985) 1529.
4 J.B. Byass and J.R. Lake, Pestic. Sci., 8 (1977) 117.
5 S. Jellinek, Fed. Reg., 44 (1979) 59956.
6 J.N. Seiber and J.E. Woodrow, Arch. Environ. Contam. Toxicol., 10 (1981) 133.
7 D. Nigel, This Poisoned Earth: The Truth About Pesticides, Judy Piatkus, London, 1987, p. 5.
8 C.J. Soderquist and D.G. Crosby, Bull. Environ, Contam. Toxicol., 8 (1972) 363.
9 A. Van Dijk, R. Ebberinck, G. DeGroot, R. Maes, J. Douze and A. Van Heyst, J. Anal. Toxicol., 1 (1977) 151.
10 R. Gill, S.C. Qua and A.C. Moffat, J. Chromatogr., 255 (1983) 483.
11 I. Ahmad, J. Assoc. Off. Anal. Chem., 66 (1983) 663.
12 I. Nakagiri, K. Suzuki, Y. Shiaku, Y. Kuroda, N. Takasu and A. Kohama, J. Chromatogr., 481 (1989) 434.
13 V.A. Simon, LC-GC, 5 (1987) 899.
14 V.A. Simon and A. Taylor, J. Chromatogr., 479 (1989) 153.
15 M. Ganesan, S. Natesan and V. Ranganathan, Analyst, 104 (1979) 258.
16 P. Yanez-Sedeno and L.M. Polo Diez, Talanta, 33 (1986) 745.
17 A. Calderbank and S.H. Yuen, Analyst, 90 (1965) 99.
18 S.H. Yuen, J.E. Baggness and D. Myles, Analyst, 92 (1967) 375.
19 A.A. Carlstrom, J. Assoc. Off. Anal. Chem., 51 (1967) 1306.
20 P.W. Lott, J.W. Lott and D.J. Doms, J. Chromatogr. Sci., 16 (1978) 390.
21 A.F. Fell, D.R. Jarvie and M.J. Stewart, Clin. Chem. (N.Y.), 27 (1981) 286.
22 T. Kuo, Clin. Chem. (N.Y.), 32 (1986) 337.
23 Z. Stransky, J. Chromatogr., 320 (1985) 219.
24 E.C. Guijarro, P. Yanez-Sedeno and L.M. Polo Diez, Anal. Chim. Acta, 199 (1987) 203.
25 P. Shivhare and V.K. Gupta, Analyst, 116 (1991) 391.
26 J.C. Miller and J.N. Miller, Statistics for Analytical Chemistry, Ellis Horwood, Chichester, 3rd edn., 1992, p. 116.
27 K.K. Verma, A. Jain, A. Verma and A. Chaurasia, Analyst, 116 (1991) 641.
28 T.M. Chichila and S.M. Walters, J. Assoc. Off. Anal. Chem., 74 (1991) 961.

Analytica Chimica Acta, 284 (1993) 281–290
Elsevier Science Publishers B.V., Amsterdam

Characterization of an immobilized hexose oxidase reactor for mono- and oligosaccharide determination by liquid chromatography

P.C. Maes and L.J. Nagels

Chemistry Department, University of Antwerp RUCA, Groenenborgerlaan 171, B-2020 Antwerp (Belgium)

(Received 18th May 1993; revised manuscript received 23rd August 1993)

Abstract

The enzyme hexose oxidase was extracted from the red sea-weed *Chondrus crispus* and immobilized in an enzyme reactor. The characteristics of this reactor were studied for the post-column liquid chromatographic detection of carbohydrates (separation on a cation exchange column). The reactor converted the eluting carbohydrates to hydrogen peroxide, which was detected amperometrically. Several saccharides could be determined at low μg levels. Conversion efficiencies for 12 mono- and oligosaccharides were measured at different flow-rates. The flow-rate versus conversion efficiency behaviour of the reactor and its selectivity is compared to the behaviour of a glucose oxidase reactor with very high enzyme loading in this respect. The differences between both reactors are explained theoretically. The practical use of both reactors in chromatographic analysis of carbohydrates is discussed and demonstrated.

Keywords: Liquid chromatography; Hexose oxidase reactor; Monosaccharides; Oligosaccharides; Immobilized hexose oxidase reactor

Liquid chromatographic (LC) methods continue to provide improved tools for the analysis of mono- and oligosaccharides in the food and in the biotechnology sectors. There is, however, still a great need for selective and sensitive detection methods, adapted to the type of sample and chromatographic system. Recent work includes evaporative light scattering detection [1], pulsed amperometric detection [2], pre-column- [3] and post-column [4] derivatization, chemically modified electrodes for direct oxidation at constant potential [5], and the use of immobilized enzyme reactors [6].

Correspondence to: P.C. Maes, Chemistry Department, University of Antwerp RUCA, Groenenborgerlaan 171, B-2020 Antwerp (Belgium).

Enzyme reactors have been described [6–14] which convert carbohydrates, eluting from an LC column into more easily detectable products. Mostly, glucose oxidase and glucose dehydrogenase have been immobilized for the post-column detection of carbohydrates. Glucose oxidase is known for its high selectivity for β-D-glucose, and was therefore applied only for the detection of glucose containing saccharides. The only other oxidase which has been used in analytical enzyme reactors was galactose oxidase [13] (determination of galactose, melibiose, raffinose and stachyose), and recently pyranose oxidase [15]. Dehydrogenases such as glucose dehydrogenase show a broad selectivity range and therefore can be used to detect several different monosaccharides, as was demonstrated by Marko-Varga et al. [16]. The system developed by these authors was

SSDI 0003-2670(93)E0489-T

capable of detecting D-cellobiose, D-glucose, D-xylose, D-galactose, L-arabinose, D-mannose and D-xylulose. Other dehydrogenases used in enzyme reactors include fructose dehydrogenase [17] (determination of D-fructose), sorbitol dehydrogenase [18] (determination of D-fructose, L-sorbose, D-xylose, L-xylose, D-sucrose) and mannitol dehydrogenase [19] (determination of D-fructose). Reactors with immobilized dehydrogenases require post-column addition of NAD^+as the electron acceptor, producing the reduced form NADH, which can than be detected by UV absorbance or by amperometric methods [20]. Immobilized oxidases do not require this post-column addition since oxygen, which is present in the eluent, acts as the electron acceptor. The hydrogen peroxide formed can be detected amperometrically [6], or fluorimetrically [21]. Working with oxidases is thus more economical, but for chromatographic applications there is the disadvantage of the high selectivity of these enzymes. Except for the readily available glucose and galactose oxidases, no investigations have been performed on the use of immobilized oxidases for the detection of carbohydrates after chromatographic separation.

In a former paper of our laboratory on the subject [6], β-glucans were detected after LC separation by the use of immobilized cellulase (splitting the oligosaccharides to monosaccharides), and glucose oxidase (producing hydrogen peroxide from the monomers). The same technique could be useful for the detection of more complex types of oligosaccharides which contain several different monosaccharides. Besides efficient hydrolytic enzymes, non-selective oxidative enzymes are needed for the post-column detection of this type of products. It is the aim of this paper to investigate the use of a less readily available "hexose oxidase" in enzyme reactors for this purpose, as such oxidases are claimed to be less selective.

In our search for a less selective oxidase, capable of oxidizing several different saccharides, our attention was attracted to a series of papers which reported on a "hexose oxidase". In 1956, Bean and Hassid [22] published a paper in which they described an extract from the red sea-weed *Iridophycus flaccidum*, which consumed oxygen when several different mono- and disaccharides were added. A similar enzyme capable of oxidizing several saccharides was found in the juice vesicles of young citrus fruits by Bean et al. [23]. Later, Sullivan and Ikawa [24,25] reported on a hexose oxidase extracted from the red sea-weed *Chondrus crispus*. As the latter sea-weed was readily available to us, we purified this relatively unknown hexose oxidase, and immobilized it in a reactor. The properties of this reactor for carbohydrate detection in chromatographic applications are compared with the properties of an immobilized glucose oxidase reactor with very high enzyme loading in this respect.

EXPERIMENTAL

Purification of the enzyme

The purification is based on the procedure of Sullivan and Ikawa [24]. Most steps were performed at 4°C. A 0.1 M sodium phosphate buffer of pH 6.8 was used during all purification steps.

Chondrus crispus was collected in March and April at the intertidal zone at the shore of Wimereux, France. Freshly collected sea-weed was rinsed with cold water and stored at −18°C. 400 g sea-weed were ground with a mixer in 1 l buffer solution. The mixture was regularly shaken over a period of two days and filtered through cheese cloth. The filtrate was centrifuged at 20 000 *g* for 30 min. The supernatant was shaken with an equal volume of *n*-butanol and centrifuged at 10 000 *g* for 30 min. To every 100 ml of the aqueous phase, 45 g of ammonium sulphate were slowly added, the solution was stirred for several hours, and centrifuged at 12 000 *g* for 20 min. The pellets were redissolved in a minimum of 0.01 M phosphate buffer of pH 6.8 and dialyzed against distilled water during 3 days. The retentate was centrifuged at 10 000 *g* for 10 min. Sodium phosphate solution of pH 6.8 was added to the supernatant in order to make the solution 0.1 M. A glass column of 120 × 15 mm i.d. was packed with Whatman DE-52 ion exchange cellulose and equilibrated with buffer solution. The buffered supernatant was poured onto the column which was rinsed with 500 ml buffer. The

enzyme was eluted from the column using the buffer solution containing 0.3 M NaCl. Fractions of 3–4 ml were collected and active fractions were pooled and concentrated to a final volume of 2 ml using ultrafiltration membrane cones (Centriflo CF 50A, Amicon, Lexington, MA). A column of 650 × 30 mm was packed with Sephadex G-200 superfine (Pharmacia, Uppsala) and the concentrated sample was placed on the column. The column was eluted with buffer solution, and 3-ml fractions were collected. Active fractions were pooled and concentrated using the membrane cones. Fast protein liquid chromatography (FPLC) was performed on a FPLC System (Pharmacia) using a MonoQ HR 5/5 column (50 × 5 mm, Pharmacia). A gradient was applied starting from pure buffer to 1 M NaCl in 20 min. Active fractions were pooled and concentrated using membrane cones to a final volume of 4 ml. 15 injections of 1 ml were performed to purify an extract from 2 kg of sea-weed as starting material.

Assay for activity

200 μl of a sample were mixed with 100 μl *o*-dianisidine (Merck) solution (30 mg/ml), 1.6 ml 0.1 M glucose (Merck) solution and 100 μl peroxidase (Serva, Heidelberg) solution (1 mg/ml). After 15 min, the absorbance was read at 420 nm. 1 unit (U) was defined arbitrarily as the amount of enzyme which catalyses the formation of 1 μmole H_2O_2 per minute at room temperature, at a pH of 6.8 and at a glucose concentration of 0.08 M. Protein was determined according to Lowry using bovine serum albumin (BSA) as a standard.

Preparation of enzyme reactors

150 mg of aminopropylglass (50 nm pore size, 200–400 mesh, Sigma, St. Louis, MO) were added to 3 ml of a 2.5% glutaraldehyde (grade I, Sigma) solution of pH 7 (sodium phosphate buffer). After standing at reduced pressure for 90 min, the activated glass beads were filtered and carefully rinsed with water. 5 ml of an enzyme preparation were added to these glass beads, and immobilization took place at 4°C at reduced pressure (15 Torr). After one night, the immobilized enzyme beads were slurry packed into 50 × 2.1 mm i.d. stainless-steel columns.

LC and flow injection

The experimental setup for flow-injection analysis (FIA) consisted of a Waters M 6000 (Waters, Milford, MA) pump equipped with a Valco EC10U injector (VICI, Houston, TX). 0.1 M sodium phosphate solution of pH 4.6 was used as the eluent. Since O_2 must be present as a cosubstrate, the eluent should not be thoroughly degassed. The amperometric detector consisted of a laboratory-made large-volume wall-jet electrochemical cell controlled by a three-electrode potentiostat [26]. The working electrode was a 3 mm diameter platinum disc, operated at +750 mV vs. a saturated calomel electrode (SCE). For LC analysis of carbohydrates, a Varian 5000 liquid chromatograph (Varian, Palo Alto, CA) was used in combination with a Bio-Rad Aminex HPX 87P column (Bio-Rad, Richmond, CA), operated at 85°C, and eluted with water at 0.4 ml min^{-1}. Between the column and the enzyme reactor, 0.2 M sodium phosphate was added at 0.1 ml min^{-1} through a mixing tee, with a Waters M 6000 pump. Chromatograms were recorded with a SP4100 computing integrator (Spectra-Physics).

Reagents

D-Glucose and D-lactose were from Merck (Darmstadt), D-mannose, *N*-acetyl-D-glucosamine, *N*-acetyl-D-galactosamine, D-glucuronic acid lactone, D-maltose, D-isomaltose, D-gentiobiose, D-maltotriose, pepsin and trypsin were from Sigma (St. Louis, MO), D-galactose, D-fructose, D-xylose, D-arabinose, L-arabinose, D-lyxose, L-rhamnose, L-sorbose, D-cellobiose and D-melibiose were from Nutritional Chemical (Cleveland, OH). Glucose oxidase (ex. *Aspergillus niger*, 200 U/mg) was from Serva (Heidelberg). Moisture contents of all carbohydrates were monitored by thermogravimetry with Dupont analyzers 951 and R90. For quantitations, concentrations were corrected accordingly.

RESULTS AND DISCUSSION

Purification and immobilization of hexose oxidase

The different purification steps, and the obtained activities are shown in Table 1. The purification procedure was comparable to the one published by Sullivan and Ikawa [24], except for the pepsin/trypsin treatment after DEAE chromatography. These authors used this treatment in order to remove the chromoprotein phycoerythrin, which co-elutes with the hexose oxidase in the next purification step [gel permeation chromatography (GPC)]. The pepsin/trypsin treatment was omitted, as in our hands it removed over 90% of the hexose oxidase activity. Instead, we separated phycoerythrin and hexose oxidase on Sephadex G-200 superfine as shown in Fig. 1. 5 U of activity were obtained at this stage, starting from 1 kg of crude sea-weed. An additional FPLC purification step was applied.

During the entire course of the purification, the activity and protein content were monitored. The ability to use partially purified extracts for the preparation of enzyme reactors was evaluated. After each purification step, 5-ml aliquots were taken from the partially purified extract and immobilized onto activated carrier beads as described in the Experimental section. Before and after immobilization, the protein content and the activity of the samples was measured, and the amount of immobilized protein and enzyme activity were calculated. For a rapid evaluation of the resulting reactor, the detection limit was determined for mannose.

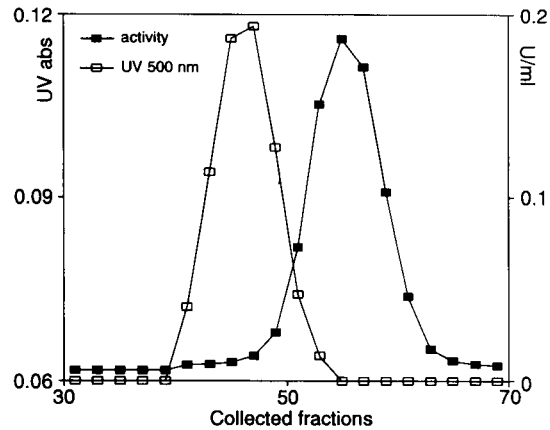

Fig. 1. Separation of phycoerythrin (□) and hexose oxidase (■) on Sephadex G-200 superfine.

As can be concluded from the detection limits given in Table 1, enzyme reactors prepared from partially purified extracts do not allow sensitive determinations. On the other hand, FPLC did not substantially improve the reactor, indicating that the enzyme is already relatively pure after the GPC step. Useful reactors were therefore obtained after the GPC step. Unless otherwise specified, the enzyme reactors used in this study were prepared from enzyme preparations purified by FPLC. Typically, 2 kg of sea-weed were extracted and purified to make one enzyme reac-

TABLE 1

Purification stages and detection limit for mannose obtained with enzyme reactors prepared after immobilization of 5 ml aliquots taken from the indicated purification stage on 150 mg controlled pore glass as described in the Experimental section (Detection limit determined as signal = $10\sigma_{noise}$ using 0.1 M sodium phosphate solution of pH 6.8 at 1 ml min^{-1} in a FIA setup)

Stage of purification	Specific activity (U/mg protein)	Amount of immobilized protein (mg)	Amount of immobilized activity (U)	Detection limit for mannose (μg)
Buffer extract	0.01	6.2	0.1	3.6
n-BuOH	0.01	6.4	0.1	3.6
$(NH_4)_2SO_4$	0.25	1.6	0.38	3.6
DEAE-cellulose	0.42	2.9	0.84	1.8
GPC	–	–	9	0.5
FPLC	–	–	9	0.5

tor. This yielded purified extracts containing 10 activity units, which were immobilized.

Comparison of the immobilized hexose oxidase reactor with an immobilized glucose oxidase reactor

Glucose oxidase is readily available, and it is possible to make a reactor with a large overcapacity for efficient conversion of glucose. In such circumstances, the reactor becomes less selective, and can be used for the detection of monosaccharides other than glucose. It is therefore interesting to compare the glucose oxidase reactor in this respect to a hexose oxidase reactor, as the latter enzyme is much less abundant and extraction is quite labour-intensive.

Both enzymes produce hydrogen peroxide when the appropriate substrates are added. The redox processes at glucose oxidase involve two molecules of FAD (flavin adenine dinucleotide) coenzyme, while hexose oxidase is a copper containing enzyme (12 atoms of copper per mole of enzyme). The molecular masses of both enzymes are comparable, being 150 000 for glucose oxidase and 130 000 for hexose oxidase. Both glucose oxidase and hexose oxidase have a broad pH working range in solution, from 4 to 7 with maxima of 5.5 and 6.8 respectively. The pH dependence of the immobilized hexose oxidase was evaluated by injecting glucose, galactose and mannose solutions using appropriate phosphate buffers as the eluent. Maximum conversion efficiencies were obtained at pH 5.5 (conversion efficiency differences less than a factor 1.8 over the entire range). Immobilized glucose oxidase also shows a broad pH working range with a slight maximum at pH 4.5 [27]. 200 U of glucose oxidase were immobilized in the glucose oxidase reactor (a large overcapacity for efficient conversion of glucose in the experimental conditions), versus 10 U for the hexose oxidase reactor.

The conversion efficiencies obtained with the immobilized enzyme reactors were measured for several mono- and disaccharides. Conversion efficiencies were determined by measuring the amount of hydrogen peroxide produced by the reactors, relative to the amount of hydrogen peroxide that could theoretically be produced at 100% conversion. These measurements were performed in a FIA setup by injecting known concentrations of carbohydrates with standard additions of hydrogen peroxide (at least 5 injections for each measurement). In Table 2, the conversion efficiencies, measured at a flow-rate of 0.2 ml min^{-1} and 50 mm reactor length, are given for 12 mono- and disaccharides. The conversion efficiencies obtained with the immobilized enzyme reactors are compared to the relative rates of substrate conversion by the enzymes in solution.

TABLE 2

Conversion efficiencies X for some saccharides on a hexose oxidase and on a glucose oxidase reactor of 50×2.1 mm i.d. at a flow-rate of 0.2 ml min^{-1} compared to the relative rates of the enzymes in solution according to [24] for hexose oxidase and to Refs. 28 and 29 for glucose oxidase (– = no data)

	Fract. conv. X by immobilized hexose oxidase	Relative rates soluble hexose oxidase	Fract. conv. X by immobilized glucose oxidase	Relative rates soluble glucose oxidase
D-Glucose	75	100	60	100
D-Galactose	79	82	3.3	0.5
D-Mannose	0.4	8	14	1
D-Xylose	0.4	1	2.8	1
L-Arabinose	1.1	–	0.03	–
Maltose	27	40	–	–
Cellobiose	18	32	0.26	–
Lactose	11	22	0.01	–
Isomaltose	0.2	–	0.22	–
Gentiobiose	0.7	–	1.8	–
Melibiose	0.04	–	0.5	–
Maltotriose	4.7	–	–	–

The following products were also tested, but gave no response (conversion efficiency less than 0.01%): L-fucose, D-fructose, D-lyxose, D-arabinose, L-sorbose, *N*-acetyl-D-glucosamine, *N*-acetyl-D-galactosamine and D-glucuronic acid lactone.

Glucose oxidase is highly selective for the β-anomer of glucose. The experimentally found maximum conversion efficiency for glucose on the glucose oxidase reactor is 60%, which corresponds within the experimental error to the percentage of the β-anomeric form present in aqueous solution at 25°C. From Table 2, it is clear that the hexose oxidase reactor is less selective for the anomeric form of the sugar: glucose is converted at a higher efficiency (75%) than would be expected on the basis of β-anomer conversion alone. This suggests that either the enzyme is capable of α-anomer oxidation at a higher rate compared to glucose oxidase, or that the reactor contains some mutarotase activity. The selectivities (relative conversion efficiencies) shown by the hexose oxidase reactor are relatively well correlated to the selectivity of this enzyme in solution (relative rates). This is not the case for the glucose oxidase reactor, where relatively high conversion efficiencies are obtained for sugars such as D-galactose, D-mannose and D-xylose, and to a smaller extent for D-cellobiose, D-isomaltose and D-gentiobiose. The relation between the relative rate of reaction catalyzed by an enzyme in solution K_{ps}, and the relative conversion efficiency (X) obtained with the immobilized enzyme reactor is not straightforward. The relation between X obtained with an enzyme reactor, and the apparent pseudo first-order rate constant $K_{ps}^{(app)}$ is given by

$$X = 1 - e^{-K_{ps}^{(app)}\tau} \quad (1)$$

where τ is the residence time of the substance in the reactor. This expression describes product formation as a function of time in an enzyme reactor. It is comparable to the expression for product buildup as a function of time for an enzyme reaction in solution which is first-order in the substrate concentration (low substrate to enzyme ratio). For solution kinetics, $K_{ps}^{(app)}$ has to be replaced by K_{ps} in this equation. Using Eqn. 1, we can predict the selectivity of a reactor towards different substrates, if we know the $K_{ps}^{(app)}$ values. Usually, however, only K_{ps} values (rate constants for reaction in solution) will be found in the literature. We can make some simplifications, and assume that there is a relation between the rate constant of the reaction in solution (K_{ps}) and of the reaction in the enzyme reactor ($K_{ps}^{(app)}$). In such a case, good estimates of reaction conversion efficiencies could be obtained by inserting K_{ps} values into Eqn. 1. Equation 1 is graphically represented in Fig. 2a, for two different substances, having $K_{ps}^{(app)}$ values which differ by a factor 10. It is clear from this figure, that if we use the enzyme reactor in conditions indicated by the shaded zone (high residence times τ), the conversion efficiencies will differ much less than the $K_{ps}^{(app)}$ values. In the limit, even for products with very small $K_{ps}^{(app)}$ values, nearly 100% con-

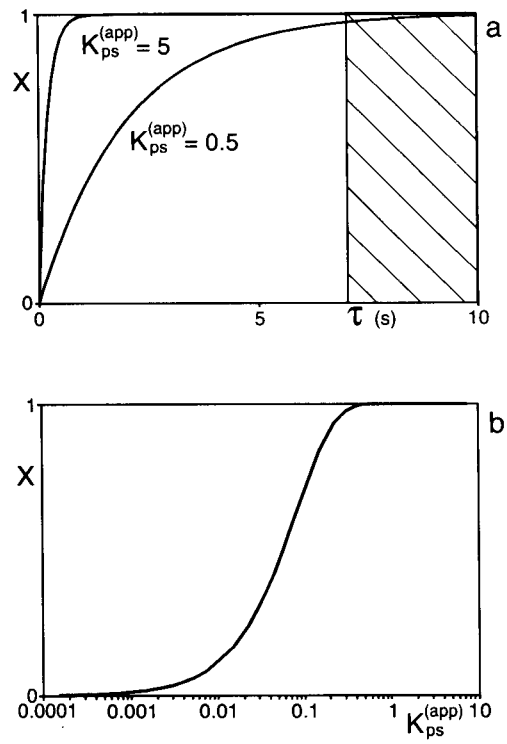

Fig. 2. Graphical representation of Eqn. 1. (a) The dependence of conversion efficiency X on residence time τ for two apparent pseudo first order rate constants $K_{ps}^{(app)}$. (b) The effect of $K_{ps}^{(app)}$ on conversion efficiency X at a given residence time τ (12 s).

version efficiencies will be obtained. A plot of conversion efficiency as a function of $K_{ps}^{(app)}$ values is given by Fig. 2b for an enzyme reactor of 50×2.1 mm i.d. and a residence time of 12 s (experimentally found at 1 ml min^{-1}). From this figure, one can deduce that for differences in $K_{ps}^{(app)}$ varying from 10 to 0.1, the conversion efficiency decreases from 100 to 70% only. When the relative rate constants differ by a factor 100 for an enzyme in solution, the enzyme can be called selective for the substrate having the higher rate constant. However, if the rate constants for the reactions in the enzyme reactor differ by a factor 100 ($K_{ps}^{(app)}$ values usually are between 0.1 and 10), the resulting selectivity will be less pronounced (100% vs. 70% conversion efficiency). Therefore, it is possible to produce efficient enzyme reactors which catalyse reactions having relatively small $K_{ps}^{(app)}$ values.

The above model explains the data given in Table 2. The glucose oxidase reactor has a large overcapacity for the conversion of glucose (high $K_{ps}^{(app)} \times \tau$ values in the experimental conditions used). For some saccharides having small $K_{ps}^{(app)}$ values, the residence times are large enough to obtain relatively high conversion efficiencies. This means that it is very well possible to use even relatively specific oxidases (large differences in K_{ps} values) to construct enzyme reactors with a broader specificity range (small differences in conversion efficiency). The hexose oxidase reactor has relatively small $K_{ps}^{(app)}$ values for all injected saccharides. In the latter reactor, conversion efficiencies are therefore a better reflection of $K_{ps}^{(app)}$ or K_{ps} rate constants. In this case, it is difficult to decrease the reactor selectivity by using a higher loading of enzyme activity, unless more abundant sources of the enzyme can be found. As a result, the specific glucose oxidase yields a reactor which is as broad in selectivity as the reactor obtained from the much less selective hexose oxidase. The validity of the applied model will be tested further by observation of the flow-rate (residence time) versus conversion efficiency behaviour of both reactors.

Figure 3a shows the conversion efficiencies of glucose on a glucose oxidase reactor, and on a hexose oxidase reactor as a function of the flow-

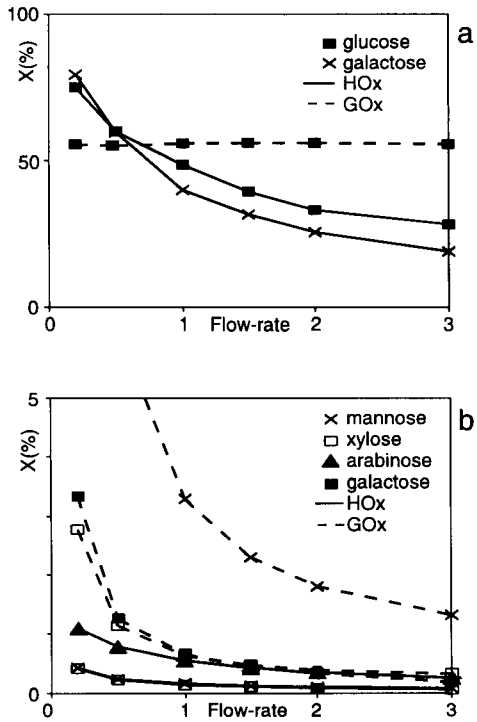

Fig. 3. Conversion efficiency X for some monosaccharides at different flow-rates F on a hexose oxidase and on a glucose oxidase reactor (50×2.1 mm i.d.).

rate. The glucose oxidase reactor efficiently oxidizes glucose throughout the whole flow-rate region (high $K_{ps}^{(app)} \times \tau$ case described above). The efficiency of the hexose oxidase reactor on the other hand, is steadily decreasing at increasing flow-rates, as well for glucose as for galactose (a case of a small $K_{ps}^{(app)}$ value compared to the residence time). This means that the first reactor has a large overcapacity for the oxidation of glucose at the flow-rates used, whereas the second has not. This is confirmed by calculations of half-length values (the reactor length needed to convert 50% of the substrate: see [6]) for the oxidation of glucose on both reactors: values of 3.8 mm for the glucose oxidase and 25 mm for the hexose oxidase reactor are obtained respectively, at a flow-rate of 1 ml min^{-1}.

Both reactors show flow-rate dependent conversion efficiencies for the less readily oxidized substrates (see Fig. 3b). From this figure, it is clear that the efficiency of the glucose oxidase

reactor is much more affected by changes in flow-rate than the efficiency of the hexose oxidase reactor. The dependency of enzyme reactor efficiency on flow-rate changes was derived by Johansson et al. [30]. These authors used Eqn. 2 to describe the dependence of $K_{ps}^{(app)}$ on reaction kinetics (K_{ps}) related and on diffusion related phenomena for packed bed reactors:

$$\left(K_{ps}^{(app)}\right)^{-1} = d_p^{3/2} B^{-1} F^{-1/2} + \left(K_{ps}\right)^{-1} \quad (2)$$

where d_p is the mean particle size, B is a constant (depending on the external void fraction, diffusion coefficient and kinematic viscosity) and K_{ps} is the pseudo first-order rate constant, without diffusional limitations and therefore directly correlated to kinetic parameters. The apparent pseudo first-order rate constant $K_{ps}^{(app)}$ is dependent on two important phenomena, i.e., reaction kinetics and mass transfer (it is therefore called an "apparent" rate constant). Substitution of Eqn. 1 into Eqn. 2 gives:

$$-\ln(1-X) = \left(d_p^{3/2} B^{-1} V^{-1} F^{-1/2} + K_{ps}^{-1} V^{-1} F\right)^{-1} \quad (3)$$

where V is the volume of the reactor. Using this equation, two extreme cases can be visualized. When the first term on the right hand side becomes dominant, the second term can be ignored and we have:

$$-\ln(1-X) = d_p^{-3/2} B V F^{-1/2} \quad (4)$$

This equation contains only parameters which are related to diffusional processes, and an enzyme reactor which is described by this equation is therefore said to be under diffusion control, which means that diffusion phenomena are rate determining. Plots of $\ln(1-X)$ against $F^{-1/2}$ will give linear graphs in this case. On the other hand, when the first term of the right hand side of Eqn. 3 can be ignored, we have:

$$-\ln(1-X) = K_{ps} V F^{-1} \quad (5)$$

In this case, the equation is dependent on kinetic parameters only, and the enzyme reactor is said to be under kinetic control. In the latter case, diffusion of a substrate to the immobilized enzyme is much faster than the rate of substrate conversion. Plots of $\ln(1-X)$ against F^{-1} will give linear graphs. In between these two extreme cases, there will be a mixed behaviour of the reactor.

The data from Fig. 3a and b were transformed into $-\ln(1-X)$ against F^{-1} or $F^{-1/2}$ plots, to see whether diffusion-controlled or kinetically controlled behaviour is predominant. The data from the glucose oxidase reactor showed a linear variation of $-\ln(1-X)$ versus F^{-1} (kinetic control), while the data from the hexose oxidase reactor showed linear $-\ln(1-X)$ versus $F^{-1/2}$ plots (diffusion control). It is not yet clear why the two reactors show different behaviour in this respect. It is important to know however, that the flow-rate dependence of the conversion efficiencies is exponential for the glucose oxidase reactor, and less pronounced for the hexose oxidase reactor. In practice, diminishing the flow-rate from 0.5 ml min^{-1} to 0.2 ml min^{-1} increased the conversion efficiencies by 92% and by 65% for the glucose oxidase reactor and for the hexose oxidase reactor respectively (mean values for the carbohydrates given in Table 2 results not shown). For the electrochemical detector, the limiting current (signal response) increases with the 3/4 power of the flow-rate (wall-jet detector: see [31]). Efficiency of enzyme reactors, and signal response of electrochemical detectors therefore have inverse relationships to flow-rate. In our experience, it is most practical to choose an optimum flow-rate for the chromatography/electrochemical detection system first and to adjust the enzyme reactor dimensions afterwards to provide a good compromise between conversion efficiency and peak broadening. The limits of detection and upper linear response levels obtained with the hexose oxidase and glucose oxidase reactors of 50 × 2.1 mm i.d. in FIA at 0.5 ml min^{-1} are given in Table 3.

Chromatographic application of the reactors

The enzyme reactors were evaluated for the post-column detection of carbohydrates in a chromatographic setup. A cation exchange column in the Pb^{2+} form was chosen for combined use with the enzyme reactors since it gives good results for monosaccharide separation with aqueous solu-

TABLE 3

Detection limits (signal = $5\sigma_{noise}$) and upper limit of linear response in FIA for some carbohydrates on hexose oxidase (HOx) and glucose oxidase (GOx) reactors of 50×2.1 mm i.d. (Conditions: injection volume 10 μl, flow-rate 0.5 ml min^{-1})

	Detection limit (ng)		Upper linearity limit (μg)	
	HOx	GOx	HOx	GOx
Glucose	2	2	2	2
Galactose	2	150	2	200
Mannose	500	20	200	20
Xylose	800	150	200	200
Maltose	40	–	40	–
Cellobiose	40	500	40	200
Lactose	40	20 000	40	200

tions. This column requires elution with pure water, since addition of salts will cause precipitation of the Pb^{2+}. Therefore, 0.2 M sodium phosphate was added between the column and the reactor with a second pump, since both the enzyme reactor and the electrochemical detector require salt solutions for proper functioning. A final flow-rate of 0.5 ml min^{-1} was used (0.4 ml min^{-1} water + 0.1 ml min^{-1} phosphate), as a compromise between optimum number of plates for the cation exchange column, conversion efficiency for the enzyme reactors, and signal-to-noise ratio for the electrochemical detector.

Figure 4 shows chromatograms obtained using this column in combination with the enzyme reactors. The same mixture of carbohydrates, containing cellobiose, maltose, glucose, xylose, galactose and mannose, was injected in all cases. As can be expected from the data in Table 2, the hexose oxidase reactor was most sensitive for glucose and galactose, the disaccharides cellobiose and maltose were also well detected, xylose and mannose were more difficult to detect (Fig. 4a). The disaccharide lactose was detected at a similar sensitivity as the other disaccharides. Since it had a similar retention time to maltose, it was omitted from the test mixture. As mentioned above, the glucose oxidase reactor showed less selectivity than would be expected on the basis of relative reaction rates of the enzyme in solution (Fig. 4b). Besides the sensitive determination of glucose, the saccharides mannose, cellobiose and xylose were also readily detected (lactose was not detected). All carbohydrates from the test mixture were detected when both reactors were placed in series (see Fig. 4c). The reactors were used for

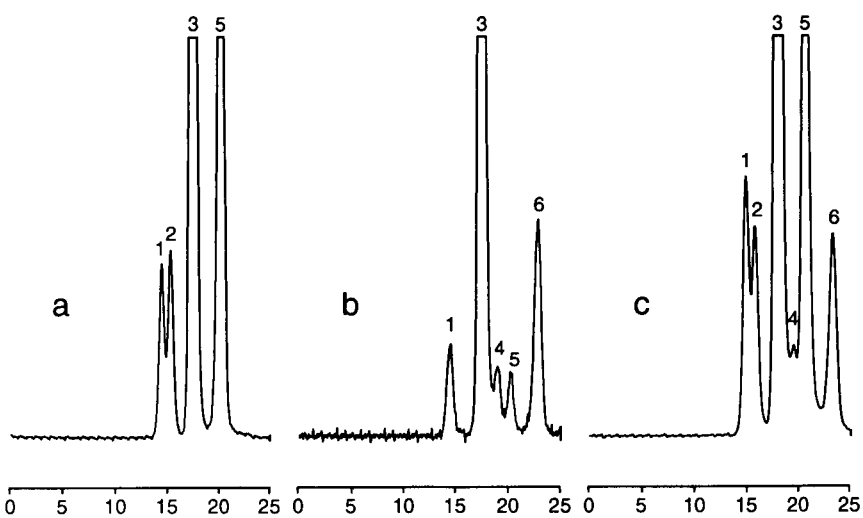

Fig. 4. Chromatograms of a carbohydrate mixture on an Aminex HPX87P column using enzyme reactor detection. (a) Hexose oxidase reactor (50 × 2.1 mm i.d.), (b) glucose oxidase reactor reactor (50 × 2.1 mm i.d.), (c) hexose oxidase and glucose oxidase reactors placed in series. Sample: 100 μl mixture containing cellobiose (1), maltose (2), glucose (3), xylose (4), galactose (5) and mannose (6), all 10^{-3} M; mobile phase: water at 0.4 ml min^{-1} + 0.2 M sodium phosphate pH 4.6 at 0.1 ml min^{-1} added between column and enzyme reactor; amperometric detection of H_2O_2 on Pt at 750 mV vs. SCE.

more than one year in our laboratory, with no signs of diminishing performance. The use of enzyme reactors proved very practical and reliable. They therefore are an interesting alternative or complement to other carbohydrate detectors. In view of the results obtained with the immobilized glucose oxidase reactor, it would be interesting to evaluate other readily available oxidases for use in a carbohydrate detector with relatively broad specificity. From inspection of relative rates of reaction in solution, galactose oxidase seems promising in this regard, as well as pyranose oxidase, an enzyme which recently was found to achieve an even better conversion efficiency for glucose than immobilized glucose oxidase [32]. The availability of other oxidases for carbohydrates, however, is still problematic. The synthesis of new efficient enzyme reactors in this field therefore depends on progress made in the isolation of new oxidases.

Conclusions

In combination with an electrochemical detector, an immobilized hexose oxidase reactor provides a stable and sensitive means for detecting several mono- and disaccharides in FIA and chromatographic systems. Analogous results can be obtained with a glucose oxidase reactor in conditions where the reactor length largely exceeds the minimum requirements for efficient conversion of glucose. Future work of our laboratory will be directed towards the use of other oxidases for the construction of reactors with relatively broad selectivity towards carbohydrates.

REFERENCES

1 A. Clement, D. Yong and C. Brechet, J. Liq. Chromatogr., 15 (1992) 805.
2 D.C. Johnson and W.R. LaCourse, Electroanalysis, 4 (1992) 367.
3 N.O. Maness, E.T. Miranda and A.J. Mort, J. Chromatogr., 587 (1991) 177.
4 U.A.Th. Brinkman, R.W. Frei and H. Lingeman, J. Chromatogr., 492 (1989) 251.
5 S.V. Prabhu and R.P. Baldwin, J. Chromatogr., 503 (1990) 227.
6 P.C. Maes, L.J. Nagels, C. Dewaele and F.C. Alderweireldt, J. Chromatogr., 558 (1991) 343.
7 G. Marko-Varga, E. Dominguez, B. Hahn-Hägerdal and L. Gorton, J. Chromatogr., 506 (1990) 423.
8 G. Marko-Varga, E. Dominguez, B. Hahn-Hägerdal, L. Gorton, H. Irth, G.J. De Jong, R.W. Frei and U.A. Th. Brinkman, J. Chromatogr., 523 (1990) 173.
9 J. Emnéus and L. Gorton, Anal. Chim. Acta, 234 (1990) 97.
10 G. Marko-Varga, Anal. Chem., 61 (1989) 831.
11 G. Marko-Varga, J. Chromatogr., 408 (1987) 157.
12 R. Mögele, B. Pabel and R. Galensa, J. Chromatogr., 591 (1992) 165.
13 N. Kiba, K. Shitara and M. Furusawa, J. Chromatogr., 463 (1989) 183.
14 F. Ortega, Anal. Chim. Acta, 257 (1992) 79.
15 N. Kiba, F. Ueda, K. Saegusa, Y. Goto, M. Furusawa and T. Yamane, Anal. Chim. Acta, 271 (1993) 47.
16 G. Marko-Varga, E. Dominguez, B. Hahn-Hägerdahl and L. Gorton, J. Chromatogr., 506 (1990) 423.
17 K. Matsumoto, O. Hamada, H. Ukeda and Y. Osajima, Anal. Chem., 58 (1986) 2732.
18 N. Kiba, R. Matsushita and M. Furusawa, Anal. Chim. Acta, 259 (1992) 15.
19 N. Kiba, Y. Inoue and M. Furusawa, Anal. Chim. Acta, 243 (1991) 183.
20 L. Gorton, J. Chem. Soc., Faraday Trans. 1, 82 (1986) 1245.
21 C.A. (Koerner) Swindlehurst and T.A. Nieman, Anal. Chim. Acta, 205 (1988) 195.
22 R.C. Bean and W.Z. Hassid, J. Biol. Chem., 218 (1956) 425.
23 R.C. Bean, G.G. Porter and B.M. Steinberg, J. Biol. Chem., 236 (1961) 1235.
24 J.D. Sullivan and M. Ikawa, Biochim. Biophys. Acta, 309 (1973) 11.
25 M. Ikawa, Methods Enzymol., 89 (1982) 143.
26 L.J. Nagels, J.M. Kauffmann, C. Dewaele and F. Parmentier, Anal. Chim. Acta, 234 (1990) 75.
27 M. Masoom and A. Townshend, Anal. Chim. Acta, 166 (1984) 111.
28 M. Dixon and E.C. Webb, Enzymes, Longmans, London, 1971.
29 J.H. Pazur and K. Kleppe, Biochemistry, 3 (1964) 578.
30 G. Johansson, L. Ögren and B. Olsson, Anal. Chim. Acta, 145 (1983) 71.
31 H. Gunasingham, B.T. Tay, K.P. Ang and L.L. Koh, J. Chromatogr., 285 (1984) 103.
32 M. Tabata, T. Murachi, J. Endo and M. Totani, J. Chromatogr., 597 (1992) 435.

Analytica Chimica Acta, 284 (1993) 291–299
Elsevier Science Publishers B.V., Amsterdam

Application of ion chromatography with indirect spectrophotometric detection to the sensitive determination of alkylphosphonic acids and fosfomycin

G.A. Pianetti and L.M. Moreira de Campos

Laboratoires de Chimie Analytique, Centre d'Études Pharmaceutiques, Université Paris-Sud, 1 Avenue J.B. Clément, F-92290 Châtenay-Malabry (France) and Laboratório de Controle de Qualidade de Produtos Farmacêuticos e Cosméticos, Faculdade de Farmácia da Universidade Federal de Minas Gerais, Belo Horizonte, MG (Brazil)

P. Chaminade, A. Baillet, D. Baylocq-Ferrier and G. Mahuzier

Laboratoires de Chimie Analytique, Centre d'Études Pharmaceutiques, Université Paris-Sud, 1 Avenue J.B. Clément, F-92290 Châtenay-Malabry (France)

(Received 27th April 1993; revised manuscript received 11th August 1993)

Abstract

Indirect spectrophotometric detection was investigated for application in the anion-exchange chromatography of alkylphosphonic acids and fosfomycin. Four chromophoric eluent anions were studied: phthalate, benzoate, phenylphosphonate and *p*-toluenesulphonate. Phthalate showed the best displacing power and the larger dynamic reserve whereas benzoate exhibited the highest absorptivity and transfer ratio. The optimal experimental conditions were found to be 0.4 mM phthalate (pH 8.5) as mobile phase, a flow-rate of 1 ml min^{-1} and a detection wavelength of 272 nm. Selectivity (between 1.02 and 1.85, depending on the pair of vicinal compounds), linearity over a 5–100 μg ml^{-1} concentration range ($r = 0.999$), precision (R.S.D. 0.6–5.3%) and sensitivity (0.4–1.0 μg ml^{-1} according to the phosphonic acid) were determined. The minimum detectable concentrations were improved by an average factor of 50 in comparison with direct non-suppressed conductimetric detection. The application of the technique to the determination of fosfomycin in plasma samples is described.

Keywords: Ion chromatography; Liquid chromatography; Fosfomycin; Phosphonic acids; Plasma

Phosphonic acids are mainly determined by gas or liquid chromatography after derivatization or by ion chromatography. Because these compounds do not absorb or fluoresce, some workers converted them into ester derivatives to allow their separation by gas chromatography [1–4] or to produce fluorescing [5] or UV-absorbing species [6] able to be separated by liquid chromatography. All these methods are time consuming. On the other hand, ion-exchange chromatography is known to provide excellent ion separations, with suppressed conductimetric detection [7] and with non-suppressed conductimetric or spectrophotometric detection [8,9]. Schiff et al. [10] described the determination of phosphonic acids in aqueous and biological samples using direct conductimetric detection with a suppression column.

Recently a rapid method involving anion-ex-

Correspondence to: G.A. Pianetti, Laboratoires de Chimie Analytique, Centre d'Études Pharmaceutiques, Université Paris-Sud, 1 Avenue J.B. Clément, F-92290 Châtenay-Malabry (France)

SSDI 0003-2670(93)E0476-N

change chromatography with direct conductimetric detection [11] was proposed. The separation of a series of homologous alkylphosphonic acids using capillary zone electrophoresis with indirect UV detection has also been reported [12]. Likewise, indirect spectrophotometric detection could be an alternative mode in non-suppressed ion chromatography [13,14]. It provides universal detection of inorganic anions and with the use of low eluent concentrations low limits of detection can be attained. However, the concentration of the mobile phase components cannot be lowered too much without degrading the separation.

The aim of this study was to investigate the applicability of this alternative method of detection coupled with anion-exchange separation. A simple technique was developed for the determination of monophosphonic acids using 0.4 mM potassium phthalate at pH 8.5 as the mobile phase with indirect spectrophotometric detection at 272 nm. The determination of methyl-, ethyl-, propyl- and butylphosphonic acids and fosfomycin in aqueous samples was carried out using phenylphosphonic acid as an internal standard. Detection limits were determined. The technique was then adapted to the determination of fosfomycin in plasma samples. The difficulties encountered and the analytical validation are detailed.

EXPERIMENTAL

Chemicals

Distilled, deionized water was used for liquid chromatography (LC). Methylphosphonic acid (MPA), ethylphosphonic acid (EPA), propylphosphonic acid (PPA), butylphosphonic acid (BPA) and phenylphosphonic acid (FPA) were obtained from Aldrich-Chimie (Strasbourg). The sodium salt of fosfomycin (FOF) was obtained from Clin-Midy (Paris) and sodium phenylphosphonate (SPHP) and potassium benzoate (KBEZ) from Fluka (Mulhouse). Dipotassium phthalate (KPHT) and sodium *p*-toluenesulphonate monohydrate (SPTS) were obtained from Merck (Nogent-sur-Marne). All other chemicals were of analytical-reagent grade.

Instrumentation

LC analyses were carried out using a liquid chromatograph from Touzart et Matignon (Vitry-sur-Seine) consisting of a Shimadzu LC-6A pump, a Shimadzu SPD-6A UV spectrophotometric detector and a Shimadzu CTO-6A oven. This system was connected to a Shimadzu Chromatopac CR-5A integrator which measured the detector response as peak areas. Separations were carried out using a Waters-Millipore (St. Quentin-en-Yvelines) IC-Pak Anion LC column (50×4.6 mm i.d.) with a low anion-exchange capacity (30 ± 3 μeq ml^{-1}).

Chromatographic procedure

For aqueous samples, the optimum conditions were determined for the analytical separation as 0.4 mM potassium phthalate (pH 8.5) as mobile phase, a flow-rate of 1.0 ml min^{-1}, a column temperature of 20°C, indirect UV detection at 272 nm (0.08 absorbance full-scale) and a sample size of 20 μl.

For spiked plasma samples, the mobile phase was 0.4 mM potassium phthalate (pH 9.0), the column temperature and indirect UV detection were as above with 0.04 absorbance full-scale and the sample size was 100 μl.

Optimization step

Standard aqueous solutions (100 μg ml^{-1}) of each alkylphosphonic acid and fosfomycin were injected on to the chromatographic column and their retention times were determined.

Calibration

Calibration graphs were obtained from triplicate injections of known concentrations of the phosphonic acids (5–100 μg ml^{-1}) in aqueous solutions, using the optimum mobile phase.

Spiked plasma sample treatment

To 200-μl plasma samples from healthy volunteers, 200, 100 and 40 μl of a 100 μg ml^{-1} solution of FOF dissolved in methanol were added to obtain the required plasma concentrations of 100, 50 and 20 μg ml^{-1}. The volume was completed to 1.0 ml with methanol to precipitate proteins and the solution was vortex mixed for 2

min. The sample was then centrifuged for 20 min at 6000 *g* at 0°C. The supernatant was collected and dried under nitrogen. The residue was dissolved in 1000 μl of the mobile phase, filtered through a 0.11-μm filter (Millipore) and then injected into the LC system.

RESULTS AND DISCUSSION

Several chromophoric eluent anions for the non-suppressed anion-exchange separation of phosphonates using indirect UV detection were studied: potassium phthalate, potassium benzoate, sodium phenylphosphonate and sodium *p*-toluenesulphonate (Table 1). These four UV-absorbing species were selected taking into account the type and number of acidic functional groups in an attempt to compare the displacing powers of the eluent ions. The structure of these acidic groups usually modifies the sample–eluent ion-exchange constants and gives rise to different selectivities. The charge on the eluent molecules plays an important role in the detection performance when modifying the ion-exchange stoichiometry and analysis time. Only singly and doubly charged eluents were investigated. Multiply charged eluents such as trimesate or pyromellilate were eliminated because of the poor retention obtained. All these eluents possess relatively high molar adsorptivities in the UV region. The effects of the type and concentration of

TABLE 1

Formulae of the alkylphosphonic acids and chromophoric eluent anions tested

Compound	Formula	Mol. wt.	p*K* values	λ_{max} (nm)	ϵ_{max} (l mol^{-1} cm^{-1})	Ref.
Methylphosphonic acid (MPA)	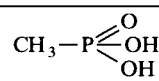	96.02	2.35 7.10	–	–	15
Ethylphosphonic acid (EPA)	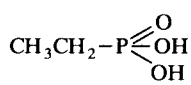	110.05	2.43 8.05	–	–	16
Propylphosphonic acid (PPA)	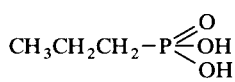	124.08	2.49 8.18	–	–	16
Butylphosphonic acid (BPA)	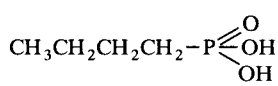	138.10	2.59 8.19	–	–	16
Sodium fosfomycin (FOF)	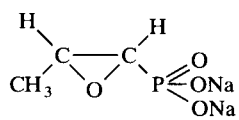	182.02	1.50 6.40	–	–	17
Sodium phenylphosphonate (SPHP)	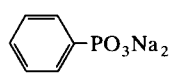	202.06	1.29 6.74	258	231	18
Potassium phthalate (KPHT)	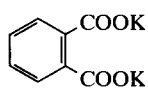	242.32	2.98 5.28	272	821	19
Potassium benzoate (KBEZ)	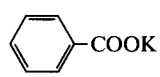	160.22	4.01	268	1634	20
Sodium *p*-toluene sulphonate (SPTS)	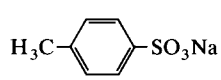	212.20	6.62	261	360	21

chromophoric anion and the wavelength of detection were studied, i.e., the parameters that can affect both the selectivity of separation and the sensitivity of detection. The chromatographic performance of the eluent also requires adjustement of the pH of the mobile phase. As phosphonates are poorly retained in their singly ionized form, the pH was set at 8.5 because at that pH the samples became 74% to 100% doubly ionized.

Anion separation

In a previous study [11], it was observed that the retention of organic anions on low-capacity anion-exchange columns can be attributed to a combination of several phenomena, as the order of elution cannot be explained only as a function of pK_a values or hydrophobicity. The retention times of analyte anions depend on both the type and concentration of the eluent. For a 1 mM concentration of the eluent, the eluting power of phthalate is higher than that of benzoate. This result follows the expected trend of polyvalent ions being stronger displacing species than monovalent ions. Moreover, the displacing power of acidic groups decreased in the order carboxylate > phosphonate > sulphonate (Fig. 1).

The retention times were also measured as a function of the chromophoric eluent anion concentration. When the concentration of the eluent anion decreased, the retention of the analytes increased as expected. Small et al. [7], demonstrated previously that the elution can be described by the expression

$$\log[V_R - V_M] = -(y/x)\log[E^{x-}] + B \qquad (1)$$

where x and y are the charges of the eluent (E) and sample ions, respectively, and B is a constant dependent on the ion-exchange equilibrium constant and the ion-exchange capacity of the stationary phase.

In Table 2, the experimentally observed slopes are compared with the theoretically calculated y/x values. Concurring values were obtained for MPA, FOF and FPA, i.e., the species which have a pK_a far from the pH of the mobile phase. In contrast, larger differences between the experimental and predicted slope values were observed for EPA, PPA and BPA ($pK_a \approx 8$) because of the large variations in the effective y/x values induced by small local pH variations in the mobile phase. pH was then a critical parameter to provide a good prediction of elution. Because of the similar y/x values obtained whatever the alkylphosphonic acid, no changes in elution order could be observed with decreasing phthalate concentration in the mobile phase. The slope values suggest that the optimum selectivity can be ob-

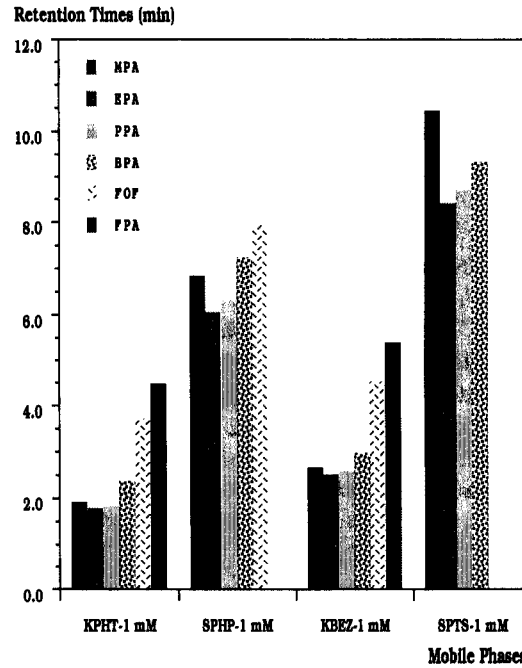

Fig. 1. Retention times of phosphonic acids in various mobile phases at pH 8.5. Elution times longer than 30 min were not determined.

TABLE 2

Comparison between theorical and observed y/x values [a]

Analyte	y/x		Difference (%)
	Calculated	Observed	
MPA	0.98	1.04 ($n = 5$)	5.8
EPA	0.87	1.03 ($n = 5$)	18.4
PPA	0.84	1.04 ($n = 5$)	23.8
BPA	0.83	1.00 ($n = 5$)	20.5
FOF	1.00	0.93 ($n = 9$)	7.0
FPA	1.00	0.94 ($n = 9$)	6.0

[a] Eluent, potassium phthalate (pH 8.5); concentration range, 0.2–2.5 mM; detection wavelength, 272 nm.

TABLE 3

Selectivities per unit time (α/Tr_2) obtained with different concentrations of various chromophoric eluent ions

α/Tr_2 [a]							
KPHT		SPHP		KBEZ		SPTS	
1.0 mM	0.7 mM	2.0 mM	1.0 mM	1.0 mM	0.4 mM	1.4 mM	1.0 mM
PPA/EPA 0.559	PPA/EPA 0.284	PPA/EPA 0.408	PPA/EPA 0.165	PPA/EPA 0.397	PPA/EPA 0.184	PPA/EPA 0.184	PPA/EPA 0.119
MPA/PPA 0.549	MPA/PPA 0.269	MPA/PPA 0.385	MPA/PPA 0.158	MPA/PPA 0.386	MPA/PPA 0.175	MPA/PPA 0.183	BPA/PPA 0.115
BPA/MPA 0.521	BPA/MPA 0.256	BPA/MPA 0.347	BPA/MPA 0.146	BPA/MPA 0.374	BPA/MPA 0.160	BPA/MPA 0.183	MPA/BPA 0.107
FOF/BPA 0.422	FOF/BPA 0.234	FOF/BPA 0.339	FOF/BPA 0.138	FOF/BPA 0.337	– [b]	FOF/MPA 0.182	– [b]
FPA/FOF 0.269	FPA/FOF 0.162	– [b]	– [b]	FPA/FOF 0.221	– [b]	–	– [b]

$\alpha = k'_2/k'_1$, selectivity between two vicinal peaks; Tr_2 = retention time of the more retained compound of the considered pair of eluents. [b] No determined retention times.

tained by increasing the eluent concentration. Indeed, the selectivity or, more accurately, the selectivity per unit time, was improved for all the pairs of compounds with increasing eluent concentration whatever the eluent used (Table 3).

Potassium phthalate was found to offer the best chromatographic performance, i.e., a good separation in a reasonable time. Fig. 2 illustrates the separation of alkylphosphonic acids and fosfomycin with phenylphosphonic acid used as the internal standard.

Sensitivity

In an attempt to study the performance of indirect UV spectrophotometric detection, the

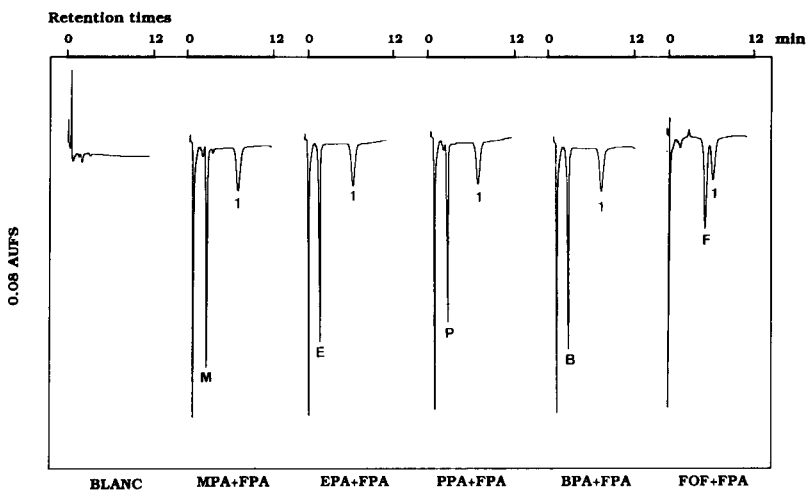

Fig. 2. Typical chromatograms of mixtures of the each alkylphosphonic acid and fosfomycin with phenylphosphonic acid as internal standard with detection at 272 nm (0.08 absorbance full-scale; attenuation = 3). Mobile phase, 0.7 mM potassium phthalate (pH 8.5); solute concentration, 50 μg ml^{-1}; injection volume, 20 μl. Peak identification: $MPA_{(M)} + FPA_{(1)}$, $\alpha = 2.83$; $EPA_{(E)} + FPA_{(1)}$, $\alpha = 3.28$; $PPA_{(P)} + FPA_{(1)}$, $\alpha = 3.21$; $BPA_{(B)} + FPA_{(1)}$, $\alpha = 2.88$; and $FOF_{(F)} + FPA_{(1)}$, $\alpha = 1.19$.

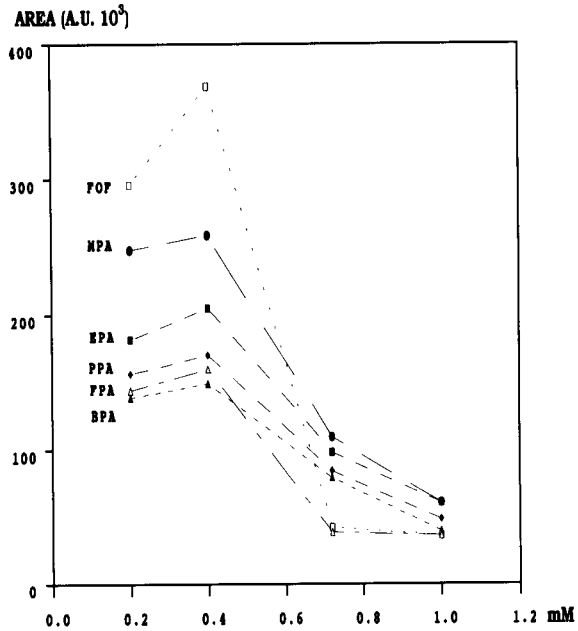

Fig. 3. Plots of peak area as a function of potassium phthalate concentration ($\lambda = 272$ nm). Solute concentration, 100 μg ml^{-1}.

sensitivities obtained when using various chromophoric eluent ions were examined.

Yeung [22] defined the concentration limit of detection, C_{lim}, as a function of the eluent ion concentration, C_m, the dynamic reserve, *DR*, viz., the ability to measure a small change on top of a large background signal, and the transfer ratio, *TR*, i.e., the number of mobile phase molecules exchanged by one analyte molecule:

$$C_{lim} = C_m/(DR \times TR) \quad (2)$$

Accordingly, higher signals were achieved using relatively dilute mobile phase concentrations, C_m. Moreover, the lower is C_m, the larger is the fractional change (larger *DR*) that results for a given analyte concentration. As an example, Fig. 3 shows the increase in area when the potassium phthalate concentration was decreased from 1 to 0.4 mM. However, concentrations less than 0.2 mM were too low to displace sample ions accurately.

The molar absorptivity, ϵ_M, of each chromophoric eluent also plays an important role in determining sensitivities. As expected, a higher *DR* was obtained when the detection wavelength was set at the maximum absorption of the chromophoric eluent.

Finally, the higher was *TR*, the larger became the change per analyte concentration.

Compared with phenylphosphonate [$\epsilon_{M\,(258\ nm)} = 231$; $0.84 < TR < 1$, depending on the analyte], *p*-toluene sulphonate [$\epsilon_{M\,(261\ nm)} = 360$; $1.67 < TR < 2$] and phthalate [$\epsilon_{M\,(272\ nm)} = 821$; $0.83 < TR < 1$], benzoate presented both the highest ϵ_M and *TR* [$\epsilon_{M\,(268\ nm)} = 1634$; $1.67 < TR < 2$] and therefore should have led to a better sensitivity. However, its use is limited by its displacing power, which is less favourable than that of phthalate. In fact, the elution of fosfomycin required a higher concentration when benzoate was used as the eluent anion compared with phthalate. This actually compromised the previous advantage.

Validation of the technique

Taking all these criteria into account, we found potassium phthalate to be the most suitable eluent. Thus, the experimental conditions were set as follows: 0.4 mM potassium phthalate as mobile phase, flow-rate 1 ml min^{-1} and detection wavelength 272 nm. The corresponding retention times were 8.6, 8.0, 8.4, 9.1, 9.6 and 13.2 min for MPA, EPA, PPA, BPA, FOF and FPA, respectively. The technique was validated for the determination of phosphonic compounds in aqueous solutions. The specificity was verified with respect to common anions, particularly chloride ($t_R = 3.4$ min), phosphate ($t_R = 15.5$ min) and sulphate ($t_R = 21.8$ min). The calibration graphs (Fig. 4) indicate a satisfactory linear dependence of area (or height) on the amount of each analyte in the range 5–100 μg ml^{-1}. The correlation coefficients were 0.999 for all the phosphonates injected. The relative standard deviation (R.S.D.) of the response factor range from 0.58 to 5.29% for six runs carried out over three days. Detection limits were calculated for a signal-to-noise ratio of 3 (attenuation = 1), corresponding to concentrations of 0.40, 0.20, 0.45, 1.0 and 0.5 μg ml^{-1} for MPA, EPA, PPA, BPA and FOF, respectively. These limits are improved by an average factor of 50 when compared with conductimetric detection [11].

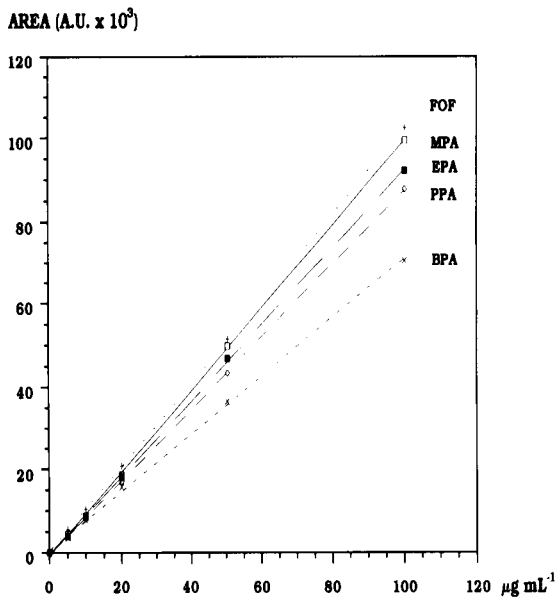

Fig. 4. Calibration graphs obtained for the different phosphonic acids. Mobile phase, 0.4 mM potassium phthalate (pH 8.5); flow-rate, 1 ml min^{-1}; detection wavelength 272 nm.

Application to plasma fosfomycin determination

The method was then applied to a plasma sample spiked at the level of 100 μg ml^{-1}. As explained in a previous paper [11], the yield of fosfomycin extraction with an organic solvent was limited by the high solubility of phosphonates in water. Consequently, the injected samples still contained anionic endogenous compounds, thus setting two problems: first, a large injection peak appeared which prevented the use of the alkylphosphonates as internal standards for the fosfomycin determination; and second, the separation of fosfomycin and phenylphosphonic acid was disturbed by the presence of two unidentified endogenous compounds.

A fivefold dilution of the sample with the mobile phase and the use of an eluent pH of 9.0 (instead of 8.5) solved the first problem, but an overlap was still observed between phenylphosphonic acid and one endogenous compound, thus preventing the use of this analyte as an internal standard.

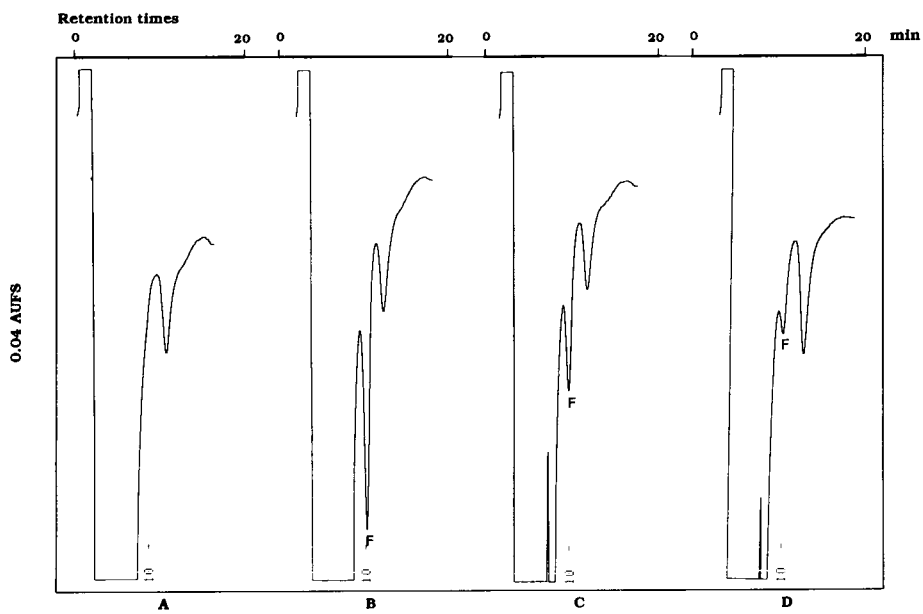

Fig. 5. Typical chromatograms for plasma samples: (A) control human plasma and human plasma spiked with (B) 100, (C) 50 and (D) 20 μg ml^{-1} of a methanolic solution of fosfomycin, both diluted fivefold in the 0.4 mM potassium phthalate mobile phase (pH 9.0). Injection volume, 100 μl; detection wavelength, 272 nm (attenuation = 2).

TABLE 4

Inter- and intra-assay precision for fosfomycin determination in human plasma

Concentration range	Concentration in spiked plasma ($\mu g\ ml^{-1}$)	Concentration found inter-assay ($n = 3$)		Concentration found intra-assay ($n = 4$)	
		Mean ± S.D. ($\mu g\ ml^{-1}$)	R.S.D.	Mean ± S.D. ($\mu g\ ml^{-1}$)	R.S.D.
Low	20	19.13 ± 0.51	2.68	18.60 ± 0.26	1.39
Medium	50	49.27 ± 0.44	0.89	49.57 ± 0.35	0.71
High	100	97.99 ± 0.99	1.01	97.85 ± 0.55	0.56

TABLE 5

Recovery of fosfomycin from human plasma

Concentration range	Concentration in spiked plasma ($\mu g\ ml^{-1}$)	Fosfomycin area		Recovery (%)
		Calibration graph	Sample determination	
Low	20	19600	18600	94.9
Medium	50	49800	49400	99.2
High	100	104700	103000	98.4

A quantitative study with external calibration was then undertaken. Typical chromatograms for spiked human plasma samples are shown in Fig. 5, for FOF plasma concentrations of 0, 100, 50 and 20 $\mu g\ ml^{-1}$. Fosfomycin eluted at ca. 9.62 ± 0.14 min (R.S.D. = 1.47%, $n = 36$) and the endogeneous peak at 12.68 ± 0.20 min (R.S.D. = 1.56%, $n = 36$). The selectivity (α) between these two peaks was 1.37. A calibration graph was obtained by analysis of plasma spiked with fosfomycin in the range 20–100 $\mu g\ ml^{-1}$. The calibration graph was linear up to a concentration (x) of 20 $\mu g\ ml^{-1}$ ($y = -1.0551 + 1.0489x$; $r = 0.993$).

To evaluate the reproducibility of the system and method, inter- and intra-assay precision studies were performed. To evaluate the intra-assay precision of the method, three different samples with high, medium and low concentrations of fosfomycin were chosen and each was injected on to the column four times. The R.S.D. for the four replicate injections for each sample ranged from 0.56 to 1.39%. For inter-assay precision, on three separate occasions different samples with three concentrations were prepared and injected on to the column. The R.S.D. ranged from 0.89 to 2.68% (Table 4). The recovery of fosfomycin in plasma, obtained from the calibration graph for spiked plasma, is shown in Table 5 and ranged from 94.9 to 99.2%.

This investigation was supported by CAPES (Coordenação de Aperfeiçoamento de Pessoal de Nível Superior do Ministério da Educação do Brasil), Brazil, and COFECUB (Comité Français d'Evaluation de la Coopération Universitaire avec le Brésil), France.

REFERENCES

1 M.L. Rueppel, L.A. Suba and J.T. Marvel, Biomed. Mass Spectrom., 3 (1976) 28.
2 C.G. Daughton, A.M. Cook and M. Alexander, Anal. Chem., 51 (1979) 1949.
3 J.Aa. Tornes and B.A. Johnsen, J. Chromatogr., 467 (1989) 129.
4 M.L. Shih, J.R. Smith, J.D. McMonagle, T.W. Dolzine and C. Greshany, Biol. Mass Spectrom., 20 (1991) 717.
5 M.C. Roach, L.W. Ungar, R.N. Zare, L.M. Reimer, D.L. Pompliano and J.W. Frost, Anal. Chem., 59 (1987) 1056.
6 P.C. Bossle, J.J. Martin, E.W. Sarver and H.Z. Sommer, J. Chromatogr., 267 (1983) 209.

7 H. Small, T.S. Stevens and W.C. Bauman, Anal. Chem., 47 (1975) 1801.
8 H. Sato, Anal. Chim. Acta, 206 (1988) 281.
9 S.A. Maki and N.D. Danielson, Anal. Chem., 63 (1991) 699.
10 L.J. Schiff, S.G. Pleva, E.W. Sarver, in J.D. Mulik and E. Sawicki (Eds.), Ion Chromatographic Analysis of Environmental Polluants, Vol. 2, Ann Arbor Sci. Publ., Ann Arbor, 1979, p. 329.
11 G.A. Pianetti, A. Baillet, F. Traoré and G. Mahuzier, Chromatographia, 36 (1993) 263.
12 G.A. Pianetti, M. Taverna, A. Baillet, G. Mahuzier and D. Baylocq-Ferrier, J. Chromatogr., 630 (1993) 371.
13 H. Small and T.E. Miller, Anal. Chem., 54 (1982) 462.
14 H. Small, Anal. Chem., 55 (1983) 235A.
15 A. Rumpf and C. Chavane, Chem. Res., 224 (1947) 919.
16 B. Crofts and K. Kosolapoff, J. Am. Chem. Soc., 75 (1953) 3382.
17 D. Baron and H. Drugeon, Sem. Hôp. Paris, 61 (1985) 2341.
18 O. Mäkitie and V. Konttinen, Acta Chem. Scand., 23 (1969) 1459.
19 W.R. Maxwell and J.R. Partington, Trans Faraday Soc., 31 (1935) 922.
20 M. Yasuda, K. Yamasaki and H. Ohtaki, Bull. Chem. Soc. Jpn., 33 (1960) 1067.
21 Dictionary of Organic Compounds, Vol. 4, Suppl., Chapman and Hall, New York, 5th edn., 1986, p. 3749.
22 E.S. Yeung, Acc. Chem. Res., 22 (1989) 125.

Analytica Chimica Acta, 284 (1993) 301–310
Elsevier Science Publishers B.V., Amsterdam

Ion chromatographic determination of selenite and selenate with selenium-specific detection by flame and graphite furnace atomic absorption spectrometry

Gottfried Kölbl, Kurt Kalcher and Kurt J. Irgolic

Institut für Analytische Chemie, Karl-Franzens-Universität, Universitätsplatz 1, A-8010 Graz (Austria)

(Received 5th May 1993)

Abstract

An ion chromatographic method for the determination of selenite and selenate using both Zeeman-effect graphite furnace atomic absorption spectrometry (GFAAS) and Zeeman-effect flame atomic absorption spectrometry (FAAS) for selenium-specific detection is described. Different mobile phases were investigated (aqueous solutions of potassium hydrogenphthalate (KHP) of various pH and concentration; KHP solutions saturated with nickel hydroxide; aqueous solutions of nickel nitrate or nickel sulphate). The pH dependence of the retention times of selenite and selenate was determined. Interferences by sulphate and sulphite in the determination of selenite and selenate were studied with conventional conductivity and GFAAS detection. The absolute detection limits for liquid chromatography (LC)–GFAAS were found to be 1 ng Se for selenite and 0.6 ng Se for selenate when a 3 mM KHP solution saturated with $Ni(OH)_2$ was used as the mobile phase. LC–FAAS had an absolute detection limit of 8 ng Se for selenite and 11 ng Se for selenate. The LC–FAAS system was used to determine selenite and selenate in different solutions used for selenium supplementation of animals. The results obtained for the selenium compounds agreed with the total selenium determinations.

Keywords: Atomic absorption spectrometry; Ion chromatography; Liquid chromatography; Selenate; Selenite; Selenium

Selenium is an essential nutrient [1] and a sufficient intake of selenium has been reported to reduce the likelihood of heart disease and the occurrence of cancer [2]. Selenium is known to prevent the appearance of toxic effects normally caused by heavy metals such as arsenic and mercury [3]. At higher doses selenium is toxic: diets containing more than 5 mg Se kg^{-1} are considered to be poisonous to man and animals [4]. The difference between the required dose and the toxic dose is small [5]. Toxicity should not be ascribed to "selenium", but to selenium compounds, because different selenium compounds do not all have the same toxicity [6]. In the aqueous environment selenites and selenates are the most common selenium compounds [7], and in biological samples inorganic and organic selenium compounds can be present. Therefore, reliable methods for the determination of selenium compounds at trace levels are required to elucidate the effects of "selenium".

Ion chromatography in the form of liquid chromatography (LC) is a promising method, because it combines a high separating capability with low detection limits (low $\mu g\ l^{-1}$). Several ion chromatographic determinations of selenite and selenate have been reported. Conductivity cells (requiring suppression of the bulk ions in the mobile

Correspondence to: K.J. Irgolic, Institut für Analytische Chemie, Karl-Franzens-Universität, Universitätsplatz 1, A-8010 Graz (Austria).

SSDI 0003-2670(93)E0480-U

phase [8–13] or low-conductivity mobile phases [14–16]), UV absorption spectrometers [17–19] and fluorescence spectrometers [20] have been used as detectors.

The large number of compounds normally present in addition to the analytes in environmental samples and extracts from biological samples may cause interferences. The selenite signal in ion chromatographic assays may be severely affected by carbonate, chloride, phosphate [10] and nitrate [21]. The selenate peaks may be obscured by sulphate [21]. Niss and Powers [8] used an aqueous carbonate solution of pH 12 as the eluent to eliminate interferences from sulphate and phosphate; this system did not give reproducible results. Williams [18] used UV detection (195 nm) for the separation of selenite and selenate. Sulphate did not interfere, because it does not absorb above 190 nm. However, the detection limits were high (0.3 mg Se l^{-1} as selenite, 8.3 mg l^{-1} as selenate). Karlson and Frankenberger [16] overcame the interference by chloride in the determination of selenite through the removal of chloride on a silver ion-loaded cation-exchange resin. Interferences by sulphate were eliminated with a barium-ion-loaded resin [9,15]. Hoover and Yager [21] separated in environmental water samples selenite and selenate from the major anions (chloride, nitrate, and sulphate) first by collecting the selenium-containing fractions after passage through the suppressor column and rechromatographing these fractions. Murayama et al. [11] used this recycle technique for the ion chromatographic determination of selenate in sulphur-containing drugs.

Very promising for the elimination of interferences by other ions is the use of selenium-specific detectors that are fairly insensitive towards sample matrices. Irgolic and co-workers used graphite furnace atomic absorption spectrometry (GFAAS) for element-specific detection for the suppressed ion chromatographic [22,23] and reversed-phase separation [24] of selenite and selenate. They observed no interference from anions at concentrations 1000 times higher than the selenium level.

Inductively coupled plasma atomic emission spectrometry (ICP-AES), which yields a continuous signal, has also been used as an element-specific detection method for the determination of selenite and selenate by ion-pair [25–27] or anion-exchange chromatography [28,29].

This paper describes an ion chromatographic separation of selenite and selenate using a single-column system. A Zeeman-effect graphite furnace and a Zeeman-effect flame atomic absorption spectrometer were employed as selenium-specific detectors. Addition of chemical modifiers commonly used in GFAAS to the mobile phase improved the detection limits of the LC–GFAAS system.

EXPERIMENTAL

Reagents

Selenium stock standard solutions (1000 mg Se l^{-1}) were prepared from anhydrous sodium selenate (Fluka) and sodium selenite pentahydrate (Merck). Working standard solutions of lower concentrations were obtained daily by appropriate dilution. Sulphate and sulphite solutions were prepared from analytical-reagent grade potassium sulphate (Merck) and sodium sulphite (Merck), respectively. Mobile phases contained potassium hydrogenphthalate (1.5–10 mM), nickel nitrate (6–20 mM) or nickel sulphate (3–15 mM) (all compounds from Merck). Potassium hydrogenphthalate solutions (3 mM) were chemically modified by stirring 2.0 l overnight with an excess (5 g) of nickel hydroxide (Fluka). Eluents with lower nickel concentrations were prepared by mixing the 3 mM phthalate solution saturated with nickel hydroxide with nickel-free 3 mM phthalate solution. The pH of the mobile phases was adjusted to the desired value with potassium hydroxide. All mobile phases were filtered through 0.2-μm cellulose nitrate filters (Sartorius) prior to use. Water was first purified by deionization and then distilled twice in a quartz still.

Instrumentation

The chromatographic system consisted of a double head pump (Waters 600 E multisolvent delivery system) with a Waters U6K injector, a precolumn and an analytical column mounted in a thermostated chamber held at 25 °C. Separa-

tions were performed on a strongly basic anion-exchange column (ESA Anion III, 250 × 4 mm i.d., 10-μm particles) with a Hamilton PRP-X100 precolumn. Solutions (100 and 250 μl) to be chromatographed were injected on to the column with a microlitre syringe (Hamilton).

Two different types of GFAAS detectors were used. A Zeeman-effect atomic absorption spectrometer (Hitachi Model 170-70) equipped with an autosampler (Hitachi 170–0125) was used for the optimization of the chromatographic parameters and for the interference studies. This spectrometer was equipped with graphite tubes (Hitachi 170-5100) and a selenium hollow-cathode lamp (Cathodeon 3QNY/Se). The lamp was operated at 9 mA. Argon at 2.5 l min^{-1} was used as the sheath gas and at 0.2 l min^{-1} as the carrier gas. The expansion setting was 3 × and the response setting was 4 ×. Aliquots (20 μl) of the effluent from the column were injected into the furnace, dried at 76°C for 30 s and atomized at 2600°C for 5 s. The ashing step was omitted. The different modules of this GFAAS system (autosampler, power unit) were controlled by a laboratory-built interface with the aid of a personal computer, which was equipped with an analogue-to-digital/digital-to-analogue converter (ADDA converter RTI 815 from Analog Devices). Signals from the spectrometer were recorded via the analogue port of the converter and processed with the computer by a laboratory-written program [30].

A simultaneous multi-element atomic absorption spectrometer (Hitachi Z-9000) operated with graphite tubes (Ringsdorff-Werke, RWO 521) was used for quantitative measurements and for the evaluation of the influence of nickel on the signals. The selenium hollow-cathode lamp was operated at 12.5 mA and argon at 0.280 l min^{-1} was employed as the carrier gas. Volumes of 20 μl were transferred into the furnace, dried at 80–120°C for 5 s and at 200°C for 5 s, ashed at 390°C for 20 s and atomized at 2600°C for 5 s. Signals from this spectrometer were processed and quantified as described [30]. The chromatographic system and the GFAAS detectors were connected with a laboratory-built flow-through cell [31] made of Teflon with a dead volume of 30 μl.

A Zeeman-effect flame atomic absorption spectrometer (Hitachi Z-6100) was operated with an air–acetylene flame (fuel pressure 15 kPa, oxidant pressure 160 kPa, optimum burner height 7.5 mm, selenium hollow-cathode lamp at 12 mA). The LC system was connected to the inlet of the atomizer with a short piece of Teflon tubing. Signals from the spectrometer were recorded with the factory-supplied recorder. Alternatively, the spectrometer signals were read into a personal computer via the Hitachi recorder interface (Hitachi 171-9124) with analogue-to-digital conversion. The data were treated by a modified version of the program for the graphite furnace spectrometer.

Conductivity measurements were performed with a conventional conductivity detector (Waters Model 431). The detector signals were stored and treated by the computer with application of a data-smoothing program [32].

Separations of selenite and selenate on the anion exchange column gave the best results when a 3 mM solution of KHP saturated with nickel hydroxide (pH 7) at a flow-rate of 0.4 ml min^{-1} was used in combination with the GFAAS detector. With the flame AAS (FAAS) detector a 10 mM solution of KHP (pH 7) at a flow-rate of 2.5 ml min^{-1} was the optimum mobile phase.

RESULTS AND DISCUSSION

Composition of the mobile phases for the separation of selenite and selenate

Potassium hydrogenphthalate, a common component of mobile phases for the chromatographic separation of anions on anion-exchange columns, was used as the eluent because its elution power even at low concentrations promises to give sufficient separation.

The dead volumes of the systems including the ESA Anion III (250 × 4 mm i.d.) column were determined by passing a solution of LiCl through the column at various flow-rates. Fractions of the effluent (LC–GFAAS system) or the total effluent (LC–FAAS system) were monitored for lithium by FAAS. The Li^+ ion should not be retained by the anion-exchange column. Therefore, the indirect linear dependence of the reten-

tion time of lithium on the flow-rate allowed the calculation of the dead volumes of the chromatographic systems. The dead volume of the LC–GFAAS system was found to be 2.22 ± 0.01 ml and that of the LC–FAAS system 2.05 ± 0.01 ml.

The retention ability of a column for a compound is expressed by the capacity factor, k'. This parameter, independent of flow-rate and the dimensions of the column, is the ratio of the retention volume at the signal maximum to the

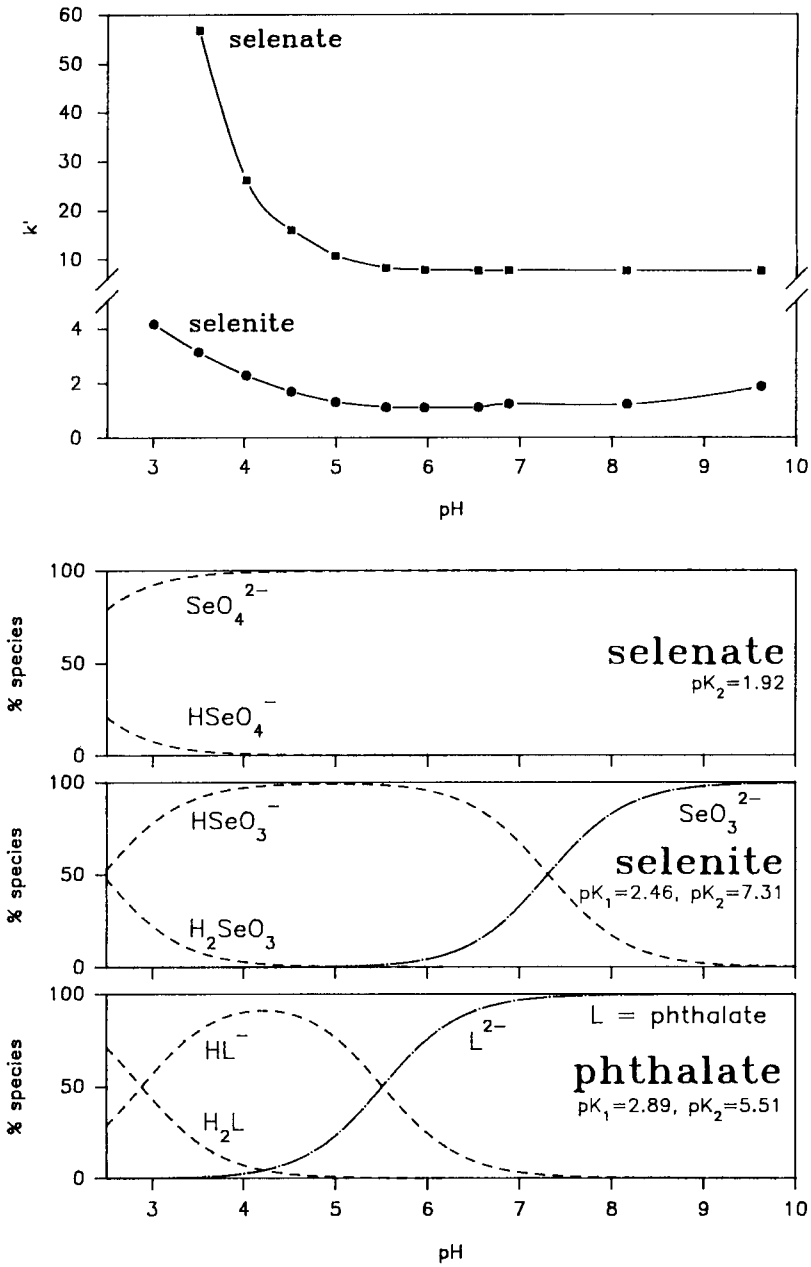

Fig. 1. Top: dependence of k' values of (●) selenite and (■) selenate on the pH of the mobile phase. Column, ESA Anion III; mobile phase, 2 mM potassium hydrogenphthalate, pH adjusted with potassium hydroxide. Standard deviations are within the symbol size. Bottom: distribution diagrams for selenate, selenite and phthalate.

column volume. The capacity factors for selenite and selenate increased in the pH range 5.5–3 (Fig. 1). Selenate could not be eluted from the column with mobile phases (2 mM potassium hydrogenphthalate) of pH $\leqslant 3$. The retention behaviour of selenite and selenate on the anion exchange column is governed by the pH-controlled protonation of the selenium anions and the phthalate anion. These anions compete for the ammonium groups of the stationary phase. Anions with higher negative charge generally have higher retention times.

As the distribution diagram (Fig. 1) shows, the completely deprotonated selenic acid (the dinegative selenate ion) is the only "selenate" species in the pH range 10–3. Only below pH 3 is the hydrogenselenate ion with one negative charge present in appreciable concentration compared with the selenate dianion. When only the charge on "selenate" is considered, the retention time/volume and k' should be constant in the pH range 10–3 and should decrease below pH 3. However, the charge on the phthalate in the mobile phase is also pH dependent (Fig. 1). Down to pH ≈ 6 the dinegative phthalate ion is the only or at least the predominant species. The constancy and the relatively low value of k' for selenate are the result of the competition between the dinegative selenate and the dinegative phthalate for the cation-exchange sites on the resin. Below pH 6 the mononegative hydrogenphthalate becomes the dominant species, which has a competitive disadvantage compared with the still dinegative selenate. Therefore, the k' value for selenate first increases slowly and then rapidly below pH 4, because an increasing fraction of the phthalate becomes completely protonated. The uncharged phthalic acid does not occupy cation-exchange sites. Although selenate is protonated below pH 3.5 to hydrogenselenate, which should have lower k' values than dinegative selenate, lack of competition from phthalate anions makes the removal of "selenate" from the column with a 2 mM phthalate-containing mobile phase of pH $\leqslant 3$ impossible.

"Selenite" has k' values over the pH range 10–3 that are approximately one tenth of the k' values of "selenate" when a 2 mM solution of potassium hydrogenphthalate was used as the mobile phase (Fig. 1). Such differences were also observed for similar pairs of anions (nitrite–nitrate, sulphite–sulphate, chlorite–chlorate [33]). For the pair selenite–selenate the difference in k' cannot be explained on the basis of the charges on the anion. At pH > 9 both selenium species carry two negative charges and would be expected, considering charges only, to have the same k' value. The experimental results do not agree with these expectations.

The k' value for "selenite" increases by a factor of four in the pH range 6–3, reaching a value of 4 at pH 3 (Fig. 1). In this pH range $HSeO_3^-$ is protonated to H_2SeO_3. As this conversion proceeds, the average charge on the selenium species decreases from ca. -1 at pH 6 to ca. -0.5 at pH 2.5. Such a decrease in average charge should produce smaller k' values, an expectation again not supported by experiment. The protonation of the hydrogenphthalate anion ($pK_1 = 2.89$) reduces the average charge on the phthalate with decreasing pH to a greater extent than is the case with hydrogenselenite. The uncharged phthalic acid, increasing in concentration with decreasing pH, does not compete with the on the average still negatively charged selenium species for the positive exchange sites on the stationary phase. The two protonation reactions with their different pH dependencies produce the observed increase in the k' values for "selenite".

In the pH range 7–10 the k' values for "selenite" increase slightly. In this range phthalate is completely ionized and cannot influence the retention behaviour of "selenite" through dissociation equilibria. Hydrogenselenite ($pK_2 = 7.31$) is converted into SeO_3^{2-} in this region. This ionization is complete above pH 9. The increase in average charge on selenite from -1.5 at pH 7.3 to -2 at pH 9 can be held responsible for the slight increase in k' values. Mehra and Frankenberger [14] assigned a similar small increase in k' for "selenite" between pH 6.5 and 8 to the deprotonation of $HSeO_3^-$ with a solution of 4-hydroxybenzoic acid ($pK_1 = 4.48$, $pK_2 = 9.32$) as mobile phase. The state of dissociation of benzoic acid does not change in this pH interval. Why the k' values for "selenite" above pH 8 are not

larger cannot be deduced from the available experimental results.

Figure 2 shows the dependence of the capacity factors of selenous and selenic acid on the concentration of potassium hydrogenphthalate, nickel sulphate, or nickel nitrate in the mobile phase at a constant pH of 7. The capacity factors for "selenite" and "selenate" decrease with increasing solute concentration, as do the selectivity factors (ratio of the capacity factors for the two species).

The chromatographic operating parameters must be selected to fit the requirements of the detector. As FAAS works continuously, sharp chromatographic peaks can be detected easily. Therefore, high concentrations of phthalate in the mobile phase can be used, permitting the separation of selenite and selenate with short analysis times. The FAAS detector needs relatively high flow-rates of the chromatographic eluent, because the normal uptake rate of the nebulizer is 6 ml min^{-1}. Such a high flow-rate is not achievable with an analytical LC column because of the build-up of back-pressure. With the anion-exchange column and the injector employed, the maximum practical back-pressure of 2500 psi allowed a flow-rate of 2.5 ml min^{-1}. The mismatch between the flow-rate through the column and the uptake rate of the atomizer caused an increase in the detection limits. A 10 mM potassium hydrogenphthalate solution (pH 7) at a flow-rate of 2.5 ml min^{-1} was found to be the optimum mobile phase for this kind of detector. Figure 3 shows a successful separation under the conditions described.

GFAAS needs only small sample volumes. For this reason, the flow-rate of the mobile phase can be kept low. Because GFAAS works discontinuously, the chromatographic peaks should be broad to obtain sufficient numbers of GFAAS signals for each selenium compound. However, the time for the total analysis should be as short as possible to avoid unnecessary consumption of graphite cuvettes and argon gas. Two fully resolved peaks for selenite and selenate were observed within 35 min when a mobile phase of 3 mM potassium hydrogenphthalate (pH 7) at flow-rates between 0.3 and 0.5 ml min^{-1} was used (Fig. 4).

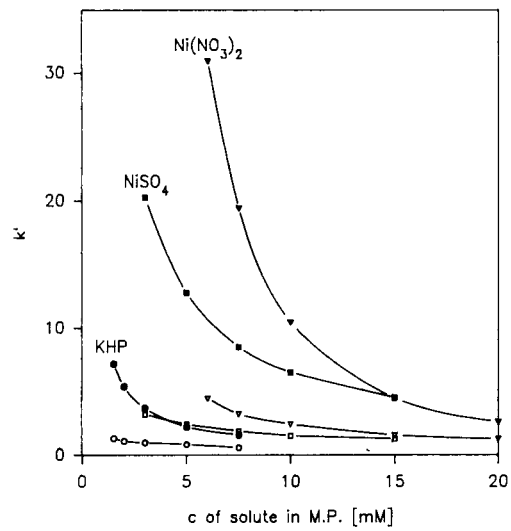

Fig. 2. Dependence of k' values of (open symbols) selenite and (closed symbols) selenate on the eluent concentration. Column, ESA Anion III. Mobile phases (pH ≈ 7): ○, ● = potassium hydrogenphthalate; □, ■ = nickel sulphate; △, ▲ = nickel nitrate.

GFAAS suffers from various interferences such as background absorption by molecular species, light scattering and detrimental reactions during atomization. Chemical modifiers prevent some of

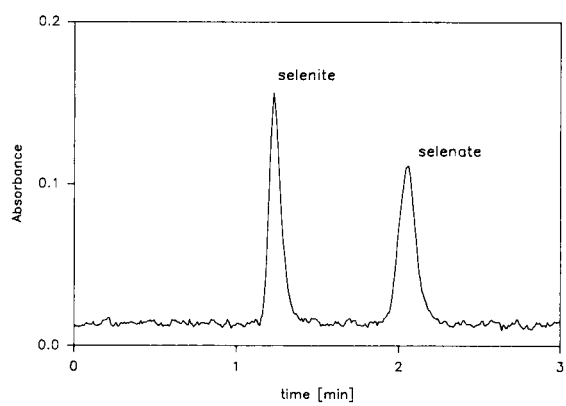

Fig. 3. Separation of selenite and selenate on an anion-exchange column. Column, ESA Anion III; mobile phase, 10 mM potassium hydrogenphthalate (pH 7); flow-rate, 2.5 ml min^{-1}; sample volume, 100 μl; detection, FAAS; 50 mg Se l^{-1} as selenite and 50 mg Se l^{-1} as selenate.

these interferences, improve the signal-to-noise ratio and may increase the signal intensity. Nickel, copper, silver, molybdenum and platinum salts have been used as modifiers in the determination of selenium with GFAAS [34]. To exploit the favourable effect of chemical modification for the element-specific detection of selenium, nickel nitrate and nickel sulphate were investigated as components of the mobile phase. With nickel sulphate and nickel nitrate solutions as mobile phase the capacity factor for selenite (ca. 2) is almost independent of the concentration of the nickel salts in the concentration range 3–15 mM. The k' values for selenate increase rapidly with decreasing concentration (Fig. 2), making the total analysis time unacceptably long (ca. 40 min at 3 mM $NiSO_4$ at a flow-rate 1.5 ml min^{-1}). At higher concentrations of nickel salts a separation of selenite and selenate is achievable in a reasonable time. However, the chromatographic signals obtained with solutions of nickel nitrate or sulphate tail badly. For these reasons, mobile phases containing these nickel salts do not have any advantages over the phthalate solutions.

To circumvent the problems associated with mobile phases containing nickel sulphate or nickel nitrate, a 3 mM solution of potassium hydrogenphthalate was shaken with nickel hydroxide (Fluka). The saturated solution had a nickel concentration of 1.6 mM. The phthalate/Ni^{2+} mole ratio is almost 2:1. Solutions with concentrations less than 1.6 mM Ni^{2+} were prepared by diluting the 1.6 mM solution with 3 mM KHP. Chromatograms of selenate–selenite mixtures obtained with these mobile phases (constant KHP concentration of 3 mM, Ni concentration in the range 0.3–1.6 mM) showed that the k' values for selenite are independent of the Ni concentration, whereas the k' values for selenate increase with increasing Ni concentration (Fig. 5). Nickel is known to form 1:1 compounds with phthalate (log $K = 2.9$) [35]. As the Ni concentration increases, the free phthalate concentration will decrease and the k' value for selenate will concomitantly increase (Fig. 2). The free phthalate concentrations were calculated on the assumption of a 1:1 compound and the reported formation constant. The k' values expected for the calculated free phthalate concentrations were estimated from the data in Fig. 2. The "theoretical" k' values for selenate agree acceptably with the experimental values (Fig. 5). The k' values for

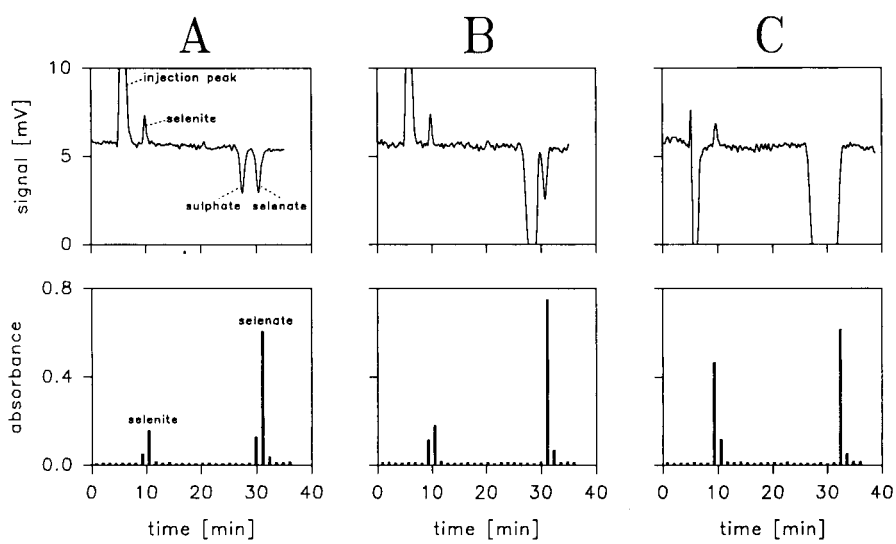

Fig. 4. Comparison of (top) conductivity and (bottom) GFAAS detection. Column, ESA Anion III; mobile phase, 3 mM potassium hydrogenphthalate (pH 7); flow-rate, 0.4 ml min^{-1}; sample volume, 100 μl; detectors, conductivity (10 mV = 2 μS) and GFAAS; 10 mg Se l^{-1} as selenite and 10 mg Se l^{-1} as selenate. (A) +10 mg sulphate l^{-1}; (B) +100 mg sulphate l^{-1}; (C) +500 mg sulphate l^{-1}.

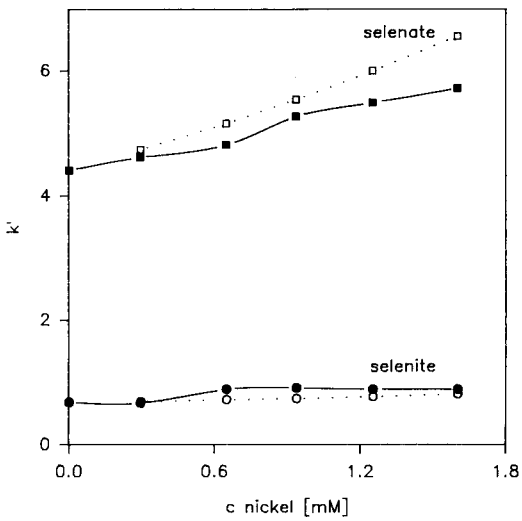

Fig. 5. Influence of nickel in the mobile phase on the retention behaviour of (●) selenite and (■) selenate. Column, ESA Anion III; mobile phase, 3 mM potassium hydrogenphthalate (pH 7). Calculated values are shown as corresponding open symbols.

selenite are almost independent of the phthalate concentration in the range 1.5–7.5 mM (Fig. 2). Therefore, the change in phthalate concentration caused by the nickel ions should not and does not influence the k' values (Fig. 5). The dependence of the signal areas on the Ni^{2+} concentration in the mobile phase (Fig. 6) shows the expected increase. Additionally, the background absorption is lowered to 50% of the value characteristic for the 3 mM potassium hydrogenphthalate solution.

Detectors and quantification

A Zeeman-effect graphite furnace atomic absorption spectrometer (Hitachi Z-9000) and a Zeeman-effect flame atomic absorption spectrometer were evaluated as selenium-specific detectors. The GFAAS instrument operates discontinuously, allowing measurements at ca. 1-min intervals. Therefore, the chromatographic bands consist of relatively few signals. The chromatographic peaks were reconstructed from these signals with interpolated Gaussian curves [30]. Calibration graphs were constructed with the calculated areas under these fitted Gaussian curves. Calibration graphs of peak area versus the concentration of selenite and selenate were linear from 0.5 to 12 mg Se l^{-1} with correlation coefficients of 0.98 for an injection volume of 100 μl. The absolute detection limits (3σ) for this system (3 mM KHP as mobile phase) were found to be 6 ng Se for selenite and 2 ng Se for selenate. With the chemically modified mobile phase (3 mM potassium hydrogenphthalate saturated with nickel hydroxide), lower detection limits of 1 ng Se for selenite and 0.6 ng Se for selenate were achieved.

Chromatograms obtained with FAAS detection were quantified similarly. The calibration graphs were linear with correlation coefficients of 0.9998 from 10 to 100 mg Se l^{-1} for selenite and selenate with a 100-μl injection. The calculated detection limits (10 mmol l^{-1} KHP) were 8 ng Se for selenite and 11 ng Se for selenate.

GFAAS and FAAS instruments can be used as selenium-specific detectors. The system with the 3 mM KHP solution saturated with nickel hydroxide as mobile phase and GFAAS detection showed the lowest absolute detection limits (ca. 1

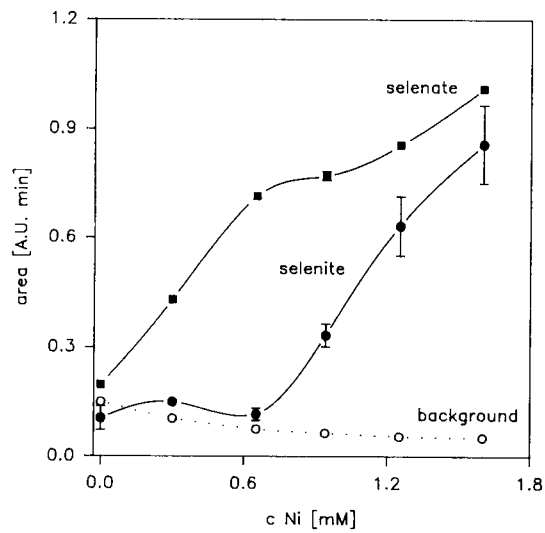

Fig. 6. Influence of nickel in the mobile phase on (●) selenite and (■) selenate signals. Column, ESA Anion III; mobile phase, 3 mM potassium hydrogenphthalate (pH 7); flow-rate, 0.4 ml min^{-1}; sample volume, 100 μl; detection, GFAAS; 3 mg Se l^{-1} as selenite and 3 mg Se l^{-1} as selenate. Standard deviations are within the symbol size if not shown.

ng Se with a 100-μl injection). With larger injection volumes (up to 500 μl), selenium compounds could be determined in samples, in which the selenium concentration is in the μg l^{-1} range. The detection limits with the FAAS detector are one order of magnitude higher than the those with GFAAS. However, the quantification is more reliable with the FAAS detector.

Interferences

Severe interferences by several common inorganic ions, such as chloride, nitrate, and sulphate, are reported with the ion chromatographic detection of selenite and selenate when a conductivity detector is used. Selenium-specific detectors largely circumvent these interferences. The effects of sulphite and sulphate on the GFAAS response to selenite and selenate were evaluated. Under the chromatographic conditions used, sulphite and sulphate were not separated from each other. The sulphite/sulphate signals were far removed from the selenite but close to the selenate signals (Fig. 4). As expected, selenite is not affected by sulphite and sulphate. The selenate signals decrease with increasing sulphite/sulphate concentration (Fig. 7). However, the detection of selenate is still possible at 1000 mg sulphate l^{-1}, the highest concentration of sulphate examined. The decrease in the selenate signals can be explained by a suppressing effect of sulphate and sulphite on the atomic absorption signals of selenium [36,37]. Sulphite suppresses the signals for selenate less than sulphate.

Applications

To demonstrate the practical applicability of the LC–FAAS system (mobile phase 10 mM KHP, pH 7; flow-rate 2.5 ml min^{-1}), selenite/selenate were determined with this method in the following samples: aqueous solutions used to supply selenium to animals by subcutaneous or intramuscular injection, which contain selenium as selenite in addition to a variety of organic compounds such as vitamin E, sorbic acid and benzoic acid in great excess over selenium; an animal food premix (1 g was stirred in 100 ml of water for 2 h and the suspension was then centrifuged and filtered); and a solution prepared by stirring

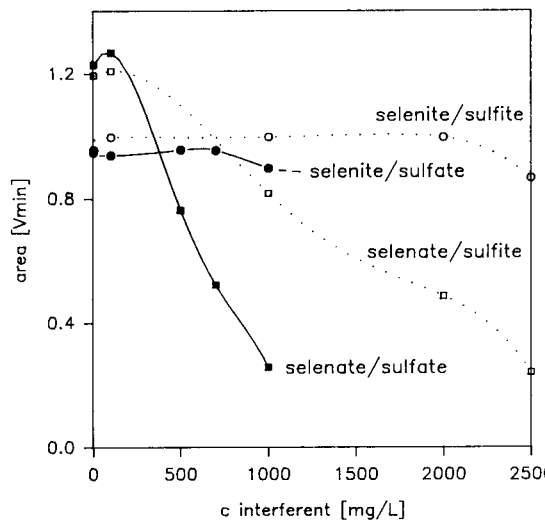

Fig. 7. Influence of (open symbols) sulphite and (closed symbols) sulphate on (○, ●) selenite and (□, ■) selenate signals. Column, ESA Anion III; mobile phase, 3 mM potassium hydrogenphthalate saturated with $Ni(OH)_2$ (pH 7); flow-rate, 0.4 ml min^{-1}; sample volume, 100 μl; detection, GFAAS; 10 mg Se l^{-1} as selenite and 10 mg Se l^{-1} as selenate.

a soluble glass bolus (13.4% copper, 0.5% cobalt and 0.3% selenium) in 0.1 M hydrochloric acid overnight; such boluses are used for supplementation of animals with trace elements [38].

All samples were diluted if necessary, filtered through a micropore filter and injected on to the column. Internal standard addition was employed for quantification. The total selenium concentration was determined by FAAS using standard conditions (digestion with nitric acid). Table 1 gives the results of these determinations. The glass bolus solution contained only selenate and all other samples only selenite. The concentra-

TABLE 1

Determination of selenite and selenate in different samples [a]

Sample	FAAS: total Se (mg l^{-1})	LC–FAAS: Se (mg l^{-1})
Solution 1 [b]	513 ±3	495 ±20 as selenite
Solution 2 [b]	497 ±3	485 ±20 as selenite
Food premix	33.0±0.3	32.0± 1.0 as selenite
Glass bolus	26.8±0.3	26.0± 1.0 as selenate

[a] Means ± standard deviations ($n = 3$). [b] For injection into animals.

tions obtained by chromatography agree within the statistical errors with the concentrations of total selenium.

Conclusion

Selenium-specific detection for LC separations is useful for the identification and determination of selenite and selenate. The coupled systems allow the identification and determination of these selenium compounds even in complex matrices. However, the LC–GFAAS system (absolute detection limit ≈ 1 ng Se) has some disadvantages: the limited number of signals forming a chromatogram can make the quantification difficult and may adversely affect the reproducibility whenever the sampling rates and flow-rates are not optimal; additionally, the analysis time is long in comparison with conventional LC procedures. FAAS for selenium-specific detection provides a continuous signal and is characterized by better reproducibility and shorter analysis times, but has higher limits of detection (absolute detection limit ≈ 10 ng Se).

REFERENCES

1 K. Schwarz and C.M. Foltz, J. Am. Chem. Soc., 79 (1957) 3292.
2 M.L. Jackson, Appl. Geochem., 1 (1986) 175.
3 O.A. Levander, Curr. Top. Nutr. Dis. (Clin. Biochem., Nutr. Aspects Trace Elem.), 6 (1982) 345.
4 L.P. Gough, H.T. Shacklette and A.A. Case, U.S. Geol. Surv. Bull., No. 1466 (1979) 42.
5 K. Forchhammer and A. Böck, Naturwissenschaften, 78 (1991) 497.
6 R.J. Shamberger, Biochemistry of Selenium, Plenum Press, New York, 1983.
7 J.M. McNeal and L.S. Balistrieri, Soil Sci. Soc. Am., Spec. Publ. (Selenium Agric. Environ.), 23 (1989) 1.
8 N.D. Niss and C.R. Powers, Determination of Selenium Species in Spent Oil Shale Leachates by Ion Chromatography, Report DOE/MC/11076-2685, Order No. DE 89000965, 1988; C.A., 113 (1990) 64 924p.
9 C. Sarzanini, O. Abollino, E. Mentasti and V. Porta, Chromatographia, 30 (1990) 293.
10 M. Murayama, M. Suzuki and S. Takitani, Anal. Sci., 4 (1988) 389.
11 M. Murayama, M. Suzuki and S. Takitani, J. Chromatogr., 463 (1989) 147.
12 Yu.A. Zolotov, O.A. Shpigun and L.A. Bubchikova, Fresenius' Z. Anal. Chem., 316 (1983) 8.
13 S.L. McGeehan and D.V. Naylor, J. Environ. Qual., 21 (1992) 68.
14 H.C. Mehra and W.T. Frankenberger, Jr., Chromatographia, 25 (1988) 585.
15 U. Karlson and W.T. Frankenberger, Jr., J. Chromatogr., 368 (1986) 153.
16 U. Karlson and W.T. Frankenberger, Jr., Anal. Chem., 58 (1986) 2704.
17 R.G. Gerritse and J.A. Adeney, J. Chromatogr., 347 (1985) 419.
18 R.J. Williams, Anal. Chem., 55 (1983) 851.
19 S.S. Goyal, A. Hafez and D.W. Rains, J. Chromatogr., 537 (1991) 269.
20 Y. Shibata, M. Morita and K. Fuwa, Analyst, 110 (1985) 1269.
21 T.B. Hoover and G.D. Yager, Anal. Chem., 56 (1984) 221.
22 D. Chakraborti, D.C.J. Hillman, K.J. Irgolic and R.A. Zingaro, J. Chromatogr., 249 (1982) 81.
23 K.J. Irgolic, C.H. Banks, N.R. Bottino, D. Chakraborti, J.M. Gennity, D.C. Hillman, D.H. O'Brien, R.A. Pyles, R.A. Stockton, A.E. Wheeler and R.A. Zingaro, in F.E. Brinckman and R.H. Fish (Eds.), Environmental Speciation and Monitoring Needs for Trace Metal-Containing Substances from Energy-Related Processes, Proceedings of the DoE/NBS Workshop (Gaithersburg, MD USA, May 18–20, 1981), Natl. Bur. Stand. (U.S.) Spec. Publ., No. 618 (1981) 244.
24 D. Chakraborti and K.J. Irgolic, in T.D. Lekkas (Ed.), Heavy Metals in the Environment, Proceedings of the 5th International Conference (Athens, Greece, Sept. 10–13, 1985), Vol. 2, CEP Consultants, Edinburgh, 1985, p. 484.
25 K.E. La Freniere, V.A. Fassel and D.E. Eckels, Anal. Chem., 59 (1987) 879.
26 S.R. Wang and S.J. Jiang, J. Chin. Chem. Soc. (Taipei), 38 (1991) 327.
27 K.J. Irgolic, R.A. Stockton, D. Chakraborti and W. Beyer, Spectrochim. Acta, Part B, 38 (1983) 437.
28 F. Laborda, M.T.C. de Loos-Vollebregt and L. de Galan, Spectrochim. Acta, Part B, 46 (1991) 1089.
29 J.P. McCarthy, J.A. Caruso and F.L. Fricke, J. Chromatogr. Sci., 21 (1983) 389.
30 G. Kölbl, K. Kalcher and K.J. Irgolic, J. Autom. Chem., 15 (1993) 37.
31 F.E. Brinckman, W.R. Blair, K.L. Jewett and W.P. Iverson, J. Chromatogr. Sci., 15 (1977) 493.
32 W.H. Press, B.P. Flannery, S.A. Teukolsky and W.T. Vetterling, Numerical Recipes – the Art of Scientific Computing, Cambridge University Press, Cambridge, 1989, p. 495.
33 O. Shpigun and Yu.A. Zolotov, Ion Chromatography in Water Analysis, Ellis Horwood, Chichester, 1988, p. 116.
34 M. Verlinden, H. Deelstra and E. Adriaenssens, Talanta, 28 (1981) 637.
35 I.R. Desai and V.S.K. Nair, J. Chem. Soc., (1962) 2360.
36 G. Bozsai, B. Welz, B. Radziuk and M. Sperling, in B. Welz (Ed.), 5th Colloq. Atomspektr. Spurenanal., Universität Konstanz, April 3–7, 1989, Bodenseewerk Perkin-Elmer, Überlingen, 1989, p. 235.
37 B. Welz, G. Bozsai, M. Sperling and B. Radziuk, J. Anal. At. Spectrom., 7 (1992) 505.
38 P. Knott, B. Algar, G. Zervas and S.B. Telfer, in C.F. Mills, I. Bremner and J.K. Chesters (Eds.), Trace Elem. Man Anim. - TEMA 5 Proc. 5th Int. Symp. on Trace Elements in Man and Animals, Aberdeen, June 29–July 4, 1984, CAB Farnham Royal, Slough, 1985, p. 708.

Analytica Chimica Acta, 284 (1993) 311–316
Elsevier Science Publishers B.V., Amsterdam

Liquid chromatographic determination of carotenoids using dual-beam continuous-wave laser thermal lens detection

A. Chartier and J. Georges

Laboratoire des Sciences Analytiques, Bât. 308, 43 Bd. du 11 Novembre 1918, F-69622 Villeurbanne (France)

(Received 8th April 1993; revised manuscript received 3rd August 1993)

Abstract

Chromatographic separations of carotenoids were carried out with a conventional column (4.6 mm i.d.) with an analytical flow cell (10 mm path length) and a microbore column (1.0 mm i.d.) with a microcell (3 mm path length) using dual-beam thermal lens detection. The technique was compared with conventional UV–visible spectrophotometry under static conditions and with both chromatographic systems. The comparison was made in terms of signal-to-noise ratios and detection limits. The linear absorbance range was from 10^{-3} to 10^{-5} and from 10^{-2} to 10^{-4} with the analytical cell and the microcell, respectively. For three carotenoids, the minimum observable absorbance at the top of the peak was 2.4×10^{-5} and 1.1×10^{-4} in conventional and microbore chromatography, respectively.

Keywords: Liquid chromatography; Carotenoids; Thermal lens detection

To improve absorbance detection limits, it may be advantageous to detect signals associated with photophysical processes which occur after light absorption. When the analytes have low fluorescence quantum yields, it is possible to use a photothermal method that detects a temperature rise associated with non-radiative relaxation of excited states. The practical use of thermal lens spectrometry for detection in liquid chromatography has been described [1–8]. The sensitivity of the method, which is directly proportional to the derivative of the refractive index with temperature, is low in water but is improved in organic solvents such as those used in liquid chromatography. Neverthless, developments in open-tubular [9] and microbore [10,11] liquid chromatographic columns require lower detection volumes and higher sensitivity. This goal is reached by the use of laser beams which can be focused in a tiny volume. To carry out these measurements, dual-beam configurations with continuous-wave (cw) laser excitation are generally used. The main advantage of this experimental set-up is working in the mode mismatched configuration where the excitation beam waist is centred in the cell which is located at $3^{1/2}$ the confocal distance after the waist of the probe beam [12,13]. Moreover, the combination of modulated cw excitation and lock-in detection improves the sensitivity and precision of the measurements. The thermal effect is measured by monitoring, in the far field, the relative change in the beam centre intensity of the probe

Correspondence to: J. Georges, Laboratoire des Sciences Analytiques, Bât. 308, 43 Bd. du 11 Novembre 1918, F-69622 Villeurbanne (France).

SSDI 0003-2670(93)E0472-J

beam. The time-dependent signal is conveniently expressed as

$$S(t) = 2.3EA\left(1 + \frac{t_c}{2t}\right)^{-1} \quad (1)$$

where A is the decadic absorbance and t_c is the characteristic time constant which represents the response time of the medium to the heat input or dissipation. The parameter E is called the enhancement factor because it indicates the sensitivity of the thermal lens method relative to that achieved with conventional spectrophotometry. E is proportional to the power of the excitation laser and to the refractive index gradient, and inversely proportional to the thermal conductivity of the solvent.

Liquid chromatography (LC) has been widely applied to the qualitative and quantitative analysis of carotenoids from different plants and materials [14]. A wide variety of octadecyl-bonded and other reversed phases with different solvent systems have been investigated. It has been demonstrated that the most appropriate system, in terms of selectivity and recovery for the separation of carotenoids, should include a polymeric C_{18} column and a methanol-based mobile phase [15–17]. Also, it has been demonstrated [18] that microcolumns can offer significant advantages over conventional columns in terms of solvent consumption and peak height. However, to obtain good performance with microcolumn chromatography, it is necessary to reduce the dead volume of the chromatographic system and therefore to use a low-volume detector with a short optical path length. In this instance, to cross the sample cell conveniently, both laser beams need to be focused with shorter focal length lenses. Because tightly focused beams diverge more quickly, the implementation of the thermal lens method with microcells involves some optical constraints [19]. As a result of the smaller beam waist and therefore shorter confocal distance, the sample path length should not exceed a maximum value in order to achieve optimum sensitivity and reduced noise.

The aim of this work was to compare thermal lens spectrometry with conventional spectrophotometry for detection in the chromatographic determination of carotenoids. Two chromatographic systems, based on octadecyl-bonded stationary phases and methanol–tetrahydrofuran mobile phases, were investigated using either a conventional column (4.6 mm i.d.) with an analytical flow cell (8 μl) or a microbore column (1.0 mm i.d.) with a microcell (0.6 μl). The analytical performances of the thermal lens method with each flow cell were first optimized and compared with those obtained with a 1-cm quartz cuvette

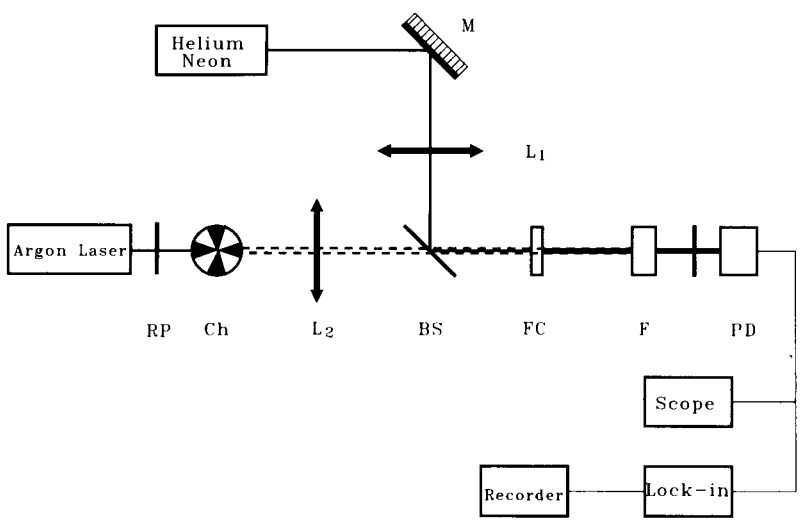

Fig. 1. Schematic diagram of the experimental set-up. M = mirror; RP = retardation plate; L_1,L_2 = focusing lenses; Ch = chopper; BS = beam splitter; FC = flow cell; F = filter; PD = photodiode.

under static conditions. The method was then applied to the detection of three carotenoids. The results obtained are compared in terms of detection limits and signal-to-noise ratio.

EXPERIMENTAL

Thermal lens detection

The thermal lens experimental set-up is depicted in Fig. 1. The excitation radiation was provided by an air-cooled argon ion laser (ILT, Model 5490A) operated in the single-wavelength mode with a maximum power of 40 mW at 488 nm. The beam diameter was 0.65 mm and the divergence θ was 0.95 mrad. A half-wave mica retardation plate (Melles Griot, 02WRM023) was used to allow the plane of polarization of the argon laser to be rotated. For better reliability, the laser was used at half its maximum power, so that the excitation power at the sample cell was about 10 mW. The cw-laser beam was then modulated by a variable-frequency optical chopper (Scitec, Model 300). The probe beam was supplied by a 6.2 mW helium–neon laser (Optilas, Model H7500P) at 632 nm. The beam diameter was 0.83 and the divergence θ was 0.96 mrad. In order to avoid saturation of the photodiode, the laser power was lowered by rotating the laser head. The excitation and the probe beams were focused independently by two lenses ($L_1 = 80$ mm; $L_2 = 80$ mm). Both beams were then recombined and made co-linear by means of a polarizing beamsplitter held on an X–Y–Z translator. After the sample cell, the excitation beam was blocked by a bandpass interference filter. The sample cell and the interference filter were tilted slightly to avoid interference effects resulting from back-reflection. The thermal lens signal was detected through a 1-mm pinhole with a silicon photodiode operated in the photovoltaic mode. Its output was sent via a 10-kΩ resistor to a lock-in amplifier (Brookdeal, Model 9503). The reference signal for the lock-in amplifier was generated within the chopper head.

Chromatographic system

The chromatographic system consisted of a Merck L6000 pump, a Rheodyne injection valve, a column and a variable-wavelength UV–visible detector (Shimadzu, SPD6AV) operated at 488 nm and equipped with either the analytical flow cell or the microcell. Conventional chromatography was carried out with a 250 mm × 4.6 mm i.d. Vydac 201 TP (5 μm) column, a 10-μl sample loop and a flow-rate of 0.8 ml min^{-1}. For microbore chromatography, a 250 mm × 1 mm i.d. (5 μm) Alltech microcolumn was used with a 0.5-μl sample loop and a flow-rate of 0.035 ml min^{-1}. In both instances, the i.d. of the capillary tubing was 0.15 mm.

Three sample cells were used, a 1-cm quartz cuvette for static experiments and two flow cells for chromatographic experiments. The analytical flow cell was an 8-μl, 1 mm i.d. tubular cell with a path length of 10 mm and the microcell was a 0.6-μl, 0.5 mm i.d. tubular cell with a path length of 3 mm. In order to keep constant the optical and geometrical characteristics of both laser beams set by the lenses L_1 and L_2, the input and output quartz lenses of the flow cells were removed and replaced with flat quartz windows. The cell axis and therefore the stream were parallel to the laser beams.

Reagents

The mobile phase was methanol–tetrahydrofuran (85:15, v/v) for conventional separation. The composition was adjusted to 82:18 (v/v) for microbore separation. The mobile phase was prepared daily and filtered through a Millipore filter (pore size 0.45 μm).

Canthaxanthin and β-carotene were purchased from Fluka and α-carotene, free from β-carotene, from Sigma. The absorption bands of the three carotenoids overlap with the 488-nm emission line of the argon ion laser. Stock solutions of each carotenoid were prepared in tetrahydrofuran and stored in brown flasks at less than 0°C.

RESULTS AND DISCUSSION

The performances of the thermal lens method were first investigated under static conditions with the three different sample cells. With the mode-

TABLE 1

Analytical performances of the thermal lens method with different cells for ferrocene in ethanol

Cell type	Path length (mm)	Relative signal for 10^{-3} absorbance	Limit of detection [a]	Noise [a]
Quartz cell	10	10.6	1.1×10^{-5}	1.9×10^{-5}
Analytical flow cell (8 μl)	10	12.1	8.6×10^{-6}	1.4×10^{-5}
Microcell (0.6 μl)	3	3.2	3.3×10^{-5}	5.5×10^{-5}

[a] Limits of detection and noise are expressed in absorbance.

mismatched configuration, the sensitivity of the method depends on the positioning of the pump and probe beam waists with respect to the sample cell and also on the relative diameter of the two beams inside the cell [12,20]. The optimum position, ensuring maximized sensitivity together with linear calibration graphs, was obtained experimentally, with the cell positioned near the waist of the excitation beam, by translating the lens of the probe beam and monitoring the thermal lens signal. The signal-to-noise ratio was then optimized by adjusting the chopper frequency and the time constant of the lock-in amplifier. The best compromise was obtained with a frequency of 40 Hz and a time constant of 1 s [21]. The response of the thermal lens detector was linear versus sample absorbance, from 10^{-3} to 10^{-5} with the 1-cm quartz cell and the analytical flow cell and from 10^{-2} to 10^{-4} with the microcell.

A comparison of relative signals, noises and detection limits taken as three times (3σ) the standard deviation of the background is shown in Table 1. Although a slight increase in the thermal lens signal is observed with the analytical flow cell compared with that obtained with the quartz cell, the results are consistent with the respective

TABLE 2

Comparison of thermal lens spectrometry and conventional spectrophotometry for 10^{-2} absorbance canthaxanthin in both chromatographic experiments

Detection method	Analytical flow cell (10 μl injected)			Micro-flow cell (0.5 μl injected)		
	Noise [a]	Relative intensity	Signal-to-noise ratio [a]	Noise [a]	Relative intensity	Signal-to-noise ratio [a]
Thermal lens	1.2×10^{-5}	21	175	5.7×10^{-5}	6	30
UV–visible	1.8×10^{-5}	9.8	109	1.0×10^{-4}	2.5	15.6

[a] Noise and signal-to-noise ratio are expressed in absorbance.

TABLE 3

Detection limits obtained for the chromatographic separation of three carotenoids and expressed as the minimum concentration injected (M) and the minimum absorbance at the top of the peak (A)

Solute	Method [a]	Analytical flow cell		Micro flow cell	
		M	A	M	A
Canthaxanthin	1	6.8×10^{-10}	2.4×10^{-5}	3.7×10^{-9}	1.1×10^{-4}
	2	1.8×10^{-9}	3.6×10^{-5}	8.8×10^{-9}	2×10^{-4}
α-Carotene	1	1.4×10^{-9}	2.4×10^{-5}	2.4×10^{-8}	1.1×10^{-4}
	2	4.5×10^{-9}	3.6×10^{-5}	5.5×10^{-8}	2×10^{-4}
β-Carotene	1	2.5×10^{-9}	2.4×10^{-5}	6.0×10^{-8}	1.1×10^{-4}
	2	6.9×10^{-9}	3.6×10^{-5}	9.6×10^{-8}	2×10^{-4}

[a] 1 = thermal spectrometry; 2 = UV–visible spectrometry.

optical path lengths. This result means that, even with tightly focused beams, the pump–probe interaction length at the sample cell is longer than the longest optical path used. Also, the optical requirements between the confocal distance of the probe beam and the path length are satisfied. However, the noise which is equivalent in both 10-mm cells is significantly greater in the microcell. This arises from the fact that noise, expressed in absorbance compared with an analytical signal, includes the difference in optical path length. Moreover, the alignment of the laser beams is more difficult in the microcell and back-reflection is more important.

Thermal lens detection was then compared with conventional UV–visible spectrophotometry in flowing conditions with both chromatographic systems. The results obtained for canthaxanthin are reported in Table 2. As shown, the noise obtained in thermal lens spectrometry was not affected by the flow, especially because a high chopping frequency (40 Hz) necessary to achieve good peak resolution was used. The ratio of the peak height obtained with the conventional column and the analytical cell to that obtained with the microcolumn and the microcell is 3.5 and 3.9 in thermal lens spectrometry and conventional spectrophotometry, respectively. These ratios include the optical path length ratio (3.3) and the relative mass sensitivities of the columns. Microchromatography is a sensitive method which can allow a significant improvement of the detection limits [18]. Indeed, for columns having the same length and efficiency and packed with the same material, and for the same injected masses, an improvement of a factor of 21 in the peak height can be expected by using microbore columns. However, in order to minimize the band broadening, one has to decrease the detector volume, which is partly obtained by reducing the optical path length of the cell. Thus, in this instance, the overall sensitivity ratio is 6.4. This is no longer true with respect to the injected mass, which was twenty times lower in the microcolumn experiment. The result is that the peak height with the microcolumn should be about three times lower than the peak height with the conventional column for the same sample concentration; this expectation is consistent with the experimental values obtained for canthaxantin with both detection systems (Table 2). As it was not possible to compare directly the electrical signals provided by thermal lens spectrometry and conventional UV–visible spectrophotometry, the two detection methods were compared with respect to the signal-to-noise ratios obtained for the same sample injected. The sensitivity enhancement obtained with the thermal lens method is only 1.6 and 1.9 in conventional chromatography and microchromatography, respectively. As it has been demonstrated that the flow-rate has little effect on the

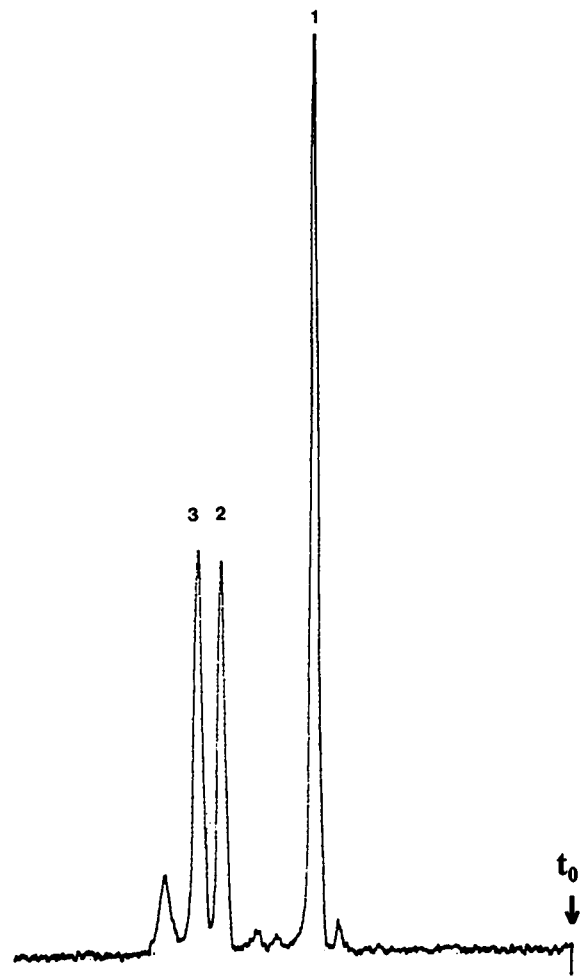

Fig. 2. Chromatographic separation of three carotenoids (5×10^{-8} M) on the conventional column (4.6 mm i.d.) using thermal lens detection. 1 = Canthaxanthin; 2 = α-carotene; 3 = β-carotene. The other four peaks are impurities

amplitude of the thermal lens signal under our experimental conditions [21,22], this result seems disappointing. It is clear that the intrinsic sensitivity of the thermal lens method is outweighed by the disavantage of it being more difficult to implement and more susceptible to variations.

The results for the chromatographic separation of three carotenoids (Fig. 2) are given in Table 3. The limits of detection were defined as the sample concentration yielding a peak height twice (10σ) the background noise, and were also expressed as the absorbance at the top of the peak. The results corroborate the previous comparison made with canthaxanthin on the basis of the results reported in Table 2. The sensitivity enhancement provided by the thermal lens method is almost the same for the three solutes in both chromatographic separations. Also, the average absorbance ratio for the microcolumn over the conventional column is 5, which is of the same order of magnitude as the theoretical peak-height ratio calculated previously (3) and the experimental signal ratio (3.5) given in Table 2. However, if these results agree for canthaxanthin owing to equivalent dilution factors obtained for both columns (about 7), this is no longer true for carotenes, where the dilution factor increased from 10 in the conventional separation to 50 in the microbore separation. As a result, the minimum detectable concentrations for carotenes are much lower with the microcolumn than with the conventional column.

Conclusion

Thermal lens detection is suitable for microbore chromatography. It is possible to use a dual-laser experimental set-up with a microcell using tightly focused beams without sensitivity loss. However, owing to a shorter optical path length and a greater sensitivity to beam alignment, the noise is comparatively greater than that experienced with the analytical flow cell. Owing to the low excitation power used in this work, the limits of detection obtained by the thermal lens method are those expected and compare favourably with results reported by other workers. However, it is not advantageous to compare a commercially available UV–visible detector that has been optimized for chromatographic applications and a laboratory-made device that is more sensitive to laser stability, alignment drift and mechanical vibrations.

REFERENCES

1 E.S. Yeung, LC·GC Int., 2 (1989) 38.
2 B.G. Belenkii, J. Chromatogr., 434 (1988) 337.
3 E.S. Yeung, in E.H. Piepmeier (Ed.), Analytical Applications of Lasers, Wiley-Interscience, New York, 1986, Chap. 17.
4 E.S. Yeung, in F.J. Yang (Ed.), Microbore Column Chromatography, Dekker, New York, 1988, Chap. 4, p. 117.
5 M.D. Morris, in E.S. Yeung (Ed.), Detectors for Liquid Chromatography, Wiley-Interscience, New York, 1986, Chap. 4, p. 124.
6 A. Berthod, Spectrochim. Acta Rev., 13 (1990) 11.
7 C.E. Buffett and M.D. Morris, Anal. Chem., 54 (1982) 1824.
8 Y. Yang and T.V. Ho, Appl. Spectrosc., 41 (1987) 583.
9 M.J. Sepaniak, J.D. Vargo, C.N. Kettler and M.P. Maskarinec, Anal. Chem., 56 (1984) 1252.
10 T.G. Nolan and N.J. Dovichi, Anal. Chem., 59 (1987) 2803.
11 C.E. Buffett and M.D. Morris, Anal. Chem., 55 (1983) 376.
12 T. Berthoud, N. Delorme and P. Mauchien, Anal. Chem., 57 (1985) 1216.
13 S.J. Sheldon, L.V. Knight and J.M. Thorne, Appl. Opt., 21 (1982) 1663.
14 R.J. Bushway, J. Liq. Chromatogr., 8 (1985) 1527.
15 H.C. Furr, A.B. Barua and J.A. Olson, in A.P. De Leenheer, W.E. Lambert and H.J. Nelis (Eds.), Modern Chromatographic Analysis of Vitamins, Vol. 60, Dekker, New York, 2nd edn., 1992, p. 47.
16 K.S. Epler, L.C. Sander, R.G. Ziegler, S.A. Wise and N.E. Craft, J. Chromatogr., 595 (1992) 89.
17 H.J. Nelis and A.P. De Leenheer, Anal. Chem., 55 (1983) 270.
18 R.P.W. Scott and P. Kucera, J. Chromatogr., 185 (1979) 27.
19 C.A. Carter and J.M. Harris, Anal. Chem., 56 (1984) 922.
20 J. Shen, R.D. Lowe and R.D. Snook, Chem. Phys., 165 (1992) 385.
21 A. Chartier, C.G. Fox and J. Georges, Analyst, 118 (1993) 157.
22 J. Georges and J.M. Mermet, Analyst, 114 (1989) 541.

Analytica Chimica Acta, 284 (1993) 317–326
Elsevier Science Publishers B.V., Amsterdam

Comparison of on-line enrichment based on ion-pair and cation-exchange liquid chromatography for the trace-level determination of 3-amino-1,2,4-triazole (aminotriazole) in water

V. Pichon and M.-C. Hennion

Ecole Supérieure de Physique et de Chimie de Paris, Laboratoire de Chimie Analytique (URA CNRS 437), 10 rue Vauquelin, 75005 Paris (France)

(Received 11th June 1993; revised manuscript received 10th August 1993)

Abstract

Aminotriazole is a polar and water-soluble organic pesticide and its preconcentration cannot be performed using either liquid–liquid extraction or solid-phase extraction with reversed-phase sorbents such as C_{18} silica, apolar copolymers or porous graphitic carbon. Aminotriazole can be ionised and its ionisation constants have been measured in order to select the best conditions for both the chromatographic analysis using ion-pair chromatography and the extraction from water in its cationic form. On-line preconcentration based on cation-exchange and ion-pair chromatography have been investigated. Breakthrough volumes measured on small precolumns were higher than 50 ml with spiked deionised LC-grade water and detection limits as low as 0.1 $\mu g\ l^{-1}$ have been obtained. In real samples, a competition with inorganic cations occurs lowering the cation-exchange capacity. A chemical pretreatment consisting of oxalate precipitation and EDTA complexation was applied in order to remove inorganic cations, but the sample volume that could be handled without breakthrough was lower and quantitative determination was obtained at the 0.5 $\mu g\ l^{-1}$ level. The same competition occurred when carrying out preconcentration based on ion-pair chromatography with a precolumn packed with an apolar copolymer that has been preloaded with a sodium dodecylsulfate solution.

Keywords: Liquid chromatography; Ion exchange; Aminotriazole; Trace determinations; Waters

The pesticide 3-amino-1,2,4-triazole (aminotriazole or amitrole) is widely used in France and other European countries as an industrial herbicide, along roads and railway tracks, and also in agriculture in mixed formulations containing other herbicides [1]. Its low volatility and high solubility in water indicate a possible leaching especially in sandy soils [2–4]. The lack of data in environmental water is easily explained by the difficulty of determining this compound at trace levels in water, because there is no efficient analytical procedure allowing its extraction from aqueous samples. Its solubility is low in non-water miscible organic solvents (about 10 mg l^{-1} in methylene chloride) and is 280 g l^{-1} in water, so that its extraction from aquatic media using liquid–liquid extraction is impossible [3]. The logarithm of its water–octanol partition coefficient (K_{ow}) is -0.5, so that this analyte is certainly too polar for being sufficiently retained by the widely

Correspondence to: M.-C. Hennion, Ecole Supérieure de Physique et de Chimie de Paris, Laboratoire de Chimie Analytique (URA CNRS 437), 10 rue Vauquelin, 75005 Paris (France).

SSDI 0003-2670(93)E0479-Q

used C_{18} silica in solid-phase extraction systems. This explains why the only methods of preconcentration described in the literature are evaporation of water [5,6]. Its analysis by gas chromatography is difficult owing to its high polarity and low volatility. A method based on an acetylation with acetic anhydride has been reported [3,4]. Liquid chromatography (LC) is more convenient for this polar analyte, but UV detection is not sensitive owing to its small extinction coefficient. Liquid chromatography with electrochemical detection or with UV detection after derivatization have been described [5–9].

Owing to its molecular structure, this compound can be ionised by adjusting the pH of water samples and therefore, its preconcentration using either cation-exchange or ion-pair extraction can be investigated. When percolating samples through cation-exchange sorbents and looking for less than 1 $\mu g\ l^{-1}$ of an organic cation, the much higher amounts of inorganic cations which are present in natural waters rapidly overload the cation-exchange capacity. A chemical clean-up pretreament consisting of oxalate precipitation of calcium ions and of EDTA complexation of metal ions has been described in order to remove most of the inorganic cations before preconcentration [10–12]. Nevertheless, previous experiments have shown that overloading still occurs rapidly after this pretreatment [13].

For ionisable analytes which are sufficiently retained on reversed-phase sorbents in their neutral form, a two-step preconcentration on two precolumns was carried out [13]. Compounds were first trapped on a non-polar sorbent in their neutral form. After the sample percolation, a second precolumn packed with a cation exchanger was coupled in series with the non-polar one. A small volume of well-deionised water adjusted to acidic pH allowed the analytes to be desorbed from the reversed-phase sorbent in their ionic form and to be preconcentrated again on the cation exchanger. The inherent advantage of this two-step procedure is that detection limits as low as several $ng\ l^{-1}$ have been obtained because of the selectivity of the cation-exchange preconcentration which eliminates many interfering compounds [13–15].

In this work, it is shown that aminotriazole cannot be retained in its undissociated form by reversed-phase sorbents. Therefore, the two-step preconcentration cannot be applied and the direct percolation of samples through the cation exchanger has to be carried out. In the literature, on-line trace enrichment based on ion-pair and cation-exchange extraction has been used for the determination of some aniline derivatives and polar pollutants in river waters from 10 ml samples [11,16]. The sample volume has to be increased for the determination of concentrations of the order of 0.1 $\mu g\ l^{-1}$ in drinking waters. The objective of that work was to investigate both ion-pair and cation-exchange extraction with real drinking water samples containing a high amount of inorganic cations. On-line techniques have been used because they provide more rapid measurements on the main extraction parameters, especially the breakthrough volumes. It has also been shown that it is possible to perform trace-level determinations with the handling of smaller sample volumes in comparison with off-line procedures because the whole amount preconcentrated is on-line transferred into the analytical column and analysed.

EXPERIMENTAL

Apparatus

Percolation of water samples was performed with a Chromatem pump (Touzart et Matignon, Paris). Precolumn elution and analyses were carried out with a Varian 5060 liquid chromatograph (Palo Alto, CA) equipped with a variable-wavelength UV 200 spectrophotometer and a Coulochem Model 5100 electrochemical detector (ESA, Bedford, MA). Precolumn and analytical column switching was accomplished with Rheodyne valves (Berkeley, CA). Quantitative measurements of peak areas were provided by a CR3A integrator-computer from Shimadzu (Kyoto).

Stationary phases and columns

The analytical columns were a 15 cm × 4.6 mm i.d. column prepacked with spherical 10-μm octylsilica RP-8 (Merck, Darmstadt), a 15 cm ×

0.46 cm i.d. column prepacked with 5-μm octadecylsilica Nucleosil C_{18} (Interchim, Paris), a 20 cm × 0.46 i.d. prepacked with 10-μm PRP-1 sorbent (Hamilton, Reno, NV) and a 10 cm × 0.46 cm i.d. column prepacked with 7-μm Hypercarb carbon (Shandon, Runcorn). For the ion-pair extraction, samples were preconcentrated on a 23 mm × 4.6 mm i.d. laboratory-made precolumn and packed with 10-μm PRP-1 sorbent. The cation-exchange precolumn was a 10 mm × 2 mm i.d. stainless-steel precolumn available from Chrompack (Middelburg) which was laboratory-packed with the sulphonic acid-type resin-based cation exchangers BC-X8, 15–20 μm (Benson, Reno, NV).

Chemicals

HPLC-grade acetonitrile was from Rathburn (Walkerburn) and methanol from Prolabo (Paris). LC-grade water was prepared by purifying demineralized water in a milli-Q filtration system (Millipore, Bedford, MA). Other chemicals were from Prolabo, Merck or Fluka (Buchs). Stock solutions of selected solutes were prepared by weighing and dissolving them in methanol. LC-grade water samples were spiked with these solutions at the $\mu g\ l^{-1}$ or $ng\ l^{-1}$ level. Final standard solutions did not contain more than 0.5% methanol.

Analytical procedures

The experimental set-up using a precolumn is now well known and has been described in Ref. 12. The following procedure was adopted for the ion-pair extraction. The PRP-1 precolumn was conditioned with 100 ml of 0.05 M sodium dodecylsulfate (SDS) and with 20 ml of LC-grade water before percolation of the water sample adjusted to pH 3. After flushing it with 2 ml of LC-grade water, the precolumn was coupled to the analytical column and desorption occurred by elution with the analytical mobile phase made of acetonitrile and a solution of 0.05 M SDS adjusted to pH 3 with perchloric acid.

In the preconcentration procedure using a cation-exchange precolumn, the precolumn was first conditioned by 100 ml of a solution of 0.1 M perchloric acid before the percolation of samples which have been adjusted to pH 3 by addition of perchloric acid. The precolumn was coupled to the analytical column and desorption occurred by elution of the same analytical mobile phase as that used in ion-pair extraction.

The pretreatment of natural water samples was made as follows: 0.2 g of sodium oxalate were added to 200 ml of water. The solution was then filtered through a 0.45-μm disk (Millipore) and 0.8 g of EDTA was added. The sample was adjusted to pH 3 with perchloric acid.

RESULTS AND DISCUSSION

As aminotriazole is rather a polar analyte, it should be weakly retained in water by the commonly used sorbents in liquid–solid extraction, i.e., C_{18} silicas or apolar copolymers [17] and ion exchangers should be used. But, in order to select the convenient pH, ionisation constants of aminotriazole have to be accurately known and were determined by simple titration methods.

Determination of ionisation constants

1,2,3- and 1,2,4-triazole heterocycles can become protonated in water with pK_a values of 1.17 and 2.30, respectively [18,19]. It is also reported that 1,2,3-triazole can loose one proton ($pK_a = 9.42$), but no value was found for the 1,2,4-triazole. Owing to the amino group substituted to the triazole ring, aminotriazole may pick up to two protons at acidic pH and also loose one at basic pH.

An aqueous of 0.096 M aminotriazole was titrated by a solution of hydrochloric acid 0.1 M (Fig. 1). The two ionisation constants corresponding to the protonation with one and two protons were determined approximately from experimental values of the initial pH, the pH at the first half equivalence ($pH = pK_{a2}$) and the pH value at the first inflexion point [$pH = 1/2(pK_{a1} + pK_{a2})$]. A similar experimental titration of the same solution was made with 0.1 M sodium hydroxide and the pK_{a3} value corresponding to the loss of one proton was found to 10.6 ± 0.2. More accurate values of ionisation constants were determined by

fitting experimental and calculated titration curves using laboratory-made software [20]. The calculated titration curve with three ionisation constants of 1.6, 4.2 and 10.5 is also represented in Fig. 1 and an excellent agreement can be observed. Aminotriazole can be negatively ionised at pH above 11 and positively ionised at pH below 4.2. The calculated distribution of the different species of aminotriazole depending on the pH are also given in Fig. 1. At pH 3, 90% of the aminotriazole is singly ionised and at pH below 3, there is a mixture of aminotriazoles with one and two positive charges. At pH 7, aminotriazole is not dissociated at all.

These results indicate that preconcentration using cation-exchange or ion-pair chromatography will require an adjustment of the water sample to pH 3 or below.

Determination of chromatographic data

Several methods were tested with the aim of investigating (i) the retention of aminotriazole in its neutral form in water with reversed-phase materials, (ii) the retention in ion-pair chromatography when the aminotriazole is in its cationic form, (iii) its electrochemical detection.

Reversed-phase chromatography. The capacity factor was measured in water–methanol mobile phases with C_{18} silica, the apolar copolymer PRP-1 and the graphitic carbon Hypercarb. No retention at all was obtained with C_{18} silica even in pure water, due to the high polarity of this analyte. PRP-1 usually shows higher retention for aromatic compounds due to stronger interactions between the aromatic matrix of the styrene divinylbenzene polymer and the π cloud of the double bonds in the solute molecule [21,22]. Aminotriazole is slightly retained in water ($k' = 0.5$) (as shown in Table 1). Previous studies have indicated a higher affinity of the graphitic carbon for polar analytes [22,23] and this is confirmed here by the higher value of the capacity factor of 5 in water. Nevertheless, this value is not high enough to allow preconcentration from a suffi-

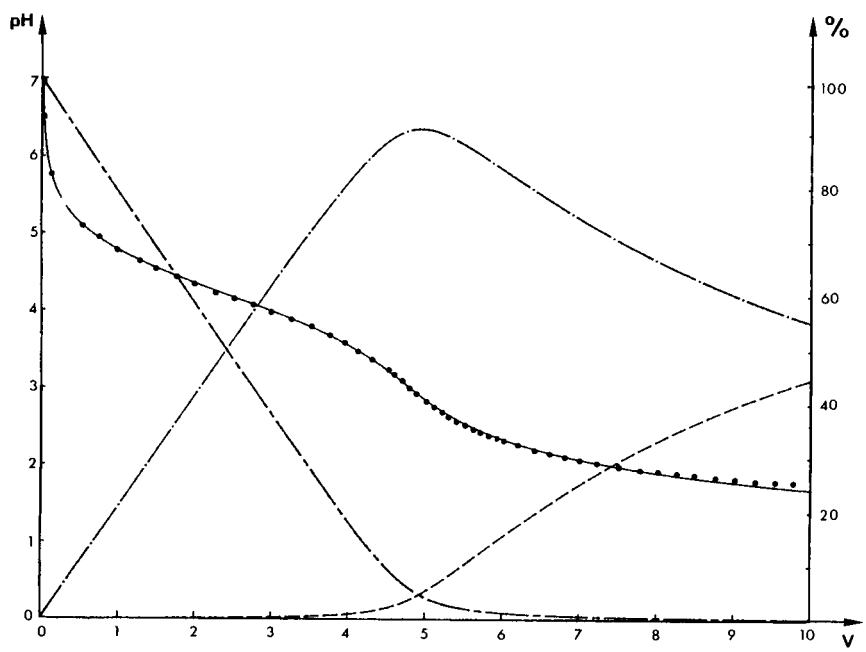

Fig. 1. Experimental (●) and simulated (———) pH titration curves of 5 ml of a solution of aminotriazole at a concentration of 0.096 M by addition of a volume (V, in ml) of 0.1 M HCl solution. The pK_a values used for the calculations of the simulated curve are 1.6, 4.2 and 10.5. The distribution in % of the forms of aminotriazole have been calculated and corresponds to (– – –) undissociated form, (–·–) cationic form with one proton and (- - - - -) cationic form with two protons.

ciently large volume. As predicted from the K_{ow} value, it is impossible to extract aminotriazole from water samples using liquid–solid extraction with reversed-phase sorbents.

Ion-pair chromatography. The capacity factor was measured using a C_{18} and a C_8 silica analytical column and various mobile phases were made of acetonitrile and a solution of 0.05 M sodium dodecylsulfate adjusted to pH 3 with perchloric acid. The variations of the logarithm of the capacity factor with the acetonitrile content are represented in Fig. 2. Capacity factors obtained with ion-pair chromatography are much higher than those in reversed-phase chromatography. The retention increases when the acetonitrile content in the mobile phase decreases, which is easily explained by the fact that the amount of counter-ion that is fixed on the C_{18} or C_8 silica is higher at low acetonitrile content. As expected also, a higher retention is obtained with C_{18} silica than with C_8 silica.

Therefore, ion-pair chromatography allows an easy determination of aminotriazole and the retention time, which is a characteristic parameter in the identification of aminotriazole in unknown samples, can be chosen by selection of the acetonitrile content of the mobile phase. Figure 3 represents the variation of the capacity factor

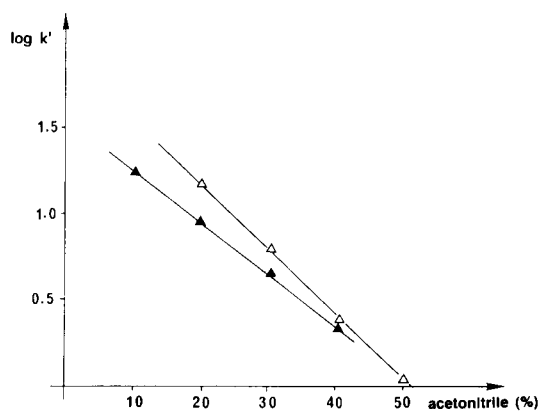

Fig. 2. Variations of the capacity factor with the acetonitrile content (%) of the mobile phase. (△) C_{18} column, 15 cm × 0.46 cm i.d., (▲) C_8 column, 15 cm × 0.46 cm i.d. Mobile phase: 0.05 M SDS adjusted to pH 3 with perchloric acid and acetonitrile.

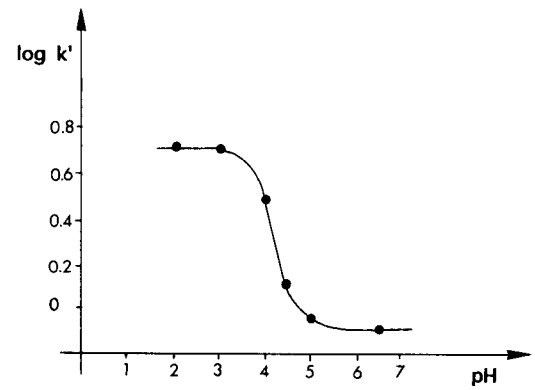

Fig. 3. Variation of the capacity factor of aminotriazole with the pH of the mobile phase. Analytical column: RP 8, 15 cm × 0.46 cm i.d.; mobile phase: 30% acetonitrile with 0.05 M SDS adjusted to different pH with perchloric acid.

with the pH of the mobile phase. The capacity factor decreases with increasing pH and aminotriazole is no longer retained above pH 5 because it is in its neutral form. These measurements provide also a rapid way for the determination of the ionisation constant which can be estimated at the inflexion point. The capacity factor is not increased at pH 2 although the content of doubly-charged analyte is higher than at pH 3.

The high retention in water indicates also that preconcentration based on ion-pair chromatography will allow the handling of a larger volume than reversed-phase chromatography.

Electrochemical detection. UV and electrochemical detection were coupled in series to the analytical column. The UV response is low and the detection limit at 210 nm is about 50 ng injected. However, UV detection is useful for the confirmation of aminotriazole in unknown samples; a weak signal or zero signal (depending on the concentration) should be recorded at the retention time of aminotriazole in the UV chromatogram. The electrochemical response was found to be much higher than the UV response and the maximal signal was obtained by setting up the potential at 0.85 V (vs. Ag/AgCl). The response was linear in the range of 1–500 ng injected. The advantage of a highly porous carbon electrode which allows the column eluent to flow through the electrode is that reproducibility

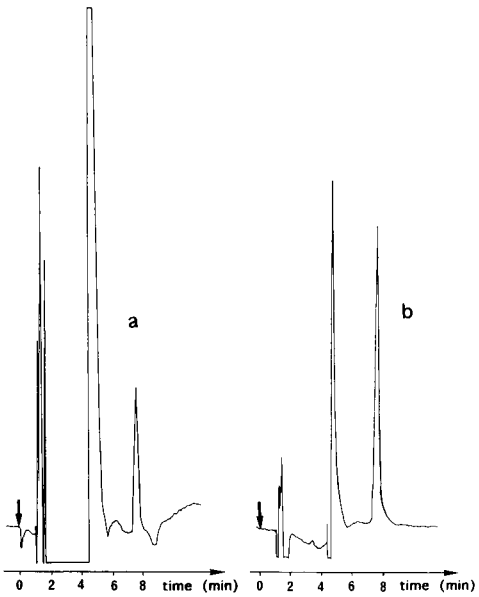

Fig. 4. Detection limit and system peaks. Column: C_{18} silica, 5 μm, 15 cm×0.46 cm i.d.; mobile phase: 65% 0.05 M SDS at pH 3 with perchloric acid and 35% acetonitrile; electrochemical detection at 0.85 V (vs. Ag/AgCl). (a) Injection of 100 μl of a 0.05 mg l^{-1} solution, 1 μA full scale and (b) injection of 100 μl of a 0.5 mg l^{-1} solution, 5 μA full scale.

was obtained over a long period. The detection limit can be calculated from Fig. 4a which represents the chromatogram corresponding to an injection of 100 μl of a solution containing 50 μg l^{-1} of aminotriazole, i.e., an amount injected of 5 ng. The detection limit is around 1 ng (signal-to-noise ratio of 5) and is of the same order than that reported by Pachinger et al. [6]. These workers calculated that by evaporation of 5 ml of water and by injection of a 250 μl extract, aminotriazole can be detected at a 0.1 μg l^{-1} concentration. But they also mentioned that the shortcoming of their method was a fast contamination of the glassy carbon electrode of the amperometric detector which required a regeneration of the electrode surface after each determination. This is a severe shortcoming of the method for quantitative measurements and also because after each regeneration, the stability of the detector at a very low attenuation range is often not obtained rapidly. It is also important to note in Fig. 4a that a large peak is obtained at the beginning of the chromatogram, owing to the injection of a relatively large volume of 100 μl. This peak system does not appear at the void volume of the column as can be seen in Fig. 4b, when injecting a more concentrated solution. The retention time of this system peak depends on the solvent used for the preparation of the standard solution. It was also noticed that these peaks were more important with the C_{18} silica than with the C_8 silica. On-line techniques were performed with the C_8 analytical column, although the efficiency was lower. The detection limit was 3 ng injected with this column.

Taking into account that 1 ng is the detection limit of the system and that, with on-line techniques, the total amount preconcentrated is transferred into the analytical column, a rapid calculation indicates that the preconcentration from a volume of 10 ml will allow a limit of detection of 0.1 μg l^{-1}. But, previous studies have shown that there is always a difference between detection limits obtained with spiked LC-grade water samples and spiked real samples, because of the presence of interfering species that are preconcentrated and that co-elute with analytes of interest. If quantitative determinations are required at the 0.1 μg l^{-1} level, the detection limit obtained with LC-grade water samples has to be about 30 ng l^{-1}. That means that it will be necessary to handle at least a volume of 30 ml of natural water without breakthrough of aminotriazole.

Preconcentration

The on-line methodology was selected for studying the sample volume that can be handled without breakthrough of aminotriazole. As de-

TABLE 1

Variation of the aminotriazole capacity factor with the methanol content of the mobile phase (pH 7) measured on PRP-1 and Hypercarb columns

Column	Methanol content (%)			
	0	10	20	30
PRP-1	0.52	0.31	0.19	0.15
Hypercarb	5.0	2.0	0.83	0.15

scribed above, the two preconcentration procedures are based on ion-exchange and ion-pair chromatography and the inherent problem of removing inorganic cations has to be studied in detail.

Cation-exchange extraction. A precolumn (1 cm × 0.2 cm i.d.) packed with a polymer-based cation exchanger has been selected owing to the higher capacity of polymer-based over silica-based cation exchanger [11]. The coupling of the cation-exchange precolumn and the chromatographic characterisation by ion-pair chromatography was first studied by comparison of direct-loop injection of 0.5 μg and the on-line preconcentration of a 30 ml sample of LC-grade water spiked with 16.7 μg l^{-1} of aminotriazole and therefore containing also 0.5 μg. The results are shown in Fig. 5a and b, respectively. The peak of aminotriazole in Fig. 5b after elution from the cation-exchange precolumn is larger and smaller than that in Fig. 5a.

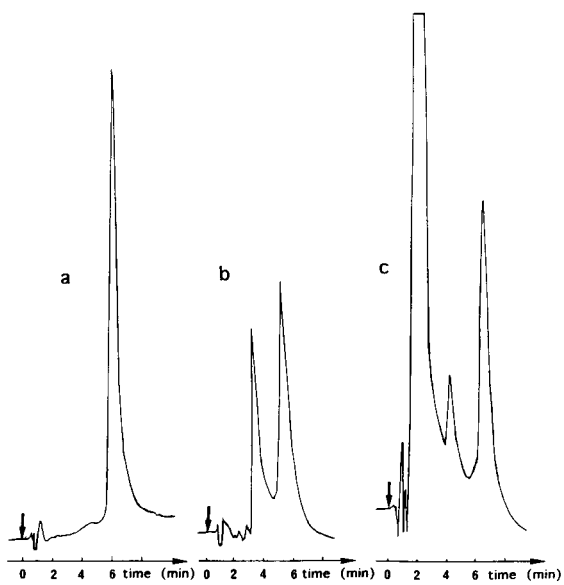

Fig. 5. Comparison of (a) direct injection, (b) on-line preconcentration using the cation-exchange precolumn and (c) on-line ion-pair extraction with the PRP-1 precolumn of a 30 ml LC-grade water sample spiked with 16.7 μg l^{-1} of aminotriazole. Analytical column: RP 8, 10 μm, 15 cm × 0.46 cm i.d.; mobile phase: 30% acetonitrile and 70% 0.05 M SDS adjusted to pH 3; electrochemical detection at 0.85 V (vs. Ag/AgCl), 5 μA full scale.

TABLE 2

Variations of the recovery with the sample volume using a cation-exchange precolumn or ion-pair preconcentration with a PRP-1 precolumn previously loaded with SDS (Concentrations have been adjusted in order to have 0.5 μg of aminotriazole in each sample. Recoveries were calculated according to Ref. 21)

Precolumn	Volume (ml)									
	10	25	50	70	80	90	100	150	175	200
Cation exchanger	100	102	98				97	98	73	50
PRP-1 with SDS	100	95	97	98	65	30				

This is due to the band broadening that occurs when transferring the compound from the precolumn to the analytical column with the isocratic mobile phase. No difference was observed when eluting the precolumn in the backflush way. A large system peak is also observed.

The breakthrough volume was estimated first with LC-grade (deionised) spiked solution adjusted to pH 3 by perchloric acid, according to an experimental method described in Ref. 21. The results are reported in Table 2 and the breakthrough volume can be estimated to 150 ± 10 ml. It was therefore possible to obtain quantitative results below the 0.1 μg l^{-1} level in LC-grade water samples. The regeneration of the cation-exchange precolumn was obtained with 100 ml of 0.1 M perchloric acid at each analysis.

Application to spiked raw drinking water samples containing high amounts of inorganic cations were then carried out. First, 30 ml of drinking water spiked with 16.7 μg l^{-1} were percolated through the cation-exchange precolumn and no signal was obtained when the precolumn was eluted on-line. The capacity of the ion exchanger has obviously been overloaded with ionic inorganic cations. A new precolumn was packed and the chemical pretreatment consisting of oxalate precipitation and EDTA complexation was applied to the spiked sample before percolation. In comparison with the results obtained with the same volume of deionised LC-grade spiked water, the recovery was 18%. The chemical pretreat-

ment was closely examined and the solubility of calcium oxalate was found to increase slightly at acidic pH. Therefore, sodium oxalate was added to the raw sample and filtration was carried out in order to remove the precipitate before addition of EDTA and acidification to pH 3. Three similar experiments with different drinking water samples chemically pretreated led to average recoveries of $20 \pm 7\%$. Regeneration of the precolumn could not be realized with 100 ml of perchloric acid and a new precolumn has to be prepared each time. The conclusions are that (i) there is a great difference between the handling of LC-grade water samples and real sample; (ii) the chemical pretreatment does not totally remove inorganic cations and there is still a competition between ionised aminotriazole and traces of inorganic cations. The treatment is either not reproducible or depends on the nature of the drinking water samples, as shown by the poor reproducibility of recoveries; (iii) the sample handling of a 30 ml sample volume is not possible and quantitative determination at the 0.1 $\mu g\ l^{-1}$ level cannot be obtained with the on-line system; (iv) since regeneration of the precolumn is impossible, an off-line method should certainly be more convenient provided that inorganic cations can be efficiently removed.

Ion-pair extraction. Taking into account the results obtained with ion-exchange extraction, a larger precolumn was selected (2.3×0.46 cm i.d.) and packed with the copolymer PRP-1. After conditioning with a solution of 0.05 M SDS and water, 30 ml of LC-grade water spiked with 16.7 $\mu g\ l^{-1}$ of aminotriazole were preconcentrated and on-line analysed. The chromatogram is represented in Fig. 5c. By coupling preconcentration and analysis both based on ion-pair, a better coupling was expected. In fact, the peak is slightly higher in Fig. 5c in comparison with Fig. 5b, but the band broadening is of the same order and is due to the large dimension of the precolumn [12,21].

The breakthrough volume was measured using the same method as described with the cation-exchange precolumn. Results are reported in Table 2. The breakthrough volume is about 70 ml and is lower than that obtained with the much smaller cation-exchange precolumn. This is inherent to the ion-pair mechanism. The PRP-1 loaded with SDS acts as dynamic cation exchanger with a lower capacity in comparison with the capacity of the fixed polymeric cation exchanger.

The results obtained after percolation of 30 ml of chemically pretreated and spiked drinking water with 16.7 $\mu g\ l^{-1}$ gave an average recovery of 15%. The effect of the inorganic interferences is exactly similar to that observed with ion-exchange extraction. The sample volume was therefore reduced to 10 ml and the recovery was around 20% without any pretreatment and around 70% with the pretreatment.

Different results have been reported by Brouwer et al. [16] who reported that the advantage of ion-pair extraction was that precipitation and complexation were superfluous. They found out that no chemical pretreatment was necessary for the trace-level determination of aniline and chloridazon [3(2*H*)-Pyridazinone-5-amino-4-chloro-2-phenyl] from a 10 ml sample using on-line ion-pair extraction with a similar copolymer (PLRP-S) loaded with a solution of SDS. They did not observe any difference after spiking tap water with 500 $mg\ l^{-1}$ of calcium chloride. One explanation is that ion pairs formed with ionised aniline or chloridazon are certainly more hydrophobic than those formed with ionised aminotriazole. The difference in hydrophobicity between aniline and aminotriazole can be estimated from the difference in the logarithm of the water–octanol constant which is 0.9 for aniline and -0.5 for aminotriazole. During the percolation of natural samples, a competitive process occurs between ion pairs formed with inorganic cations and those formed with organic cations. When ion pairs are hydrophobic, this competitive process is in favour of the sorption of hydrophobic cations and the effect of interfering inorganics is weak. Since the ion pairs formed with aminotriazole are more polar, the competitive process is more important and the ion-pair extraction is then closer to a simple ion-exchange mechanism.

As pointed out by the same authors, it was also found that one advantage of ion-pair extraction over cation-exchange extraction is the easy regeneration of the precolumn which is simply reloaded

with a solution of 0.05 M SDS after analysis of drinking water samples.

Detection limits

Taking into account the detection limit of the system, it was shown that the handling of at least a volume of 30 ml without breakthrough was necessary for quantitative measurements at the 0.1 $\mu g\ l^{-1}$ level. The average recoveries of 20% with a 30 ml sample or of 70% with a 10 ml sample indicate that quantitative determination cannot be obtained accurately below the 0.5 $\mu g\ l^{-1}$ level in drinking water samples containing high amounts of inorganic compounds. About 50% of the drinking water in the area of Paris originates from river water after purification in a treatment plant and therefore contains higher amounts of inorganics than some ground waters. The detection limit was also experimentally determined using on-line ion-pair extraction with 30 ml of drinking water samples spiked with amounts of aminotriazole in the 1–15 $\mu g\ l^{-1}$ range. The calibration graph was only roughly linear ($r = 0.98$ with 5 data points) which is due to the poor reproducibility of the chemical pretreatment. The relative standard deviation obtained from three experiments with drinking water samples from the same origin and spiked with 5 $\mu g\ l^{-1}$ was 13%. The detection limit calculated with a signal-to-noise ratio of 5 was 0.4 $\mu g\ l^{-1}$.

Off-line preconcentration using simple evaporation of the water in samples was also carried out. A sample volume of 100 ml of LC-grade water spiked at the 0.1 $\mu g\ l^{-1}$ level was evaporated to dryness and the residue dissolved in 300 μl of the mobile phase used for the chromatographic characterization by ion-pair chromatography. Quantitative determination at the 0.1 $\mu g\ l^{-1}$ was obtained. The same experiment was performed with a drinking water sample containing a high amount of inorganic cations. It was impossible to dissolve the residue in less than 1 ml of the mobile phase. The peak systems were broad due to the inorganic salts that were also preconcentrated, so that the retention time of aminotriazole has to be delayed and the detection limit of 0.1 $\mu g\ l^{-1}$ was not obtained.

The difference in detection limits obtained with LC-grade water and real water samples is large, whatever the preconcentration techniques may be, showing the necessity of always studying real spiked samples when setting up a new method.

Conclusions

Results from the literature have shown that preconcentrations based on ion-exchange or on ion-pair chromatography can be performed with moderately polar organic cations such as aniline. Nevertheless, their application to more polar organic cations such as aminotriazole has shown that competition from inorganic cations does not allow the handling of a large volume of natural samples pointing out the necessity of always testing the methodology with real samples. Our experimental results demonstrate that more efficient and reproducible methods have to be carried out which are able to remove inorganic cations, in order to obtained the detection limits required in drinking water by the EEC regulations. New methods involving chelating sorbents are now under investigation.

REFERENCES

1 M. Fielding, D. Barcelo, A. Helweg, S. Galassi, L. Tortenson, P. Van Zoonen, R. Wolter and G. Angeletti, in Pesticides in ground and drinking water, Water Pollution Research Report 27, Commission of the European Communities, Directorate-General for Science, Research and Development, 1991.
2 D. Barcelo, Analyst (London), 116 (1991) 681.
3 J.M. van der Poll, M. Vink and J.K. Quirijns, Chromatographia, 25 (1988) 511.
4 J.M. van der Poll, M. Vink and J.K. Quirijns, Chromatographia, 30 (1990) 155.
5 M.F. Legrand, E. Costentin and A. Bruchet, Environ. Technol., 12 (1991) 985.
6 A. Pachinger, E. Eisner, H. Begutter and H. Klus, Fresenius' J. Anal. Chem., 342 (1992) 413.
7 H. Lokke, J. Chromatogr., 200 (1980) 234.
8 A.W. Archer, J. Chromatogr., 303 (1984) 267
9 W. Ternes and H.A. Rüssel-Sinn, Fresenius' Z. Anal. Chem., 326 (1987) 757.
10 M.W.F. Nielen, U.A.Th. Brinkman and R.W. Frei, Anal. Chem., 57 (1985) 806.

11 M.W.F. Nielen, U.A.Th. Brinkman and R.W. Frei, J. Chromatogr., 317 (1984) 557.
12 M.W.F. Nielen, R.W. Frei and U.A.Th. Brinkman, in R.W. Frei and A. Zech (Eds.), Selective Sample Handling and Detection in High-performance Liquid Chromatography, Part A, Elsevier, Amsterdam, 1988, Chap. 1, pp. 5–80.
13 M.-C. Hennion, P. Subra, V. Coquart and R. Rosset, Fresenius' J. Anal. Chem., 339 (1991) 488.
14 V. Coquart and M.-C. Hennion, J. Chromatogr., 585 (1991) 67.
15 V. Coquart, P. Garcia Camacho and M.-C. Hennion, Int. J. Environ. Anal. Chem., 52 (1993) 99.
16 E.R. Brouwer, I. Liska, R.B. Geerdink, P.C.M. Fintrop, W.H. Mulder, H. Lingeman and U.A.Th. Brinkman, Chromatographia, 32 (1991) 445.
17 M.-C. Hennion, Trends Anal. Chem., 10 (1992) 318.
18 A. Albert, in A.R. Katritzky (Ed.), Physical Methods in Heterocycle Chemistry, Vol. 1, 1963, Academic Press, New York, pp. 45 and 96.
19 D.D. Perrin, Dissociation Constants of Organic Bases in Aqueous Solutions, IUPAC Series, Butterworths, London, 1965.
20 R. Rosset, D. Bauer and J. Desbarres, Chimie Analytique des Solutions et Informatique, Masson, Paris, 1991, Chap. 2, pp. 7–39.
21 P. Subra, M.-C. Hennion, R. Rosset and R.W. Frei, J. Chromatogr., 456 (1988) 121.
22 V. Coquart and M.-C. Hennion, J. Chromatogr., 600 (1992) 195.
23 M.-C. Hennion and V. Coquart, J. Chromatogr., 642 (1993) 211.

Analytica Chimica Acta, 284 (1993) 327–335
Elsevier Science Publishers B.V., Amsterdam

Multi-element speciation of trace metals in fresh water adapted to plasma source mass spectrometry

Conny Haraldsson, Benny Lyvén, Marianne Pollak and Annelie Skoog

Department of Analytical and Marine Chemistry, University of Göteborg and Chalmers University of Technology, S-412 96 Göteborg (Sweden)

(Received 21st January 1993; revised manuscript received 11th August 1993)

Abstract

A method for speciation of trace metals at natural concentration levels has been developed. The speciation is carried out in a cleanroom laboratory and the determination is performed with an ICP–MS. The method is based on fractionation of metal species on three adsorbents, Chelex-100, Sep-Pak C-18 and Fractogel DEAE. The method distinguishes between labile complexes, non-polar organic adsorbable matter and ion exchangeable substances. The filtered water samples are pumped through columns with the adsorbents. Following a prefraction, samples for determination of metal concentrations are taken. The adsorbents are not eluted. After extensive cleaning, the used adsorbents have blank values that are low enough for trace metal analysis in fresh water. Concentration and speciation data for Al, Cd, Co, Cu, Fe, Pb, Mn, Mo, Ni and Zn are obtained.

Keywords: Mass spectrometry; Metal speciation; Trace metals; Waters

It is becoming increasingly clear that the total concentration of a metal in an ecosystem gives only a limited amount of information about its effects. Morel et al. [1] state that only a few metal species are available to plankton, since most metal uptake occurs using a complexing agent produced by the plankton. The uptake mechanism includes a reaction step where M^{n+} reacts with the chelator [1], either as active sites in a cell membrane or as an excreted chelator. Thus, essentially only rapidly dissociating complexes, with a formation constant below a certain value, are available for uptake.

In waters with a lowered pH due to acid precipitation, there is likely to be an increase of the inorganic fraction of trace metal species. This is of environmental importance because the inorganic fraction is the most active fraction in biological systems. A metal can either have toxic effects [2] or function as a nutrient [1]. In both cases, changes in the metal species present can have a significant impact on a biological system.

The term lability is used to describe the availability of an ion for biological reactions. This can be simulated by extraction with Chelex-100 during a specified time [3,4] or by electroactivity [2]. The electrochemical response, which depends on the ability of the complex to dissociate at the surface of the electrode, can be considered to be analogous to parts of the uptake mechanism in a biological cell [2].

One of the earliest and most well known speciation schemes is the one presented by Florence and Batley [5] and modified by Florence [6]. The authors distinguish between total concentration and several groups of anodic stripping voltammetry (ASV) labile metals. Further fractions are defined based on the fraction that adsorbs to

Correspondence to: C. Haraldsson, Department of Analytical and Marine Chemistry, University of Göteborg and Chalmers University of Technology, S-412 96 Göteborg (Sweden).

SSDI 0003-2670(93)E0473-K

Chelex-100 with or without pre-treatment, e.g. UV irradiation. Electrochemistry is still frequently used for the speciation of trace metals. Coale and Bruland [7] used ASV to study copper speciation in sea water. They found that > 99.7% of the dissolved copper in the upper 100 m of the north-east Pacific is complexed by organics.

Other types of speciation includes methods where different species are adsorbed to matrixes with well-defined chemical properties. Resins containing the diethylaminoethyl (DEAE) functional group have been used to collect dissolved humic substances from natural waters around neutral pH, and would be predicted to collect anionic metal–organic complexes as well [8].

Lipophilic matter in natural waters includes small, often highly toxic metal complexes [9] and humic substances. This fraction can be collected with a non-polar adsorbent, e.g., C-18 chains immobilised on silica gel [10]. The immobilised C-18 was used to quantify a fraction of copper bound to organics in the Pacific Ocean [11]. The fact that C-18 has affinity for both small lipophilic compounds and humic substances raises questions about its usefulness for speciation studies, since these two groups of substances have different biological effects. However, it is included for comparison since it has been used in previous studies.

Theoretical calculations are an alternative approach to experimental work in elucidating metal speciation. These are of only limited value in practice, since knowledge of the species present and the equilibrium constants needed to describe the system is incomplete. There is no doubt that a significant amount of metal is complexed in the natural environment, but for any given stream the relative importance of organic to inorganic metal binding can be evaluated only after experimental studies. Thus, the experimental approach is the most relevant at present.

Humic substances comprise a general class of biogenic, refractory, yellow–black, organic substances known to be ubiquitous to all environments including soils, ground waters, streams, estuaries, and oceans. The concentrations and characteristics of humic substances vary with water mass and time. Humic substances have strong complexing abilities and carry significant amounts of metal [12]. Humic complexes often show low lability, and it has been shown that the presence of humic matter decreases the toxicity of metal ions [13]. An interesting observation made by Forsberg [14] is that the concentration of humic matter has increased by 5–20% in Swedish lakes over the past 20 years.

The aim of this work is to separate different fractions of metals in fresh water. The metals divide into three fractions. Metal bound to polar organic compounds, non-polar organic compounds and labile metal complexes. Since the use of the inductively coupled plasma mass spectrometry (ICP–MS) technique is becoming widespread, the development of a speciation method with special attention to ICP–MS is considered useful. The multielement capacity of the instrument makes it possible to study the speciation of the elements Al, Mn, Fe, Co, Ni, Cu, Zn, Mo, Cd, and Pb simultaneously.

EXPERIMENTAL

Reagents

All experimental work, except filtration of the samples, is done in a clean room laboratory (a positive pressure laboratory with Class-100 filtered air supply).

High purity water is prepared using a Milli-Q (Millipore) system. Calcium chloride (2 M) is prepared from calcium chloride dihydrate (Merck p.a.). Sodium hydroxide (2 M) is prepared from sodium hydroxide pastille p.a. (EKA Bohus). High-purity acids are prepared in the clean lab by sub boiling point quartz distillation of analytical grade HCl and HNO_3.

Sampling

Sampling bottles made of polyethylene are extensively cleaned as described by Danielsson et al. [15]. The samples are collected and immediately filtered. There is no further manipulation of the samples before they are passed through the columns with adsorbent. The samples are pumped over the adsorbents within 24 h after collection.

Filtration

The filters are 0.45 μm pore size cellulose acetate filters (Millipore HA) with a diameter of 45 mm, cleaned by soaking in 0.5 M HCl for at least two weeks. Prior to sampling, the filters are rinsed with Milli-Q water several times to obtain a pH > 5. After sampling the filtration is done immediately.

Adsorbents

The adsorbents used are: Chelex-100 with 200–400 mesh pore size (Bio-Rad); Fractogel TSK DEAE-650 with 200–400 mesh pore size (Merck) and Sep-Pak C-18 cartridges (Waters).

Chelex collects free metal ions and ions in complexes that dissociate to be available for Chelex during the passage through the column. The DEAE resin retains humic complexes and the metal ions that are bound to these complexes. The C-18 traps non-polar organic compounds.

Pretreatment of adsorbents

Chelex-100 consists of iminodiacetate groups on a styrene–divinylbenzene matrix. The resin is cleaned and transferred to its calcium form according to the method of Figura and McDuffie [3] with minor modifications because of blank problems. The problems came from contaminated calcium chloride. To remove the impurities, 1 g of Chelex was added to 100 ml 2 M calcium chloride and the mixture was shaken for 30 min. After allowing 30 min for the resin to settle, the supernatant was withdrawn. The procedure was repeated twice.

Fractogel TSK consists of diethylaminoethyl groups on a styrene–divinylbenzene matrix. Before use the resin is cleaned using the following procedure: It is first soaked in a mixture of toluene and methanol with 1 M HCl and 10 M HF for approximately 1 week. The organic solvents are used in order to swell the resin, making it more susceptible to cleaning. HF is used since it is effective in removing iron without being too aggressive towards the resin. The TSK matrix contains iron at levels that make it necessary to take these precautions. Following this the resin is rinsed with 1 M HCl and then soaked in 0.1 M HCl for at least 2 weeks. The same acid concentration is also used for storage, since the low pH prevents bacteria from destroying the DEAE groups. Immediately prior to sample treatment and as a final cleaning and conditioning step, 1 ml of the resin is rinsed first with 50 ml of a mixture of 0.1 M HNO_3 and 2 M HCl and then twice with 50 ml Milli-Q water.

Sep-Pak C-18 cartridges have a silica bonded C-18 phase and adsorbs non-polar species. Before use, the cartridges are cleaned with 100 ml of 0.6 M HCl, 100 ml of methanol–water (1:1), followed by 200 ml of water. This procedure is repeated twice, the last time being just prior to use.

Apparatus

For pH measurements we use a Ross combination electrode Model 81-55 (Orion Research). It is calibrated with Orion low ionic strength pH buffers with pH 6.97 and pH 4.10.

The instrument, a plasma source mass spectrometer (ICP–MS), employed is a VG-PQ 1 with a PQ 1 + sampling interface (VG Elemental), furnished with a Babbington V-grove nebulizer. The sample uptake rate is 0.9 ml/min and we use a standard Scott spray chamber cooled to 10°C. The plasma torch is of the standard quartz design, mounted at a distance of 10 mm from the nickel sampling cone. The instrument is tuned to get a maximum response at mass 115 Indium. The sensitivity varies between 9×10^6 counts s^{-1} ppm^{-1} and 30×10^6 counts s^{-1} ppm^{-1}. Table 1 gives the operating conditions of the ICP–MS.

A Gilson 222 autosampler is used. A waiting time of 60 s is used to allow the sample to reach the nebulizer and equilibrate with the spray chamber. Between the samples the system rinses for 20 s with Milli-Q water. The short rinsing

TABLE 1

Operating conditions for the ICP–MS

Cool gas flow	13 l/min
Auxiliary gas flow	0.9 l/min
Nebulizer gas flow	0.9 l/min
RF power	1300 W
Sampling cone orifice	1.0 mm
Skimmer cone orifice	0.7 mm

time is possible after the construction of a system with two channels, controlled by magnetic valves positioned close to the nebulizer. One of the channels connects the nebulizer to a tube through which 1% nitric acid is pumped and the other channel introduces the sample. After completing the data acquisition, the valves are automatically set to the rinsing position. This makes it possible to rinse the system while there is still sample in the tubing from the autosampler. The advantage, apart from a higher sample throughput, is reduction by approximately one-third of the sample amount reaching the plasma. This decreases the drift in sensitivity caused by the formation of a salt layer on the cones.

When data is acquired the following parameters are used: 3 points per mass, 0.04 a.m.u. apart. The selected masses (Table 2) are scanned 20 times with the dwell times shown in Table 2. The analysis time is less than 3 min per sample including rinsing and sample uptake.

The detection limits of the instrument, with the conditions described above, are shown in Table 3. Detection limits of an ICP–MS depend on two things; the sensitivity and the background signal. The signal caused by photons reaching the detector sets the lower limit for the background signal at 5–20 Hz, but in the low nM range carry over from previous samples and standards will increase this background. Table 3 presents the detection limits calculated as 3σ for samples containing Milli-Q water and nitric acid (0.015 M) placed between the natural samples in the run. The relatively poor detection limits, as compared with other reported for ICP–MS, depend on the short rinsing time used to increase sample throughput. The detection limits are significantly lower when only low concentration standards and blanks are analysed. In the river samples analysed, cadmium is the only element with a concentration that is not always well above the instrumental detection limits.

TABLE 2

Data acquisition parameters for ICP–MS

Element	Mass	Dwell s/point
Aluminium	27	0.1
Cadmium	114	0.2
Cobalt	59	0.2
Copper	65	0.1
Iron	57	0.1
Lead	208	0.1
Manganese	55	0.1
Molybdenum	98	0.1
Nickel	60	0.1
Zinc	66	0.1

TABLE 3

Detection limits calculated as 3σ for blanks inserted in a normal run and the concentration ranges found in natural samples

Element	Detection limit (μg/l)	Concentration range (μg/l)
Aluminium	0.05	25–200
Cadmium	0.002	0.005–0.07
Cobalt	0.01	0.04–1.2
Copper	0.03	0.5–1.9
Iron	3.0	55–1700
Lead	0.001	0.10–0.95
Manganese	0.05	30–100
Molybdenum	0.01	0.03–0.5
Nickel	0.1	0.6–1.8
Zinc	0.10	3–20

In the storage experiment, a Perkin Elmer 4000 atomic absorption spectrophotometer with a HGA 400 graphite furnace and an AS 40 autosampler was used.

Method

The speciation is performed in a cleanroom laboratory, supplied with class 100 filtered air. In the cleanroom, the filtered samples are split into fractions to determine the dissolved fraction and the fractions that adsorb to Ca–Chelex, DEAE and C-18. The adsorbable fractions are determined in the following way: approximately 150 ml filtered water is transferred to each of three PTFE separatory funnels. The funnels are connected with a polyethylene column containing 1 ml pre-cleaned Chelex, DEAE or a pre-cleaned Sep-Pak cartridge. The samples are pumped through the adsorbents at a flow-rate of 2 ml/min using a peristaltic pump (Gilson Minipuls 2). To condition the columns, 100 ml of sample is pumped through and discarded as a prefraction. The following 15 ml is collected in a polyethylene

test tube that has been cleaned in the same way as the sample containers [15]. The sample is acidified to 0.15 M with HNO_3 before storage.

RESULTS AND DISCUSSION

Storage of samples

To study the effects of storage, a sample was collected in the river Säveån, a small river close to Göteborg on the Swedish west coast. The sample was filtered immediately after collection and divided into four sub samples. These samples were speciated immediately and after one, two, or three days storage in a refrigerator. Owing to technical problems with the ICP–MS we used graphite furnace atomic absorption spectroscopy (GFAAS) for the determinations. The only elements that could be determined with a sufficient precision with GFAAS at these concentrations were aluminium, copper, iron and zinc (Fig. 1).

The results show that the samples are quite stable during short term storage. With the possible exception of zinc, storage for up to 3 days before speciation does not significantly affect the results. This is in agreement with the storage stability for aluminium species found by others [16].

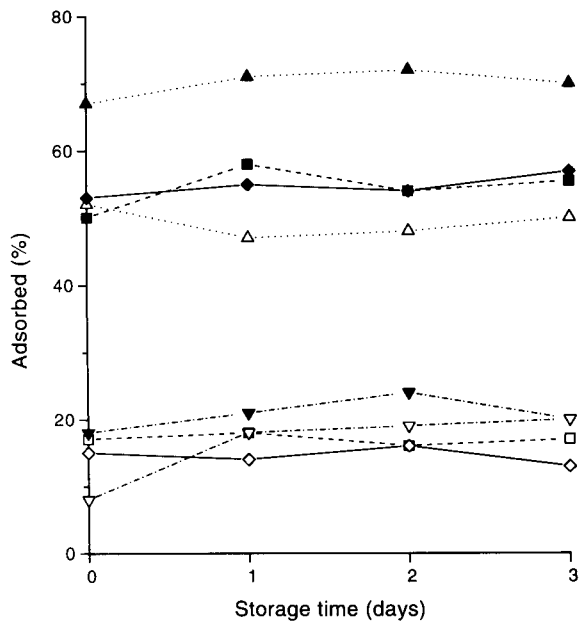

Fig. 1. Change in speciation as an effect of sample storage. The fraction of metal adsorbed on DEAE (filled symbols) and C-18 (open symbols). □ = Al; △ = Cu; ◇ = Fe; ▽ = Zn.

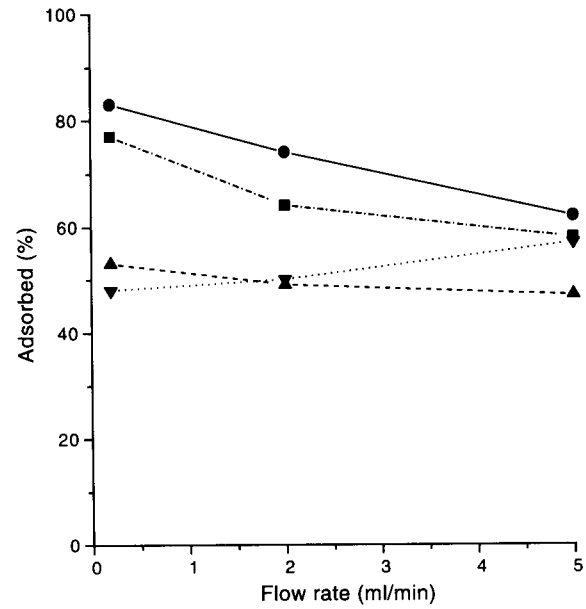

Fig. 2. The fraction of metal adsorbed on DEAE versus flow-rate. ■ = Al; ▲ = Cu; ● = Fe; ▼ = Pb.

Choice of flow-rates

The significance of the contact time between sample and adsorbent has been discussed in detail for Chelex-100 [4]. In the work mentioned above, the metal fraction collected on a column with 6–9 s contact time is defined as labile to moderately labile. This contact time was achieved using a column (0.8 cm i.d.) packed with 1.3 g Chelex-100 and a flow-rate of 2–3 ml/min.

The influence of flow-rate on the collection of organically complexed copper with C-18 in sea water has been studied [11]. No significant difference was found in the amount of copper adsorbed when varying the flow-rate between 5 and 30 ml/min.

To study the influence of flow-rate on DEAE we used a river water with a pH of 7.0 and a DOC content of 4.9 mg/l. Figure 2 shows the results for aluminium, copper, iron and lead. The dependence of flow-rate on the adsorbtion of the

other metals discussed in this paper have also been studied and no significant difference was found between the flow-rates of 0.2, 2 and 5 ml/min.

In accordance with the findings of Figura and McDuffie for Chelex [4] and due to the small dependence of the adsorption on flow-rate for C-18 and DEAE, we decided to use a flow-rate of 2 ml/min for the three adsorbents.

Environmental relevance

To study the effects of acidification on trace metal speciation, samples were taken from runoff water in the Gårdsjö area (F1 and G2) 30 km north of Göteborg. This area has been extensively studied by others [17]. In our work the lead results from the acidified area are compared with two waters less affected by acidification, taken in Göteborg; lake Bergsjön (Bs) and the creek Delsjöbäcken (Db). From Table 4 it can be seen that the pH differs by approximately three units.

Figure 3 presents the results from speciation of lead. The Chelex labile fraction is significantly higher in the area affected by acidification. The fraction adsorbing to DEAE is lower in the Gårdsjö area, while for C-18 no clear trend is observed. Similar behaviour is observed for copper and aluminium. This is the expected behaviour since hydrogen ions will replace metal ions in the complexes with humic matter. The result is an increase in the amount of free and weakly complexed metal ions, which constitute the toxic species. This occurs in spite of the fact that DOC concentration is higher in the acidified waters.

TABLE 4

Dissolved organic carbon and pH for stations F1 and G2 in the Gårdsjö area, Bergsjön (Bs) and Delsjöbäcken (Db) in Göteborg

Station	pH	DOC (mg/l)
F1	4.1	13.5
G2	3.9	16.4
Bs	6.9	3.6
Db	7.1	6.4

Results from a large scale speciation study

The method described here was applied to more than 100 samples taken from lakes and streams in southern Sweden. A detailed discussion of results from this study is beyond the scope of this paper, and the results will be presented elsewhere. Table 5 shows a brief summary and presents results from two rivers in southern Sweden (the rivers Viskan and Nissan). The table shows the average percentage of metal adsorbed

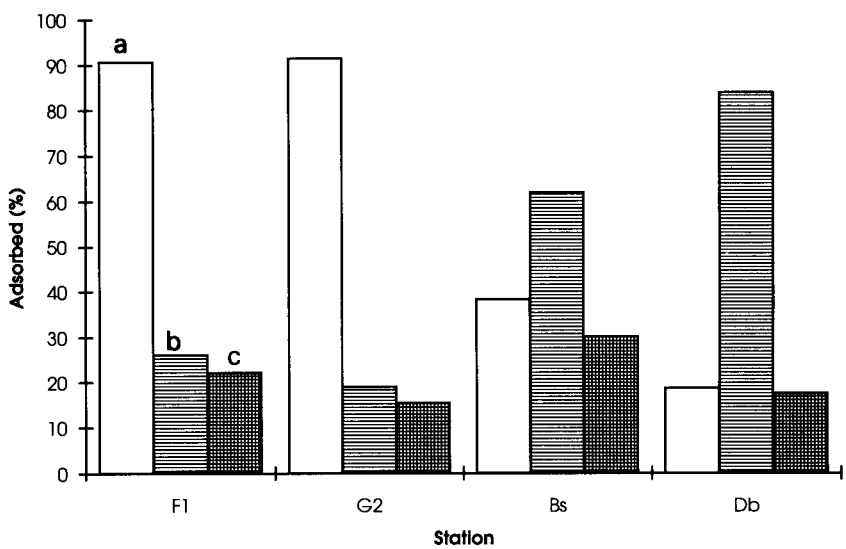

Fig. 3. Percent lead adsorbed on the three adsorbents. The concentrations (μg/l) of the filtered samples prior to passing the adsorbents were: F1 = 0.95, G2 = 1.1, Bs = 0.42 and Db = 0.43. a = Chelex; b = DEAE; c = C-18.

TABLE 5

Percent of metal adsorbed from filtered samples from the river Nissan (pH = 6.7 ± 0.24, DOC = 10.0 mg/l ± 1.7) and river Viskan (pH = 7.0 ± 0.10, DOC = 6.4 mg/l ± 2.5)

Element	Chelex		DEAE		C-18	
	Mean	S.D.	Mean	S.D.	Mean	S.D.
Aluminium	9	8	78	14	26	9
Cadmium	69	26	27	21	13	11
Cobalt	76	13	29	14	11	10
Copper	27	17	75	21	24	9
Iron	19	18	81	13	16	10
Lead	12	13	81	17	16	11
Manganese	96	2	6	3	4	3
Molybdenum	4	2	97	3	3	2
Nickel	50	14	40	15	6	5
Zinc	72	20	32	18	23	18

on the three different adsorbents and the standard deviation of the results.

The chemical forms of molybdenum and manganese in fresh waters are well known and therefore these elements can be used to validate the method. Molybdenum adsorbs almost completely to DEAE and this can be expected, since the thermodynamically stable form of molybdenum in natural water is molybdate. Manganese adsorbs to almost 100% on the Chelex, which indicates that manganese exists as Mn^{2+}. This is not the thermodynamically stable form of manganese in natural water but can be explained by leaching of manganese from the rock as Mn^{2+} and slow oxidation to MnO_2. The slow oxidation of manganese has been observed by others, e.g., Bruland et al. [18].

Interpreting C-18 data

The C-18 columns give data that are difficult to interpret. The reason is the affinity for both small lipophilic substances, which are highly toxic, and the non-polar groups of humic substances. The affinity of humic substances for C-18 is smaller than the affinity for DEAE. Figure 4 shows that the light absorbance at 460 nm is much higher after the C-18 column than after the DEAE resin, indicating that a significant amount of humic substances pass through the C-18. This breakthrough is also observed when a sample passes through the C-18 column; there is no clearly coloured zone but rather a colour gradient from dark brown at one end of the column to yellow at the other end. This can be compared with DEAE, having a clear brown band on the top 2–4 mm of the column after sample passage.

To elute or not to elute the columns

In contrast with most other speciation studies, we have not eluted the adsorbent columns, instead we have analysed the sample that has passed

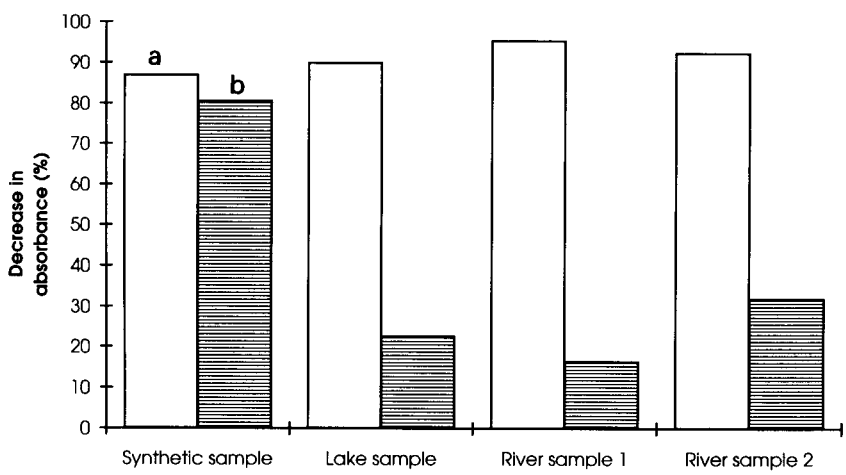

Fig. 4. Adsorption of humic matter on DEAE and C-18 measured as a decrease in absorbance (460 nm) after DEAE and C-18 columns for one synthetic and three natural samples. a = DEAE; b = C-18.

TABLE 6

Blank values for different adsorbents

Metal	Chelex-100 (ng/l)	Fractogel DEAE (ng/l)	Sep-Pak C-18 (ng/l)
Aluminium	13	11	< 2.5
Cadmium	1	1	2
Cobalt	< 0.6	< 0.6	< 0.6
Copper	< 0.6	< 0.6	1.3
Iron	1700	< 1700	< 600
Lead	5.2	6.2	7.3
Manganese	1	< 0.6	< 0.6
Molybdenum	1	< 1	< 1.9
Nickel	< 9	< 9	< 9
Zinc	5	6	13

through. This concept was selected for a number of reasons.

First of all, the problem of column blanks is reduced. Elution would mean that acid passes over the adsorbent after the sample has been pumped through. When the media passing the column changes, there is a contamination pulse caused by the changed environment at the adsorbent surface. Refraining from eluting means that this change can be avoided by preconditioning the column with sample. In this case 100 ml of water sample is used as a prefraction. The concept of preconditioning, i.e., not changing the environment which surfaces are exposed to, is commonly applied to avoid contamination problems in ultratrace determination. The blank values from the adsorbents can be seen in Table 6. The blanks vary from batch to batch with Sep-Pak C-18, which demands an extensive cleaning.

A second problem associated with eluting the adsorbents is that the elution is made with relatively strong acids [20]. The resulting samples are not suitable for determination with ICP–MS, since the acid damages the sampling cones. To avoid the problem of strong acid elution, it would be necessary to evaporate the sample and redissolve it in dilute acid. This would introduce a contamination problem and is therefore considered less suitable than the non-eluting approach.

A further problem with the eluates from the Ca–Chelex columns is that they contain high concentrations of calcium that give interferences in the ICP–MS determinations. The sensitivity drops instantly and a salt layer forms at the cones causing a further gradual drop in sensitivity. These problems are mainly of concern at lower masses. The problem with calcium can be minimised by extracting the elements of interest from the eluates with suitable extraction reagents. This would further increase the blank problems, and we have also considered this to be too tedious.

The drawback of the non-eluting approach is the difficulty to determine a specie that exists as a small fraction of the total concentration of the element, since a small fraction would be calculated as the difference between two large numbers.

Problems in verifying the performance of a speciation method

When developing an analytical method it is valuable to have a reference material to determine if the method provides accurate results. There are two approaches; either making a standard water from available compounds or using a natural water. Using a natural water is difficult because of storage problems. We tried to make synthetic fresh water in such a way that it can be prepared elsewhere to compare results from different speciation experiments and different laboratories. The water was made from 10 mg/l of a fulvic acid standard material [19] and salts (0.2 mM NaCl, 0.3 mM $CaCO_3$ and 0.2 mM $MgSO_4$) to provide fulvic acid concentration and ionic strength similar to that of the rivers investigated. As shown in Fig. 4 the purified fulvic acid have a much stronger affinity for the C-18 column than the natural samples. This led us to give up the attempt to prepare a speciation standard.

Future work

To gain a good understanding of the trace metal chemistry, it is of importance to study the influence of colloidal matter. This has been done using various size fractionating devices [21]. A comparison between different size fractionating systems has been made by Salbu [22]. The ultrafiltration units used in these works are quite expensive. We are now investigating if it is possible to use small, low-cost ultra filters, Mini-Ultrasette (Filtron). The adsorption and contamination

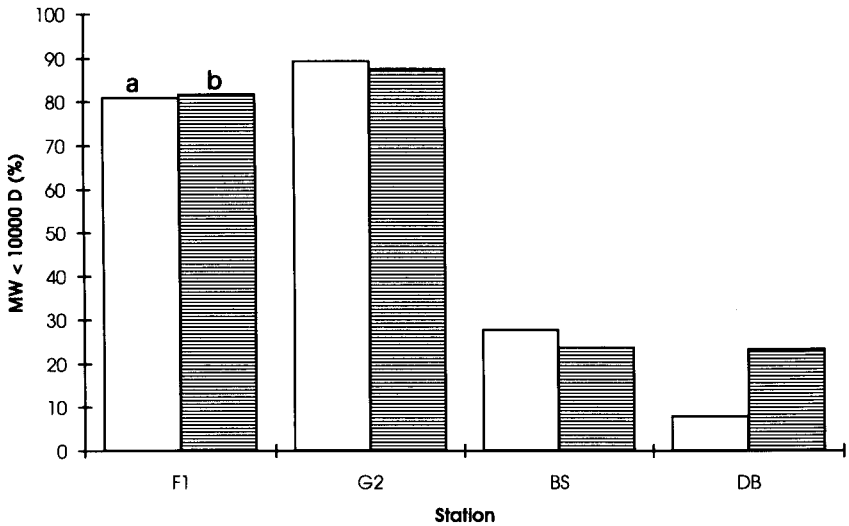

Fig. 5. Percent metal passing through an ultrafilter, with a molecular weight cutoff at 10000 Dalton. a = Pb; b = Al.

problems of this fractionation method will have to be further investigated.

The results from preliminary experiments, presented in Fig. 5, show that there is a significant increase in the low molecular weight fraction of lead and aluminium in samples from the acidified area (F1 and G2). This indicates that it would be worthwhile continuing this line of work.

Conclusions

After extensive cleaning, the chosen adsorbents give blank levels and detection limits that are within the requirements for trace metal analysis in fresh waters. The method does not provide a clear-cut distinction between different forms of metal species, but it gives information about characteristics of the metal species that are valid for natural behaviour. The attempt to prepare a speciation standard was not successful. However, a speciation standard would still be very useful if someone presents a composition that can be repeated.

The authors wish to thank the Knut and Alice Wallenberg Foundation for financial support. Constructive criticism from Stig Westerlund is gratefully acknowledged.

REFERENCES

1 F.M.M. Morel, R.J.M. Hudson and N.M. Price, Limnol. Oceanogr., 36 (1991) 1742.
2 T.M. Florence, Analyst, 111 (1986) 489.
3 P. Figura and B. McDuffie, Anal. Chem., 49 (1977) 1950.
4 P. Figura and B. McDuffie, Anal. Chem., 52 (1980) 1433.
5 T.M. Florence and G.E. Batley, Talanta, 22 (1975) 201.
6 T.M. Florence, Water Res., 11 (1977) 681.
7 K.H. Coale and K.W. Bruland. Deep-Sea Res., 37 (1990) 317.
8 C.J. Miles, J.R. Tuschall, Jr., and P.L. Brezonik, Anal. Chem., 55 (1983) 410.
9 T.M. Florence, B.G. Lumsden and J.J. Fardy, in C.J.M. Cramer and J.C. Duinker (Eds.), Complexation of Trace Metals in Natural Waters, Martinus Nijhoff/Dr W. Junk Publishers, The Hague, 1984, p. 411.
10 G.L. Mills and J.G. Quinn, Mar. Chem., 10 (1981) 93.
11 J.R. Donat, P.J. Staham and K.W. Bruland, Mar. Chem., 18 (1986) 85.
12 J.H. Reuter and E.M. Perdue, Gechim. Cosmochim. Acta, 41 (1977) 325.
13 M. van der Werff, in C.J.M. Kramer and J.C. Duinker (Eds.), Complexation of Trace Metal in Natural Waters, Martinus Nijhoff/Dr W Junk publishers, The Hague, 1984, p. 441.
14 C. Forsberg, Hydrobiologia, 229 (1992) 51.
15 L-G. Danielsson, B. Magnusson, S. Westerlund and K. Chang, Anal. Chim. Acta, 144 (1982) 183.
16 P.G.C. Campbell, D. Thomassin and A. Tessier, Water, Air and Soil Pollut., 30 (1986) 1023.
17 H. Hultberg and P. Grennfelt, Environ Polut., 75 (1992) 215.

18 K.W. Bruland, J.R. Donat and D.A. Hutchins, Limnol. Oceanogr., 36 (1991) 1555.
19 E.M. Thurman and R.L. Malcolm, Environ. Sci. Technol., 15 (1981) 463.
20 W.L. Landing, C. Haraldsson and N. Paxéus, Anal. Chem., 58 (1986) 3031.
21 C.L. Chakrabarti, Yanjia Lu, J. Cheng, M.H. Back and W.H. Schroeder, Anal. Chim. Acta, 267 (1993) 47.
22 B. Salbu and H.E. Bjørnstaad, J. Radioanal. Nucl. Chem., 138 (1990) 337.

Analytica Chimica Acta, 284 (1993) 337–344
Elsevier Science Publishers B.V., Amsterdam

Characterization of electrogenerated peroxyoxalate chemiluminescence

Katrina F. Heinze and Timothy A. Nieman

Department of Chemistry, University of Illinois, 600 South Mathews Ave., Urbana, IL 61801-3792 (USA)

(Received 14th June 1993; revised manuscript received 23rd August 1993)

Abstract

Peroxyoxalate chemiluminescence (PO-CL) is a commonly used chemiluminescent detection method for liquid chromatography. This paper concerns the electrogeneration of peroxyoxalate chemiluminescence (PO-ECL) as a means to eliminate post-column reagent addition which is required with conventional peroxyoxalate chemiluminescence detection in liquid chromatography. In acetonitrile, peroxyoxalate chemiluminescence can be electrogenerated at potentials between −1.5 and −1.9 V (versus Ag/AgCl). Imidazole, a catalyst for PO-CL, was found to interfere with the electrochemistry of the model peroxyoxalate and thus the emission of light with PO-ECL. Conversely, PO-ECL is enhanced in the presence of hydrogen peroxide. This enhancement is time dependent. Direct comparison showed PO-ECL to be less sensitive than PO-CL.

Keywords: Chemiluminescence; Electrogenerated chemiluminescence; Peroxyoxalates

Peroxyoxalate chemiluminescence (CL) has been widely used as a detection method in liquid chromatography (LC). Among the many analytes detected with this method are polycyclic aromatic hydrocarbons [1,2] and dansylated amino acids [3,4], cholesterol [5], fluorescamine-labeled catecholamines [6] and derivatized C_8–C_{16} aliphatic acids [7]. The wide use of peroxyoxalate CL (PO-CL) is due partly to the advantages that it shares with other CL systems: low detection limits and simple, inexpensive equipment. Low detection limits, as compared to other light measuring techniques (e.g., fluorescence and absorbance), are possible due to the absence of source instability and background signal from source scatter.

Another reason for the popularity of PO-CL is the reaction's ability to selectively detect fluorophores. This selectivity arises from the reaction mechanism [8]:

Correspondence to: T.A. Nieman, Department of Chemistry, University of Illinois, 600 South Mathews Ave., Urbana, IL 61801-3792 (USA).

$$\text{oxalate ester} + H_2O_2 \rightarrow \text{intermediates}$$

$$\text{intermediates} + \text{fluorophore} \rightarrow \text{fluorophore}^*$$

$$\text{fluorophore}^* \rightarrow \text{fluorophore} + h\nu$$

In this reaction the oxalate ester reacts with hydrogen peroxide to form an intermediate which then transfers its energy to fluorophores which are present. Emission is then from the excited state fluorophore. Thus, the wavelength of the emitted light depends on the fluorophore. The reaction proceeds much more readily in the presence of a catalyst [3–6], most commonly imidazole. The two most common oxalate esters are bis(2,4,6-trichlorophenyl) oxalate (TCPO) and bis(2,4-dinitrophenyl) oxalate (DNPO).

Despite PO-CL's great popularity this method suffers from several limitations. The first is the lack of solubility and stability of the oxalate esters in aqueous solvents [9]. Thus, the use of organic solvent based mobile phases is required. Com-

SSDI 0003-2670(93)E0498-V

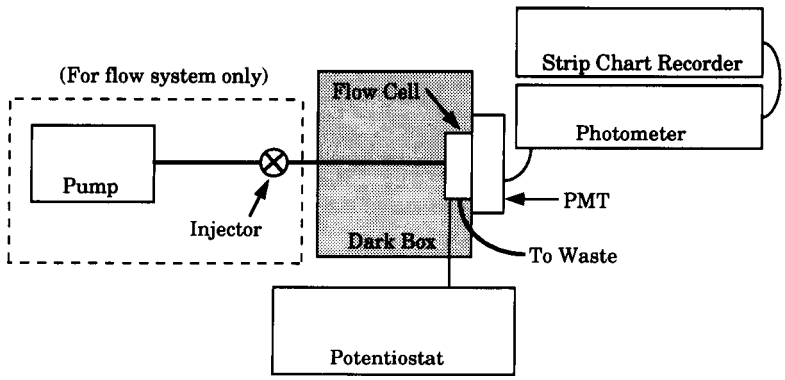

Fig. 1. Schematic of experimental set-up. For flow system, equipment in dashed box was used. For stopped-flow system, pump and injector were removed and the sample was directly injected into the flow cell with a manual syringe.

mon solvents are acetonitrile, ethyl acetate and acetone. An additional problem is created by the need for post-column reagent addition. In traditional PO-CL set-ups, the reagent mixture (oxalate ester and hydrogen peroxide) is mixed with the column eluent and the resulting CL is detected downstream. Post-column reagent addition causes undesirable band-broadening and analyte dilution. One method currently being explored to eliminate reagent stream addition in other LC and flow-injection analysis applications with CL systems is electrogenerated chemiluminescence (ECL) [10–12]. With ECL, some or all of the necessary reagents are generated in situ via an electrochemical reaction. In addition to elimination of post-column reagent addition, ECL also

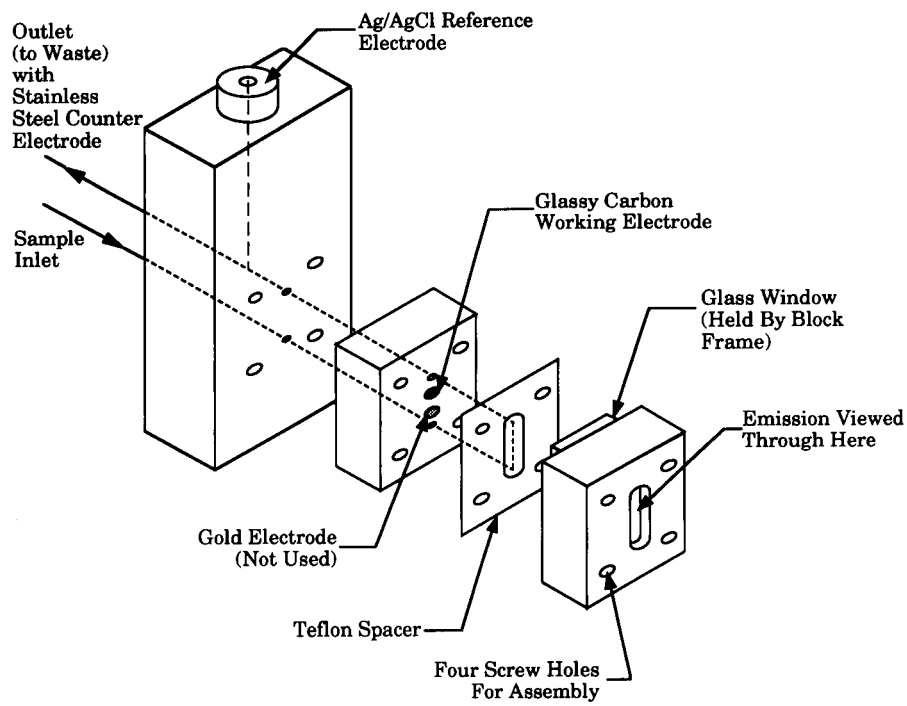

Fig. 2. Detailed schematic of flow cell.

offers the advantages of spatial and temporal control of the reaction.

In 1987, Brina and Bard [13] showed that ECL of a model peroxyoxalate, TCPO, was possible. In this paper we examine the feasibility of using electrogenerated peroxyoxalate CL (PO-ECL) for LC detection. In particular, the effects of applied potential, reaction time, and reagent concentrations on ECL intensity were investigated. Finally, the resulting light emission for PO-ECL was compared, under identical conditions, to that for conventional peroxyoxalate CL (PO-CL).

EXPERIMENTAL

Chemicals

TCPO, chosen as model oxalate ester, was purchased from Sigma (St. Louis, MO). Dansyl chloride (Dns-Cl) and 9,10-diphenylanthracene (DPA), both from Aldrich (Milwaukee, WI), were used as fluorophores. Potassium perchlorate ($KClO_4$) (Baker, Phillipsburg, NJ) and tetrabutylammonium tetrafluoroborate ($TBABF_4$) (Aldrich) were used as supporting electrolytes. All other chemicals and solvents were of reagent grade or better.

Instrumentation

Fluorescence emission wavelengths were obtained using a Hitachi F-4010 Fluorescence Spectrophotometer (Danbury, CT). Cyclic voltammograms were obtained using a Bioanalytical Systems BAS-100A Electrochemical Analyzer (West Lafayette, IN), a 3-mm glassy carbon disk working electrode, a silver/silver chloride (Ag/AgCl) reference electrode, and a platinum wire, counter electrode. Prior to obtaining the cyclic voltammograms, solutions were purged for 10 min with nitrogen gas.

The apparatus used for CL measurements is shown in Fig. 1, with a detailed schematic of the flow cell shown in Fig. 2. A Bioanalytical Systems glassy carbon working electrode block was the basis of the flow cell. The electrochemical cell was completed using a Ag/AgCl reference electrode, also from Bioanalytical Systems, and the stainless steel exit tube as counter electrode. Potential control was maintained using a Pine Instruments AFRDE4 potentiostat (Grove City, PA). An 8.4-μl flow cell, located within a light tight dark box, was created by separating a glass window from the electrode surface using a PTFE spacer. Light emitted by the chemical reaction in the flow cell was collected by a Hamamatsu 1P28 photomultiplier tube (PMT) (Bridgewater, NJ) biased at -900 V. Current from the PMT was measured using a Pacific Precision Instruments Model 126 laboratory photometer (Concord, CA), the signal from which was fed into a Pedersen Series MR strip chart recorder (Lafayette, CA).

Studies on the effect of various parameters (applied potential, imidazole concentration and hydrogen peroxide concentration) were carried out in a pseudo-stopped flow system. In these experiments, sample was introduced directly into the flow cell using a syringe. Once the solution was at rest in the flow cell, a potential step, from 0 V to the desired potential, was applied to the system. This experimental set-up allowed for the measurement of light intensity versus time at a given potential.

In addition, several experiments were carried out in a flow system. For these experiments, the carrier stream was pumped at 0.2 ml/min using an Altex Model 110A single-piston LC pump (Berkeley, CA); sample was injected into the carrier stream using a Valco Instruments two-position electric valve actuator (Houston, TX) and a standard LC six-port valve fitted with a 10-μl injection loop. After injection, sample was carried to the flow cell through 25 cm of 0.01″ PEEK tubing. For these experiments CL signal is reported as maximum peak height.

RESULTS AND DISCUSSION

Brina and Bard [13] showed that light was generated at reducing potentials during a cyclic voltammogram of TCPO and DPA in acetonitrile–benzene (2:1, v/v) with $TBABF_4$ electrolyte. Before further investigating PO-ECL, we wanted to determine that, as with PO-CL, light intensity varied linearly with fluorophore concentration for this system. This was done by making

injections of DPA into a carrier stream of acetonitrile–toluene (2:1, v/v). This solution mixed with a solution of TCPO and $TBABF_4$ also in acetonitrile–toluene (2:1, v/v) and proceeded through the flow cell where light emission was generated by the working electrode, which was held at −1.300 V versus Ag/AgCl. Light emission did indeed vary linearly with the concentration of DPA. This showed that PO-ECL had potential for analytical use.

The use of reversed-phase solvents for LC is common. Thus, we were interested in determining whether PO-ECL could be used analytically in solvents compatible with reversed-phase LC. The first step was to examine PO-ECL in 100% acetonitrile. This solvent was chosen due to its common use with conventional PO-CL. This selection led to a change in fluorophore due to DPA's extremely low solubility in acetonitrile. Dansyl chloride (Dns-Cl) was chosen as model fluorophore since it is commonly used with PO-CL [3–4,9–10,14–17]. The emission maximum for Dns-Cl is 480 nm, and for DPA is 425 nm.

Electrochemical studies

To determine the feasibility of obtaining ECL from TCPO in acetonitrile, the electrochemistry of TCPO in acetonitrile compared to that in acetonitrile–toluene (2:1, v/v) was examined. Figure 3a shows a cyclic voltammogram of TCPO

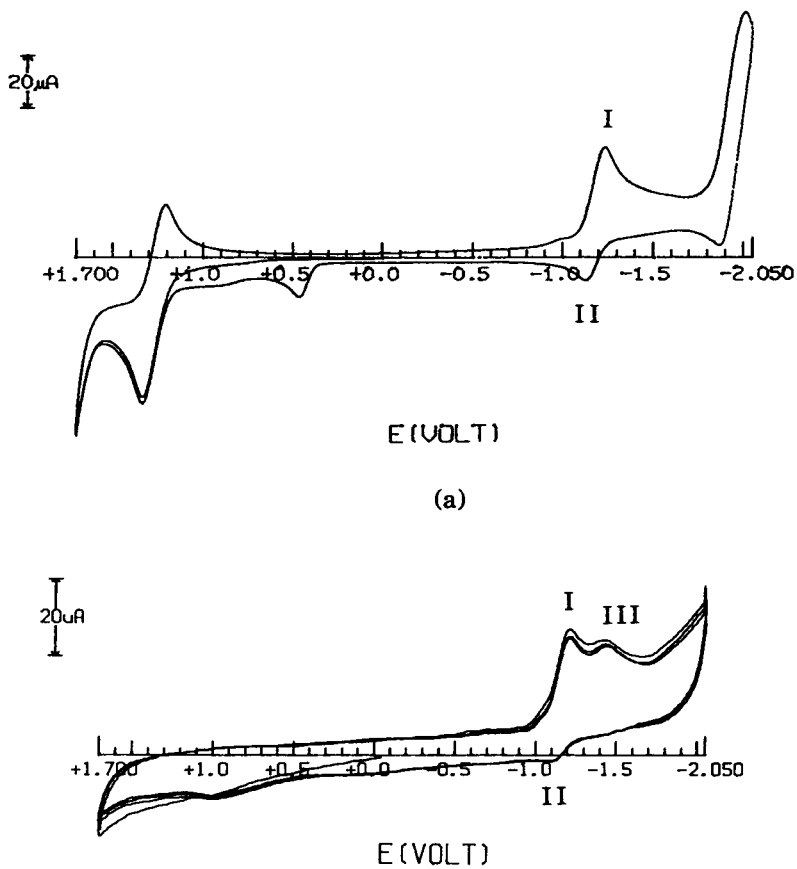

Fig. 3. Cyclic voltammograms of TCPO at 100 mV/s. (a) 2.7 mM TCPO, 2.6 mM DPA and 0.026 M $TBABF_4$ in acetonitrile–toluene (2:1, v/v). (b) 2 mM TCPO and 4 mM $KClO_4$ in acetonitrile.

in acetonitrile–toluene (2:1, v/v); Fig. 3b shows a cyclic voltammogram of TCPO in acetonitrile. The peaks associated with TCPO are peaks I, II and III. All other peaks are associated with the background. Brina and Bard [13] showed that light emission occurred when TCPO was reduced at −1.2 V versus a silver quasi-reference electrode. In Fig. 3, we see that the reduction of TCPO occurs at −1.2 V (vs. Ag/AgCl) in both acetonitrile–toluene (2:1, v/v) and acetonitrile (peak I). The conclusion is that ECL of TCPO in acetonitrile will be possible. It should be noted that the reduction of TCPO is only quasi-reversible, as shown by the ratio of anodic peak current to cathodic peak current (i_{pa}/i_{pc}) being less than 1 [$i_{pa}/i_{pc} = 0.7$ in acetonitrile–toluene (2:1, v/v) and $i_{pa}/i_{pc} = 0.4$ in acetonitrile]. This is indicative of the product of the reduction being unstable, and is not unexpected. Brina and Bard suggested that the reduced form of TCPO reacts with reduced oxygen (also reduced at −1.2 V vs. Ag/AgCl) to form $(TCPO–O_2)^{2-}$. This product then follows the pathway suggested for conventional PO-CL [8]. Thus the irreversibility of the reduction of TCPO will not interfere with ECL.

Applied potential studies

Having determined that the electrochemistry of TCPO in acetonitrile was favorable towards the use of PO-ECL, our next goal was to determine whether an optimum existed for light emission with regards to applied potential. It was anticipated that no significant light emission would occur at potentials positive of −1.2 V (vs. Ag/AgCl). However, it was not clear how overpotentials would affect light emission.

The initial experiment was very similar to that used by Brina and Bard [13]; using the stopped flow set-up, light emission as a function of applied potential was recorded during the course of a cyclic voltammogram. It quickly became apparent that, due to the apparent slow reaction rate, this experiment convoluted the effects of applied potential and reaction rate. In order to avoid this convolution, the light intensity versus time profile was measured for a series of fixed potentials. By plotting the results versus applied potential, the light emission could be optimized with regards to both applied potential and time from application of potential. To accomplish this, a recording of light intensity versus time after application of potential was obtained, using the stopped flow set-up, for applied potentials between −2.000 and −0.500 V, stepped by 0.100 V. The solution used was 0.481 mM TCPO, 0.503 mM Dns-Cl and 3 mM $KClO_4$ in acetonitrile. The results of this experiment were digitized and plotted, see Fig. 4. In addition, a reproducibility study was conducted by repeating the measurement of light intensity versus time after application of potential seven times at −1.800 V.

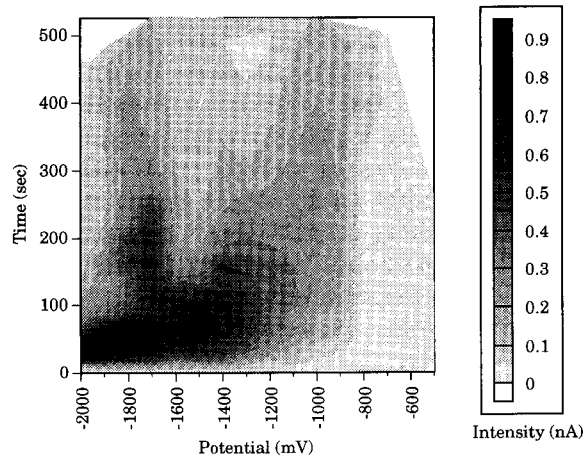

Fig. 4. Contour plot of emission intensity as a function of time and applied potential.

The reproducibility for these experiments was less than optimum. Nevertheless, some general conclusions can be drawn from Fig. 4. To obtain ECL, applied potentials of between −1.5 and −1.9 V (versus Ag/AgCl) are needed. Based on this, −1.700 V was used for all other experiments. Figure 4 also reveals that the emission of light is long lived, with maximum light intensity occurring between 25 and 100 s after potential is applied. For maximum S/N, detection should occur at the peak of the light intensity versus time profile. Thus, for PO-ECL detection in LC, low flow-rates or delayed detection would be needed in order to obtain optimal S/N. This is not the case with PO-CL, where the CL reactions are significantly faster [16].

Effect of reagent concentrations

The dependence of PO-CL on reagent concentrations has been well established [17–19]. While it was expected, and shown by our experiments, that PO-ECL light intensity would vary linearly with concentration of oxalate ester and fluorophore, we were unsure of the effect that the presence of either catalyst or hydrogen peroxide would have. A series of experiments were carried out to answer these questions.

Catalyst effect. In conventional PO-CL, imidazole is a commonly used catalyst, and an optimum imidazole concentration exists at approximately 15 mM [17,18]. At both higher and lower concentrations light intensity decreases dramatically. An experiment was performed to determine whether a similar dependence on imidazole concentration existed with PO-ECL. Using the stopped flow set-up, light intensity versus time profiles were obtained for samples containing 0.504 mM TCPO, 0.442 Dns-Cl, 3 mM $KClO_4$ and between 0 and 50 mM imidazole in acetonitrile. The applied potential for these experiments was -1.7 V. No light emission was observed for any of the solutions. This result is expected from examination of the electrochemistry in the presence of imidazole. Figure 5 shows a cyclic voltammogram of TCPO, DPA and imidazole in acetonitrile–toluene (2:1, v/v). When compared to Fig. 3a, it is clear that the addition of imidazole interferes with the reduction of TCPO at -1.2 V (vs. Ag/AgCl). Since the emission of light in PO-ECL is dependent on this reduction, it seems likely that the lack of light emission observed with imidazole in solution is due to imidazole's interference with the electrochemistry of TCPO.

Hydrogen peroxide effect. As with imidazole, the effect of hydrogen peroxide (H_2O_2) concentration on light emission with PO-CL has been studied. Sugiura et al. [19] have found that, while the H_2O_2 concentration has a minimal effect (when TCPO is the limiting reagent) on the amount of light generated from the reaction, optimum signal/noise (S/N) is observed at a H_2O_2 concentration of 13 mM. While H_2O_2 is not necessary for PO-ECL, it was thought that this reagent might have some impact on light emission.

To investigate the effect of H_2O_2 on PO-ECL, an experiment identical to that done with imidazole was planned. The light intensity versus time (after application of potential) profile obtained,

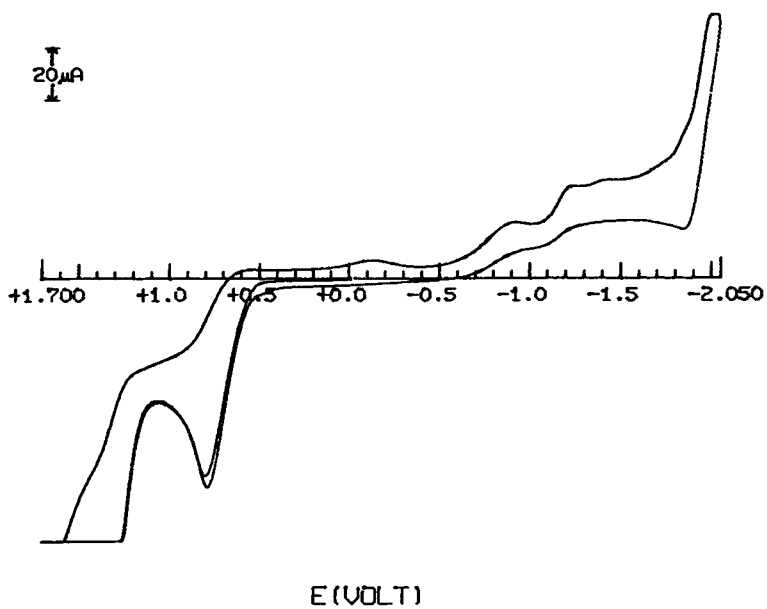

Fig. 5. Cyclic votammogram of 2.7 mM TCPO, 2.6 mM DPA, 0.026 $TBABF_4$ and 0.1 M imidazole in acetonitrile–toluene (2:1, v/v). Sweep speed, 100 mV/s.

for a solution of 0.504 mM TCPO, 0.442 mM Dns-Cl, 3 mM $KClO_4$ and 5.2 mM H_2O_2 in acetonitrile at −1.7 V, showed that hydrogen peroxide increased the maximum light intensity by approximately one order of magnitude. The total time during which light was emitted, but not the time to reach maximum light intensity, also increased significantly. As expected, even prior to applying potential to the system, light emission was observed due to the direct reaction of TCPO and H_2O_2.

Use of H_2O_2 enhanced PO-ECL would be limited if the enhancement was not stable with time. To determine whether or not this was the case, an experiment in the flow system was carried out. At time equal to 0 s, 3.00 μl of H_2O_2 was added to a solution of 0.504 mM TCPO, 0.442 mM Dns-Cl and 3 mM $KClO_4$ in acetonitrile ($[H_2O_2] = 1.95$ mM). Injections of this solution were made into a carrier stream of acetonitrile with 3 mM potassium perchlorate; the time from mixing of solutions for each injection was recorded. For approximately half of the injections no potential was applied to the system; for the other half, the applied potential was −1.700 mV. The results of this experiment are shown in Fig. 6. It is known that TCPO and H_2O_2 react to give background emission [8]. In Fig. 6 it can be seen that this reaction, and the resulting light emission, is long lived. The reaction of TCPO and H_2O_2 is another problem associated with conventional PO-CL, where the reagent mixture added post-column is usually a mixture of oxalate ester and H_2O_2. For our purposes the important conclusion that can be drawn from Fig. 6 is that the enhancement of PO-ECL by the addition of H_2O_2 is time dependent. Thus in order to obtain the reproducibility needed for detection in HPLC, the H_2O_2 and TCPO would need to be mixed at a given time prior to each injection. This reagent mixing requirement is no better than that required with conventional PO-CL. Thus for analytical purposes non-enhanced PO-ECL must be used.

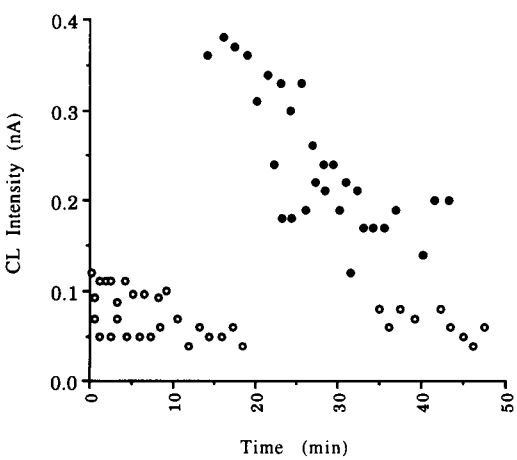

Fig. 6. Plot of high intensity versus time after mixing H_2O_2 and TCPO for (○) no applied potential and (●) applied potential of −1.7 V.

Comparison of CL to ECL

An experiment was designed to directly compare the light emission from PO-CL to that of PO-ECL with identical samples and instrumentation. The sample used was 0.503 mM TCPO, 0.221 mM Dns-Cl and 3 mM $KClO_4$ in acetonitrile. Using a carrier stream of acetonitrile containing 10.0 mM imidazole, 6.0 mM H_2O_2 and 3 mM $KClO_4$, sample was injected (with no applied potential) and light intensity recorded. This was repeated with a carrier stream of acetonitrile containing 6.0 mM H_2O_2 and 3 mM $KClO_4$, with and without applied potential. Six replicate injections were made for each condition. A similar experiment was carried out using a model normal-phase solvent system, acetonitrile–toluene (2:1, v/v). Here the sample was 0.503 mM TCPO, 0.225 mM DPA and 2 mM $KClO_4$ in acetonitrile–toluene (2:1, v/v). The carrier streams used were 6.0 mM H_2O_2 and 2 mM $KClO_4$ in acetonitrile–toluene (2:1, v/v) with either 0 or 10.0 mM imidazole. The results for these experiments are shown in Table 1. It is clear from the data that PO-ECL, even when enhanced, cannot compete with PO-CL with regards to sensitivity.

Conclusions

We have shown that electrogenerated chemiluminescence (ECL) of a model peroxyoxalate is possible in both normal- and reversed-phase LC model solvents. The ECL emission intensity has

TABLE 1

Comparison of ECL to CL
(uncertainties given at 95% confidence)

LC phase	[Imidazole] (mM)	[H_2O_2] (mM)	Potential (V)	CL int. (nA)
Reversed	10.0	6.0	–	8.70 ± 0.6
	–	6.0	–	0.07 ± 0.02
	–	6.0	−1.700	0.11 ± 0.02
Normal	10.0	6.0	–	940 ± 90
	–	6.0	–	3.7 ± 0.3
	–	6.0	−1.700	4.3 ± 0.5

been shown to vary linearly with both fluorophore and oxalate ester concentration. Unlike conventional peroxyoxalate chemiluminescence, the use of a catalyst, in this case imidazole, inhibits light emission. Additionally, ECL can be enhanced by the addition of hydrogen peroxide. Unfortunately, the amount of light generated by electrogenerated peroxyoxalate chemiluminescence (PO-ECL) is significantly less than that obtained with conventional peroxyoxalate chemiluminescence (PO-CL) for the same fluorophore and oxalate ester concentrations. Thus, for sensitivity considerations alone, PO-CL has a distinct advantage to PO-ECL. However, the temporal and spatial control of ECL can make PO-ECL desirable in appropriate situations.

This research was supported in part by a grant from the Biotechnology Research and Development Corporation. The authors also thank Dr. Andrej Wieckowski for the use of his digitizing equipment and software.

REFERENCES

1 K.W. Sigvardson and J.W. Birks, Anal. Chem., 55 (1983) 432.
2 A.N. Gachanja and P.J. Worsfold, Anal. Proc., 29 (1992) 61.
3 K. Miyaguchi, K. Honda and K. Imai, J. Chromatogr., 303 (1984) 173.
4 K. Miyaguchi, K. Honda and K. Imai, J. Chromatogr., 316 (1984) 501.
5 J.H. Mike and T.J. Cleland, Anal. Chim. Acta, 259 (1992) 73.
6 S.-I. Kobayashi, J. Sekino, K. Honda and K. Imai, Anal. Biochem., 112 (1981) 99.
7 S.W. Lewis, P.J. Worsfold, A. Lynes and E.H. McKerrell, Anal. Chim. Acta, 266 (1992) 257.
8 R.S. Givens and R.L. Schowen, in J.W. Birks (Ed.), Chemiluminescence and Photochemical Reaction Detection in Chromatography, VCH, New York, 1989, Chap. 5, pp. 125–147.
9 G. Orosz and E. Dudar, Anal. Chim. Acta, 247 (1991) 141.
10 J.S. Littig and T.A. Nieman, Anal. Chem., 64 (1992) 1140.
11 O.M. Steijger, G.J. de Jong, J.J.M. Holthuis and U.A.Th. Brinkman, J. Chromatogr., 557 (1991) 13.
12 T.M. Downey and T.A. Nieman, Anal. Chem., 64 (1992) 1140.
13 R. Brina and A.J. Bard, J. Electroanal. Chem., 238 (1987) 277.
14 T. Koziol, M.L. Grayeski and R. Weinberger, J. Chromatogr., 317 (1984) 355.
15 P.J.M. Kwakman, D.A. Kamminga, U.A.Th. Brinkman and G.J. de Jong, J. Chromatogr., 553 (1991) 345.
16 G.J. de Jong, N. Lammers, F.J. Spruit, U.A.Th. Brinkman and R.W. Frei, Chromatographia, 18 (1984) 129.
17 N. Hanaoka, R.S. Givens, R.L. Schowen and T. Kuwana, Anal. Chem., 60 (1988) 2193.
18 N. Hanaoka, J. Chromatogr., 503 (1990) 155.
19 M. Sugiura, S. Kanda and K. Imai, Anal. Chim. Acta, 266 (1992) 225.

Analytica Chimica Acta, 284 (1993) 345–349
Elsevier Science Publishers B.V., Amsterdam

pH and concentration response surfaces for the luminol–H_2O_2 electrogenerated chemiluminescence reaction

Glenn P. Jirka, Alice F. Martin and Timothy A. Nieman

Department of Chemistry, University of Illinois at Urbana-Champaign, 600 South Mathews Avenue, Urbana, IL 61801-3792 (USA)

(Received 17th June 1993; revised manuscript received 23rd August 1993)

Abstract

A response surface for the luminol–H_2O_2 electrogenerated chemiluminescence (ECL) reaction is constructed by systematically altering the pH and reagent concentration while determining luminol or H_2O_2. Ranges covered are 0.5 through 500 μM H_2O_2 and pH 7 through 10 for luminol determinations and 0.1 through 1000 μM luminol and pH 7 through 10 for H_2O_2 determinations. At a given luminol or H_2O_2 concentration the ECL response surface with respect to pH and reagent concentration is essentially identical in general shape to the response surface observed at any other concentration. With this information one can predict the change in ECL response between any two sets of conditions or maintain the same ECL response with two sets of conditions if appropriately chosen. In general, monotonically sloping contours are observed such that as the pH or the luminol or H_2O_2 concentration is increased, there is a corresponding increase in ECL response.

Keywords: Chemiluminescence; Electrogenerated chemiluminescence; Luminol; Response surfaces

Luminol electrogenerated chemiluminescence (ECL) has attracted our interest for a variety of reasons. The luminol ECL system is useful in the determination of species labelled with luminol or luminol-like compounds, H_2O_2 and species that can be enzymatically converted to H_2O_2 [1–3]. In addition to this versatility and the low detection limits characteristic of CL systems, ECL offers the advantages of both spatial and temporal control of the emission process via regulation of the working electrode potential.

A number of other laboratories have also shown interest in luminol electrogenerated chemiluminescence. Kuwana and co-workers [4–9] have performed a series of investigations on the mechanism of luminol ECL. Engstrom et al. [10] have similarly studied the luminol mechanism as well as the effect various of electrode materials on luminol ECL. Luminol ECL has also been used as the basis for a fiber optic probe developed by Van Dyke and Cheng [11]. Sakura [12,13] has utilized the luminol ECL reaction to determine H_2O_2 as well as demonstrate its utility in the determination of lipid hydroperoxides [14,15].

Examination of the literature cited above revealed that a wide pH range with various H_2O_2 and luminol concentrations had been used in the ECL experiments. It also became apparent that there was not a clear understanding of how ECL intensity under one set of reaction conditions is related to the intensity under another set of conditions. Our goal was to gain an understanding of the general shape of the ECL response surface as a function of pH, H_2O_2 concentration, and lumi-

Correspondence to: T.A. Nieman, Department of Chemistry, University of Illinois at Urbana-Champaign, 600 South Mathews Avenue, Urbana, IL 61801-3792 (USA).

SSDI 0003-2670(93)E0496-T

nol concentration in order to facilitate a more effective use of the luminol ECL reaction. The specific mode of operation was to generate a series of H_2O_2 working curves at different pH and luminol concentrations, and to generate a series of luminol working curves at different pH and H_2O_2 concentrations.

EXPERIMENTAL

Flow-injection determination of luminol

The flow system for these experiments utilized two flow channels, both pumped by a single Rainin Rabbit peristaltic pump (Woburn, MA), with a flow of 1.4 ml/min through each channel. A continuous stream of aqueous H_2O_2 solution was pumped through channel A. A pH buffer solution of either sodium borate or potassium phosphate was pumped through channel B. Luminol solutions, prepared in the appropriate buffer, were injected into the buffer stream (stream B) using a Rheodyne Type 50 valve (Cotati, CA) having a 200-μl injection loop. The two streams were joined at a mixing tee approximately four inches prior to an observation cell with a volume of 120 μl. Because the luminol determination experiments were done in a flow system that merged two streams, the concentration values reported here have been divided by 2 to give the concentration flowing through the observation cell.

Flow-injection determination of hydrogen peroxide

A single channel flow-injection system pumped by an Altex Model 110A HPLC pump (Berkely, CA) was utilized for this set of experiments. An Alcott Model 732 injection valve (Norcross, GA), with a 25-μl injection loop, was used to make injections of H_2O_2 samples into a stream of 0.2 M KNO_3 flowing at 2 ml/min. The H_2O_2 samples, which also contained luminol and buffer, proceeded downstream to an observation cell with a volume of 3.5 μl.

Electrogenerated chemiluminescence

The observation cell contained a Bioanalytical Systems glassy carbon working electrode (West Lafayette, IN), a Ag/AgCl reference electrode (Bioanalytical Systems), a stainless steel outlet tube which served as a counter electrode, a Plexiglas® window, and a suitable spacer to define a flow channel between the electrode and window [16]. The flow cell was placed in front of a Hamamatsu 1P28 photomultiplier tube (Bridgewater, NJ) biased at −900 V and contained inside a light tight box. The output current of the PMT was measured by Pacific Instruments Model 124 photometer (Concord, CA) and recorded on a strip chart recorder. During luminol determinations, a Bioanalytical Systems LC-4B potentiostat was used to hold the working electrode potential at 0.650 V vs. Ag/AgCl. During H_2O_2 determinations, a Bioanalytical Systems 100A potentiostat was used to step the working electrode potential between 0.950 V and −0.200 V vs. Ag/AgCl at 20 ms intervals.

Reagents and solutions

All solutions were made using water from a Millipore Milli-Q (Bedford, MA) water purification system. Luminol (5-amino-2,3-dihydro-1,4-phthalazinedione) was used as purchased from Sigma (St. Louis, MO). All other chemicals were of reagent grade. A 0.1 M sodium phosphate buffer was used for work at pH 7, and buffers 0.05 M in sodium borate and 0.20 M in potassium nitrate were used for work at pH 8 through pH 11.

RESULTS AND DISCUSSION

Luminol determination

A series of luminol working curves were obtained at H_2O_2 concentrations of 0.5, 5, 50 and 500 μM each at pH values of 7, 8, 9 and 10. We were particularly interested in use of H_2O_2 concentrations of 500 μM or lower because such concentrations can be obtained by electrogeneration [17]. Figure 1a pictures a series of luminol working curves obtained at pH 7 and various H_2O_2 concentrations. This plot is also representative of the series of working curves obtained for similar experiments at pH 8, 9 and 10. Figure 1b pictures a series of working curves obtained at a

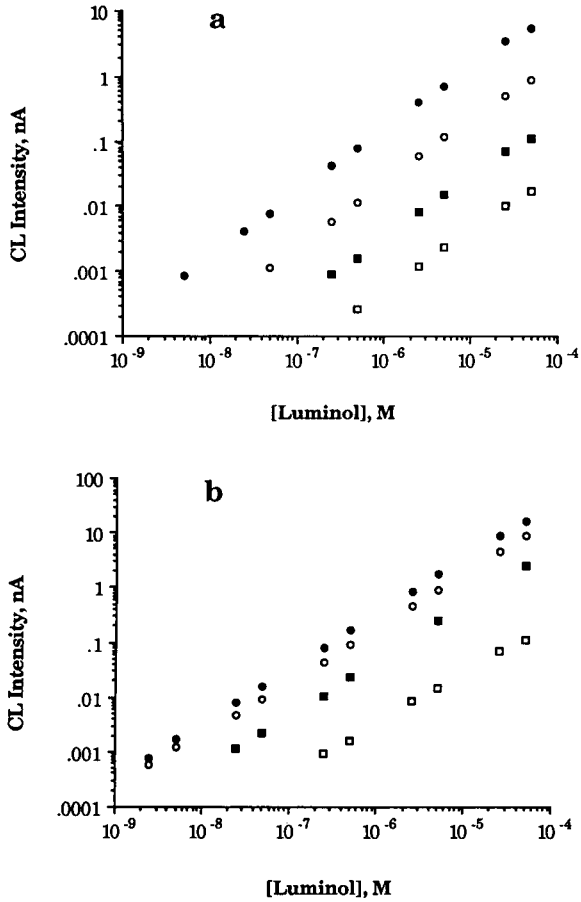

Fig. 1. (a) Luminol determination at pH 7 for ●, 5000 μM, ○, 500 μM, ■, 50 μM, □, 5 μM hydrogen peroxide. (b) Luminol determination with 50 μM H_2O_2 for ●, pH 10, ○, pH 9, ■, pH 8, □, pH 7.

constant H_2O_2 concentration (50 μM) under various pH conditions. This plot is also representative of the series of working curves obtained at 0.5, 5 and 500 μM H_2O_2 concentrations. The curve obtained using pH 7 with 50 μM H_2O_2 is shown in both Fig. 1a and b to facilitate interpretation of the data. This shows that the working curves obtained at a constant pH are parallel with those obtained at constant H_2O_2 concentration. Although not shown due to the congested nature of the plot, a single graph containing all the working curves obtained clearly reveals that all working curves are indeed parallel. This result implies that the ECL response surface varies as a function of pH and H_2O_2 concentration similarly at all luminol concentrations. Therefore, a characteristic response surface shown in Fig. 3a was constructed from data obtained at a luminol concentration of 500 nM. The numbers along the contour lines are the logarithms of the ECL emission intensity. The response surface illustrates that as either pH or H_2O_2 is increased, a corresponding increase in ECL response for luminol is observed. There is over a thousand-fold intensity increase going from lower left (pH 7 and 5 μM H_2O_2) to upper right (pH 10 and 500 μM H_2O_2) on the response surface. There are various combinations of pH and H_2O_2 concentration which can be implemented to achieve a similar ECL response. For example, the intensities obtained at pH 7 with 500 μM H_2O_2 are the same as obtained at pH 10 with 10 μM H_2O_2.

Hydrogen peroxide determination

A series of H_2O_2 working curves were obtained at luminol concentrations of 0.1, 1, 10, 100, and 1000 μM each at pH 8, 9 and 10, and at 10, 100 and 1000 μM luminol at pH 7. Past experience in our laboratory has shown that electrode fouling by luminol oxidation products considerably decreases the catalytic activity of the electrode and hence decreases the ECL intensity [1]. In order to minimize fouling of the electrode over time, the electrode potential was repetitively stepped between 0.950 and −0.200 V vs. Ag/AgCl at 20 ms intervals. With such a potential program, luminol is oxidized at the positive potential, to initiate ECL, and the electrode activity is restored at the negative potential, presumably by reduction of products which foul the electrode. A sample containing 100 μM luminol and 10 μM H_2O_2 at pH 8 was chosen as a standard to be tested along with each working curve in order to account for any degradation of the electrode activity. All ECL intensities were scaled to the signal recorded for this standard. Also, each signal was corrected for background ECL resulting from luminol oxidation in the absence of H_2O_2.

Figure 2a pictures a set of working curves for H_2O_2 at pH 9 for various luminol concentrations. This plot is also representative of the trends seen at pH 7, 8, and 10. Figure 2b pictures a set of

working curves obtained at constant luminol concentration (100 μM) under various pH conditions. This plot is also representative of the trends at 0.1, 10, and 1000 μM luminol. However, when looking at the collective set of plots one observes that the curves lie closer together at pH values 8, 9, and 10 than shown in Fig. 2b. Overall, the working curves of Fig. 2a and b along with those not presented simply show that as each of the 3 variables (H_2O_2 concentration, luminol concentration and pH) are increased, a corresponding increase in ECL is observed. This is further illustrated in Fig. 3b showing the response surface for a single concentration of H_2O_2 (100 μM). Note the similarity between Fig. 3a for luminol determination and that of 3b for H_2O_2 determination. In this case it is also seen that there are various combinations of pH and luminol concentration which can be implemented to achieve a similar ECL response. For example, the intensities obtained at pH 7 with 1 μM luminol are the same as those obtained at pH 10 with 0.15 μM luminol.

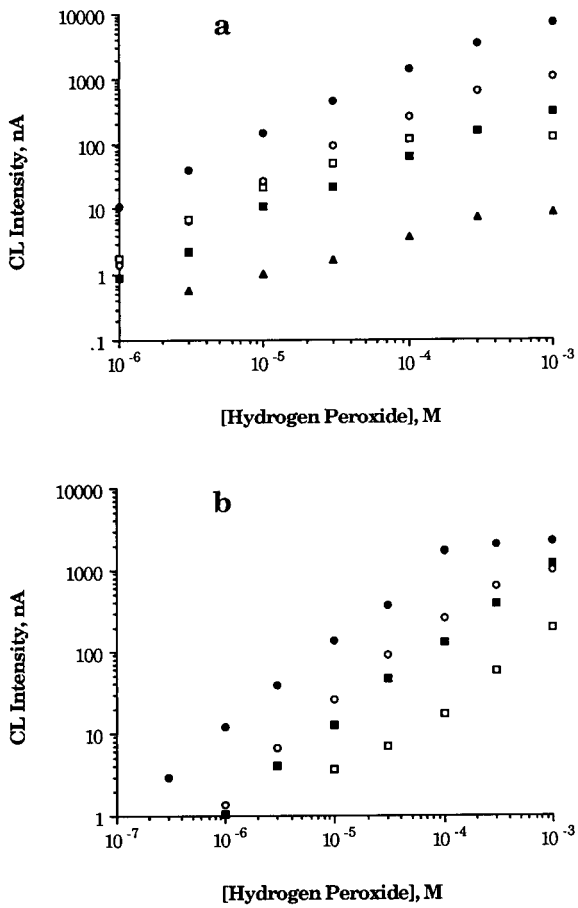

Fig. 2. (a) H_2O_2 determination at pH 9 for ●, 1000 μM, ○, 100 μM, ■, 10 μM, □, 1 μM, ▲, 0.1 μM luminol. (b) H_2O_2 determination with 100 μM luminol for ●, pH 10, ○, pH 9, ■, pH 8, □, pH 7.

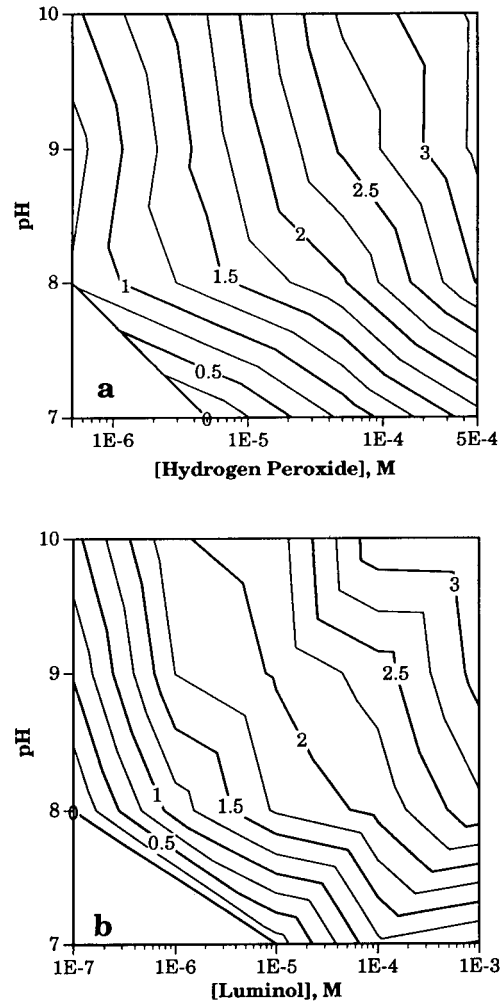

Fig. 3. (a) ECL surface response for 500 nM luminol. [pH, log(H_2O_2) and log(normalized CL intensity)]. (b) ECL surface response for 100 μM H_2O_2. [pH, log(luminol) and log(normalized CL intensity)].

Conclusions

Response surfaces of ECL emission intensity vs. pH and reagent concentration in the luminol–

H_2O_2 electrogenerated chemiluminescence reaction are virtually the same shape at any set of conditions over the ranges we examined. The overall response surface plot would be the 4-dimensional combination of the data presented in Figs. 1–3. Because of the simple monotonic shape of the plots in Fig 3a and 3b, the shape of the overall plot can be appreciated. With an increase in either pH, luminol concentration, or H_2O_2 concentration there is an increase in ECL response. The response surfaces indicate how the magnitude of this response can be controlled by the appropriate choice of pH, luminol or H_2O_2 concentration as well as predict the change in ECL response between any two sets of conditions. Luminol CL and ECL are most commonly performed in fairly alkaline solutions in order to achieve intense emission. There are times however, when the overall analytical scheme makes operation at near neutral pH more desirable. This could be for coupling to various enzymatic reactions (for generation of H_2O_2 from the analyte substrate) or for coupling to LC (with a silica column that is unstable above pH 8). In the near-neutral pH 7–8 region, increased emission intensities can be obtained by use of H_2O_2 concentrations greater than 500 μM (and we have examined up through 5 mM); such higher concentrations could not be achieved by electrogeneration of the H_2O_2 (if that ability was desired), but must be reached via addition of a conventional solution of H_2O_2. The response surfaces reported here provide a guide to utilization of luminol ECL over a very wide range of conditions.

REFERENCES

1 D.A. Van Dyke, Ph.D. Thesis, University of Illinois at Urbana, 1986.
2 T.A. Nieman, Mikrochim. Acta, 3 (1980) 239.
3 T.A. Nieman, J. Res. Natl. Bur. Stand., 93 (1988) 501.
4 T. Kuwana, J. Phys. Chem., 67 (1963) 2243.
5 T. Kuwana, J. Electroanal. Chem., 6 (1963) 164.
6 T. Kuwana, J. Electroanal. Chem., 6 (1963) 417.
7 B. Epstein and T. Kuwana, Photochem. Photobiol., 4 (1965) 1157.
8 B. Epstein and T. Kuwana, J. Electroanal. Chem., 15 (1967) 389.
9 B. Epstein and T. Kuwana, Photochem. Photobiol., 6 (1967) 605.
10 R.C. Engstrom, J.E. Vitt and D.C. Johnson, J. Electrochem. Soc., 138 (1991) 1637
11 D.A. Van Dyke and H.Y. Cheng, Anal. Chem., 61 (1989) 633.
12 S. Sakura and H. Imai, Anal. Sci., 4 (1988) 9.
13 S. Sakura, Anal. Chim. Acta, 262 (1992) 49.
14 S. Sakura, Anal. Chim. Acta, 262 (1992) 59.
15 S. Sakura and J. Terao, Anal. Chim. Acta, 262 (1992) 217.
16 T. Malcom Downey and T.A. Nieman, Anal Chem., 64 (1992) 261.
17 J. Littig and T.A. Nieman, Anal. Chem., 64 (1992) 1140.

Analytica Chimica Acta, 284 (1993) 351–360
Elsevier Science Publishers B.V., Amsterdam

Assessment of the population of neutral and singly ionized zinc species in argon and argon–nitrogen inductively coupled plasma by atomic absorption spectrometry

Kazuaki Wagatsuma and Kichinosuke Hirokawa

Institute for Materials Research, Tohoku University, Katahira 2-2-1, Sendai 980 (Japan)

(Received 15th June 1993; revised manuscript received 23rd July 1993)

Abstract

Atomic absorption measurements were used to determine the relative number densities of both zinc atoms and ions in an inductively coupled plasma (ICP). Variations in the absorbance obtained with the zinc atomic and ionic resonance lines reflect the dynamic equilibrium between the number of atoms and ions in the plasma. Absorbance changes as a function of the carrier gas flow-rate were investigated at several incident power values. Ionization is drastically reduced at higher carrier gas flow-rates. Measurements at different observation heights were carried out with widely differing flow-rates of the carrier gas. The results obtained for the tail plume zone are different from those for other zones of the ICP. The characteristics of the ICP using argon–nitrogen mixed gas instead of argon alone were also examined by atomic absorption spectrometry.

Keywords: Atomic absorption spectrometry; Inductively coupled; Plasma spectrometry; Zinc

Atomic emission spectrometry using an inductively coupled plasma (ICP) has become a powerful technique for routine use. A variety of factors influence the analytical performance of ICP spectrometry. In ordinary operations, analyses under so-called compromise conditions [1] usually provide results that exhibit good precision and accuracy. However, the selection of the optimum parameters should be based on studies of the behaviour of the plasma itself. Spectrochemical characteristics of the ICP must therefore be elucidated.

Some experimental approaches in plasma diagnostics have been suggested in order to understand the fundamental characteristics of ICPs [2]. The electron number density and the electron temperature are typical characteristics in the plasma, and great efforts have been made to elucidate these parameters in the plasma [3–6].

Atomic absorption occurring through the body of the plasma also gives useful information for the plasma studies. Assuming that the Lambert–Beer law is satisfied, atomic absorption spectrometry (AAS) can provide the relative population of chemical species in the plasma [7–11]. Nojiri et al. [7] reported the radial distribution of calcium atoms and found calcium atoms also at off-centre positions. The spatial distribution of argon atoms in the metastable state, which would play a significant role in the excitation and ionization processes in the plasma, was investigated by Uchida et al. [8], and it was pointed out that the most abundant proportion of the metastable argon atoms was in the induction region of the ICP.

Correspondence to: K. Wagatsuma, Institute for Materials Research, Tohoku University, Katahira 2-2-1, Sendai 980 (Japan).

SSDI 0003-2670(93)E0431-6

Plasma evaluation by AAS offers several advantages: remote measurement that hardly influences the plasma itself; straightforward knowledge obtained as the relative densities of various species in the plasma; and simple instrumentation.

In selecting the element to be employed as a probe in the AAS method, it is desirable that both ionic and atomic resonance emission lines are in the wavelength region above 200 nm so that they can be measured with an air-path spectrometer. Zinc is a suitable element for this approach. Further, atomic absorption employing these resonance lines faithfully reflects the state density of each species in the plasma because both the neutral zinc atom and the singly ionized ion have a single ground-state level. Based on AAS determinations, it is possible to measure the relative populations of singly ionized ions zinc and neutral zinc atoms. Previous investigations have revealed that the carrier gas flow-rate, observation height and incident power are the major parameters that influence emission intensities in ICP emission spectrometry [12]. This paper describes the behaviour of zinc species in an ICP as a function of these three parameters. Particular attention is paid to the flow-rate of the carrier gas, which seriously affects the excitation efficiency at the central channel of the ICP.

It has been reported that the characteristics of an argon matrix ICP containing small amounts of nitrogen gas are considerably different from those of an argon ICP [13–16]. The behaviour of the zinc species in the mixed gas ICP was also investigated by AAS.

EXPERIMENTAL

Apparatus

A schematic diagram of the apparatus used is illustrated in Fig. 1. A zinc hollow-cathode lamp was employed as a primary light source for AAS. The power supply for driving the lamp was controlled by a signal generator in order to effect a pulsed discharge in the lamp. Emission radiation emanating from the lamp was modulated at the frequency of the discharge. The radiation passed through the body of the plasma and was then dispersed and detected using a sequentially scanning spectrometer. The modulated component in the source radiation was selected from the overall signals using a lock-in amplifier tuned to the frequency of the light modulation. The unmodulated components, mainly from the radiation

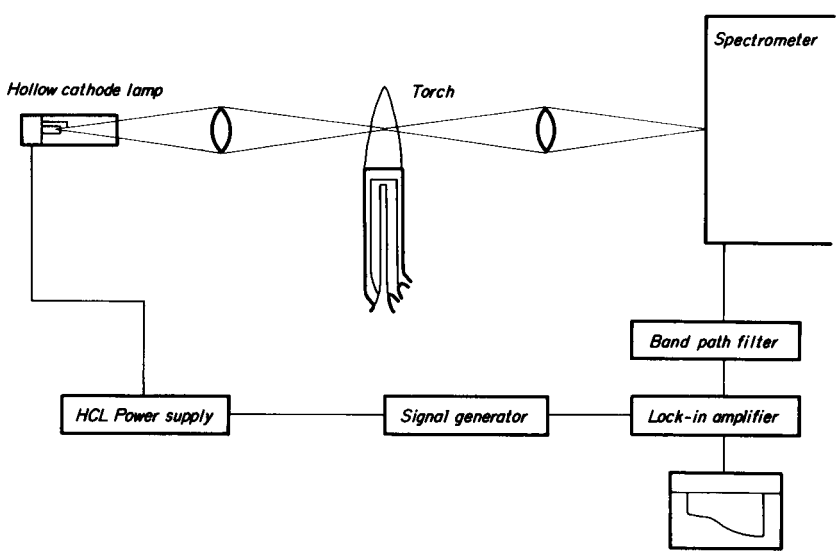

Fig. 1. Schematic diagram of the instrumentation.

emitted from the ICP itself, could be discriminated.

The plasma source unit consisted of a plasma torch, a matching box and a radiofrequency generator. Argon gas or argon–nitrogen mixed gas was used for supporting the plasma. The procedure for gas mixing has been described elsewhere [17]. A Fastie–Ebert mounting spectrograph, equipped with a photomultiplier tube, was employed. Table 1 gives all the other instrumentation and operating conditions.

Reagents

A stock standard solution of zinc was made by dissolving 2.5 g of high-purity zinc metal (> 99.999%) in small amounts of heated hydrochloric acid (6 M) and subsequent dilution to 10 mg ml^{-1} with distilled water. Test solutions were prepared by dilution of this solution with the appropriate amounts of dilute hydrochloric acid. All the test solutions contained ca. 0.06 M hydrochloric acid.

TABLE 1

Instrumental and operating conditions

Plasma source unit	ICPS-2H (Shimadzu)
R.f. generator	Frequency 27.12 MHz
	Nominal output power range 0–2.7 kW (continuous rating)
Induction coil	Two turns, 30 mm i.d., water cooled
Torch	Fassel-type, outer gas tube 18 mm i.d.
Nebulizer	Pneumatic
Spray chamber	Scott-type double pass
Spectrometer	GE-340 (Shimadzu)
	Focal length 3.4 m
	Grating 1200 grooves mm^{-1}
	Blaze wavelength 300 nm
	Slit width 30 μm
	Slit height 3 mm
Optics	Two fused-silica lenses, focusing 1 : 1 images of the light source on the centre of the ICP and on the entrance slit
Lock-in amplifier	LI-574A (NF Electronics)
Bandpass filter	FV-651 (NF Electronics)
Signal generator	E-1202 model (NF Electronics)
Hollow-cathode lamp	L233-30NQ (Hamamatsu Photonics)
	Modulation frequency 264 Hz
	Average current 25 mA
Incident r.f. power	0.6–1.6 kW (as parameter)
Reflected power	< 10 W (Ar ICP)
	< 40 W (Ar–N_2 ICP)
Outer gas	16.0 l min^{-1} Ar (fixed)
	16.0 l min^{-1} Ar and 0–0.6 l min^{-1} N_2 (Ar–N_2 ICP)
Intermediate gas	1.45 l min^{-1} Ar (fixed)
Carrier gas	0.75–1.65 l min^{-1} Ar (as parameter)
Observation height	5–33 mm above load coil (as parameter)
Sample uptake rate	See Fig. 4

TABLE 2

Assignment of zinc emission lines employed

Wavelength (nm)	Assignment	
	Upper (eV)	Lower (eV)
Zn I 213.86	5.796, $4s4p\ ^1P_1$	0.000, $(4s)^2\ ^1S_0$
Zn II 202.55	6.119, $4p\ ^2P_{3/2}$	0.000, $4s\ ^2S_{1/2}$

Analytical lines

The Zn I 213.86-nm and Zn II 202.55-nm lines were selected as the analytical lines for zinc atom and ion, respectively. The assignment for each line is summarized in Table 2. Both lines are the resonance lines. Therefore, one can calculate the relative number densities of the ground-state levels from the atomic absorption for these lines.

Procedures

After the ICP had been ignited and stabilized, distilled water was introduced into the plasma and the peak intensities (I_0) of the zinc analytical lines were recorded as blanks corresponding to a zinc-free solution. Then a test solution containing a certain amount of zinc was aspirated into the plasma. The peak intensities were lowered owing to the atomic absorption by zinc atoms or ions. When the signals had reached approximately constant levels, the decreased line intensities were monitored for ca. 5 min. The average value (I) was converted into the absorbance [$\log(I_0/I)$] for the sample solution. Again, the intensities for the blank solution were measured with distilled water. It was checked that there was little change in the source light intensities before and after the test solution was injected. It was further established that the intensities of the primary light source hardly changed when the ICP was on and off, indicating that the plasma in which only distilled water was introduced was transparent for the zinc analytical lines.

RESULTS AND DISCUSSION

Non-resonance absorption

Absorption phenomena also originate from non-resonance processes such as light scattering and molecular absorption, resulting in experimental errors in the determination of analyte species [18,19]. The non-resonance absorption is significant when particles of salts are decomposed incompletely in high-concentration solutions. In such a case, one can observe continuous absorption over a certain wavelength range [19], while the resonance absorption has a very narrow bandwidth.

To determine the non-resonance absorption in the present measurements, the degree of absorption by the zinc species at a wavelength of 217.0 nm in the neighbourhood of the zinc analytical lines was investigated. For this purpose, a lead hollow-cathode lamp was utilized as the light source (Pb I 217.00 nm). The open circles in Fig. 2 indicate the absorbance at 217.0 nm for several test solutions with relatively high zinc contents. All the absorbance values are almost zero, independent of the zinc concentration. Accordingly, it is assumed that the contribution of the non-resonance absorption can be neglected and that it is unnecessary to perform any background corrections. These results probably arise because the absorption path length in the ICP is much shorter compared to that of chemical flame atomizers used for conventional AAS.

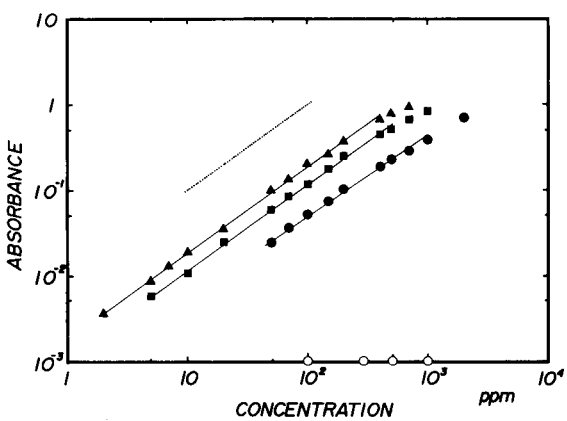

Fig. 2. Calibration graphs of absorbance at the Zn I 213.9-nm line with incident powers of (▲) 0.6, (■) 1.0 and (●) 1.6 kW. Observation height, 14 mm ALC; carrier gas flow-rate, 1.0 l min^{-1}. ○ = Absorbance measured at a wavelength of 217.0 nm. Dotted line expresses the slope of unity.

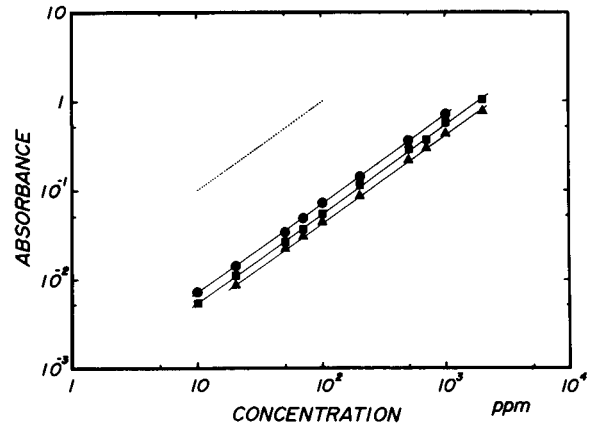

Fig. 3. Calibration graphs of absorbance at the Zn II 202.5-nm line. Operating conditions for the ICP as in Fig. 2.

Dynamic range

A major problem in AAS is that the concentration range over which the calibration graph is linear is not very wide. Saturation in the absorbance readily takes place at high analyte concentrations.

For subsequent measurements, it should be confirmed that the absorbance values obtained correspond linearly to the densities of the zinc species in the plasma. The linearity of the calibration graphs for both zinc analytical lines under different conditions was examined.

Figure 2 shows calibration graphs of the absorbance at the Zn I 213.9-nm line under several operating conditions. The manufacturer recommends a setting of the parameters used in Fig. 2 as the compromise conditions in this ICP system. Although saturation occurs at higher zinc concentrations, straight lines can be observed for three different incident powers. The slope of these graphs is almost unity, implying that the Lambert–Beer law is obeyed. In such a case, the absorbance data provide quantitative information on the density of zinc atoms and ions in the plasma. It is also found that the absorbance at the Zn I 213.9-nm line increases with a decrease in the incident power. Figure 3 shows calibration

graphs for the Zn II 202.5-nm line under the same ICP conditions as in Fig. 1. These graphs remain linear up to a zinc concentration of 2 mg ml^{-1} (the highest zinc content in the test solutions prepared), whereas saturation takes place for the Zn I line. Because the sensitivity of the Zn II line is lower compared than that of the Zn I line, the dynamic range shifts towards higher zinc concentrations. In addition, the absorbance at the Zn II 202.5-nm line increases with increase in the incident power, in contrast to the results obtained with the Zn I 213.9-nm line.

As indicated in Fig. 2, test solutions where the absorbance is less than about 0.5 give results within the linear range of the absorbance for the Zn I 213.9-nm line regardless of the incident power. The absorbance value increases with increasing flow-rate of the carrier gas, as described later (see Fig. 5), and then the dynamic range of the calibration graph shifts towards lower zinc concentrations although the upper absorbance of the linear calibrations is maintained at ca. 0.5. Considering these effects, a zinc concentration of 0.1 mg ml^{-1} was selected for the test solution used in the subsequent experiments.

Precision of measurements

The precision of the measurements becomes worse at higher concentrations of zinc. In this case, the ability to eliminate the radiation emitted from the ICP is a major factor in determining the stability of the detected absorption signals because the zinc emission lines from the ICP become more intense with increasing amounts of zinc in the test solution. When the intensity of the ICP emission becomes much greater than that of the primary light from the hollow-cathode lamp, it is difficult to obtain the absorbance of the zinc analytical lines with small deviations. In most instances, however, 0.1 mg ml^{-1} zinc solutions employed in the following measurements caused no problems with the precision of the measured absorbance, the relative standard deviations being within a few percent. Further, the precision of the absorbance determination is decreased for larger incident radiofrequency (r.f.) power levels. Under extremely high power conditions (more than 2.0 kW in the present instrumentation), it is almost impossible to estimate the absorbance values owing to the large signal drifts. This effect can also be explained by the increased emission intensities from the ICP.

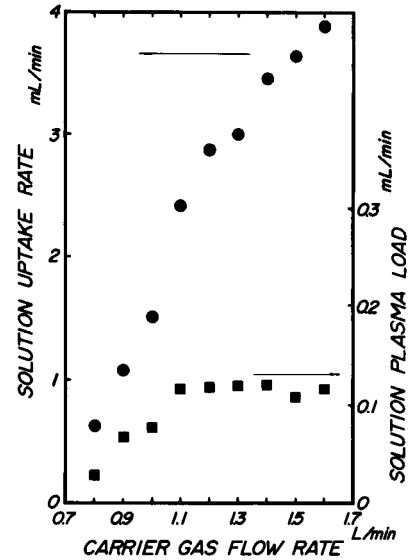

Fig. 4. Variation of (●) the solution uptake rate and (■) the rate of the solution actually loaded into the plasma as a function of the carrier gas flow-rate when distilled water was aspirated.

Absorbance versus flow-rate of carrier gas

The carrier gas flow-rate is a very critical parameter in ICP emission spectrometry. Changes in spectral line intensities with variation in the flow-rate of the carrier gas lead to the changes in both the flow-rate of the aerosol and the characteristics of the plasma itself [12]. Therefore, this parameter has to optimized.

Figure 4 shows the variation in the uptake rate of the solution as a function of the carrier gas flow-rate when distilled water is aspirated. The uptake rate is approximately proportional to the carrier gas flow-rate although the absolute values may vary slightly depending on the experimental conditions. In the nebulizer used, the solution uptake rate is increased by a factor of ca. 6 when the carrier gas flow-rate is increased from 0.8 to 1.6 l min^{-1}. However, it has been reported that the solution uptake rate does not always correspond to the actual solution plasma load [20–23].

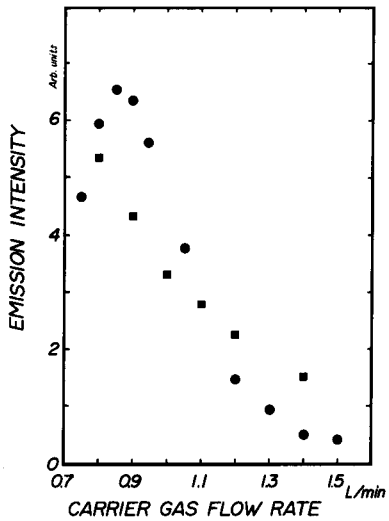

Fig. 5. Relationship between emission intensities of the (●) the Zn II 202.5-nm and the (■) the Ar I 404.4-nm lines and the carrier gas flow-rate. Incident power, 1.5 kW; observation height, 14 mm ALC.

The rate of the solution loaded into the plasma was roughly estimated from the weight difference between the solution uptake and the drain when distilled water was aspirated, as shown by solid squares in Fig. 4. The results indicate that the solution load rate reaches a plateau above a carrier gas flow-rate of ca. 1.1 l min^{-1}. This value agrees with that reported by Boorn et al. [20]. Hence the uptake rate of the sample is an insignificant parameter, especially at higher flow-rates of the carrier gas.

The influence of the carrier gas flow-rate on the emission intensities of the Zn II 202.5-nm and the Ar I 404.4-nm lines is illustrated in Fig. 5. The zinc line intensity (solid circles) reaches a maximum at a flow-rate of 0.85 l min^{-1} and then decreases. The peak position of the maximum depends on the operating conditions of the ICP. Apparently, the decrease in the zinc emission intensity cannot be explained by the variation in the rate of the solution plasma load. As pointed out by Bates and Olesik [24], the change in the ion emission intensities is not due to variation in the number of zinc ions per unit amount of sample entering the plasma, but to the decreasing fraction of the ions. The intensity of the argon line (solid squares) decreases with increasing flow-rate of the carrier gas. It is considered that the results in Fig. 5 can be attributed to the decreased efficiency in ionizing and exciting the analyte species caused by larger amounts of the carrier gas in the plasma.

Figure 6 shows the variations in the absorbance at the Zn I 213.9-nm (open circles) and the Zn II 202.5-nm lines (solid circles) as a function of the carrier gas flow-rate. The absorbance at the Zn II 202.5-nm line reaches a maximum when the carrier gas flow-rate is about 1.3 l min^{-1}. On the other hand, the absorbance at the Zn I 213.9-nm line increases with increase in the flow-rate of the carrier gas and the variation is sigmoid shaped. It can be assumed that the abrupt increase in the absorbance for flow-rates of 1.1–1.4 l min^{-1} is derived principally from alterations in the plasma characteristics, whereas below a carrier gas flow-rate of 1.1 l min^{-1} the gradual increase in the absorbance may be caused by the variation in the solvent plasma load (solid squares in Fig. 4). Recently, Hobbs and Olesik [25] reported that the electron number densities of the ICP are changed by the degree of desolvation of the aerosol aspirated in the plasma. It was eluci-

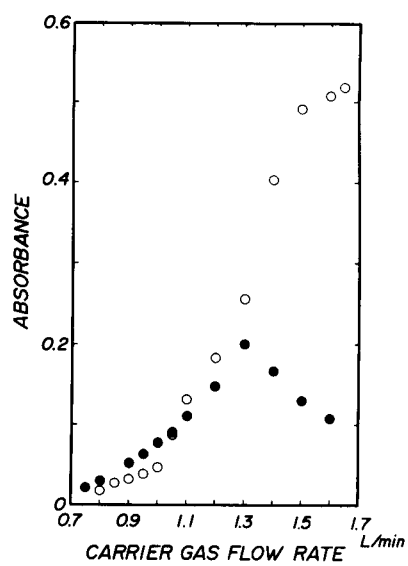

Fig. 6. Effect of flow-rate of the carrier gas on the absorbances estimated at (○) the Zn I 213.9-nm and (●) the Zn II 202.5-nm lines. Incident power, 1.5 kW; observation height, 14 mm ALC.

dated from their study that the properties of the droplets entering the plasma, which can be controlled by the transport rates of the carrier gas, are an important factor determining ionization in the plasma. Therefore, the results presented in Fig. 6 can be explained in the following way: the degree of zinc ionization is lowered owing to the decrease in the plasma temperature when the carrier gas flow-rate increases. It should be noted that the peak position of the ionic absorbance corresponds approximately to the portion of the rapid increase in the atomic absorbance. These changes can be attributed to a shift in the dynamic equilibrium between the atomic and ionic states of zinc.

Effect of incident r.f. power

Figure 7 shows variations in the absorbance at (a) the Zn I 213.9-nm and (b) the Zn II 202.5-nm lines as a function of the carrier gas flow-rate for several different r.f. power levels. The peak position of the ionic absorbance is shifted towards higher carrier gas flow-rates along with an increase in the incident power, and the maximum value of the absorbance becomes greater. Variations in the atomic absorbance follow those in the ionic absorbance; abrupt rises occur in the vicinity of the maximum position of the corresponding ionic absorbance. It is interesting that, at an r.f. power of 0.6 kW, the atomic absorbances of zinc are always the highest. The ICP loaded at 0.6 kW is very faint and emits weak spectra of both argon and the analyte species. Under such operating conditions, the atomization of zinc takes place with high efficiency, probably because the degree of ionization is lower.

Because the plasma temperature is raised with increase in the incident r.f. power, it is expected that the atom–ion equilibrium, which is affected by the flow-rate of the carrier gas, depends strongly on the r.f. power levels supplied. One can assume a norm temperature [12] at which the relative number density of zinc ions in the ground state is at a maximum, derived from the scheme $Zn \rightleftharpoons Zn^{+} \rightleftharpoons Zn^{2+}$ (or $Zn^{+}*$) [12]. Changes in the plasma temperature caused by the carrier gas flow will pass through the norm temperature at higher flow-rates when the plasma is generated at higher r.f. power.

Effect of observation height

The investigations described above were carried out at an observation height of 14 mm above the load coil (ALC): a so-called normal analytical

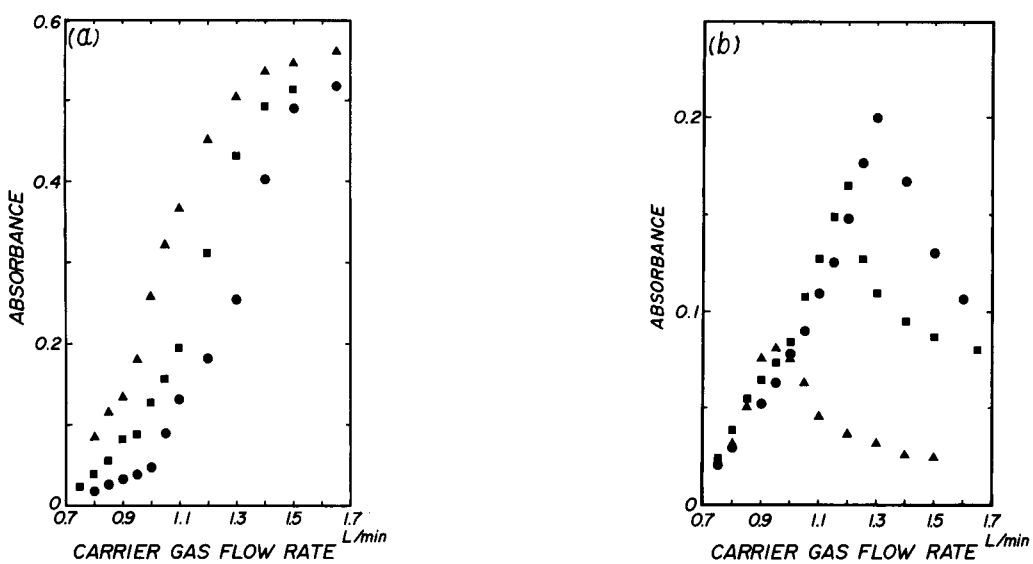

Fig. 7. Variation of the absorbance at (a) the Zn I 213.9-nm and (b) the Zn II 202.5-nm lines with increase in the carrier gas flow-rate for incident powers of (▲) 0.6, (■) 1.0 and (●) 1.5 kW. Observation height, 14 mm ALC.

zone [26] which is best suited for ICP emission analyses. The behaviour of the atomic and ionic absorbances of zinc for the different regions of the ICP was examined.

Figure 8 shows the variations in the absorbance at (a) the Zn I 213.9-nm and (b) the Zn II 202.5-nm lines as a function of the carrier gas flow-rate for three different observation heights. In the measurement at 5 mm ALC (solid triangles), the position of the maximum ionic absorbance is moved towards lower flow-rates of the carrier gas compared with that obtained at 14 mm ALC (solid circles). The result at 5 mm ALC follows typical changes in the population of zinc ions in the initial radiation zone of the ICP [26]. Because the plasma temperature in this region is relatively low, one can expect a similar behaviour to be observed when the r.f. power is decreased at an observation height of 14 mm ALC (Fig. 7). With an observation height of 29 mm ALC (solid squares), the maximum in the ionic absorbance disappears and the latter increases monotonously with increasing carrier gas flow-rate. However, the absorbance values are lower than those at 5 or 14 mm ALC. The observation at 29 mm ALC was carried out in order to survey a portion of the tail plume [26] above the normal analytical zone. The induction zone of ICP [26], which forms the core of the plasma as a hot region, surrounds the normal analytical zone and the initial radiation zone. However, the portion of the tail plume is not affected directly by the plasma core and is far above the plasma core where the atom–ion equilibrium is principally determined. Both the ionic and the atomic absorbance vary with similar dependences on the carrier gas flow-rate in contrast with the tendency at 5 or 14 mm ALC. It seems that, in this region, the number densities of both atomic and ionic zinc change with variation in the flow-rate of the argon carrier gas which transports surviving atomic and ionic zinc from the plasma core.

Atom–ion equilibrium in argon–nitrogen mixed gas ICP

Several workers have pointed out that, in an argon matrix ICP containing small amounts of nitrogen, the emission intensities are enhanced compared with those in a conventional argon ICP [13–17]. This phenomenon can be explained by variations in the plasma temperature caused by the differences in the physical properties such as heat content and heat conductivity, between argon and nitrogen [12]. It has also been observed

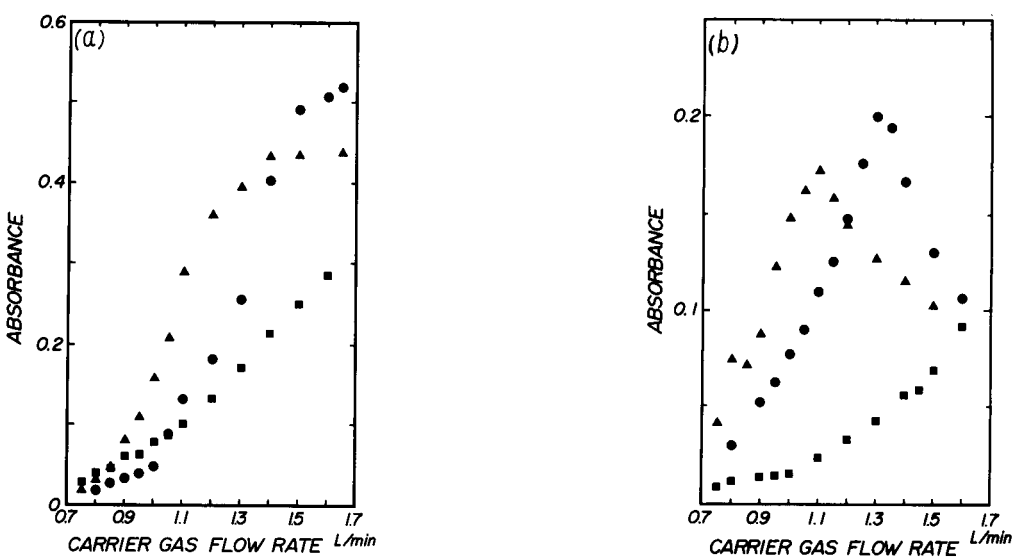

Fig. 8. Variation of the absorbance at (a) the Zn I 213.9-nm and (b) the Zn II 202.5-nm lines with increase in the carrier gas flow-rate for observation heights of (▲) 5, (●) 14 and (■) 29 mm ALC. Incident power, 1.5 kW.

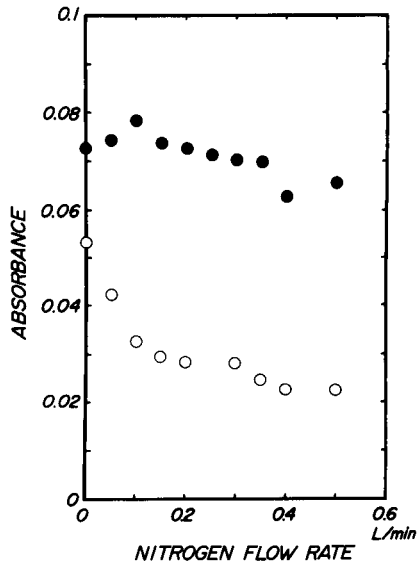

Fig. 9. Change in the absorbance at (○) the Zn I 213.9-nm and (●) the Zn II 202.5-nm lines as a function of the nitrogen flow-rate added to the plasma outer gas flow. Incident power, 1.5 kW; observation height, 14 mm ALC; argon flow-rate in the outer gas, 16.0 l min^{-1} (fixed).

that the emission intensities of both the Zn I 213.9-nm and Zn II 202.5-nm lines increased when nitrogen gas was added to the argon ICP [17].

Figure 9 shows the changes in the absorbance at the Zn I 213.9-nm (open circles) and the Zn II 202.5-nm lines (solid circles) as a function of the nitrogen flow-rate added to argon. The mixed gas was introduced only as the outer gas flow of the ICP. For the intermediate gas flow and the carrier gas flow, only argon was employed. The atomic absorbance decreases with increase in the nitrogen flow-rate and then reaches a steady state at about 0.4 l min^{-1}. The ionic absorbance shows a slight decrease with increasing nitrogen flow-rate added.

It seems likely that the decrease in the atomic absorbance results from the increase in the plasma temperature caused by the nitrogen addition. The zinc atom–ion equilibrium shifts to the ionic side, which results in a reduced population of zinc atoms in the ground state. On the other hand, as shown in Fig. 9 (solid circles), the relative population of zinc ground-state ions experiences only a slight alteration as the nitrogen flow-rate is varied. The shift in the atom–ion equilibrium to the ionic species can cause an increase in the overall population of zinc ions. However, it should be noted that only the ground-state ions are detected by atomic absorption at the Zn II 202.5-nm

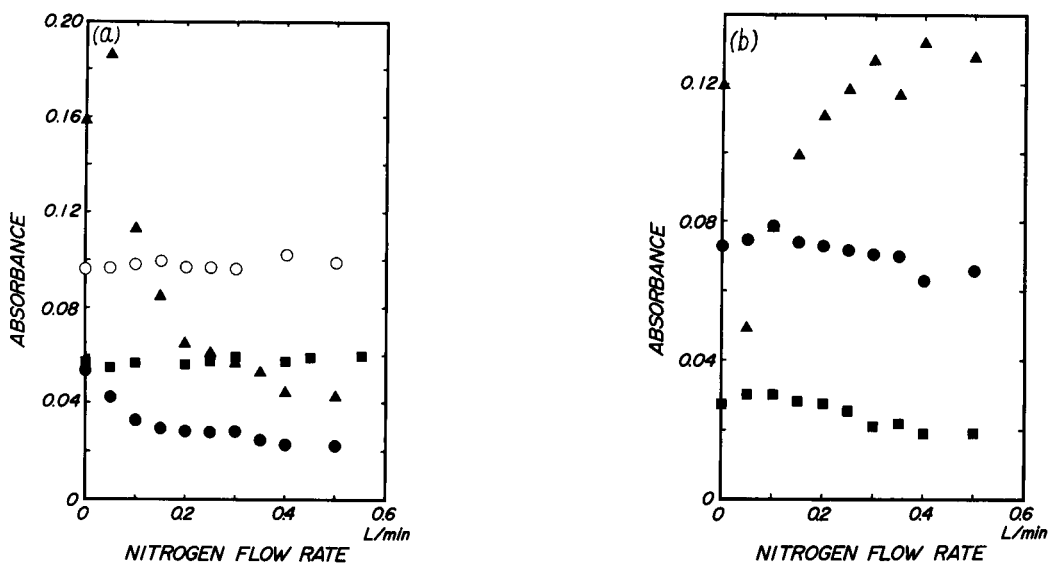

Fig. 10. Variation of the absorbance at (a) the Zn I 213.9-nm and (b) the Zn II 202.5-nm lines as a function of the nitrogen flow-rate in the argon–nitrogen ICP for observation heights of (▲) 5, (●) 14, (■) 24 and (○) 33 mm ALC. Incident power, 1.5 kW; argon flow-rate in the outer gas, 16 l min^{-1} (fixed).

line. The distribution between the ground and the excited states of zinc ion is also affected by variations in the plasma temperature. The number of zinc ions in the ground state is offset by redistribution among various excited states of zinc ion. As a result, the resulting population of the ion ground state may not be greatly changed.

Figure 10 shows the relationships between the absorbance at (a) the Zn I 213.9-nm and (b) the Zn II 202.5-nm lines and the nitrogen flow-rate for different observation heights. It should be noted that the atomic absorbances are almost constant and independent of the nitrogen concentration at observation heights of 24 mm (solid squares) and 33 mm ALC (open circles). This result implies that the nitrogen addition has little influence on the atom–ion equilibrium in the tail plume zone [26] of the ICP. In the measurement at 5 mm ALC, the ionic absorbance exhibits a temporal decrease at a nitrogen flow-rate of ca. 0.05 l min^{-1}, in contrast with the atomic absorbance (solid triangles in Fig. 10). This suggests that de-excitation towards zinc atoms in the ground state takes place in the initial radiation zone of the plasma.

REFERENCES

1 P.W.J.M. Boumans and F.J. de Boer, Spectrochim. Acta, Part B, 30 (1975) 309.
2 P.W.J.M. Boumans (Ed.), Inductively Coupled Plasma Emission Spectrometry, Part II, Wiley, New York, 1987, Chap. 10.
3 B.L. Caughlin and M.W. Blades, Spectrochim., Acta, Part B, 40 (1985) 98.
4 A. Montaser, V.A. Fassel and G. Larsen, Appl. Spectrosc., 35 (1981) 385.
5 D.J. Kalnicky, R.N. Kniseley and V.A. Fassel, Spectrochim. Acta, Part B, 30 (1975) 511.
6 G.R. Kornblum and L. de Galan, Spectrochim. Acta, Part B, 29 (1974) 249.
7 Y. Nojiri, K. Tanabe, H. Uchida, H. Haraguchi, K. Fuwa and J.D. Winefordner, Spectrochim. Acta, Part B, 38 (1983) 61.
8 H. Uchida, K. Tanabe, Y. Nojiri, H. Haraguchi and K. Fuwa, Spectrochim. Acta, Part B, 36 (1981) 711.
9 L.P. Hart, B.W. Smith and N. Omenetto, Spectrochim. Acta, Part B, 41 (1986) 1367.
10 J.P. Rybarczyk, C.P. Jester, D.A. Yates and S.R. Koirtyohann, Anal. Chem., 54 (1982) 2162.
11 G. Gillson and G. Horlick, Spectrochim. Acta, Part B, 41 (1986) 1986.
12 P.W.J.M. Boumans (Ed.), Inductively Coupled Plasma Emission Spectrometry, Part I, Wiley, New York, 1987, Chap. 4.
13 A. Montaser and J. Mortazavi, Anal. Chem., 52 (1980) 225.
14 A. Montaser, V.A. Fassel and J. Zalewski, Appl. Spectrosc., 35 (1981) 292.
15 E.H. Choot and G. Horlick, Spectrochim. Acta, Part B, 41 (1986) 889.
16 E.H. Choot and G. Horlick, Spectrochim. Acta, Part B, 41 (1986) 925.
17 K. Wagatsuma and K. Hirokawa, Anal. Sci., 9 (1993) 509.
18 I. Rubeska, Anal. Chim. Acta, 40 (1968) 187.
19 K. Yasuda and N. Hasegawa, Atomic Absorption Analysis, Kohdansha, Tokyo, 1972, Chap. 1.
20 A.W. Boorn, M.S. Cresser and R.F. Browner, Spectrochim. Acta, Part B, 35 (1980) 823.
22 R.F. Browner and A.W. Boorn, Anal. Chem., 56 (1984) 786.
23 F.J.M.J. Maessen, P. Coevert and J. Balke, Anal. Chem., 56 (1984) 899.
24 L.C. Bates and J.W. Olesik, J. Anal. At. Spectrom., 5 (1990) 239.
25 S.E. Hobbs and J.W. Olesik, Spectrochim. Acta, Part B, 48 (1993) 817.
26 S.R. Koirtyohann, J.S. Jones, C.P. Jester and D.A. Yates, Spectrochim. Acta, Part B, 36 (1981) 53.

Analytica Chimica Acta, 284 (1993) 361–366
Elsevier Science Publishers B.V., Amsterdam

Roll-over effect in graphite furnace atomic absorption spectrometry with a gold pulsed hollow-cathode lamp

A.J. Aller

Department of Biochemistry and Molecular Biology, University of León, E-24071 León (Spain)

(Received 13th May 1993; revised manuscript received 6th August 1993)

Abstract

The presence of stray light in graphite furnace atomic absorption spectrometry causes errors in background correction at high analyte concentrations. The stray light level originates in the hollow-cathode lamp, but can be modified in the atomizer. Some differences were noted for both wall and platform atomization. Other factors, such as the presence of matrix components (copper) or chemical modifiers (vanadium), also affect the sensitivity for gold and consequently have an effect on the roll-over phenomenon. Experimental results show that the stray radiation depends on the wavelength region used for the determination of gold.

Keywords: Atomic absorption spectrophotometry; Gold; Roll-over

In graphite furnace atomic absorption spectrometry (GFAAS), the shapes of the absorbance–time profiles for certain analyte concentrations are different for both normal and background-corrected AAS signals if the phenomenon of roll-over takes place. With analyte concentrations high enough to cause roll-over, the absorption signal of the analyte shows a dip, i.e., the absorbance–time profile rises with increasing atom concentration in the furnace, but before reaching the maximum atom population the absorbance decreases. Then the atom concentration in the furnace decreases but the signal rises again to the initial maximum before declining to zero.

The roll-over phenomenon has been extensively studied in Zeeman-effect AAS [1–4]. The roll-over absorbance has been correlated with self-absorption differences of emission lines in hollow-cathode lamps for Zeeman-effect AAS [5], while the roles of various parameters, such as overlapping factors, Zeeman splitting ratios, non-linear coefficients [6], applied field strength, excitation wavelength and spectral profile [7], were also investigated as causes of calibration graph roll-over.

The Smith–Hieftje technique for background correction in AAS was initially accepted as a roll-over-free system [8,9]. However, the roll-over phenomenon has also been observed for the Smith–Hieftje background correction system in both the flame and furnace atomization of a few elements: Al, Cu, Cd, Fe, Mn, V [10–12], Cr, Ni [12] and Au [13]. From the studies of De Galan and De Loos-Vollebregt, some statements have been derived: the maximum values on either side of the dip remain at a constant value, the roll-over phenomenon originates in the hollow-cathode lamp and the relatively low maxima in the Smith–Hieftje curves result from a strongly reduced sensitivity or a high stray light level during the low lamp current pulse. Roll-over was attributed [10,11] to non-absorbable stray light, which is mainly constituted by general scatter. However, weak non-absorbable spectral lines, near the resonance line and increasing in relative

SSDI 0003-2670(93)E0477-O

intensity on pulsing, can also behave as stray light. Nonetheless, the shape of the absorbance curve obtained is different from that which would be given by stray light [12]. Larkins [12] has shown that the influence of weak line-wings (the Lorentz component) on the shape of absorbance curves at high analyte concentrations is the main cause of the flattening of the calibration graph in the Smith–Hieftje technique. As a result, stray light from any source can leads to errors in background correction when it is not completely absorbed [11,12].

From a theoretical analysis, De Galan and De Loos-Vollebregt [10] revealed an interdependence between roll-over of the analytical curve, analytical sensitivity and wavelength proximity of the background correction systems. However, some instrumental parameters, such as atomizer type and temperature programme, could affect this interrelationship and consequently the roll-over phenomenon. Previous studies have considered the roll-over effect for single analyte solutions, although the analyte was usually determined in a complex matrix and concomitant species and chemical modifiers could also modify the roll-over conditions. Hence some single analyte concentrations, for which the roll-over effect is not observed, could show this effect if they are atomized in the presence of other metals. The general aim of this paper is to show the influence of the atomizer type, concomitant species and pyrolysis temperature on the roll-over effect.

EXPERIMENTAL

Apparatus

All AAS experiments were made on a Thermo Jarrel Ash (TJA) SH-11 spectrophotometer with a CTF-188 controlled-temperature graphite furnace atomizer. Pyrolytic graphite-coated cylindrical (Part No. 124544-02) and uncoated rectangular (Part No. 124544-04) graphite tubes were used. Pyrolytic graphite-coated micro-boats were used with rectangular tubes. In TJA instruments micro-boats can be used in either a horizontal or vertical arrangement; both possibilities were explored in this work. Holes in all rectangular graphite tubes used with a horizontal platform were made with a drill. The spectrometer was provided with a Smith–Hieftje background-correction system. A Visimax II gold hollow-cathode lamp and an Epson 118 recorder were used. Samples for the furnace studies were injected as a cloud by means of an automatic nebulization system, whereas for the flame studies the usual nebulizer system was used. Argon was used as the purge gas. The operating conditions were selected as given in Table 1.

TABLE 1

Instrumental components and experimental parameters

Wavelength (nm)	242.8, 267.6, 274.8
Spectral band width (nm)	From 1.0 to 0.3
Lamp current (mA)	5
Fastac delay (s)	6.0
Injection volume (μl)	10

Furnace programme

	Temperature (°C)	Time (s)		Purge (Position)
		Ramp	Hold	
Dry	150	2	0	1
Pyrolysis 1	450	20	0	2
Pyrolysis 2	600–900	20	0	1
Atomization	2200	0	4	0
Cleaning	2400	–	0	2

Reagents

Working standard solutions were prepared by conventional dilution of concentrated stock standard solutions. All chemicals were of analytical-reagent grade, and distilled, deionized water was used for the preparation of sample and standard solutions.

Procedure

The effects of both chemical modification and interferences were studied as described later. The read-out system was used in the both integrated absorbance and peak-height modes in all measurements. All results presented are averages of at least three measurements.

The total stray light was derived from the limiting absorbance measured at a low lamp cur-

rent. However, the stray light level during the high-current pulses cannot be obtained directly, but it can be deduced indirectly from the net absorbance signal. The net absorbance signal is obtained by subtraction of the gross absorbance and the high-current data. The gross absorbance is the absorbance obtained at low current, being the signal provided by the analyte and the matrix (background).

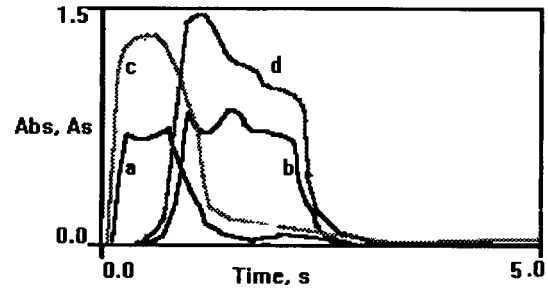

Fig. 1. Background-corrected AAS signal for (a) wall (1.5 μg ml^{-1} Au) and (b) horizontal (200 ng ml^{-1} Au) platform atomization. Lines (c) and (d) are the background plus analyte signals of lines (a) and (b), respectively. Ashing temperature = 600°C.

RESULTS AND DISCUSSION

Effect of atomizer type on roll-over and stray light

In Fig. 1 the furnace AAS signals for the wall atomization and horizontal platform atomization of gold aqueous solutions are shown. In the platform atomization mode the analyte curve levels off at a lower concentration than the corresponding curve for wall atomization, which is the result of the higher sensitivity for that atomization mode. The peak for the horizontal platform atomization is blunted at a limiting absorbance of about 1.31 absorbance, which corresponds to a stray light level of 0.49%. The Smith–Hieftje signal at high analyte concentrations is slightly higher for the platform atomization (0.75 absorbance) than for the wall atomization mode (0.65 absorbance). The stray light level is higher for the vertical platform atomization (Table 2). The relative sensitivity and the maximum absorbance of the Smith–Hieftje curves are also presented in Table 2.

The dip level of the Smith–Hieftje signal decreases with increasing gold concentration for both wall and platform atomization. However, lower dip level of the Smith–Hieftje signals and higher gross signals were obtained for both wall and horizontal platform atomization in comparison with those obtained for the vertical platform atomization mode. These results suggest that the

TABLE 2

Stray light levels at low and high current and relative sensitivity loss for the atomization of gold

Atomization mode	AAS curves level off at (absorbance)	Stray light level at low current (%)	Peak area (absorbance)	Smith–Hieftje signal at high analyte concentration (absorbance)		Stray light level at high current (%)		Relative sensitivity (% loss)
				Maximum	Dip	Measured	Required to prevent roll-over	
Wall [a] (242.8 nm)	1.31	0.490	1.395 [a1]	0.90	0.82	2.73	11.0	45.0
	1.38 (1st peak)	0.417	2.622 [a2]	0.88	0.45	2.80	12.3	44.0
	1.41 (2nd peak)	0.389		0.91	0.74	2.69	10.9	45.5
Wall [b] (267.6 nm)	1.46	0.347	1.624	1.11	0.97	1.96	7.3	55.5
Horizontal platform [c] (242.8 nm)	1.25	0.562	1.068	0.75	0.69	3.27	16.3	37.5
Vertical platform [d] (242.8 nm)	1.16	0.860	0.893	0.73	0.70	5.10	18.5	36.5

[a] 3 μg ml^{-1} Au from an ore concentrate without (a_1) and with (a_2) 2.0% V. [b] 1.8 μg ml^{-1} Au + 1.0% V. [c] 3 μg ml^{-1} Au. [d] 3μg ml^{-1} Au.

TABLE 3

Stray light levels for both the air–acetylene (A–A) and nitrous oxide–acetylene (N–A) flames at two wavelengths

Flame	Wavelength (nm)	Stray light level (%)
A–A	242.8	0.59
N–A	242.8	0.88
A–A	267.6	0.38
N–A	267.6	0.50

stray light level during the high lamp current pulses behaves differently depending on the atomization mode. As the limiting absorbance measured with both wall and platform atomization shows slightly different values, the roll-over phenomenon, originating in the hollow-cathode lamp, can be modified in the atomizer. This conclusion is supported by the results obtained with flame AAS. The stray light level obtained for gold alone in flame AAS depends on the flame composition (Table 3), thus differing in turn from those obtained for the furnace atomization mode.

The stray light originating from the radiation source scatter background depends on the wavelength region [14] (Fig. 2). The roll-over phenomenon observed at 242.8 nm shows a stray light level higher than that observed at both 267.6 and 274.8 nm, where roll-over was not detected. These findings were also observed in flame AAS (Table 3). From these results, it can be concluded that the roll-over effect is not dependent on the background level (at least for some levels of stray

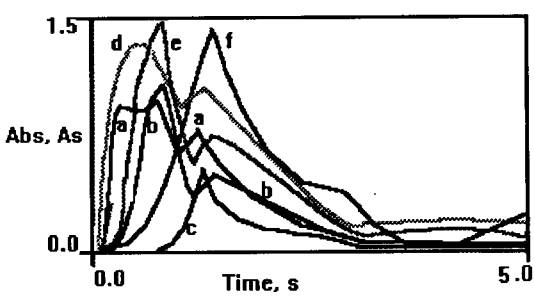

Fig. 2. (a)–(c) Analyte and (d)–(f) background plus analyte peak profile signals for gold [(a), (d) 3 μg ml^{-1} + 1.0% V; (b), (e) 1200 μg ml^{-1}; and (c), (f) 1995 μg ml^{-1}] at three wavelengths [(a), (d) 242.8 nm; (b), (e) 267.6 nm; and (c), (f) 274.8 nm] for wall atomization. Ashing temperature = 600°C. Note that a higher background is found at 274.8 nm.

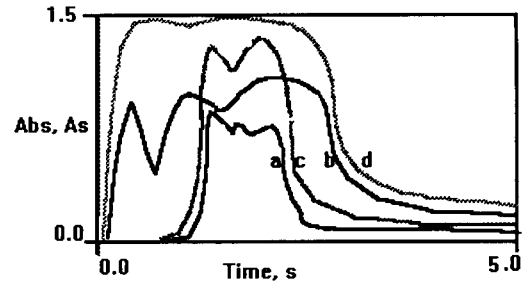

Fig. 3. Effect of (a) copper (2000 μg ml^{-1}; horizontal platform atomization) and (b) vanadium (2.0%; wall atomization from an ore concentrate) on the dip of the roll-over phenomenon for the atomization of gold [(a) 50 ng ml^{-1}; (b) 3 μg ml^{-1}]. Lines (c) and (d) are the background plus analyte signals of lines (a) and (b), respectively. Ashing temperature 600°C.

light), because the higher background is obtained for the wavelength of lower sensitivity (274.8 nm) (Fig. 2).

Effect of concomitant species on roll-over

The effect of the copper and vanadium concentration on the roll-over phenomenon was also studied for gold GFAAS. The gold atomic absorption peak profile shows two peaks in the presence of either vanadium or copper; the first and second peaks are referred to as the peaks appearing at short and long atomization times, respectively. When the phenomenon of roll-over is present, a dip is observed for these peaks appearing for the conventional AAS signal (Fig. 3). The roll-over effect increases with increasing vanadium concentration, which can be largely explained by the fact that the presence of vanadium favours gold atomization. The presence of copper can also affect the roll-over phenomenon, but a few differences are noted for these peak profiles obtained for the gold atomization in the presence of each concomitant. The roll-over effect for gold is stronger and appears earlier in the first peak as the vanadium concentration increases, but in the presence of copper the roll-over is observed earlier in the second peak. This difference occurs when accompanying metals affect the atomization rate of gold in a different way. Figure 3 also shows that the roll-over observed for gold in the presence of copper appears at a

gross absorbance (0.75) lower than the corresponding value (0.90) when vanadium is used. These results suggest that a higher stray light level is observed if copper is present (horizontal platform atomization). In conclusion, copper appears to be not as good a chemical modifier for gold as is vanadium or, alternatively, matrix components could show an absorption coefficient in the background channel higher than that in the gross channel.

The maxima on both sides of the dip do not remain at a constant value, because in the presence of vanadium the second peak shows higher absorbance values (wall atomization), while in the presence of copper higher absorbance values are obtained for the first peak (platform atomization). In other words, in the presence of copper the peak-height signal for the second peak (where the roll-over is observed) is slightly lower than the corresponding signal for the first peak (where the roll-over phenomenon is not observed). This could probably be a consequence of either a difference in the temporal behaviour of the atomization of both the analyte and concomitant species or a change in the absorption line profile (a modification of the absorption coefficient) as a result of the presence of concomitants (vanadium or copper).

From the influence of the vanadium concentration on the gold atomization, some interesting conclusions can be derived. Thus, the stray light level derived from the second peak of the gold atomic absorption peak profile decreases as the levelling off of the line increases with increasing vanadium concentration (Fig. 4, lines a and d). These results suggest that some vanadium species, vaporized during the course of the second peak, absorb some of the stray light, so diminishing the stray light level reaching the detector and simultaneously increasing the absorption at the high current channel. Unlike vanadium, other species from the matrix components probably do not take part in this absorption process because they were also present, and at the same concentration, in every experiment (in the absence and presence of vanadium).

The Smith–Hieftje signals for the gold atomization show some minimum differences for each

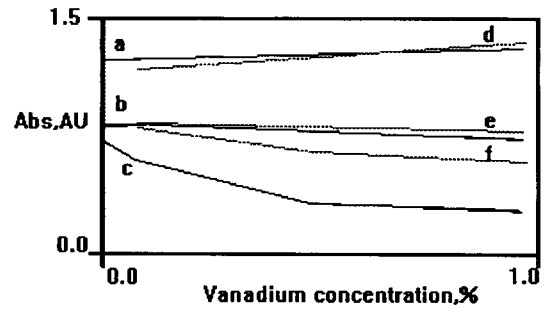

Fig. 4. Variation of the peak heights for (a), (d) the gross AAS signal (b), (e) net absorbance and (c), (f) dip for the wall atomization of gold as a function of the vanadium concentration. Solid [(a)–(c)] and dashed [(d)–(f)] lines refer to the first and second peaks, respectively.

of the two peaks depending on the vanadium concentration. The height of the second peak is always constant and slightly greater than the corresponding height for the first peak (Fig. 4, lines b and e). However, the height of the first peak increases slightly and then decreases with increasing vanadium concentration. This means that the sensitivity loss differs for each peak (Table 2), suggesting that any matrix element absorbs radiation at a wavelength very close to the analyte one when the first peak appears.

The dip height decreases (the dip is larger, which means that the roll-over effect is stronger) at higher vanadium concentrations (Fig. 4, lines c and f). The decrease in the dip height differs slightly for both peaks, suggesting that those parameters contributing to the formation of roll-over act to a different extent on every peak. Additionally, the gross signal height increases more slowly than the dip decreases with increasing vanadium concentration (Fig. 4). This means that the increase in the background with increasing vanadium concentration does not counteract the decrease in stray light. In other words, as both the light source and the readout system were the same in all the measurements, these results suggest that additional unabsorbed stray light would be generated in the atomizer. This additional stray light increases with increasing vanadium concentration.

Effect of ashing temperature

The temperature programme can also affect the roll-over effect because it can modify the stray light level and the relative sensitivity. Thus, a greater dip height is noted with increasing ashing temperature from 600 to 800°C. However, for a maximum temperature of 900°C the roll-over phenomenon disappears, probably because higher analyte losses are present. As a result, a decreased absorbance will be obtained. It is interesting that the stray light level is not modified by the ashing temperature, but the background is lowered. The background level is slightly higher for the wall atomization compared with that obtained for the platform atomization.

Conclusion

The roll-over effect, affected mainly by the relative sensitivity and stray light level, can be modified in the atomizer as a result of the presence of elements accompanying gold during the atomization path. The stray light produced in the hollow-cathode lamp differs for every wavelength range and its level during the low lamp current pulse can be modified by the presence in the atomizer of some matrix components (vanadium, copper). Stray light can also originate from the atomizer to an extent that depends on the furnace and platform geometry and flame composition. In some instances, the maximum on both sides of the dip does not remain at a constant value.

REFERENCES

1 M.T.C. de Loos-Vollebregt and L. de Galan, Appl. Spectrosc., 34 (1980) 464.
2 M.T.C. de Loos-Vollebregt and L. de Galan, Spectrochim. Acta, Part B, 37 (1982) 659.
3 H. Koizumi, H. Sawakabu and M. Koga, Anal. Chem., 54 (1982) 1029.
4 M.T.C. de Loos-Vollebregt and L. de Galan, Appl. Spectrosc., 38 (1984) 141.
5 B.V. L'vov, N.V. Kocharova, L.K. Polzik, N.P. Romanova and Yu.I. Yarmak, Spectrochim. Acta, Part B, 47 (1992) 843.
6 X. Feng and Y. Ma, Guangpuxue Yu Guangpu Fenxi, 6 (1986) 28.
7 F.R. Preli, Jr., J.P. Dougherty and R.G. Michel, Spectrochim. Acta, Part B, 43 (1988) 501.
8 S.B. Smith, Jr. and G.M. Hieftje, Appl. Spectrosc., 37 (1983) 419.
9 J.J. Sotera and H.L. Kahn, Am. Lab., 14 (1982) 100.
10 L. de Galan and M.T.C. de Loos-Vollebregt, Spectrochim. Acta, Part B, 39 (1984) 1011.
11 M.T.C. de Loos-Vollebregt and L. de Galan, Spectrochim. Acta, Part B, 41 (1986) 597.
12 P.L. Larkins, Spectrochim. Acta, Part B, 43 (1988)1175.
13 C. García-Olalla and A.J. Aller, Anal. Chim. Acta, 252 (1991) 97.
14 M.-L.W. Wu and R.G. Michel, Analyst, 110 (1985) 937.

Analytica Chimica Acta, 284 (1993) 367–377
Elsevier Science Publishers B.V., Amsterdam

Some processes occuring in graphite furnaces used for electrothermal atomic absorption spectrometry in the presence of organic chemical modifiers

Anatoly B. Volynsky

Laboratory of Organic Analysis, Department of Chemistry, Moscow State University, 119899 Moscow (Russian Federation)

Sergei V. Tikhomirov

Erratum

Some processes occurring in graphite furnaces used for electrothermal atomic absorption spectrometry in the presence of organic chemical modifiers, *Analytica Chimica Acta*, 284 (1993) 367–377, by A.B. Volynsky, S.V. Tikhomirov, V.G. Senin and A.N. Kashin

p. 367, 11th line of the Abstract, and p. 368, 14th line, left column: analyser should read atomizer.

p. 368, 5th line of the Experimental section: "graphite-coated" should be deleted.

p. 375, 7th and 9th line of the right column: m_{crit} should read $m_{crit}g$. It represents the weight of the particles that can be kept at the liquid–gas boundary.

ascorbic acid is a result of their diffusion from the carbon residue at the ... enhancement in the presence of ascorbic acid, which was observed earlier for lead, tin and a number of other elements, was caused by the substantial changes in the composition of the gas phase in the electrothermal analyser under non-STPF conditions.

Keywords: Atomic absorption spectrometry; Chemical modifier; Graphite furnaces

The first paper on the application of the sodium salt of EDTA to suppress the matrix interferences when determining Pb, Cd and Cu in natural waters and industrial wastes [1] was published 2 years before the term "matrix modifier", now more correctly termed "chemical modifier", had actually appeared [2]. Organic chemical modifiers, especially ascorbic acid [3] and the sodium and ammonium salts of EDTA and citric acid [4] are now widely used. In comparison with palla-

Correspondence to: A.B. Volynsky, Laboratory of Organic Analysis, Department of Chemistry, Moscow State University, 119899 Moscow (Russian federation).

SSDI 0003-2670(93)E0414-3

dium-based modifiers, the organic compounds are less often used, but for some analytical tasks the effectiveness of organic chemical modifiers is significantly higher [5].

The processes that occur in graphite atomizers in the presence of organic chemical modifiers are complex. Even for the simplest system (analysis of samples without a matrix) the mechanism of their action is still unclear. For instance, the decrease in the appearance temperature (t_{app}) for lead and some other elements in the presence of ascorbic acid [6–9] is usually explained by the change in the composition of the gas phase in the electrothermal analyser (ETA).

The fact that ascorbic acid decreases the partial pressure of free oxygen (p_{O_2}) in the ETA gas phase was proved in 1984 by the "calibration graph displacement method" [10]. Later, Gilchrist et al. [11] showed by means of gas chromatography and thermodynamic calculations that free oxygen from the ETA gas phase interacts with the gaseous products of the thermal destruction of ascorbic acid, i.e., CO and H_2. In addition, free oxygen may be removed from the ETA gas phase as a result of interaction with active carbon [10,12] formed as a result of the thermal decomposition of ascorbic acid [13].

The magnitudes of the experimental and theoretical characteristic masses for most elements differ insignificantly [14,15]. Hence, for the analysis of "pure" solutions under stabilized-temperature platform furnace (STPF) conditions [16], and especially for sample evaporation from the L'vov platform in the "gas-stop" mode, the degree of dissociation of the oxides for most of the analytes in the ETA gas phase is close to 100% even in the absence of organic chemical modifiers. The exception is a group of elements that have monoxides with decomposition energy $D_0 > 650$ kJ mol^{-1} (Ge, B and, possibly, Si). Factors that decrease the oxygen partial pressure p_{O_2} in a graphite furnace increase the sensitivity of determination of Ge and B even under STPF conditions [5,17]. However, the influence of these factors on the analytical signals of tin (for SnO, $D_0 = 528$ kJ mol^{-1}) is almost negligible [17].

Consequently, a decrease in p_{O_2} during the atomization stage in the presence of organic chemical modifiers in principle cannot increase the sensitivity of determination for elements with relatively weakly bound oxides (such as lead) under STPF conditions. The main reason for the enhancement of the sensitivity for Pb, In, Ga and some other elements in the presence of organic chemical modifiers reported previously [6–9,18,19] is a lack of adherence to STPF conditions. Evaporation of the samples from the wall of the graphite tube [6–9,18,19] and especially the use of "mini-flow" [8,9,18,19] and "full-flow" [6] modes led to an increase in p_{O_2} in the ETA gas phase at the atomization stage. As a result, the degree of dissociation of the monoxides of the analytes was decreased and the values of t_{app} were enhanced [20].

In spite of various hypotheses, the differences in the behaviours of organic chemical modifiers also do not yet have any convincing explanation [4,21]. Recent studies on the action of organic chemical modifiers in graphite furnaces were carried out mainly with ascorbic acid as the most effective chemical modifier [8,9,11,19].

The aim of this work was to study the reasons for the great effectiveness of ascorbic acid as a chemical modifier in comparison with its analogues under STPF conditions.

EXPERIMENTAL

Equipment

Measurements were performed using a Perkin-Elmer Model 3030Z atomic absorption spectrometer with an HGA-600 atomizer. Standard graphite tubes without a pyrolytic graphite coating were used together with Perkin-Elmer pyrolytic graphite-coated graphite platforms. Argon with an oxygen content of less than 7×10^{-4}% (v/v) was used as the sheath gas. Atomic absorption signals were recorded on a Perkin-Elmer Model 100 graphics plotter. Analyte solutions (5–10 μl each) and solutions of chemical modifiers (5–10 μl) were introduced into the graphite atomizer manually. Samples were dried for 10–20 s at 110°C and ashed for 15 s at 400°C. The heating rate was 5 s for each stage. Other instrumental parameters are given in Table 1. For all elements

TABLE 1

Instrumental parameters

Parameter	Element		
	Ga	Pb	Sn
Wavelength (nm)	287.4	283.3	286.3
Slit width (nm)	0.7	0.7	0.7
Hollow cathode lamp type	Pye Unicam	Pye Unicam	Perkin-Elmer
Lamp current (mA)	14	10	30
Atomization [a,b]	2400/0/2	2200/0/3	2500/0/3
Cleaning [a]	2600/1/2	2400/1/2	2600/1/2

[a] The order of the parameters is temperature (°C)/ramp time (s)/hold time (s). [b] "Gas-stop" mode.

studied peak area (integrated absorbance) data are presented if not stated otherwise.

Thermal analysis was performed using a Q-1500D derivatograph. A quartz crucible containing 52 ± 2 mg of the sample was heated to 400–475°C at a rate of 5–10°C min^{-1} in an argon or nitrogen atmosphere (the inert gas flow-rate was 60 ml min^{-1}). In the individual experiments the given weight of the organic chemical modifier was preliminarily moistened with 0.1 ml of 0.1 M HNO_3. Elemental analysis of the carbon deposits formed was performed using a Carlo Erba Model 1106 analyser. The gallium and lead distribution in the carbon matrix was studied using a Camebax Microbeam electron microprobe.

Procedure

Determination of edge angles. Wetting of the metal oxides with the organic compound melts was studied using a quartz cell with an optical quartz window. The plates were formed from PbO and Ga_2O_3 under a pressure of 1.45×10^9 Pa for 2 min. Lead oxide was preliminarily calcined for 25 min at 400°C in an argon flow to decompose any $PbCO_3$ ($t_{dec} = 315$°C) present. The plate with 14–20 mg of ascorbic acid or glucose was placed carefully in the cell, which was purged using argon at 50 ml min^{-1}. The cell was then electrically heated using a wire winding on its surface. The temperature was monitored by using a thermocouple inside the cell. Immediately after the visually determined start of melting of the organic compound the heating was turned off. The plate was then removed from the cell to measure the diameter ($2r$) of the drop formed; the precision of this measurement was ± 0.1 mm. To calculate the edge angle, θ, it is proposed that the drops formed have a shape of a spherical segment (hatched in Fig. 1). Such an approximation is correct for small values of the angles. The volume of the drop was found from the equation $V = m/\rho$, where m is the mass of the organic compound and ρ is its density. The height of the spherical segment, h, and the radius of the sphere, R, were then found from the equation $V = \pi h(3r^2 + h^2)/6$ and $R = (r^2 + h^2)/2h$; $\sin \theta = r/R$ (Fig. 1).

Determination of appearance time and appearance temperature. The time corresponding to a signal-to-noise ratio of 2 was adopted as the appearance time (τ_{app}). Examples of the determination of τ_{app} for signals of complex shape are given in Fig. 2. The rate of heating for a graphite tube with the L'vov platform in the mode "ramp time = 0 s" was assumed to be 1700°C s^{-1} for the HGA-600 atomizer [22]. To calculate the appearance temperatures the relationship between the temperatures of the graphite tube wall and of the L'vov platform for the HGA-400 according to Welz et al. [23] was used. As the error for the absolute temperature values obtained is large, the

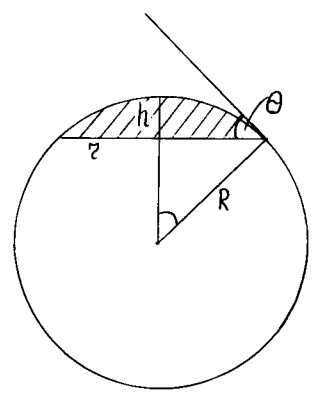

Fig. 1. Calculation of θ.

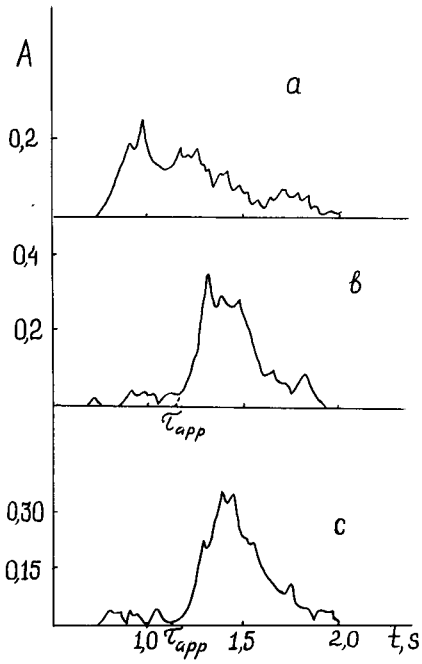

Fig. 2. Analytical signals for 0.6 ng of gallium in 0.1 M HNO_3 in the presence of (a) 5, (b) 50 and (c) 250 μg of ascorbic acid.

relative changes in t_{app} in the presence of the organic chemical modifiers are of more interest.

Study of lead and gallium distribution in the carbon residues of the organic chemical modifiers. For the first experimental series, 50 μl of 20% ascorbic acid or glucose solution and 20 μl of a 1 M HCl–1 M HNO_3 mixture (1 + 1) containing 1 mg ml^{-1} of lead and 2.5 mg ml^{-1} of gallium were placed in the quartz crucible. For the blank experiment 20 μl of 1 M HCl–1 M HNO_3 (1 + 1) were added to the solution of the organic chemical modifier. After removing water in a dry-box at ca. 110°C, the crucibles were placed in the quartz tube purged with argon (at ca. 0.5 l min^{-1}), which was heated in the furnace at rate of 220°C min^{-1}. Immediately after reaching 500°C the tube was removed from the furnace and the crucibles were cooled to room temperature in an argon flow. For the second experimental series only the organic chemical modifier solution was dried and ashed in the quartz crucible. Then 50 μl of 1 M HCl–1 M HNO_3 mixture (1 + 1) containing 0.4 mg ml^{-1} of lead and 1 mg ml^{-1} of gallium were placed on the carbon residue and dried in the dry-box.

The structure of the carbon residues formed and the distribution of lead and gallium in the residues were studied by using the electron microprobe with the Pb Mα and Ga Lα lines. The optimum experimental conditions were electron beam current 30 nA and accelerating voltage 10 kV. All samples were carbon coated to ensure electrical conduction. For each sample the number of x-ray pulses was measured for 40 s over a surface area of 500 × 500 μm. The relative standard deviation obtained was < 1% for each point on the sample surface ($n = 5$, $\alpha = 0.95$). Considerable irregularities of the sample surface dramatically reduced the reproducibility when scanning over the surface was done. The average relative standard deviation for the samples studied was 25% (8–12 points of the surface were scanned for every sample).

The data obtained were calculated assuming that 100% of the metals used are on the surface of the samples of the second series and that the microprobe detection is equally effective for the samples of both series. The x-ray intensities for the samples of the first and second series were compared after subtracting the background values obtained for the corresponding pure carbon residues.

Reagents

Analytical-reagent grade reagents and distilled water were used. A standard tin solution was prepared by dissolving 38.3 mg of tin in 5 ml of concentrated HCl with slight heating. The solution was diluted to 50 ml with 2 M HCl. Standard gallium solution, containing 4.71 mg ml^{-1} of gallium in 3 M HCl, was prepared by dissolving gallium oxide in a 3 + 1 (v/v) mixture of concentrated HCl and HNO_3. To obtain a standard lead solution, 107.884 mg of lead nitrate were dissolved in 50 ml of 1 M HNO_3. Metals solutions with concentrations of the order 0.1 μg ml^{-1} were prepared in 0.1 M HNO_3 immediately before use. The concentration of HCl in dilute solutions of tin and gallium did not exceed 3×10^{-4} M. Solutions of the organic chemical modi-

TABLE 2

Relative sensitivity of gallium determination in the presence of 250 μg of the organic chemical modifiers

Chemical modifier	Relative sensitivity	Chemical modifier	Relative sensitivity
None	1.00	Polyethylene glycol (av. M.W. 1000)	0.75
Glycerol	1.03	Sucrose	1.10
Oxalic acid	1.08	Glucose	1.21
Citric acid	1.28	Fructose	1.34
Tartaric acid	0.75	Ascorbic acid	1.37
Mannitol	1.18		

fiers in water [usually 5% (w/v)] were also prepared immediately before use.

RESULTS AND DISCUSSION

Influence of organic chemical modifiers on the atomic absorption spectrometric determination of Ga, Pb and Sn

Among the organic compounds studied, ascorbic acid increases both the areas and heights of the gallium signals to the greatest extent (Table 2). The effectiveness of the action decreases for fructose, which is the closest analogue of the ascorbic acid among hexoses, and less for glucose. The addition to the graphite furnace of 250 μg of ascorbic acid slightly decreases the area of the lead analytical signals, although the corresponding peak heights are increased 1.6-fold (Table 3). Both the height and area of the tin signals are decreased in the presence of ascorbic acid with an ashing temperature of 400°C (Table 3), but increasing the ashing temperature to 750°C almost suppresses the negative influence of ascorbic acid [5].

In the presence of organic chemical modifiers, the tin and especially the gallium analytical signals become more noisy (Figs. 2 and 3). Sometimes relatively large spikes could be observed (Fig. 3b). The largest spikes were observed for the determination of gallium in the presence of both an organic chemical modifier and chloroform [24]. Evidently the spikes result from some fast processes in the graphite furnace. Although the number of spikes and their intensity vary, ascorbic acid insignificantly influences the reproducibility of the determination for the elements studied (in both peak height and area modes, Table 3).

In the presence of the organic chemical modifiers the gallium and tin analytical signals may be jagged (Figs. 3 and 4). For example, side-by-side with a "low-temperature" peak (τ_{max} = 0.72–0.90 s) on the gallium signal there appears a "high-temperature" peak (τ_{max} = 1.07–1.20 s). The "low-temperature" peak almost completely disappears in the presence of ascorbic acid solution of concentration $\geqslant$ 1% (Fig. 2). As a result, t_{app} for gallium is increased from 1020 to 1620°C (Table 3). Ascorbic acid also increases t_{app} for tin and lead under STPF conditions (Table 3). In the presence of ascorbic acid the maximum of the analytical signals shifts to lower temperatures for

TABLE 3

Influence of ascorbic acid on the determination of Ga, Pb and Sn (n = 4–9; mean ± S.D.; α = 0.95)

System	τ_{app}(s)	t_{app}(°C)		Absorbance (A)	A s
		Wall	Platform		
0.6 ng Ga	0.64 ± 0.03	1480 ± 40	1020	0.209 ± 0.016	0.090 ± 0.007
0.6 ng Ga + 500 μg ascorbic acid	1.16 ± 0.05	2370 ± 80	1620	0.364 ± 0.033	0.118 ± 0.002
0.5 ng Pb	0.67 ± 0.03	1540 ± 50	1020	0.265 ± 0.025	0.145 ± 0.010
0.5 ng Pb + 250 μg ascorbic acid	0.74 ± 0.03	1660 ± 50	1150	0.420 ± 0.015	0.137 ± 0.007
1.5 ng Sn	0.82 ± 0.06	1790 ± 100	1270	0.307 ± 0.036	0.186 ± 0.005
1.5 ng Sn + 250 μg ascorbic acid	0.95 ± 0.06	2010 ± 90	1310	0.221 ± 0.004	0.156 ± 0.011

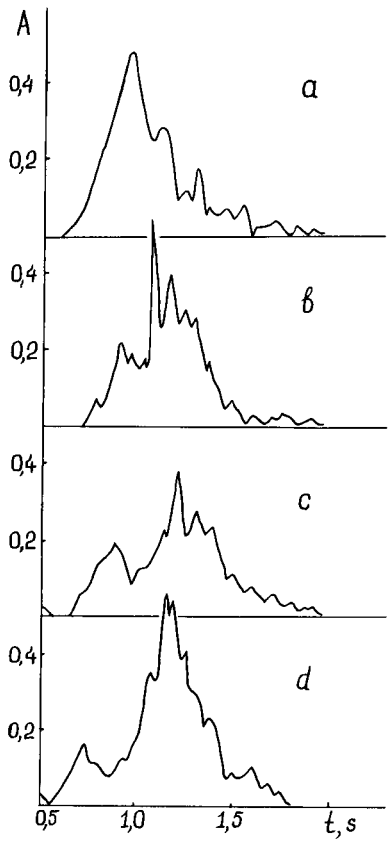

Fig. 3. Analytical signals for 1.0 ng of gallium in 0.1 M HNO_3: (a) in the absence of chemical modifier; (b) in the presence of 250 μg of tartaric acid; (c) in the presence of 250 μg of glucose; (d) in the presence of 250 μg of fructose.

lead (Fig. 5) and to higher temperatures for tin (Fig. 4).

The data obtained (the slight decrease in the areas of the tin and lead analytical signals and the enhancement of t_{app} for these elements in the presence of ascorbic acid) differ significantly from previous data [9,11]. This corroborates the supposition about the primary influence of the composition of the ETA gas phase on the results of atomic absorption measurements under the conditions used here and the absence of such an influence under STPF conditions.

Thermal analysis of organic chemical modifiers

Usually during thermal analysis ca. 50 mg of the sample are heated at a rate of ca. 5–10°C min^{-1}. These conditions differ sharply from the

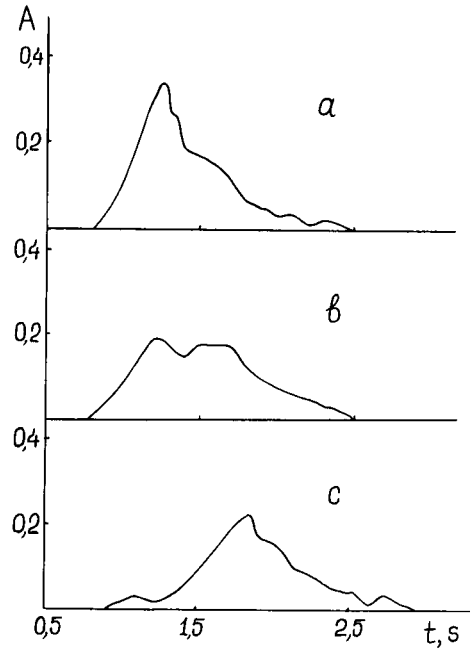

Fig. 4. Analytical signals for 2.0 ng of tin in 0.1 M HNO_3: (a) in the absence of chemical modifier; (b) in the presence of 250 μg of glucose; (c) in the presence of 250 μg of ascorbic acid.

typical conditions for the analyte during the atomization stage (the mass is of the order of 1 ng and the heating rate is about 1500°C s^{-1}). Therefore, the use of the thermal analysis data for the interpretation of the processes in the atomization stage is doubtful. However, thermal analysis may be used for the qualitative estimation of the transformations of the organic chemical modifiers

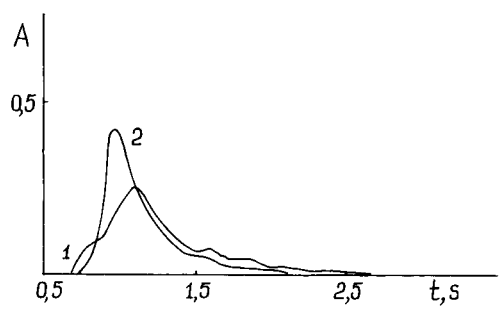

Fig. 5. Analytical signals for 0.5 ng of lead in 0.1 M HNO_3: (1) in the absence of chemical modifier; (2) in the presence of 250 μg of ascorbic acid.

in the ashing stage. The parameters of such processes (the mass is of the order of 0.25 mg and the heating rate is ca. 50°C s^{-1}) are similar to the conditions of thermal analysis.

It was ascertained that thermal decomposition of the organic compounds studied is mainly complete by 400°C. The largest carbon deposits are formed during the thermal decomposition of glucose, fructose and ascorbic acid (Table 4). These chemical modifiers are the most effective for gallium determination in dilute HNO_3 (Table 2) and in the presence of chloroform [24]. For understanding the reasons for the great effectiveness of ascorbic acid as a chemical modifier, the main attention was subsequently devoted to the investigation of these three compounds with intimate compositions and properties.

By the use of elemental analysis it was deter-

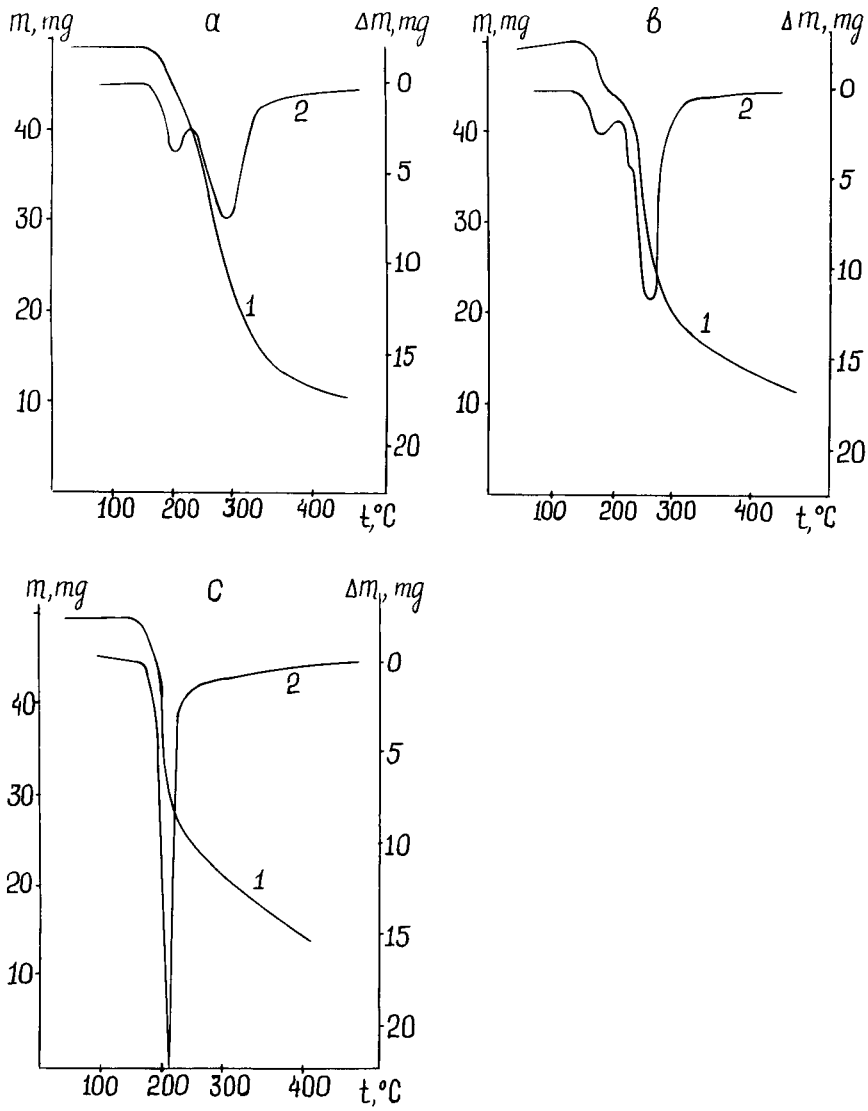

Fig. 6. Thermal decomposition of (a) glucose, (b) fructose and (c) ascorbic acid. 1 = Thermogravimetric curves; 2 = differential thermogravimetric curves.

TABLE 4

Thermal decomposition of the organic chemical modifiers (in the presence of 0.1 M HNO_3; heating rate 10°C min^{-1}; final temperature 400°C)

Chemical modifier	Onset of decomposition (°C)	Carbon residue (%)
Oxalic acid	140 [a]	0
Citric acid	314	5.7
Mannitol	197	5.9
Polyethylene glycol	362	16.5
Glucose	235	29.5
Fructose	210	31.9
Ascorbic acid	186	32.5

[a] Sublimation.

mined that the carbon residues contain up to 4% of hydrogen and 10.5–34.2% of oxygen. The oxygen content in the residues increases with decrease in the purity of the argon used for the thermal analysis and during storage of the carbon residues over silica gel in a desiccator. Obviously in both instances oxygen is sorbed by the active sites on the carbon surface [25]. This hinders the determination of reliable data on the elemental composition of the carbon residues and their interpretation.

On going from ascorbic acid to fructose and further to glucose the temperature of the onset of their thermal decomposition (186, 210 and 235°C, respectively) increases. An increase in temperature is also observed for this sequence which corresponds to the maximum rate of decomposition (215, 262 and 284°C, respectively). The absolute value of the rate of decomposition decreases on going from ascorbic acid to fructose and further to glucose (Fig. 6). According to the literature, a further increase in thermal stability is observed on going from monosaccharides (glucose, fructose) to disaccharides (e.g., sucrose) [26]. For carbohydrates and ascorbic acid the higher thermal stability correlates with lower enhancement of the gallium signal (Table 2). The reasons for this are not yet clear.

After melting carbohydrates, the processes of anomerization, thermal decomposition, polymerization and inter- and intramolecular condensation start [27]. Lewis acids are active catalysts of the polymerization and polycondensation reactions [28,29]. The polymers formed are non-volatile; they are ashed and dehydrogenated during further temperature increases under vacuum or in an inert atmosphere. As a result, in the presence of Lewis acids the mass of carbon residue is increased [30].

Gallium oxide is formed from gallium nitrate at 200°C. It exhibits relatively high aprotic acidity at the expense of a free electron orbital for each gallium atom. It is well known that gallium oxide is catalytically active in reactions proceeding by an acid–base mechanism [31]. However, the temperatures of onset of thermal decomposition and the carbon residue masses for ascorbic acid alone and in the presence of 5% (w/w) gallium oxide are not statistically different. Hence the assumption that the sample may influence the thermal decomposition of the organic chemical modifier [32] is not applicable in this instance. Oxides of lead and tin are not Lewis acids, so their influence on the thermal decomposition of the organic chemical modifiers was not studied.

It has been hypothesized that the influence of ascorbic acid on the determination of lead is caused by the formation of a pyrolytic graphite layer on the ETA surface [9]. However, it is well known that not all carbon materials form graphite at 2800–3000°C. The degree of graphitization is in inverse proportion to the O : H atomic ratio for the initial organic compound [33]. For ascorbic acid this ratio (0.75) is higher than that for sucrose (0.50). However, the sucrose carbon is a typical non-graphitizable material [34]. The relatively low thermal stability of ascorbic acid (Table 5) is also characteristic of materials that form a non-graphitizable carbon on thermal decomposition [33]. The formation of graphite from such

TABLE 5

Properties of the organic chemical modifiers

Substance	Formula	Melting point (°C)	σ_{lg} (dyn cm^{-1})
Ascorbic acid	$C_6H_8O_6$	190 [a]	51.27
Glucose	$C_6H_{12}O_6$	146	84.73
Fructose	$C_6H_{12}O_6$	102–104	115.62
Sucrose	$C_{12}H_{22}O_{11}$	186 [a]	84.63

[a] Decomposition.

carbon is possible in the presence of some metals that catalyse this process, but lead is not one of them [35].

Wetting metal oxides with melts of organic chemical modifiers

The amount of organic chemical modifier in the graphite tube is 10^5–10^6 times higher than that of the analyte. During drying, co-crystallization [36] and occlusion of the analyte by the crystals of the chemical modifier [37] are possible, but in the absence of any specific interaction the crystals of the chemical modifier will deposit first on the surface of the atomizer during steady evaporation of the analyte solution. Most of the analytes will deposit on the surface of these crystals at the end of the drying stage. At the beginning of the ashing stage the crystals of most of the organic chemical modifiers are molten. The main factors that influence the interaction of liquid with the solid particles are the surface tension at the liquid–gas boundary, σ_{lg}, and the edge angle, θ, for the liquid–solid pair used [38].

The experimental measurement of σ_{lg} for ascorbic acid is difficult because it melts with partial decomposition. Therefore, the empirical relationship between the surface tension, elemental composition and the structure of the compound [39] was used to estimate the surface tension for the melts of a number of organic compounds.

These melts wet the plates of lead and gallium oxides fairly well (Table 6). The values of θ for the melt of ascorbic acid are significantly lower. During the ashing stage such good wetting should allow the analyte oxide particles to fall through the melt.

If the only mechanism for the interaction of the organic chemical modifier melts and the analyte oxides is contact flotation (forming of a three-phase perimeter of wetting), $\sigma_{lg}(1 - \cos\theta) = m_{crit}$ [40], where $\sigma_{lg}(1 - \cos\theta)$ is the force holding the particle on the surface of the liquid (f_h) and m_{crit} is the mass in grams of the particles that can be kept at the liquid–gas boundary. For the glucose melt the values of f_h are an order of magnitude higher than for the melt of ascorbic acid. Hence the relatively light particles that fall through into an ascorbic acid melt will remain on the surface of a glucose melt. However, the absolute values of m_{crit} (e.g., 0.65 mg of gallium oxide for ascorbic acid and 10.97 mg for glucose) are significantly higher than the typical masses of the analytes in an ETA when used for atomic absorption spectrometry. The reason for this is that contact flotation is the predominant mechanism of wetting only for relatively large particles. The smaller the particles the greater is the influence of non-contact flotation, most of which is due to London–Van der Waals forces of molecular adhesion [41].

Interaction of very small amounts of lead and gallium compounds with melts of glucose and ascorbic acid

For the electron microprobe the typical absolute detection limits are of the order of 6×10^{-16} g [42]. However, these amounts are present in a volume of ca. 4 μm^3, so the concentration detection limits are high (ca. 50 $\mu g\ ml^{-1}$) [42]. The

TABLE 6

Interaction of lead and gallium oxides with the melts of ascorbic acid and glucose

Parameter	Ascorbic acid		Glucose	
	PbO	Ga_2O_3	PbO	Ga_2O_3
θ(°) ($n = 3$)	6.5 ± 1.4	8.7 ± 0.8	24.8 ± 2.5	29.2 ± 1.9
Fraction of metal on the carbon surface (1st series) (%)	7	14	25	30
Fraction of "low-temperature" atomic absorption signal (%) ($n = 5$)	–	5.5 ± 1.4	–	21.9 ± 3.6

ratio of organic chemical modifier to the analyte in the experiments was 10000 μg:20 μg for lead and 10000 μg:50 μg for gallium.

The carbon formed as a result of the thermal decomposition of ascorbic acid and glucose has a net-like structure. No significant difference in the structures of these two carbon residues can be observed up to 2000 × magnification. The amounts of lead and gallium studied evidently do not influence the carbon structure.

The surface concentration of lead and gallium is much less for the samples with joint ashing of the organic chemical modifier and the analytes (first series) than for the samples for which the analyte solution was pipetted on to an already formed carbon deposit (second series). On the basis that in the latter instance 100% of the metals used are on the surface of the sample, the concentration of lead and gallium on the surface of the samples of the first series is 3–4 times lower for glucose and 7–14 times lower for ascorbic acid (Table 6).

On the surface of the samples of the second series, irregular particles consisting of lead and gallium compounds are observed; the masses of these particles are 0.5–1.0 ng. The distribution of lead and gallium on the surface of the samples of the first series is more uniform. For the samples based on ascorbic acid sometimes sphere-type lead-containing particles were observed. No gallium-containing particles were observed for these samples up to 3000 × magnification.

Therefore, during ashing particles of lead and gallium compounds with a mass of $\leqslant 0.1$ ng were absorbed to a great extent by the ascorbic acid or glucose melt. The relatively good wetting by the ascorbic acid melt that was observed earlier at a macrolevel was retained for the much smaller amounts of the metal oxides.

Behaviour of analyte compounds in the carbon matrix

The transformations of the particles of the analyte oxides that fell into the melt of the organic chemical modifier at ca. 150–200°C will now be considered. With a further increase in temperature the organic compounds decompose, evolving active reductants such as hydrogen and carbon monoxide [11]. They reduce gallium oxide and lead oxide to metallic gallium and lead at ca. 600 and 300°C, respectively [43,44]. The reduction of tin dioxide by hydrogen starts at 170°C [44]. Therefore, it is suggested that gallium, lead and tin oxides in the carbon matrix are reduced to the free metals in the ashing stage. The acceleration of the reduction of the analyte compounds in the presence of organic compounds in graphite furnaces is well known [45–47].

The behaviour of the analytes in the carbon matrix will also be determined by their chemical properties and by the properties of the matrix. The average radius of the pores for the carbon formed as a result of the thermal decomposition of sucrose is 1–2 nm [48]. Such a microporous structure of carbon is caused by the melting of sucrose at the onset of its decomposition [49]. Glucose, fructose and ascorbic acid also melt under heating. Their elemental composition and the composition of the "carbon" formed as a result of their thermal decomposition are close to the corresponding properties of sucrose. Hence it is positively proposed that their structures are also analogous.

Diffusion of the elements in carbon is a complex process. Its main components are diffusion through the carbon lattice, diffusion of solid (or liquid) substances over the pore surface and diffusion of gases through the pores of carbon [50]. Lead, tin and gallium do not form thermostable compounds with carbon and their melts do not wet it [51]. Hence the most probable mechanism of "liberating" the metals from the carbon matrix is diffusion of their vapours through the carbon pores.

Conclusion

The influence of the organic chemical modifiers on the analytes and the sample matrix is polyfunctional. The elements studied (Ga, Pb and Sn) do not form high-melting carbides and have relatively weak monoxides and organoelemental compounds. Therefore, under STPF conditions the organic chemical modifiers do not influence significantly the sensitivity of their determination in pure solutions under STPF conditions. The modification of the shape of their analytical sig-

nals is caused by the "fall-through" of the analyte compounds into the melt of the organic chemical modifier and by further relatively slow diffusion of the metal vapours to the ETA gas phase from the carbon matrix. Evidently if Ga, Pb, Sn and their analogues form the matrix of the sample (e.g., in alloys), their oxides also will fall into the melt of ascorbic acid or other organic chemical modifier. The influence of this effect on the analysis of real samples demands special investigations.

The authors thank B.D. Summ, E.M. Sedykh and O.R. Valedinskaya for valuable assistance.

REFERENCES

1 F. Dolinsek and J. Stupar, Analyst, 98 (1973) 841.
2 R.D. Ediger, At. Absorpt. Newsl., 14 (1975) 127.
3 J.G.T. Regan and J. Warren, Analyst, 101 (1976) 220.
4 Z.-M. Ni and X.-Q. Shan, Spectrochim. Acta, Part B, 42 (1987) 937.
5 A.B. Volynsky, E.M. Sedykh and L.N. Bannykh, Talanta, 38 (1991) 761.
6 L.R. Hageman, J.A. Nichols, P. Viswanadham and R. Woodriff, Anal. Chem., 51 (1979) 1406.
7 R.E. Sturgeon and S.S. Berman, Anal. Chem., 57 (1985) 1268.
8 G.F.R. Gilchrist, C.L. Chakrabarti and J.P. Byrne, J. Anal. At. Spectrom., 4 (1989) 533.
9 S. Imai and Y. Hayashi, Anal. Chem., 63 (1991) 772.
10 A.B. Volynsky and E.M. Sedykh, Zh. Anal. Khim., 39 (1984) 1197.
11 G.F.R. Gilchrist, C.L. Chakrabarti, J.P. Byrne and M. Lamoureux, J. Anal. At. Spectrom., 5 (1990) 175.
12 R.E. Sturgeon, K.W.M. Siu, G.J. Gardner and S.S. Berman, Anal. Chem., 58 (1986) 42.
13 V.I. Scherbakov, Yu.I. Belyaev, B.F. Myasoedov, I.N. Marov and N.B. Kalinichenko, Zh. Anal. Khim., 37 (1982) 1717
14 B.V. L'vov, V.G. Nikolaev, E.A. Norman, L.K. Polzik and M. Mojika, Spectrochim. Acta, Part B, 41 (1986) 1043.
15 W. Frech, D.C. Baxter and E. Lundberg, J. Anal. At. Spectrom., 3 (1988) 21.
16 W. Slavin, D.C. Manning and G.R. Carnrick, At. Spectrosc., 2 (1981) 137.
17 A.B. Volynsky and E.M. Sedykh, J. Anal. At. Spectrom., 4 (1989) 71.
18 M. Taddia and G. Clauser, Fresenius' Z. Anal. Chem., 334 (1989) 148.
19 T. Shirasaki, A. Yonetani, K. Uchino and K. Sakai, Bunseki Kagaku, 40 (1991) 163.
20 S.G. Salmon, R.H. Davis, Jr., and J.A. Holcombe, Anal. Chem., 53 (1981) 324.
21 J. Komarek and L. Sommer, Chem. Listy, 82 (1988) 1151.
22 W. Frech, M. Arshadi, D.C. Baxter and B. Hutsch, J. Anal. At. Spectrom., 4 (1989) 625.
23 B. Welz, M. Sperling, G. Schlemmer, N. Wenzel and G. Marowsky, Spectrochim. Acta, Part B, 43 (1988) 1187.
24 A.B. Volynsky, O.R. Valedinskaya and N.K. Kutseva, Zh. Anal. Khim., 47 (1992) 493.
25 W.V. Loebenstein and V.R. Deitz, J. Phys. Chem., 59 (1955) 481.
26 C. Ramos-Sanchez, F.J. Rey, L. Rodriguez-Mendez, F.J. Martin-Gil and J. Martin-Gil, Thermochim. Acta, 134 (1988) 55.
27 K. Heyns and M. Klier, Carbohydr. Res., 6 (1968) 436.
28 H.W. Durand, M.F. Dull and R.S. Tipson, J. Am. Chem. Soc., 80 (1958) 3691.
29 C. Schuerch, Adv. Carbohydr. Chem. Biochem., 39 (1981) 157.
30 F. Shafizadeh, C.W. Philpot and N. Ostojic, Carbohydr. Res., 16 (1971) 279.
31 D.K. Simmons, R. Szostak, P.K. Agraval and T.L. Thomas, J. Catal., 106 (1987) 287.
32 R. Guevremont, Anal. Chem., 52 (1980) 1574.
33 A. Oberlin, M. Villey and A. Combaz, Carbon, 18 (1980) 347.
34 J.N. Rouzaud and A. Oberlin, Carbon, 27 (1989) 517.
35 A. Oya and S. Otani, Carbon, 17 (1979) 131.
36 V.I. Slaveykova and D.L. Tsalev, Anal. Lett., 23 (1990) 1921.
37 J.A. Krasowski and T.R. Copeland, Anal. Chem., 51 (1979) 1843.
38 B.D. Summ and Yu. B. Gorjunov, Physico-chemical Bases of Wetting and Spreading, Khimiya, Moscow, 1976 (in Russian).
39 S. Sugden, J. Chem. Soc., 125 (1923) 1185.
40 D.A. Fridrihsberg, Course of Colloid Chemistry, Khimiya, Leningrad, 1984 (in Russian).
41 B.V. Derjagin, S.S. Dukhin and I.N. Rulev, Usp. Khim., 51 (1982) 92.
42 S.J.B. Reed, Chem. Geol., 83 (1990) 1.
43 J.C. Bailar, Jr., H.J. Emeleus, R. Nyholm and A.F. Trotman-Dickenson (Eds.), Comprehensive Inorganic Chemistry, Vol. 1, Pergamon Press, Oxford, 1973.
44 J.W. Mellor, A Comprehensive Treatise on Inorganic and Theoretical Chemistry, Vol. 7, Longmans, Green, London, 1947.
45 T. Kantor and L. Bezur, J. Anal. At. Spectrom., 1 (1986) 9.
46 B.V. L'vov and L.F. Yatsenko, Zh. Anal. Khim., 39 (1984) 1773.
47 E. Iwamoto, N. Miyazaki, S. Ohkubo and T. Kumamaru, J. Anal. At. Spectrom., 4 (1989) 433.
48 M.M. Dubinin, in M.M. Dubinin (Ed.), Methods for Investigation of the Structure of High-dispersive and Porous Bodies, USSR Academy of Sciences, Moscow, 1953, p. 72 (in Russian).
49 M.M. Dubinin and E.D. Zaverina, Zh. Fiz. Khim., 23 (1949) 469.
50 G.N. Walton, Nucl. Eng., 7 (1962) 97.
51 Yu.V. Naiditch, Contact Phenomena in Metal Melts, Naukova Dumka, Kiev, 1972 (in Russian).

Analytica Chimica Acta, 284 (1993) 379–384
Elsevier Science Publishers B.V., Amsterdam

Spectrophotometric determination of the dissociation constant (pK_a) of arsenous acid

H. Yamazaki [1], R.P. Sperline and H. Freiser

Strategic Metals Recovery Research Facility, Department of Chemistry, University of Arizona, Tucson, AZ 85721 (USA)

(Received 4th May 1993; revised manuscript received 2nd August 1993)

Abstract

The dissociation constant of *meta*-arsenous acid ($HAsO_2$) was accurately determined from spectrophotometric measurements, combined with volumetric methods. The measurement of pH of the analyte solution containing $HAsO_2$, which was titrated with sodium hydroxide, was achieved by the spectrophotometric method using thymol blue as a pH indicator. Acetic acid and aqueous ammonia were used as primary standards. The pK_a of $HAsO_2$ was determined to an accuracy of ± 0.005 pK_a units at temperatures between 25 and 65°C, and ionic strengths between 0 and 3 M. The standard enthalpy change of $HAsO_2$, $\Delta H°$, which was calculated from its dissociation constants, was 29.59 ± 0.78 kJ/mol. Determination of the pK_a values is necessary for the characterization of As_2O_3 as a dual purpose acid–base and oxidation–reduction primary standard reagent under various conditions.

Keywords: Spectrophotometry; Arsenous acid; Dissociation constants

Accurate determination of thermodynamic equilibrium constants (pK_a) is of sufficient importance in analytical chemistry to warrant a detailed study of chemical reaction. Many studies of the determination of pK_a of assorted materials have been reported. The pK_a of a weak acid can be simply determined by using a glass-electrode pH meter and spectrophotometric measurements, according to Eqn. 1,

$$K_i = \left(\frac{(A_o - A)}{(A - A_i)}\right)[H^+] = \rho[H^+], \quad (1)$$

where K_i is the dissociation constant of the weak acid, A is the absorbance observed in the sample at a given wavelength and at a pH corresponding to $[H^+]$, and A_o and A_i are the absorbances for the acid and conjugate forms of the weak acid at the given wavelength. The bracketed term ρ, known as the "upper–lower absorbance ratio", is a function of A, A_o, and A_i. Using this equation, it is not necessary to know the molar absorptivities of the species.

In general, however, it is difficult to accurately measure pH values in solutions at high ionic strength (I) and/or high temperatures (T); the accuracy of the pK_a value is governed by that of the pH measurement. The accuracy of pH measurements using glass-electrodes is usually take as ± 0.02 pH [1]. In addition, the accuracy of a glass electrode may decrease with an increase in I and/or T. We have developed a method for the accurate determination of pH through a combination of spectrophotometric measurements and activity coefficient corrections based on experi-

Correspondence to: H. Freiser, Strategic Metals Recovery Research Facility, Department of Chemistry, University of Arizona, Tucson, AZ 85721 (USA).

[1] Present address: Department of Nuclear Reactor Engineering, Kinki University, Kowakae, Higashiosaka 577 (Japan).

SSDI 0003-2670(93)E0493-Q

mental γ values. Computers were used to eliminate otherwise tedious calculation. As in our previous work, advantage was taken of the redundant data available with digitized spectra [2]

Currently available spectrophotometers are capable of measuring absorbances of high accuracy. This suggests a reevaluation of the role of spectrophotometry in the determination of concentrations and the parameters of equilibria. As our earlier paper demonstrated, the use of standardized acid–base indicators led to the development of a convenient spectrophotometric method for pH determinations having a high level of accuracy. In the same way, oxidation potentials might also be accurately measured by the use of standardized colored redox indicators. In this report, we make use of our spectrophotometric pH method to obtain accurate pK_a values for $HAsO_2$ ($pK_a \pm 0.005$) over a range of ionic strengths (I, 0–3 M) and temperatures (T, 25–65°C) in order to characterize As_2O_3 as a primary standard in reduction potential measurements. Evaluation of redox indicators for accurate spectrophotometric E° measurements is now underway.

EXPERIMENTAL

Reagents

Both the preparation of reagents and the procedures used were similar to those employed previously, but the differences are important. Stock solutions of arsenous acid (0.1800 M) were prepared by dissolving arsenic(III) oxide (Johnson Matthey Electronics, ACS primary standard) in deionized water. Thymol blue (TB) (Aldrich) was purified by repeated recrystallization from acetic acid solution. The initial purity was estimated at 96.0%. UV–Visible spectra of the solutions, taken before and after recrystallization, showed the impurities to be nearly colorless; the extent of their removal has insignificant effect on subsequent spectra. The stock solution of TB (1.20×10^{-4} M) was prepared in deionized water and was stored in glass bottles shielded from light. Potassium nitrate (Mallinckrodt) was used for controlling I of the solutions. Sodium hydroxide solution was prepared by dissolving sodium hydroxide from a freshly opened bottle (Mallinckrodt) in carbon dioxide-free water and was stored in a polyethylene bottle under nitrogen. The solution was standardized by titrating against primary standard potassium hydrogen phthalate (Aldrich).

The Gran method for location of the titration end points was applied on the spreadsheet software Quattro (Borland) [3]. Reproducibility in these procedures is principally determined by the volumetric accuracies. For example, the As concentrations were determined, in triplicate, to 0.05% relative standard deviation.

Apparatus

A Perkin-Elmer Lambda Array 3840 UV/VIS spectrophotometer equipped with a Perkin Elmer 7500 computer was used for measurement of the absorbance spectra and data storage. An IBM compatible computer was linked to the Perkin Elmer computer using data transmission–conversion software [4].

An Orion 801 pH meter equipped with a Corning 476560 Rugged Bulb Combination glass electrode was used for pH measurement. The pH meter was calibrated over the appropriated ranges using pH buffers. The pH buffer solutions were prepared according to procedures outlined by the IUPAC [5].

The titration procedure was carried out using a Mettler V10 10-ml digital burette, calibrated by delivered weight of water, which gave volumetric accuracy of ± 0.0018 ml (10 replicates) for any delivered volume. The temperature of the reaction vessel and absorption cell was controlled to within ± 0.1°C of the desired temperature using a VWR 1155 constant temperature water bath.

Procedures

Spectrophotometric measurement of pH of analyte solutions. The fundamental procedure for the spectrophotometric measurement of pH has been described previously. The sample solution (360 ml) was prepared by diluting stock solution with water to give initial concentrations of 0.028 M for arsenous acid and 2.0×10^{-5} M for TB. The pH of the solution was adjusted through additions of sodium hydroxide solution using the digital bu-

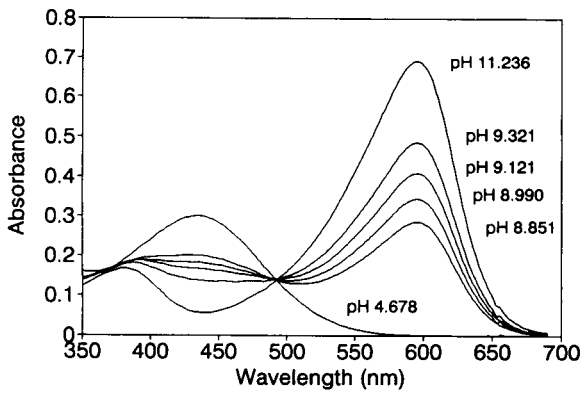

Fig. 1. Electronic spectra of thymol blue vs. pH in the presence of $HAsO_2$ and AsO_2^-.

rette. The pH of the solution was monitored with the pH meter after each addition. Absorption spectra of protonated and deprotonated species were measured at pH 4.7 and 11.1, respectively, at wavelengths between 350 and 690 nm. Spectra at intermediate degrees of protonation were taken for determinations of pH. These procedures were repeated at 13 volume-added increments through the titration range. Typical absorption spectra of the analyte solution are shown in Fig. 1.

Methods of calculation. The pH of the analyte solution was calculated by the previous method. In this study, the experiments were carried out by titrating $HAsO_2$ with sodium hydroxide in the presence of TB. The absorption ratio (ρ) was found from spectrophotometric measurements of the solution, and the pH of the solution was calculated from Eqn. 1 using the K_i value of TB previously determined. The dissociation constant of TB (pK_i), as a function of T and I, was taken from our previous work. Those values were accurate to ± 0.003 pK units under the conditions used here. The dissociation constant of $HAsO_2$ in the titration, which is a weak acid–strong base titration system, can be calculated using Eqn. 2,

$$K_a = [H^+]\left(\frac{[Na^+] + [H^+] + [OH^-]}{C_a - ([Na^+] + [H^+] - [OH^-])}\right), \quad (2)$$

where K_a is the dissociation constant of $HAsO_2$, C_a is the total concentration of As(III), and $[Na^+]$ is the total concentration of added sodium hydroxide [6].

These calculations were performed using the spreadsheet software Quattro. Statistical errors for the experiments were calculated by the method described in our previous report [2].

RESULTS AND DISCUSSION

pH of analyte solution

The pH of the analyte solution was determined by the spectrophotometric method and was monitored by a glass-electrode pH meter. The pH values from the two measurements were compared to indicate the possible errors introduced by relying on the glass-electrode. In the NH_4OH–HCl–TB titration system, the pH values from the two methods agreed to within analytical error at I between 0.005 and 0.5 M and T between 25 and 45°C. The pH difference, however, changed with increasing I and T.

pH results for the $HAsO_2$–NaOH–TB titration system are shown in Fig. 2. A significant difference between the spectrophotometric method and the glass-electrode method was observed. In particular, the difference became progressively greater as I decreased.

It was found that the glass-electrode results varied with the total concentration of As. To

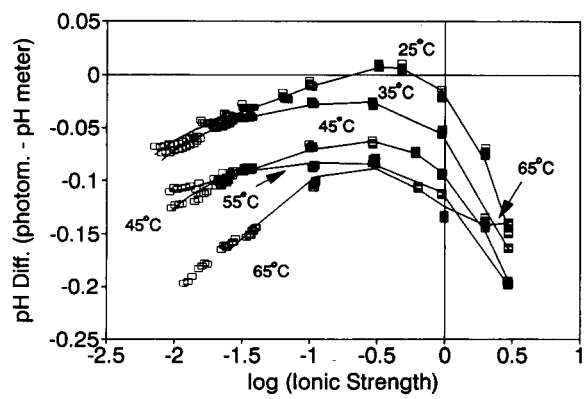

Fig. 2. Difference between pH determined photometrically and by glass-electrode/pH meter vs. ionic strength and solution temperature. pH 8.8–9.2. Lines are guides to the eye only.

TABLE 1

Dissociation constant of arsenous acid

Temp. (°C)	Ionic strength	pK_a of $HAsO_2$		Ionic strength	pK_a of $HAsO_2$	
		Spectroscopic method [a]	pH meter [b]		Spectroscopic method [a]	pH meter [b]
25	0	9.2426 ± 0.0026[c]	9.348	0.5	9.1318 ± 0.0043	9.127
	0.02	9.2144 ± 0.0026[c]	9.262	1.0	9.1034 ± 0.0043	9.116
	0.05	9.1984 ± 0.0036	9.227	2.0	9.0693 ± 0.0042	9.146
	0.1	9.1825 ± 0.0043	9.197	3.0	9.0453 ± 0.0042	9.198
	0.2	9.1631 ± 0.0043	9.165			
35	0	9.0892 ± 0.0033[c]	9.203	0.5	8.9442 ± 0.0044	8.975
	0.02	9.0603 ± 0.0032[c]	9.114	1.0	8.9132 ± 0.0044	8.964
	0.05	9.0361 ± 0.0047	9.079	2.0	8.8870 ± 0.0043	8.993
	0.1	9.0127 ± 0.0047	9.048	3.0	8.8763 ± 0.0043	9.045
	0.2	8.9851 ± 0.0044	9.015			
45	0	8.9330 ± 0.0043[c]	9.061	0.5	8.7881 ± 0.0044	8.859
	0.02	8.8954 ± 0.0043[c]	8.994	1.0	8.7586 ± 0.0044	8.847
	0.05	8.8732 ± 0.0048	8.961	2.0	8.7323 ± 0.0042	8.874
	0.1	8.8517 ± 0.0048	8.931	3.0	8.7202 ± 0.0042	8.922
	0.2	8.8262 ± 0.0044	8.898			
55	0	8.7896 ± 0.0033[c]	8.966	0.5	8.6523 ± 0.0038	8.737
	0.02	8.7693 ± 0.0033[c]	8.876	1.0	8.6205 ± 0.0038	8.742
	0.05	8.7450 ± 0.0032	8.839	2.0	8.5925 ± 0.0036	8.756
	0.1	8.7215 ± 0.0038	8.806	3.0	8.5802 ± 0.0036	8.779
	0.2	8.6937 ± 0.0038	8.771			
65	0	8.6251 ± 0.0026[c]	8.863	0.5	8.5435 ± 0.0043	8.635
	0.02	8.6091 ± 0.0026[c]	8.778	1.0	8.5104 ± 0.0026	8.644
	0.05	8.5995 ± 0.0037	8.737	2.0	8.5269 ± 0.0026	8.665
	0.1	8.5890 ± 0.0036	8.700	3.0	8.5440 ± 0.0026	8.685
	0.2	8.5742 ± 0.0043	8.663			

[a] Calculated using spectrophotometric pH values. [b] Calculated using glass electrode-pH meter pH values. [c] pK_a values were extrapolated from regression lines of pK_a against $I^{1/2}/(1+I^{1/2})$, using only data at $I < 0.05$ M.

examine this effect, the pH measured by the glass-electrode pH meter was compared with the pH calculated from the concentration and corrected K_a of $HAsO_2$ (Tables 1 and 2), as a function of ionic strength. The results are shown in Fig. 3, for pH values between 5.0 and 5.5, at

TABLE 2

Multiple linear regression coefficients for the pK_a of arsenous acid by Eqn. 3

Temp. (°C)	Ionic strength	A	B	C	r^2
25	0.05–3.0	9.248 ± 0.003	−0.0112 ± 0.0006	−0.266 ± 0.003	0.9976
35	0.05–3.0	9.112 ± 0.004	0.0094 ± 0.0009	−0.416 ± 0.005	0.9973
45	0.05–3.0	8.942 ± 0.004	0.0062 ± 0.0008	−0.380 ± 0.004	0.9971
55	0.05–3.0	8.821 ± 0.006	0.0077 ± 0.0015	−0.416 ± 0.008	0.9937
65	0.05–3.0	8.839 ± 0.011	0.0725 ± 0.002	−0.564 ± 0.015	0.9558
65	0.05–1.0	8.627 ± 0.003	−0.0553 ± 0.004	−0.135 ± 0.009	0.9909
65	1.0 –3.0	8.501 ± 0.002	0.0179 ± 0.003	−0.017 ± 0.042	0.9821

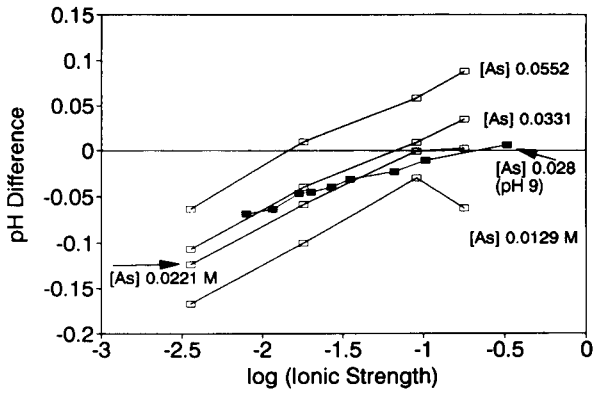

Fig. 3. Effect of As concentration on glass-electrode/pH meter readings vs. ionic strength at 25°C. □ = Difference between pH calculated from pK_a of $HAsO_2$ and pH meter readings, pH 5.0–5.5; ■ = difference between photometric pH (thymol blue) and pH meter readings, pH 8.8–9.2, [As] = 0.028 M.

25°C, where nearly all the As is present in neutral species. The differences found roughly agreed with the differences between the values obtained by spectrophotometric measurement and by pH meter measurement (pH 8.8–9.2, also shown in Fig. 3.). The slope is lower at the higher pH, where some of the As is present as the *meta*-arsenite ion, AsO_2^-. This suggests that the glass electrode is affected by the presence of either $HAsO_2$ or AsO_2^-, though to a lesser extent by the latter. In this study, therefore, the pH value determined from spectrophotometric measurements was adopted in the calculation of the pK_a value of $HAsO_2$.

pK_a of arsenous acid

pK_a values (non-thermodynamic values) were determined for ca. 100 points at I between 0.006 and 3 M, at each temperature in the range of 25 to 65°C. The pK_a generally decreased with both increasing I and increasing T, as shown in Table 1. At I between 0.05 and 3 M, the calculated pK_a curves were fitted with a three term empirical expression analogous to the Davies equation:

$$pK_a = A + BI + C\left(\frac{I^{1/2}}{1+I^{1/2}}\right), \qquad (3)$$

where A, B and C are constants, and I is the ionic strength. Multiple regression on these data gave the values of A, B and C and the correlation coefficient (r^2) shown in Table 2. The values of r^2 indicate that Eqn. 3 represents the data reasonably, except at 65°C.

When the pK_a values at I below 0.05 M were fitted, the B term in Eqn. 3 was essentially zero. The pK_a values of $HAsO_2$ for $I = 0$ and T between 25 and 65°C, were extrapolated from the fitting after setting $B = 0.0$. The results are given in Table 1. The results for the pK_a values determined from the pH meter measurements are also shown in Table 1.

The accuracy of the pK_a values of $HAsO_2$ can be calculated from the statistical errors of the spectrophotometric pH measurements and the accuracy of the pK_i values for TB. These errors have been detailed in the previous report; accuracies were estimated as ±0.003 pH for the spectrophotometric pH measurement, principally due to the ±0.003 accuracy in the pK_i of TB. Overall errors in pK_a of $HAsO_2$ are shown in Table 1.

Standard enthalpy change of arsenous acid

The free energy, $\Delta G°$ (extrapolated to $I = 0$), of $HAsO_2$ was calculated at several temperatures; the results are shown in Table 3. The standard enthalpy change of $HAsO_2$, $\Delta H°$, calcu-

TABLE 3

Temperature, pK_a^*, and free energy change of arsenous acid

Temp. (°C)	$1/T$ (K^{-1})	pK_a^* of $HAsO_2$	$\Delta G°$ (kJ/mol)
25	0.003354	9.243 ± 0.003	52.76 ± 0.02
35	0.003245	9.089 ± 0.003	53.62 ± 0.02
45	0.003143	8.933 ± 0.004	54.41 ± 0.02
55	0.003047	8.790 ± 0.003	55.22 ± 0.02
65	0.002957	8.625 ± 0.003	55.84 ± 0.02

lated from the regression line of $\ln(K_a)$ on $1/T$, was 29.59 ± 0.78 kJ/mol. This value is in good agreement with published values, which were determined at 25° and I between 0.0 and 0.3 M [7–10].

Conclusions

This method can be regarded as a new method for the pK_a measurement without the use of a pH meter and can be applied to the accurate determination of pK_a at high temperatures and ionic strengths. The pH values of an $HAsO_2$–NaOH–TB titration system were accurately determined from spectrophotometric measurements. The fraction of $HAsO_2$ deprotonated at each pH was determined volumetrically. When those results were combined with the spectrophotometric pH values, the pK_a of $HAsO_2$ was accurately determined at ionic strengths between 0 and 3 M and temperatures between 25 and 65°C. The accuracy of this method was estimated as ± 0.005 pK_a units.

As_2O_3 is already established as a primary redox standard because of its high purity, stability, and known constants. The results of this study make As_2O_3 into an acid–base standard as well. The range of conditions for its use as a primary redox standard have also been extended by allowing improved Nernst equation calculations of its formal potentials.

This work was supported by a grant from the Magma Power Company.

REFERENCES

1 C.C. Westcott, pH Measurement, Academic Press, New York, 1978, pp. 106–109.
2 H. Yamazaki, R.P. Sperline and H. Freiser, Anal. Chem., 64 (1992) 2720.
3 M. Meloun, J. Havel and E. Högfeldt, Computation of Solution Equilibria, Wiley, New York, 1990, pp. 37–42.
4 R.P. Sperline, Appl. Spectrosc., 45 (1991) 1046.
5 Manual of Symbols and Terminology for Physicochemical Quantities and Units, IUPAC Additional Publication, Butterworths, London, 1975, p. 30.
6 H. Freiser and Q. Fernando, Ionic Equilibria in Analytical Chemistry, Wiley, New York, 1963, pp. 227–233.
7 P. Sellers, S. Sunner and I. Wadsö, Acta Chem. Scand., 18 (1964) 202–206.
8 J.J. Christensen, L.D. Hansen and R.M. Izatt, Handbook of Proton Ionization Heats, Wiley, New York, 1976, p. 27.
9 R.M. Smith and A.E. Martell, Critical Stability Constants, Plenum Press, New York, 1976, p. 132.
10 L.G. Sillén, Stability Constants of Metal-Ion Complexes, Supplement No. 1, Burlington House, London, 1971, p. 121.

Analytica Chimica Acta, 284 (1993) 385–391
Elsevier Science Publishers B.V., Amsterdam

Fumed-silica containing carbon-paste dehydrogenase biosensors

Joseph Wang and Jie Liu

Department of Chemistry and Biochemistry, New Mexico State University, Las Cruces, NM 88003 (USA)

(Received 8th June 1993; revised manuscript received 23rd August 1993)

Abstract

The sensitivity and stability of dehydrogenase-based carbon paste biosensors are greatly improved upon adding fumed-silica nanoparticles into the electrode matrix. The enhanced performance is attributed to improved retention of the dehydrogenases and their NAD^+ cofactor on the silica support, and to an electrocatalytic action of fumed silica towards the detection of NADH. Such advantages of the silica modified carbon paste are illustrated with the enzymes alcohol and lactate dehydrogenase, and using batch and flow conditions. The response is characterized with respect to various experimental variables.

Keywords: Biosensors; Alcohol; Fumed silica; Lactate

Dehydrogenase-catalyzed enzymatic reactions play an important role in biosensor development [1–5]. The large number of commercially available dehydrogenases opens the prospect for many useful sensing devices of great relevance to clinical, food, forensic or environmental analysis. Such bioprobes usually rely on the anodic detection of the reduced form of the cofactor (NADH or NADPH), which results with regeneration of the NAD^+ or $NADP^+$ cofactor. Problems inherent to such operation are the large overvoltage, gradual passivation of the surface, and the solubility of the cofactors [3]. Some of these difficulties can be minimized through the use of redox mediators which shuttle electrons between the cofactor and the electrode surface [3]. The coimmobilization of the enzyme, the cofactor and the redox mediator within the bulk of a carbon paste electrode has been particularly attractive for fabrication fast-responding, reagentless dehydrogenase electrodes [5,6].

Correspondence to: J. Wang, Department of Chemistry and Biochemistry, New Mexico State University, Las Cruces, NM 88003 (USA).

The aim of the present work is to improve the analytical performance of dehydrogenase-based carbon-paste biosensors through the incorporation of fumed silica within the paste matrix. Recent studies by Gorton et al. [7] illustrated the utility of polymeric additives, particularly polyethyleneimine, for enhancing the behavior of carbon paste biosensors. Similarly, we demonstrated recently that the biosensing of glucose can be greatly improved at fumed-silica containing carbon pastes [8]. Fumed silica is a huge surface area material (100–400 m^2/g), with nanoparticles of 5–25 nm diameter. The enhanced performance of the silica-containing glucose sensor was attributed to the electrocatalytic function of the silica towards the detection of the enzymatically-liberated hydrogen peroxide, and to a prolonged retention of glucose oxidase at the silica particles. Similar sensitivity and stability improvements are reported in the following sections for alcohol and lactate biosensors, at alcohol dehydrogenase

0003-2670/93/$06.00
SSDI 0003-2670(93)E0495-S

(ADH) and lactate dehydrogenase (LDH) containing carbon pastes. Such improvements are attributed to the electrocatalytic detection of the generated NADH and to stabilization of the dehydrogenase enzymes and NAD^+cofactor at the silica particles. The silica/carbon paste mixing modification strategy thus provides an effective, simple and fast route for preparing dehydrogenase-based biosensors, without the need for additional immobilization steps.

EXPERIMENTAL

Apparatus

Batch experiments were carried out in a 10-ml electrochemical cell [Model VC 2, (BAS)]. The working electrode, reference electrode (Ag/AgCl, Model RE-1, BAS), and platinum wire auxiliary electrode joined the cell through holes in its PTFE cover. The flow-injection system consisted of a 400-ml carrier reservoir, a Rainin Model 5041 sample injection valve (20-μl loop), interconnecting PTFE tubing (1.0 mm i.d.) and the large-volume wall-jet electrochemical cell. Flow of the carrier solution was maintained by gravity.

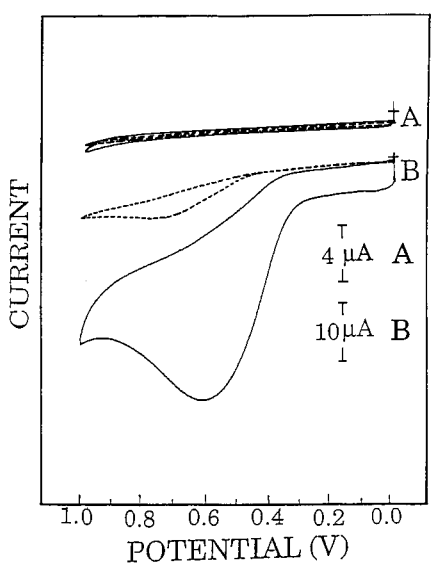

Fig. 1. Cyclic voltammograms for the blank solution (A) and for 2×10^{-3} M NADH (B) at the ordinary and fumed-silica containing (15% w/w) carbon paste electrodes (dotted and solid lines, respectively). Supporting electrolyte, 0.05 M phosphate buffer (pH 7.4); scan rate, 50 mV/s.

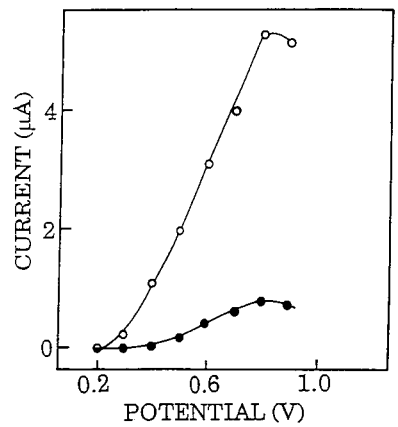

Fig. 2. Hydrodynamic voltammograms for 5×10^{-3} M ethanol at ordinary (●) and fumed-silica containing (○) carbon paste enzyme electrodes. Enzyme (ADH) loading 8% w/w; NAD^+ loading, 10% w/w; solution stirring, 300 rpm. Electrolyte and silica loading, as in Fig. 1.

All measurements were performed using an EG&G Model 264A voltammetric analyzer, with Houston Omniscribe strip-chart or Houston Omnigraphic X–Y recorder.

Reagents

Alcohol dehydrogenase (ADH, EC 1.1.1.1, from Bakers Yeast, 380 U/mg), β-nicotinamide adenine dinucleotide, NAD^+(sodium salt), its reduced form NADH, Meldola Blue (Hemi zinc chloride salt), L(+)-lactate (lithium salt), and fumed silica (particle size, 7 nm, specific area, 400 m^2/g) were purchased from Sigma. Fluka provided L-lactate dehydrogenase (LDH, EC 1.1.1.27, from rabbit muscle, 148.7 U/mg), while ethanol was received from Quantum Chemical (USI Division). A 0.05 M phosphate buffer solution (pH 7.4) served as the supporting electrolyte. All solutions were prepared with double-distilled water.

Electrode preparation

The carbon paste biosensors were prepared by hand-mixing first 20 mg of ADH (or 12 mg LDH), with 25 mg NAD^+, 120 mg graphite powder

(Fisher) and 80 mg mineral oil for 5 min. The desired amount of rehydrated fumed silica was then added and mixed with the above mixture for 10 min. The resulting carbon paste was packed into the end of a glass tube (3 mm i.d.), the inner end of which was connected to a copper wire for electrical contact. The electrode surface was smoothed on a weighing paper placed over a flat glass stand. Other paste formulations were prepared in a similar fashion.

The fumed silica was rehydrated by immersing a 1-g portion in 10 ml of water for 2 h. The excess water was removed by centrifugation (3000 rpm) for 5 min.

Procedure

Amperometric detections were carried out at room temperature by holding the working electrode at the desired operating potential and allowing the transient currents to decay to a steady-state value. Convective transport (300 rpm stirring or 1.0 ml/min flow) was maintained under the batch and flow conditions, respectively.

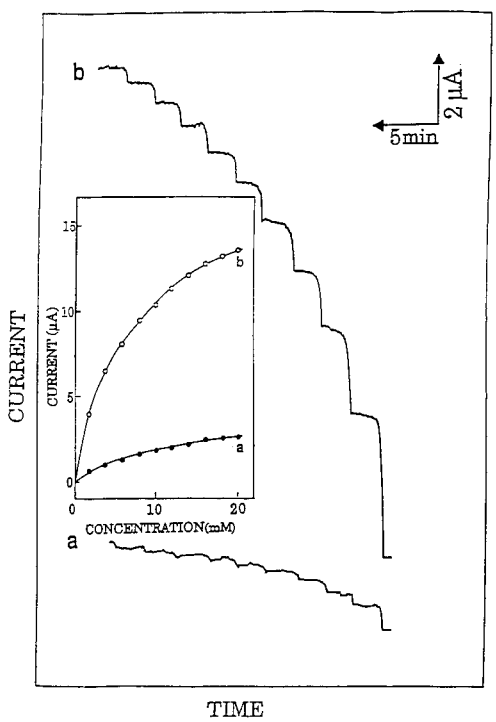

Fig. 3. Amperometric response to successive additions of 2×10^{-3} M ethanol at the ordinary (a) and fumed-silica containing (b) carbon paste enzyme electrodes. Applied potential, +0.8 V. Other conditions, as in Fig. 2. Also shown (inset) are the resulting calibration plots.

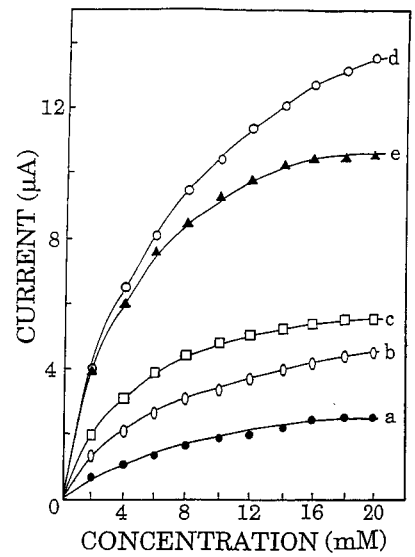

Fig. 4. Dependence of the steady-state current on the concentration of ethanol at carbon paste biosensors containing different loadings of fumed silica: 0 (a), 5 (b), 10 (c), 15 (d) and 20% (e) w/w. Other conditions, as in Fig. 3.

RESULTS AND DISCUSSION

Figure 1 compares cyclic voltammograms recorded at the ordinary and fumed-silica modified carbon paste electrodes (dotted and solid lines, respectively) for the blank solution (A) and after an addition of 2×10^{-3} M NADH (B). Several important points are noted from these data. The incorporation of fumed silica offers significant (×7 fold) enhancement of the anodic peak, and a substantial lowering of the overvoltage. At the conventional electrode, redox activity is observed only above +0.50 V (with a peak at +0.71 V). In contrast, the oxidation of NADH at the silica-based carbon paste starts around +0.30 V, and yields a maximum value at +0.58 V. Apparently, the silica modifier displays an efficient catalytic activity toward the oxidation of NADH. Metal oxide particles, particularly alu-

mina powder, are known for their catalytic action toward various solutes with slow electron transfer kinetics [9]. Silica-containing carbon paste electrodes have been shown recently to promote the oxidation of hydrogen peroxide [8]. The blank voltammogram (A) indicates that the presence of silica results in a very small increase of the background current. The main change is at the high potential region (above +0.8 V), where the silica appears to promote the oxidation of the solvent. Such background response indicates that the enhanced NADH response is not attributed to higher exposure of graphite sites (i.e., removal of the oil layer by the silica). Yet, the appearance of the silica-containing surface (under optical microscopy, 500 magnification, not shown) was distinctly different from that without the silica, with silica aggregates being visualized as a white reticular network.

The catalytic response of fumed silica toward the dissolved NADH, has prompted the incorporation (by mixing) of dehydrogenase enzymes and their NAD^+cofactor within the silica-containing paste. This results in reagentless biosensors, which are advantageous to analogous devices not containing the silica modifier. Figure 2 compares hydrodynamic voltammograms for ethanol at alcohol biosensors, in the absence (●) and presence (○) of fumed silica. In accordance with the cyclic voltammetric data of Fig. 1, the silica-containing surface greatly lowers the operating potential (with ethanol sensing starting at +0.30 V, as compared to +0.5 V without the silica). Note also the substantial (7-fold) enhancement of the biosensor response. The silica-containing NAD^+modified electrode also displayed a 4-fold enhancement of the cathodic current of the surface-bound cofactor, compared to analogous measurements without the silica (not shown). No lowering of the peak potential (−0.50 V) was observed.

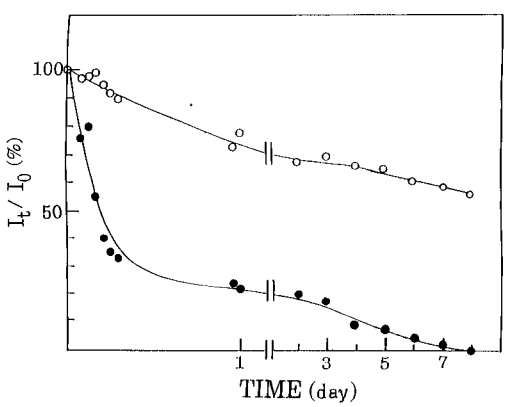

Fig. 5. Stability of the response of the carbon-paste (●) and carbon-paste/silica (○) enzyme electrodes to 5×10^{-3} M ethanol. Other conditions, as in Fig. 3. The same surface was employed with dry-storage at 4°C between measurements.

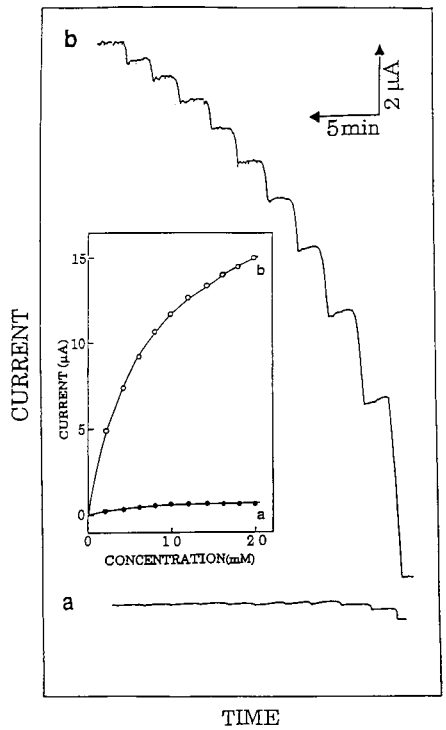

Fig. 6. Amperometric response to successive additions of 2×10^{-3} M lactate at the ordinary (a) and fumed-silica containing (b) carbon paste enzyme electrodes. Enzyme (LDH) loading, 5% w/w. Applied potential, +0.8 V. Other conditions, as in Fig. 5. Also shown (inset), are the resulting calibration plots.

Comparison of the actual current–time recordings for ethanol solutions of increasing concentration (2–20 mM, Fig. 3) demonstrates that the sensitivity improvement of the silica-containing carbon paste biosensor is achieved without compromising the speed advantage inherent to carbon paste biosensors ($t_{95\%} \sim 10$ s). Note also that

the silica modification does not affect the noise level. Hence, detection limits of 0.08 and 0.50 mM can be estimated based on the signal-to-noise characteristics ($S/N = 3$) of the response in the presence and absence of silica, respectively. Similar improvements are expected for other substrates of ADH. The use of nonhydrated fumed silica resulted in a similar enhancement of the ethanol response, but was accompanied by a slight increase in the response time (not shown).

The amount of silica in the paste has a profound effect upon the signal enhancement. Figure 4 shows the dependence of the steady-state amperometric response on the ethanol concentration for different silica loadings. The current signal increases rapidly (up to 6-fold) upon increasing the silica content between 0 and 15% w/w (a–d). No further increase in the sensitivity is observed at a higher (20% w/w) silica loading (e). The latter actually results in a slightly smaller response (relative to the 15% w/w silica-based bioelectrode). Apparently, there is a tradeoff between larger silica contents, and (the accompanied) small graphite fractions. All analytical work was thus carried out with the 15% w/w silica-containing biosensor.

It should be pointed out that the dramatic enhancement in the sensitivity associated with the presence of silica is attributed not only to its powerful electrocatalytic action (toward the NADH oxidation), but also to improved retention of the enzyme and its cofactor within the paste environment. Apparently, the adsorptive properties associated with the enormous surface area of the silica particles promotes the stabilization of these components in the paste matrix. without the need for time-consuming (derivatization/covalent) immobilization reactions. Such stabilization action is illustrated in Fig. 5 which compares the time dependence of the sensor response in the presence (○) and absence (●) of silica. A rapid decrease in the sensitivity (e.g., of

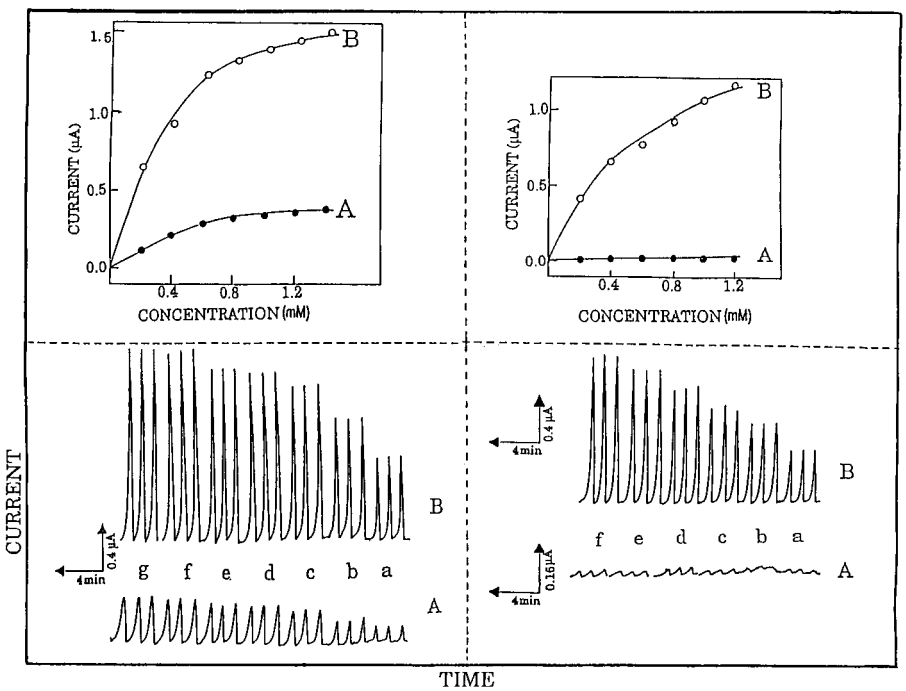

Fig. 7. Amperometric detection for injections of ethanol (left) and lactate (right) solutions of increasing concentration from 2×10^{-3} to 1.4×10^{-2} M (a–g) (left) and 2×10^{-3} to 1.2×10^{-2} M (a–f) (right) at the ordinary (A) and silica-containing (B) carbon paste biosensors. Flow-rate, 1.0 ml/min; carrier solution, 0.05 M phosphate buffer (pH 7.4). Other conditions, as in Figs. 3 and 5. Also shown (top) are the resulting calibration plots.

70 and 90% after 1 and 4 days, respectively) is observed without the silica, suggesting that the ADH and NAD^+ are rapidly diffusing away from the surface. In contrast, the silica-containing surface exhibits only a 20% decline in the response over the first day, and its sensitivity remained nearly unchanged over the next 7 days. Similar stability improvements were observed for glucose oxidase/fumed-silica carbon paste biosensors [8]. Larger silica beads have been used for immobilizing enzymes with high retention of the bioactivity [10].

Other dehydrogenase-based bioelectrodes can greatly benefit from the attractive features of the silica modifier. For example, Fig. 6 displays the response of conventional (a) and silica-containing (b) lactate dehydrogenase/NAD^+ biosensors to successive standard additions of lactate, each addition affecting a 2×10^{-3} M increase in concentration. These traces indicate that the silica-containing bioelectrode greatly enhances the sensitivity of the lactate biosensor (e.g,. ca. 18-fold current enhancement at the 2×10^{-3} M level). Such improvements are more profound than those observed in analogous biosensing of ethanol (Fig. 3). Notice also the very fast response to the changes in the substrate concentration. The resulting calibration plot (also shown) displays a curvature over the entire (2–20 mM) concentration range.

The silica-containing carbon paste biosensor holds great promise for on-line monitoring of the corresponding substrates. For example, Figure 7 displays the flow-injection response of the conventional (A) silica-containing (B) carbon paste bioelectrodes for ethanol (left) and lactate (right) solutions of increasing concentration, $(2–14) \times 10^{-3}$ M (a–g). Both silica-based detectors exhibit significant enhancement of the flow-injection peak. Note, in particular, that while the detection of lactate is not feasible at the ordinary detector, the silica-containing biosurface yields a well-defined response and offers convenient quantitation. The peak current enhancements are clearly indicated from the resulting calibration plots (also shown). A detection limits of ca. 1×10^{-4} M can be estimated for both compounds, on the basis of the favorable signal-to-noise characteristics ($S/N = 3$). The dynamic properties are not compromised by the presence of fumed silica. The silica-containing detector exhibits a very short response time and a rapid return to the baseline. The peak width is ~ 50 s, allowing a high injection rate of 60 samples/h.

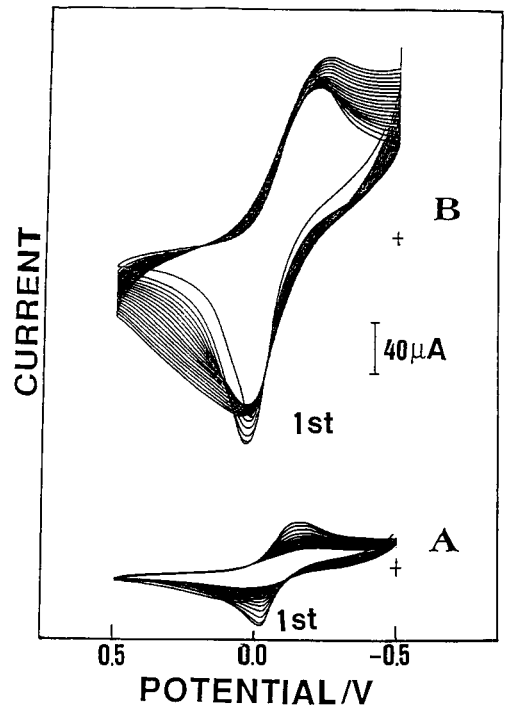

Fig. 8. Repetitive cyclic voltammograms in the blank solution at ordinary (A) and silica-containing (B) Meldola Blue modified electrodes. Meldola Blue loading, 2.5% w/w. Electrolyte, silica loading and scan rate, as in Fig. 1.

Electron acceptors (e.g., phenoxazine and phenothiazine compounds), commonly used to mediate the electrocatalytic oxidation of NADH [3], often leach rapidly from carbon paste biosensors to the contacting aqueous solution. The silica support offers stabilization of these mediators within the electrode matrix. Figure 8 compares repetitive cyclic voltammograms of ordinary (A) and silica-containing (B) Meldola-Blue (MB) modified electrodes. At the ordinary electrode, the MB peaks rapidly decrease upon repetitive scannings, and the redox activity is lost after 12 runs. In contrast, substantially larger peaks are observed at the silica-containing surface, with re-

tention of 85% of the activity after numerous repetitive scans.

In conclusion, we have illustrated that the incorporation of fumed silica within carbon paste matrices greatly enhances the sensitivity and stability of the resulting dehydrogenase biosensors. The improved performance is attributed to the adsorptive properties of the silica nanoparticles and to their electrocatalytic activity toward the oxidation of NADH. The silica-modification carbon paste strategy should be applicable to other enzyme/cofactor systems. Yet, additional work is desired to elucidate the exact microenvironmental effect and stabilization action of the fumed-silica additive, and for exploring the utility of other support matrices.

REFERENCES

1 W.J. Blaedel and R. Jenkins, Anal. Chem., 48 (1976) 1240.
2 P. Pantano and W.G. Kuhr, Anal. Chem., 65 (1993) 623.
3 L. Gorton, J. Chem. Soc., Faraday Trans., 82 (1986) 1245.
4 J. Wang, E. Gonzalez-Romero and M. Ozsoz, Electroanalysis, 4 (1992) 539.
5 G. Bremle, B. Persson and L. Gorton, Electroanalysis, 3 (1991) 77.
6 W. Kubiak and J. Wang, Anal. Chim. Acta, 221 (1989) 43.
7 L. Gorton, G. Jönsson-Pettersson, E. Czöregi, K. Johansson, E. Dominguez and G. Marko-Varga, Analyst, 117 (1992) 1235.
8 J. Wang and N. Naser, Electroanalysis, in press.
9 J. Zak and T. Kuwana, J. Am. Chem. Soc., 104 (1982) 5514.
10 A. Grumbliss, K. McLachlan, J. O'Daly and R. Henkens, Biotechnol. Bioeng., 31 (1988) 796.

Analytica Chimica Acta, 284 (1993) 393–404
Elsevier Science Publishers B.V., Amsterdam

Electrochemical behaviour of dopamine and ascorbic acid at overoxidized polypyrrole(dodecyl sulphate) film-coated electrodes

Zhiqiang Gao [1] and Ari Ivaska

Laboratory of Analytical Chemistry, Åbo Akademi University, SF-20500, Turku-Åbo (Finland)

(Received 17th May 1993)

Abstract

The electrochemical behaviour of dopamine and ascorbic acid at overoxidized polypyrrole(dodecyl sulphate) film-coated glassy carbon electrodes was investigated. It was found that dopamine can be efficiently accumulated into the film and the voltammetric detection limit of dopamine is greatly improved by this procedure. The current response was linear in the concentration range 0.1–10 μM and a detection limit of 40 nM was achieved when a 2-min preconcentration step under open-circuit conditions was used. A high selectivity for dopamine was observed owing to the exclusion of anionic species by the negative charges in the film. Chronoamperometry and chronocoulometry were used to determine the concentration and diffusion characteristics of dopamine within the film as a function of dopamine concentration in the solution and the film thickness. The film was found to protect the substrate electrode surface from poisoning by the oxidation product of dopamine. Good reproducibility was observed for multiple measurements of dopamine in 0.1 M phosphate buffer solution (pH 7.4).

Keywords: Voltammetry; Ascorbic acid; Dopamine; Film-coated electrodes; Polypyrrole(dodecyl sulphate) film-coated electrodes

In recent years, substantial efforts have been devoted to the development of electrochemical sensors based on chemically modified electrodes [1,2]. Investigations have demonstrated that coating of electrode surfaces with polymer films is an attractive means of increasing the sensitivity and selectivity of voltammetric analyses [1,2]. Preconcentration of analytes in modifier layers greatly improves the sensitivity and selectivity of voltammetric determinations. Various approaches have been proposed, including electrostatic accumulation [3], complexation [4], adsorption–extraction [5], bioaccumulation [6] and covalent reaction [7].

Chemically modified electrodes have also been developed for the electrochemical determination of neurotransmitters both in vivo and in vitro [8–12]. The use of Nafion film, a perfluorosulphonated polymer, as the electrode coating shows great affinity to large, hydrophobic cations relative to small inorganic cations [13,14]. This characteristic of Nafion films, coupled with their anion expulsion properties, has been successfully applied to the in vivo determination of primary catecholamine neurotransmitters, e.g., dopamine and norepinephrine [11,12]. In this case, the permeability of the film is particularly advantageous because all neurotransmitters are cations at physiological pH and the Nafion film, with its cation-

Correspondence to: A. Ivaska, Laboratory of Analytical Chemistry, Åbo Akademi University, SF-20500, Turku-Åbo (Finland).

[1] On leave from Henan University, Kaifeng, Henan, 475001 (China).

SSDI 0003-2670(93)E0488-S

exchange properties, shows an excellent response to them. On the other hand, major interferences such as biogenic amine metabolites, ascorbic acid and uric acid, are all anions at pH 7.4, and can therefore effectively be eliminated from the electrode surface. However, the practical utility of Nafion film-based electrochemical sensors for neurochemistry is limited by their non-uniform thickness and poor reproducibility arising from the solvent evaporation method used in the film preparation [14–16]. Undoubtedly, new polymers that are permselective or have catalytic properties are desirable for the further development of chemically modified sensors.

In this work, polypyrrole film prepared by electropolymerization in 0.1 M pyrrole and 0.1 M dodecyl sulphate solution [PPy(DS)] was first overoxidized in 0.1 M NaOH solution, and the electrochemical behaviour of dopamine at the resulting film-coated electrode was studied. The voltammetric response of ascorbic acid at these electrodes was also investigated because it is a commonly occurring interferent in the in vivo determination of neurotransmitters [17].

EXPERIMENTAL

Chemicals

Pyrrole obtained from Merck was purified by double distillation and stored at low temperature and protected from light. Dopamine (DA) and ascorbic acid (AA) from Aldrich and sodium dodecyl sulphate (NaDS) (Microselect) from Fluka were used as received. All other chemicals were of analytical-reagent grade and used as received. All solutions were prepared in distilled, deionized water obtained from a Millipore Milli-Q system. Solutions of DA and AA were prepared daily in water that had been deoxygenated with high-purity nitrogen.

Instrumentation

Voltammetric experiments were conducted with a PAR 174A polarographic analyzer (PARC, Princeton, NJ) and the results were recorded with a Model 29 000 Bryans X–Y recorder. Chronoamperometric and chronocoulometric experiments were performed with a PAR 273 potentiostat/galvanostat with the software version 3.00 (PARC). A conventional three-electrode system was used in the experiments; the working electrode was a glassy carbon disc electrode (5 mm diameter) (Metrohm, Herisau, Switzerland), the counter electrode was a platinum wire and a saturated calomel electrode (SCE) was used as the reference electrode. All potentials reported in this paper are referred to the SCE. Solutions were deoxygenated with high-purity nitrogen for at least 10 min prior to each experiment and all experiments were performed under nitrogen.

Preparation of overoxidized PPy(DS) film-coated glassy carbon electrodes

The working electrode was polished to a mirror finish successively with 1-μm diamond paste and 0.3-μm alumina slurry, rinsed with water and thoroughly polished on a clean, wet polishing cloth. It was then pretreated according to the procedure described by Anjo et al. [18] and rinsed with water again. PPy films were prepared galvanostatically with a current density of 1–2 mA cm^{-2} in oxygen-free 0.1 M NaDS solution containing 0.02–0.1 M pyrrole. The film thickness was controlled by controlling the charge of polymerization [19]. When the film deposition process was finished the electrode was rinsed with water and then transferred into a 0.1 M NaOH solution. The PPy film was overoxidized by potential cycling between -0.2 and 0.4 V with a scan rate of 20–50 mV s^{-1} until the voltammetric activity of the film had been lost completely. It usually took 20 min for a 0.3-μm thick PPy(DS) film. The electrode was then ready for use after the final wash with water. PPy in strongly alkaline medium becomes overoxidized and loses its electrochemical activity at ca. 0.3 V.

Voltammetric measurements with the PPy(DS) film-coated electrodes

The same preconcentration–quantification–renewal scheme was used in all experiments. For the preconcentration step, the film electrode was immersed under open-circuit conditions in 20 ml of 0.1 M phosphate buffer (pH 7.4) containing

the analytes. The solution was stirred by a 1.5-cm magnetic stirring bar at ca. 300 rpm. After a given period of time a linear potential scan was conducted and after the measurement the electrode was kept at 0.4 V for 1 min to ensure complete oxidation of the previously preconcentrated DA prior to the next measurement.

RESULTS AND DISCUSSION

Voltammetry of dopamine and ascorbic acid at overoxidized PPy(DS) film electrodes

Figure 1 shows cyclic voltammograms for DA and AA at both bare (solid line) and overoxidized PPy(DS) film-coated (dotted line) electrodes in 0.1 M phosphate buffer solution (pH 7.4). In this medium DA molecules are protonated as cationic species and AA molecules are deprotonated as anionic ascorbates. As can be seen in Fig. 1A, the current for negative ascorbate ions at the 0.5-μm thick PPy(DS) film electrode is less than 6% of the current measured at the bare glassy carbon electrode. In contrast, the current for oxidation of cationic DA (Fig. 1B) at the same coated electrode is more than 45 times higher than the current at the bare electrode. These results clearly indicate that the overoxidized film effectively excludes the negative ascorbate ions from the electrode but increases the sensitivity for the positive DA species. This selective retardation of electrochemical activity of ascorbate is of great importance in developing neurochemical sensors. For example, the linear-sweep voltammetric determination of 0.5 μM DA at 0.3–0.5-μm thick overoxidized PPy(DS) film coated electrodes was almost unaffected by the presence of 0.5 mM AA. On the other hand, a large overlapped anodic wave for DA and AA would be observed at the bare glassy carbon electrode. This is due to both overlapping of the oxidation potentials of these two species and the catalytic nature of AA towards the oxidation product of DA in aqueous solutions [20]. As can be seen in Fig. 1, the anodic peak potentials of both AA and DA are almost identical at both the bare and at the coated electrodes. These peak potentials are similar to those observed by Anjo et al. [18].

Overoxidation of the PPy(DS) film by potential cycling in 0.1 M NaOH is obviously the result of

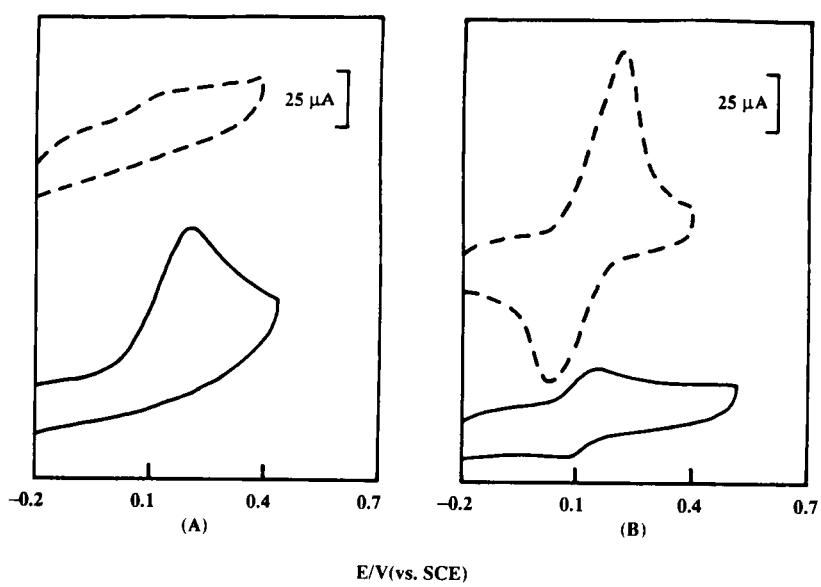

Fig. 1. Cyclic voltammograms of (A) AA and (B) DA at (solid lines) bare and (dashed lines) overoxidized PPy(DS) film-coated electrodes. Film thickness, 0.5 μm; preconcentration time, 2 min; potential scan rate, 100 mV s^{-1}. (A) 1.0 mM AA + 0.1 M phosphate buffer (pH 7.4); (B) (solid line) 50 and (dashed line) 10 μM DA + 0.1 M phosphate buffer (pH 7.4).

the nucleophilic attack of OH^- on the pyrrole units. The hydroxyl groups are then oxidized to carbonyls [21,22], resulting in the loss of conductivity and conversion of the polymer from an electronic/ionic conductor into a non-electronic but purely ionic conductor [23]. The presence of hydroxyl and carbonyl groups in overoxidized pyrrole units has previously been confirmed by Fourier transform IR spectra of the polymers [21,22]. Overoxidation of PPy in NaOH solution can therefore be regarded as resulting in a negatively charged polymer film. Cationic species such as dopamine in the solution can therefore effectively be accumulated into the film by an ion-exchange equilibrium under open-circuit conditions [24]. When the electrode is then potential scanned in the positive direction an enhanced anodic current due to oxidation of the preconcentrated DA is observed. The negative charges in the polymer, however, effectively expel negative ions from the film, as can be seen in the much lower current for ascorbate measured at the overoxidized film than at the bare electrode. Overoxidation of PPy(DS) in 0.1–1.0 M HCl obviously does not lead to the formation of any anionic sites in the polymer backbone because the polymer was found to lose only its electrochemical activity without showing any increased activity for preconcentration of positively charged DA.

Oxidation of DA and AA at an overoxidized film electrode obviously takes place at the surface of the substrate electrode rather than at the polymer/solution interface because the same peak potential is observed both at the bare electrode and at the overoxidized electrode. This is valid for both species. This conclusion can further be confirmed by studying the voltammograms of DA and AA at a free-standing PPy(DS) film electrode in 0.1 M phosphate buffer solution (pH 7.4). The free-standing PPy(DS) film electrode was prepared on indium–tin oxide glass (ITO) under identical experimental conditions as for the polymer-coated glassy carbon electrodes. After polymerization, the coated ITO glass was transferred into distilled water and the polymer film was stripped off by a stream of water. In order to ensure that the only contact between the measuring instrument and the electrolyte solution is through the PPy(DS) film, the electrical contact point was ca. 0.5 cm above the solution level. Large anodic currents for DA and AA were detected with this film electrode prior to overoxidation treatment, indicating that there is an electron transfer reaction at the polymer/solution interface. The observed redox processes of DA and AA at the PPy(DS) film are due to the fact that the film itself is in its electronically conducting state (in oxidized form) at the potentials studied. The high conductivity of this polymer film [25] makes it possible to have an electron transfer process at the polymer/solution interface. PPy film-coated electrodes can indeed be described as redox electrodes when they are in the fully oxidized form [26]. When the free-standing film electrodes were then overoxidized under identical experimental conditions as for the glassy carbon electrode coated by the polymer film, no oxidation current for DA or AA could be detected with this electrode, even in 5.0 mM solutions. This indicates that the electron-transfer reaction does not take place at the overoxidized polymer film/solution interface but rather at the electrode substrate itself.

Previous work on PPy films prepared in solution of inorganic anions (X^-), PPy(X), has shown that electrochemically active anions cannot be oxidized at overoxidized PPy(X) [27,28]. However, the voltammetric responses of electrochemically active cationic species in solution such as dopamine and methyl viologen are also slightly suppressed and the currents measured for these species are never higher than the current measured at uncoated electrodes, no matter what solution is used in overoxidation of the PPy(X) films. In contrast, the overoxidized PPy(DS) film shows a significant improvement in current sensitivity toward cationic DA. The explanation for this behaviour is evident when one considers the volume of doping ions used in the preparation of PPy films. During overoxidation, the doping ions are expelled from the polymer films [22], resulting in a porous structure of the film. The bulky dodecyl sulphate ion results in a more porous structure of the overoxidized PPy film than a film prepared in the presence of small inorganic anions. Owing to the large pores in the overoxidized

PPy(DS) film, cationic species such as DA can easily diffuse through the film and reach the substrate electrode surface, where the electron-transfer reaction takes place. It seems that the permeability of the PPy films can be flexibly controlled by a judicious choice of the size of the doping ions, providing the basis for the analytical usefulness of the overoxidized PPy film-coated electrodes.

The voltammetric response of DA at a bare glassy carbon electrode gives a typical diffusion-controlled anodic peak in the concentration range studied in this work (μM–mM). At the film-coated electrode, however, DA gives a symmetrical anodic peak that no longer is solely controlled by the diffusion process in the solution phase. An analysis of the log i_{pa} (anodic peak current) vs. log v^n (potential scan rate) plot was done in order to determine the exponent (n) of the potential scan rate as a function of the DA concentration in the solution and the film thickness. With decreasing DA concentration from mM to μM a shift of n from 0.5 to 1 was observed at films with the thickness < 0.5 μm, as would be expected for a change from a diffusion-controlled oxidation to an oxidation of surface-attached species [29]. The contribution from the mass-transport process in solution, i.e., diffusion from the bulk to the surface of the film, becomes negligible at very low concentrations, e.g., at 0.1 μM, and therefore the electrode process will be entirely controlled by the concentration of the accumulated analyte in the film The voltammograms at high concentrations, however, did not exclusively show oxidation of surface-attached species and a contribution from the solution diffusion is undoubtedly present. However, a large part of the increased sensitivity seems clearly to be the result of DA accumulation in the film. When the film thickness was increased from 0.1 to 1.0 μm the exponent of the scan rate, n, changed from 1 to 0.5 in a 10 μM solution of DA. This indicates that the diffusion of DA within the film becomes predominant in thick films. As discussed above, the electron-transfer process takes place at the substrate electrode and therefore any change in the film thickness will also result in a change in the diffusion pathway for DA. The diffusion process within the film becomes more and more important as the film thickness increases. Similar behaviour has been observed at Nafion-coated electrodes [30]. At electrodes coated with a 1.0-μm thick overoxidized PPy(DS) film the oxidation current of DA in the concentration range 0.2 μM–1.0 mM was found to be controlled almost entirely by the diffusion process of DA in the film.

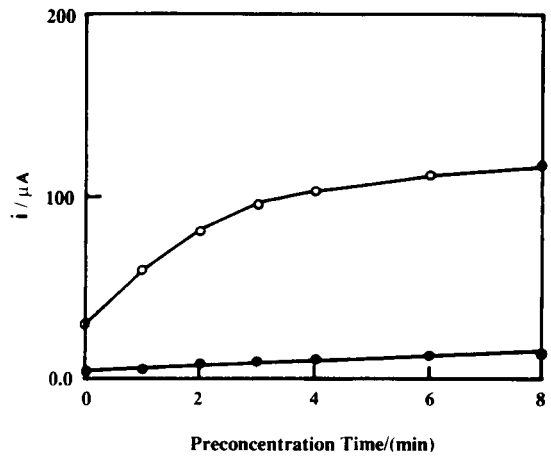

Fig. 2. Dependence of anodic peak current of DA on preconcentration time at overoxidized PPy(DS) film-coated electrodes. (●) 1.0 and (○) 10 μM DA; other conditions as in Fig. 1B.

Figure 2 shows plots of anodic peak currents, determined by linear-sweep voltammetry, versus the open-circuit immersion time in a 10 μM solution of DA at the PPy(DS) film-coated electrode in phosphate buffer solution (pH 7.4). In these experiments the voltammograms were recorded with freshly prepared and overoxidized polymer-coated electrodes. The plots in Fig. 2 indicate that the peak current for DA at the coated electrodes increases with increasing immersion time and much higher anodic currents than observed at bare glassy carbon electrodes are evident for all immersion times studied. This observation clearly supports the assumption of the high permeability and the accumulating nature of the film towards cationic DA. The rate of the DA accumulation in the film depends on the DA concentration in the solution. Generally the observed peak current, i.e., the amount of accu-

mulated DA, increases rapidly during the first few minutes, after which the rate drops significantly and finally a limiting value is reached. In all instances, the preconcentration process was found to be relatively fast, more than 70% of the final response always being obtained during the first few minutes of immersion. Similar observations have also been made at other ion-exchange film-coated electrodes [30,31]. For practical purposes, a 2-min preconcentration period was found to be sufficient in order to obtain high sensitivity in the voltammetric determination of DA. At the polymer film-coated electrode the small oxidation current of AA did not show any dependence on the immersion time, indicating that ascorbate is not preconcentrated at these polymer film-coated electrodes. At the same concentration level the peak current for DA at the bare glassy carbon electrode was 3–4 times higher than that for AA, which is due to more rapid electrode kinetics arising from the more reversible redox behaviour of DA [8].

After the first anodic scan, the preconcentrated DA in the film is not completely oxidized and therefore will affect the subsequent measurements. This effect is more pronounced at high concentrations of DA. In order to develop a highly sensitive and reproducible electrochemical sensor, different methods for effective renewal of the film had to be evaluated. It was found that renewal of the film is easily accomplished by soaking the film electrode in 0.1 M phosphate buffer solution (pH 7.4) for about 2 h. The renewal process could be greatly accelerated by applying a sufficiently positive potential to the electrode. In practical work, the electrode was polarized at 0.4 V for 1 min after each determination at a concentration lower than 1.0 mM. At higher concentrations of DA the film can only partly be renewed and therefore the electrode cannot be used in practical work at concentrations of DA higher than 1.0 mM. The effective renewal and reproducible preconcentration were studied by ten parallel determinations in 0.1 M phosphate buffer solution (pH 7.4) containing 0.5 μM DA. For a 2-min exposure time at a 0.5-μm-thick PPy(DS) film, the mean anodic current was 4.2 μA with a relative standard deviation of 5.0%

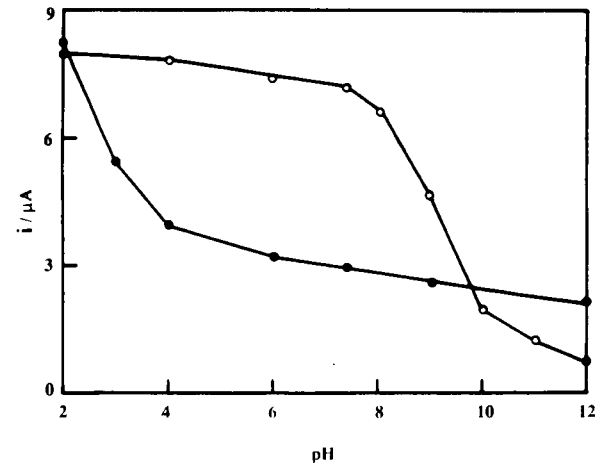

Fig. 3. Effect of pH on the anodic peak currents of (●) 1.0 mM AA and (○) 1.0 μM DA at overoxidized PPy(DS) film-coated electrodes. Conditions as in Fig. 1B.

when the scan rate of 100 mV s^{-1} was used. This is contrary to the observed fouling of the bare glassy carbon electrode by DA oxidation products resulting in shift of the anodic peak and a decrease in the anodic current [32]. Adsorption of analytes or species formed on their oxidation may be responsible for the observed fouling. A possible explanation for the anti-fouling effect of the polymer film has been given by Wang and Li [33]. A single overoxidized PPy(DS) film could be used for at least 25 determinations at μM concentration levels without any noticeable decrease in sensitivity and stability.

As discussed in the previous section, the transport rate of a solution species through the film is strongly dependent on its charging state. Therefore, in the determination of DA in the presence of AA, the acidity of the medium is also very important. The influence of the solution pH on the current sensitivity of DA and AA was investigated in 0.1 M phosphate buffer solution. The results of this study are shown in Fig. 3. Dramatic changes in the film permeability were observed around the pK_a values of the species. As can be seen, a high anodic current is observed for DA at pH < 8, indicating that DA ($pK_a \approx 8.9$) is readily preconcentrated and transported through the film as a cation, and therefore a competitive effect of

TABLE 1

Effect of film thickness on the voltammetric sensitivity of DA and selectivity towards AA [a]

Thickness (μm)	i_{pa}(DA) (μA)	i_{pa}(AA) (μA)	i_{pa}(DA)/i_{pa}(AA) [b]
0.0	1.74	53.5	3.25
0.1	50.4	11.2	450
0.3	89.5	4.71	1900
0.5	83.1	2.67	3110

[a] Concentrations of DA and AA, 10 μM and 1.0 mM, respectively; potential scan rate, 100 mV s^{-1}; preconcentration time, 2 min. [b] i_{pa}(DA)/i_{pa}(AA) was calculated at the same concentration level; i_{pa}(AA) was estimated by assuming that a linear response exists at the film coated electrode.

other cations on the ion-exchange process can be expected. At pH > 9, DA will mainly be in the form of neutral species, and therefore the current sensitivity is significantly decreased. At the same time the cation concentration in the solution was found to have only a small effect on the peak current of DA. For AA the change in the film permeability, i.e., accumulation in the film, with pH was also observed around its pK_a value (ca. 4.2). As can be seen in Fig. 3, higher currents are observed for the protonated neutral species than for deprotonated anionic species.

The sensitivity of the DA oxidation and the selectivity towards oxidation of AA are strongly dependent on the film thickness and preconcentration time. As shown in Table 1, the highest sensitivity was observed at a 0.3-μm thick film-coated electrode for a 2-min exposure time in 10 μM DA solution. At much lower DA concentrations the highest sensitivity was obtained at films thinner than 0.3 μm. On the other hand, the selectivity towards AA was found to increase when the thickness of the PPy(DS) film was increased.

The anodic peak current at 0.3–0.5-μm thick PPy(DS) films in 0.1 M phosphate buffer (pH 7.4) was found to be directly proportional to the concentration of DA in the range 0.1–10 μM with an overall relative standard deviation of 3.8%, a correlation coefficient of 0.998 and a detection limit of 40 nM (signal-to-noise ratio = 3, 2-min preconcentration time). A prolonged preconcentration time extended the low-concentration end but shortened the linear response range. For example, a detection limit down to 10 nM was obtained after 10 min of immersion, whereas increasing the film thickness both decreased the current sensitivity and increased the detection limit owing to the diffusion behaviour of the analyte within the film and the increase in the background current.

Chronoamperometry of dopamine at both bare and coated electrodes

The electrode process, especially diffusion of DA within the film, was studied by chronoamperometry. Values for the apparent diffusion coefficient, D_{app}, of DA in PPy(DS) film-coated and bare glassy carbon electrodes were determined in a 0.1 M phosphate buffer solution (pH 7.4). The electrode area (0.2 ± 0.01 cm^2) was determined by carrying out an experiment with a known system, i.e., oxidation of $Fe(CN)_6^{4-}$ in 1.0 M KCl solution. The diffusion coefficient of $Fe(CN)_6^{4-}$ is 0.68×10^{-5} cm^2 s^{-1} [34]. A typical chronoamperometric response and the plot of current (i) versus $t^{-1/2}$ (Cottrell plot) for a potential step from -0.2 to 0.4 V for DA preconcentrated from a 1.0 mM solution at pH 7.4 are shown in Figs. 4 and 5, respectively. The Cottrell plot obtained was lin-

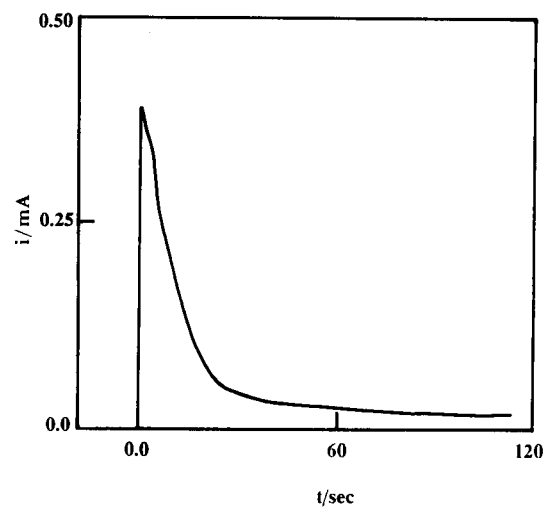

Fig. 4. Chronoamperometric response of preconcentrated DA in overoxidized PPy(DS) films. Film thickness, 1.0 μm; preconcentration time, 30 min in 1.0 mM DA + 0.01 M phosphate buffer (pH 7.4) solution; potential step from -0.2 to 0.4 V.

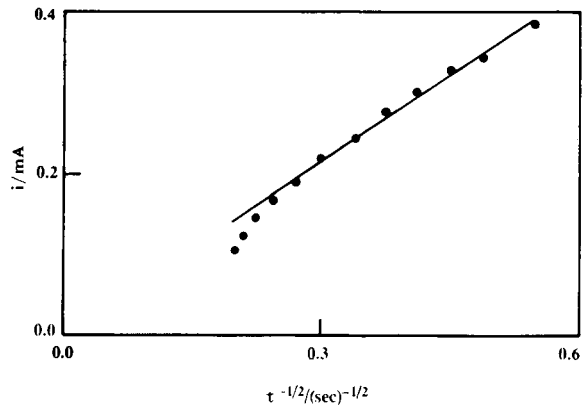

Fig. 5. Cottrell plot for oxidation of preconcentrated DA in overoxidized PPy(DS) films. Conditions as in Fig. 4.

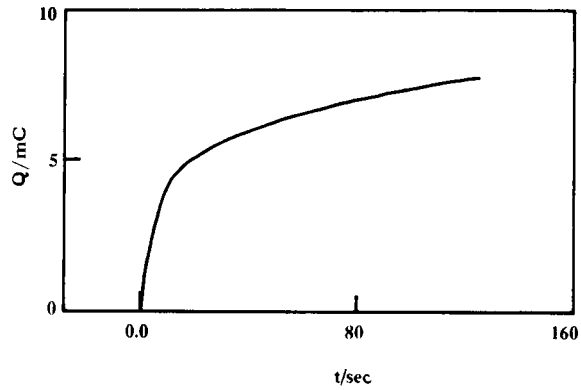

Fig. 6. Chronocoulometric response of accumulated DA in overoxidized PPy(DS) films. Conditions as in Fig. 4.

ear, as expected for a diffusion-limited process [29]:

$$i = nFAD_{app}^{1/2}C_p/(\pi^{1/2}t^{1/2}) \quad (1)$$

where n is the number of electrons transferred, A is the electrode area and D_{app} and C_p are the apparent diffusion coefficient and bulk concentration of DA in the polymer film, respectively. C_p was determined by complete coulometric oxidation of preconcentrated DA in PPy(DS) films. D_{app} was then calculated from the slope of the Cottrell plot. Values determined at different film thicknesses and DA concentrations are given in Table 2. As can be seen, similar values for D_{app} were obtained with films with different thicknesses. However, a much larger value of D_{app}, ca. 5.6×10^{-6} cm s^{-1}, was obtained for diffusion in solution when determined at a bare glassy carbon electrode. This value is comparable to the value given in the literature [35]. The different values for D_{app} observed in the measurements with the bare glassy carbon electrode and with the electrode covered with overoxidized PPy(DS) film further confirm that oxidation of DA in the latter instance takes place at the substrate electrode rather than at the polymer/solution interface.

TABLE 2

Apparent diffusion coefficient (D_{app}) of dopamine in overoxidized PPy(DS) films

Parameter	Film thickness (μm)		
	0.3	0.5	1.0
DA concentration in solution (mM)	0.2–2.0	0.2–2.0	0.2–2.0
D_{app} (10^{-10} cm^2 s^{-1}) [a]	3.3±0.5	4.2±0.6	3.5±0.6
D_{app} (10^{-10} cm^2 s^{-1}) [b]	3.2±0.5	3.7±0.6	4.0±0.6

[a] From chronoamperometric responses. [b] From chronocoulometric responses.

Chronocoulometry of preconcentrated dopamine in overoxidized PPy(DS) films

The experimental results obtained by voltammetry presented above showed that oxidation of preconcentrated DA in an overoxidized PPy(DS) film exhibits behaviour that is characteristic both for surface-attached and diffusion-controlled electrode processes. Chronocoulometry is a good technique for distinguishing these two processes. Responses were recorded after the coated electrodes had been soaked for 30 min in 1.0 mM DA solution, rinsed with water and then transferred to a blank electrolyte solution, i.e., 0.01 M phosphate buffer (pH 7.4). Figure 6 shows the charge (Q) vs. time (t) plot for a potential step from −0.2 to 0.4 V with a 1.0-μm thick PPy(DS) film. Electrochemical parameters of this system can be determined by using the integrated Cottrell equation [29]:

$$Q = 2\pi^{-1/2}nFAD^{1/2}{}_{app}t^{1/2}C_p + Q_{ads} + Q_{dl} \quad (2)$$

where Q_{ads} and Q_{dl} are the surface charge and double-layer charge, respectively, and the other

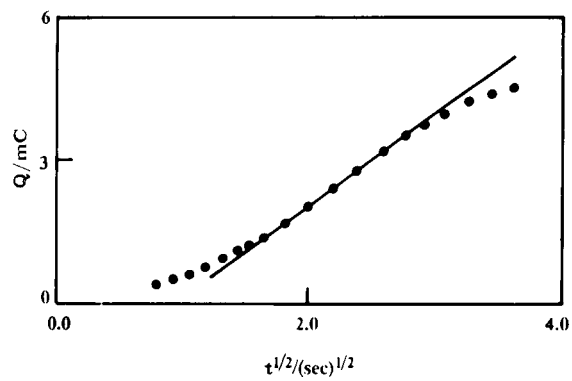

Fig. 7. Integrated Cottrell plot for oxidation of preconcentrated DA in overoxidized PPy(DS) films. Conditions as in Fig. 4.

symbols have their usual meanings. Q_{dl} can be obtained directly from the Q vs. $t^{1/2}$ plot at the unloaded, overoxidized PPy(DS) electrode. A typical plot of Q vs. $t^{1/2}$ for a potential step experiment (integrated Cottrell plot) is shown in Fig. 7. For $t < 6$ s this plot was linear, as expected for a diffusion-controlled process. At longer times the charge increased more slowly than would be expected for a diffusion-controlled process, indicating depletion of electroactive species in the film. On the other hand, however, at very short times the charge is larger than would be expected from a pure diffusional behaviour in the polymer film. This suggests that some DA behaves as surface-attached species. This is in good agreement with the observed voltammetric responses where the exponent n in the $\log i_{pa}$ vs. $\log v^n$ plot was changed from 1 to 0.5. However, for films thicker than 0.5 μm in solution and with a relatively high concentration of DA, the contribution to the overall charge from the adsorbed species is very small compared with the contribution from diffusion. Unfortunately, an attempt to determine the surface concentration of DA was unsuccessful, probably owing to the change in the double-layer capacitance after the preconcentration process of DA, i.e., Q_{ad} in Eqn. 2 cannot be determined separately when Q_{dl} cannot be kept constant. The slope of the plot of Q vs. $t^{1/2}$ was found to increase with increasing preconcentration time owing to the increase in the concentration of DA in the film, i.e., C_p, as Eqn. 2 indicates. With a 1.0-μm thick PPy(DS) film-coated electrode in 1.0 mM DA solution the slope finally reached a maximum value when the preconcentration time became longer than 10 min. This indicates that DA has reached the equilibrium distribution between the film and the solution. Essentially the same tendency was observed at lower concentrations of DA in the solution, but a much longer time was needed to reach the equilibrium state. The slope of the Q vs. $t^{1/2}$ plots for the film-coated electrode was also dependent on DA concentration in the solution. The slope increased with increasing DA concentration up to 3 mM in the solution with a 5-min preconcentration time and a virtually constant value was reached when the DA concentration increased above 5 mM.

The apparent diffusion coefficient, D_{app}, of DA in the polymer film was also determined from the slope of the Q vs. $t^{1/2}$ plot in Fig. 7 according to Eqn. 2 and the values are given in Table 2. In these experiments it was also found, as in the chronoamperometric measurements, that D_{app} did not show any dependence on the total concentration of DA in the film. As can he seen in Table 2, similar values for D_{app} were found by both techniques. The small variations are probably due to uncertainties in the film thickness, but are still much smaller than the previously reported variations in D_{app} obtained for DA at Nafion film-coated electrodes [15]. This is obviously due to the more precise control of the thickness of the PPy(DS) film by controlling the charge used during polymerization.

Equilibrium between dopamine in the overoxidized PPy(DS) film and in the solution

A 1.0-μm thick overoxidized PPy(DS) electrode was first soaked in 0.1 M phosphate buffer (pH 7.4) containing DA in the μM to mM concentration range for 30 min to ensure equilibrium between DA in the film and in the solution. This time was found to be long enough to establish the equilibrium for DA. The dependence of the concentration of dopamine in the film, C_p, and the concentration in the solution phase, C_s, is shown in Fig. 8. The concentration of preconcentrated DA in the polymer film was calculated from the

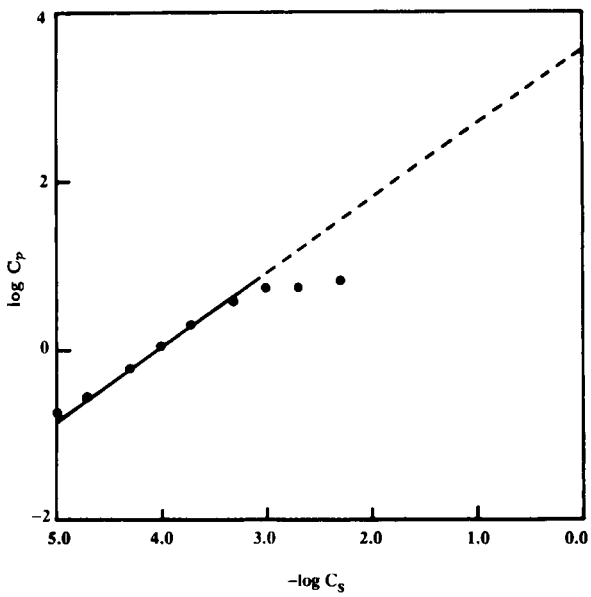

Fig. 8. Dependence of DA concentration, C_p, in the overoxidized 1.0-μm thick PPy(DS) films on the concentration of DA in the solution, C_s. The total amount of DA in the film was determined by coulometry. Conditions as in Fig. 4.

film thickness and the charge (Q) consumed for complete oxidation of DA measured in 0.01 M phosphate buffer (pH 7.4). As can be seen, the plot of log C_p vs. log C_s is linear in the C_s range 10 μM–0.5 mM. The deviation from linearity at higher concentrations indicates that the film has become saturated [36]. The saturation concentration of DA in the film was calculated to be ca. 5 M. This concentration can be considered to be the same as the concentration of negatively charged pyrrole units in the polymer film assuming 1 : 1 stoichiometry. The calculated concentration of DA in the film is probably smaller than the true value because some DA molecules may be trapped in regions inaccessible to electrochemical oxidation or diffuse to the electrolyte solution owing to the solution contact during the coulometric experiment. The distribution coefficient $K = C_p/C_s$, determined from the intercept of the plot shown in Fig. 8, was found to be $(3.6 \pm 0.6) \times 10^3$. The relatively good correlation between the concentrations in the solution and in the polymer indicates that fairly uniform films with reproducible thickness could be prepared. The plot in Fig. 8 can also be used to estimate the equilibrium concentration of DA in the film when the concentration of DA in the solution is known. Because K is large and the process of equilibration of species between the solution and the polymer is relatively slow, the rate of loss of the preconcentrated species from the polymer layer is very low. Thus the loss of electroactive species from the loaded polymer when it contacts supporting electrolyte solution is negligible over the time scale of the experiments, usually less than 5 min. However, when the electrode was immersed in blank electrolyte solution under open-circuit conditions for a long time, e.g., 3 h, only less than 10% of the original signal could be detected. The loss was found to increase with increasing electrolyte concentration, which is in good agreement with the common behaviour of ion exchangers. It was also found that the distribution coefficient is dependent on the electrolyte concentration. A 55% decrease in K was observed when the electrolyte concentration was increased from 0.01 to 1.0 M.

The influence of the cation concentration of the buffer, in this instance Na^+, was studied in phosphate buffer solution (pH 7.4) by changing the total concentration of the buffer or by adding NaCl to the solution. It was found that the anodic peak current or anodic peak area decreased with increasing cation concentration, indicating that the efficiency of the preconcentration is inversely proportional to the cation concentration. The decrease in the signal is obviously due to the fact that cations from the electrolyte solution are competing with the ion-exchange process responsible to the accumulation of DA and can therefore be regarded as the major disturbance source. The peak current as a function of the cation concentration is shown in Fig. 9. The competitive effect is much more pronounced when large hydrophobic cations, e.g., $Fe(bpy)_2^{2+}$ (bpy = 2,2′-bipyridyl), are present in the sample solution. For example, the anodic peak current of DA decreased from 8.3 to 3.5 μA when the $Fe(bpy)_2^{2+}$ concentration was increased from 0 to 0.5 μM in 1.0 μM DA solution (pH 7.4), whereas for AA a small increase in the oxidation current was observed in a similar experiment. This increase is

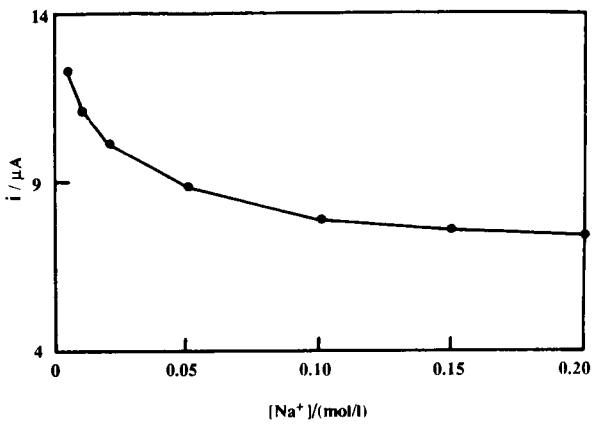

Fig. 9. Effect of buffer cation concentration on the anodic peak current of 1.0 μM DA. Conditions as in Fig. 1B.

obviously due to the decrease in the negative charge density of the polymer film resulting in a reduced repulsive force between ascorbate ions and the anionic sites in the film.

Conclusions

It has been demonstrated that overoxidized PPy(DS) films can be used for the selective voltammetric determination of cationic dopamine species in the presence of anionic ascorbate ions in solution. In particular, the enhanced selectivity obtained at the overoxidized PPy(DS) film-coated electrode could be very valuable for in vivo electrochemical determinations of biologically important ionic species. Preconcentration of cations in the films might be of general utility in developing highly sensitive electrochemical sensors. Experimental results obtained by voltammetry, chronoamperometry and chronocoulometry have shown that the overall electrode process is controlled by both surface-attached and diffusional dopamine species in the film, which mainly depends on the film thickness.

REFERENCES

1 J. Wang, in A.J. Bard (Ed.), Electroanalytical Chemistry, Vol. 16, Dekker, New York, 1989.
2 S.A. Wring and J.P. Hart, Analyst, 117 (1992) 1215.
3 J. Schneider and R.W. Murray, Anal. Chem., 54 (1982) 1508.
4 A.R. Guadalupe and H.D. Abruna, Anal. Chem., 57 (1985) 142.
5 T.B. Jarbawi and W.R. Heineman, Anal. Chim. Acta, 186 (1986) 11.
6 J. Gardea-Torresdey, D. Darnall and J. Wang, Anal. Chem., 60 (1988) 72.
7 J.F. Price and R.P. Baldwin, Anal. Chem., 52 (1980) 1940.
8 M.B. Gelbert and D.J. Curran, Anal. Chem., 58 (1986) 1028.
9 C.D. Blaha and R.F. Lane, Brain Res. Bull., 10 (1983) 861.
10 J. Wang and M.S. Lin, Electroanalysis, 2 (1990) 253.
11 P. Capella, B. Ghasemzadeh, K. Mitchell and R.N. Adams, Electroanalysis, 2 (1990) 175.
12 G.A. Gerhardt, A.F. Oke, F. Nagy, B. Moghaddam and R.N. Adams, Brain Res., 290 (1984) 390.
13 M.N. Szentirmay and C.R. Martin, Anal. Chem., 56 (1984) 1898.
14 G. Nagy, G.A. Gerhardt, A.F. Oke, M.E. Rice, R.N. Adams, R.B. Moore, M.N. Szentirmay and C.R. Martin, J. Electroanal. Chem., 188 (1985) 85.
15 H.S. White, J. Laddy and A.J. Bard, J. Am. Chem. Soc., 104 (1982) 4811.
16 A.J. Tudös, W.J.J. Ozinga, H. Poppe and W.T. Kok, Anal. Chem., 62 (1990) 367.
17 R.N. Adams, Anal. Chem., 48 (1976) 1126A.
18 D.M. Anjo, M. Kahr, M.M. Khodabakhsh, S. Nowinski and M. Wanger, Anal. Chem., 61 (1989) 2603.
19 A.F. Diaz and J.I. Castillo, J. Chem. Soc., Chem. Commun., (1980) 397.
20 M.A. Dayton, A.G. Ewing and R.M. Wightman, Anal. Chem., 52 (1980) 2392.
21 W. Wernet and G. Wegner, Makromol. Chem., 188 (1987) 1465.
22 F. Beck, P. Braun and M. Oberst, Ber. Bunsenges. Phys. Chem., 91 (1987) 967.
23 T.A. Skotheim (Ed.), Handbook of Conducting Polymers, Vol. 1, Dekker, New York, 1986.
24 R.W. Murray, A.G. Ewing and R.A. Durst, Anal. Chem., 59 (1987) 379A.
25 R.C.D. Peres, J.M. Pernaut and M.-A. De Paoli, Synth. Met., 28 (1989) C59.
26 A. Michalska, A. Lewenstam, A. Ivaska and A. Hulanicki, Electroanalysis, 5 (1993) 261.
27 M.S. Freund, L. Budabhai and A. Brajter-Toth, Talanta, 38 (1991) 95.
28 A. Witkowski, M.S. Freund and A. Brajter-Toth, Anal. Chem., 63 (1991) 622.
29 A.J. Bard and L.R. Faulkner, Electrochemical Methods, Wiley, New York, 1980.
30 L.D. Whiteley and C.R. Martin, Anal. Chem., 59 (1987) 1746.
31 Z. Gao, P. Li and Z. Zhao, Anal. Chem., 63 (1991) 953.

32 A.W. Sterson, R. McCreery, B. Feinberg and R.N. Adams, J. Electroanal. Chem., 46 (1973) 313.
33 J. Wang and R. Li, Anal. Chem., 61 (1989) 2809.
34 K. Aoki and J. Osteryoung, J. Electroanal. Chem., 125 (1981) 315.
35 S. Nowinski and D. Anjo, J. Chem. Eng. Data, 34 (1989) 265.
36 G.T. Cheek and R.F. Nelson, Anal. Lett., 11 (1978) 393.

Analytica Chimica Acta, 284 (1993) 405–411
Elsevier Science Publishers B.V., Amsterdam

Rapid adsorptive cathodic stripping voltammetry of zinc complexes in sea water

J.J. Hernández-Brito, J. Pérez-Peña, M.D. Gelado-Caballero and C. Collado-Sánchez

Chemistry Department, Faculty of Marine Sciences, University of Las Palmas de Gran Canaria, P.O. Box 550, 35017 Las Palmas de Gran Canaria (Spain)

(Received 7th June 1993; revised manuscript received 20th July 1993)

Abstract

The effects of the potential scan speed on the adsorptive cathodic stripping voltammetric determination of zinc–tetramethylenedithiocarbamate complexes in sea water were investigated. It was observed that an increase in scan speed increases the peak height and peak width, shifts the peak potential towards negative values and increases the capacitance background current. These effects were explained by taking into account the ohmic drop at high scan speeds. Several advantages of using a high scan speed in the determination of zinc were found. The faradaic current and sensitivity of the determination are noticeably increased as the whole electroactive substance is reduced in a shorter time. The stirring or turbulent motion of the solution during the scan does not perturb the zinc peak as the complete scan is done in a few milliseconds. Oxygen interference is less severe as the metal and oxygen reduction currents are now in the same current range. The entire analysis time can be markedly reduced as the purging, collection and quiescence time can be decreased. The method is proposed for use on-board oceanographic vessels where its advantages are especially valuable. All results were obtained using a laboratory-designed polarograph able to operate at very high scan speeds.

Keywords: Stripping voltammetry; Sea water; Waters; Zinc

Zinc is a metal of increasing interest to oceanographers and environmentalists [1–10]. Its dissolved concentration in open ocean surface waters is ca. 0.1 nM [11,12], being a potential limiting element [13]. Its vertical profile in the water column resembles that of silicate, with increasing concentration in deep waters (ca. 9 nM). Elucidation of zinc's biogeochemical cycle in the marine environment and monitoring require rapid and sensitive routine methods.

Electrochemical techniques are useful for environmental monitoring because of their sensitivity, accuracy and low cost. In addition, recent advances in automation and computerization have decreased analysis times and improved data treatment [14–16]. Adsorptive cathodic stripping voltammetry is especially valuable as it also allows complexation and speciation studies [2,5,13]. The conventional cathodic stripping voltammetric method for zinc determination [6] uses tetramethylenedithiocarbamate [pyrrolidinedithiocarbamate (PDC)] for complexation and a scan speed of 10 mV s^{-1}. Improvements to this method could be achieved by better electrochemical instrumentation and chemical conditions. Recently developed microelectronics hardware makes possible the design of improved, versatile potentiostats. Characteristics such as a fast response can be achieved by using high-speed and low-noise

Correspondence to: C. Collado-Sánchez, Chemistry Department, Faculty of Marine Sciences, University of Las Palmas de Gran Canaria, P.O. Box 550, 35017 Las Palmas de Gran Canaria (Spain).

SSDI 0003-2670(93)E0445-D

electronics. Fast scans could remove the interference of oxygen and noise arising from turbulence without a decrease in sensitivity. This would be especially convenient for adsorptive stripping voltammetry as the electroactive material would not need long diffusion times as in anodic stripping voltammetry.

EXPERIMENTAL

The experiments were carried out with a laboratory-designed computer-controlled polarograph [17], a PAR Model 303A electrode, a Compaq Model 386 computer and a Colour-Pro HP plotter. The entire system was specially built to operate at high scan speeds. The surface area of the hanging mercury drop electrode (HMDE) was 2.92 mm^2. Potentials are given relative to an Ag/AgCl reference electrode.

Stock aqueous zinc solutions were prepared by dilution of BDH standard solutions for atomic absorption spectrometry. Distilled water used for dilution was obtained with a Milli-Q system (Millipore) with a resistivity of 18 $M\Omega\ cm^{-1}$. Chemicals were of Suprapur grade (Merck). Solutions were purged with pure nitrogen before polarographic measurements when needed.

RESULTS AND DISCUSSION

Two types of scan waves with increasing scan speed were tested to establish the behaviour of the zinc complex. Differential-pulse operation was not considered as the capacitance currents developed at the top of the pulse using a high scan speed cannot be successfully subtracted from the currents at the bottom. The capacitance current would be too different in the two situations. In addition, the scan time cannot be sufficiently shortened.

Square-wave modulation showed better possibilities at high scan speeds. The peak currents increase at moderate scan speeds but are irrelevant at very fast scan speeds. Figure 1 shows various traces obtained for sea water by the square-wave procedure where this tendency is explained. Figure 1a shows standard square-wave polarograms at various scan speeds for zinc–PDC complexes. The peak height increases until ca. 10 $V\ s^{-1}$, decreasing at higher speeds and being almost flat, without any analytical information, above 50 $V\ s^{-1}$. Figure 1b shows an atypical "square-wave" plot in which both current components (at the top and bottom of the pulse) are added instead of subtracted. The peak height now increases continuously over the whole range studied. This suggests that the subtraction of the components removes electrochemical information at high scan speeds. The free analysis of both current components (Fig. 1c and d) confirms this assessment. The peak current at the top of the pulse rises continuously. The component at the bottom shows an oxidation peak at low scan speeds that amplifies the subtracted signal, producing better sensitivity than the staircase component alone at the same scans speeds. However, this oxidation currents turn into a reduction peak at high scan speeds, which rises in a similar way to that of the top component. At very high scan speeds, the reduction currents at the bottom of the pulse are of the same order as those at the top. The subtraction of both components produces an almost flat line without analytical information.

Figure 1 suggest that square-wave modulation is a useful technique only at moderate scans speed. Above 10 $V\ s^{-1}$ staircase modulation should be used. Figure 2 shows the peak evolution at various scan speeds using a staircase modulation wave. The peak height increases continuously, giving rise to a reduction current of several μA. The peak height using high scan speeds is increased by several orders of magnitude compared with those obtained using low scan speed modulation. The limit of the useful analytical scan speed is set by the capacitance background. Figure 2 shows that even at scan speeds as high as 100 $V\ s^{-1}$ the faradaic component is not significantly smothered by the capacitance currents. Scan speeds of 10–25 $V\ s^{-1}$ offer the best compromise between peak height and peak width.

A slight shift of the peak potentials towards negative values and peak broadening is also observed (Fig. 3). The magnitude of the change is

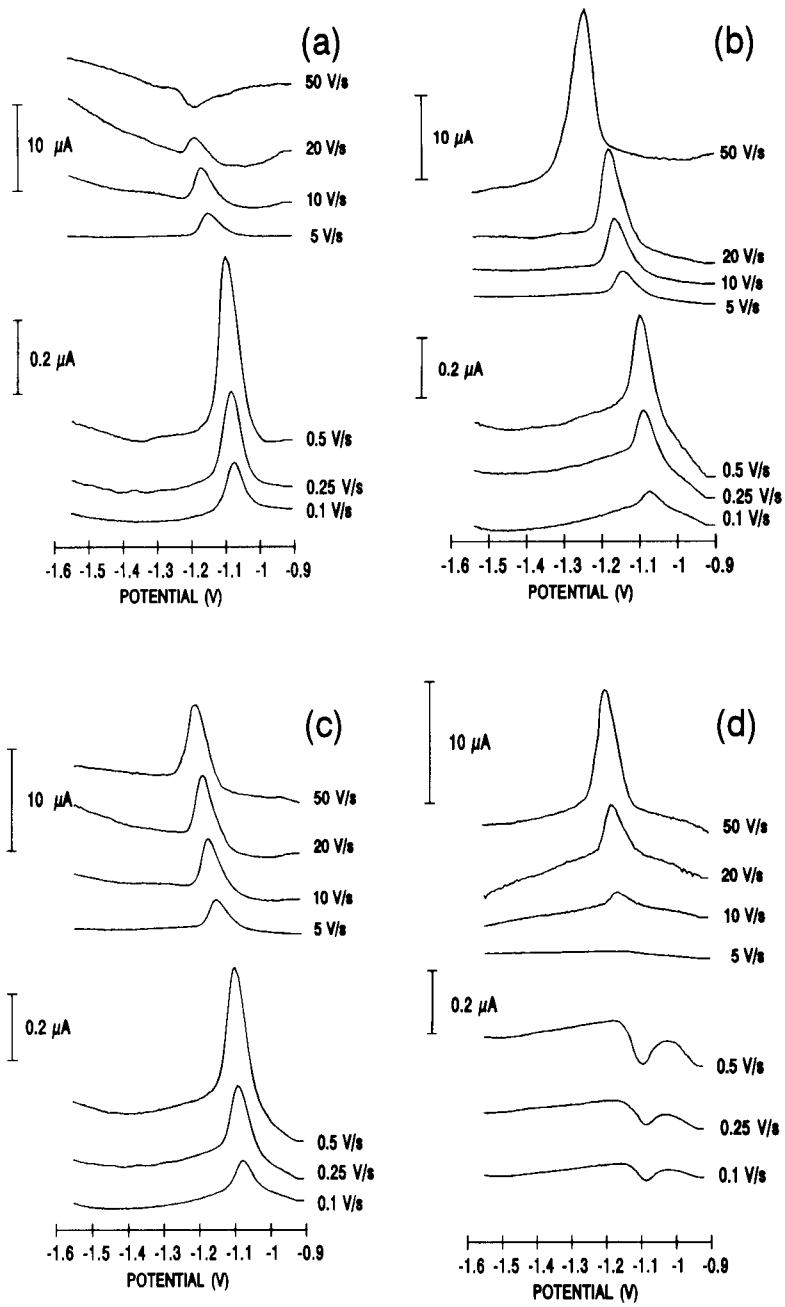

Fig. 1. Square-wave adsorptive cathodic stripping voltammetry of coastal sea water containing 31 nM Zn at various potential scan speeds. PDC concentration, 1×10^{-3} M BES [N,N′-bis(2-hydroxyethyl)(2-aminoethane)sulfonic acid], 0.01; scan increment, 5 mV; potential pulse, 50 mV; deposition time, 60 s at −1.3 V; stripping, 10 s at −0.9 V. (a) Standard difference between top and bottom components; (b) sum of both components; (c) top components; (d) bottom components.

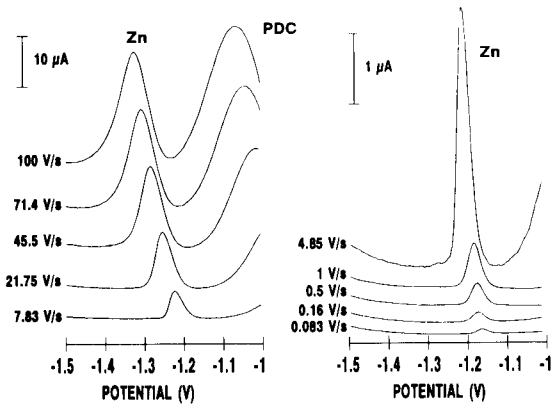

Fig. 2. Staircase wave adsorptive cathodic stripping voltammetry of coastal sea water containing 31 nM Zn at various potential scan speeds. Conditions otherwise as Fig. 1.

not linearly correlated with the scan speed. A preliminary explanation of this behaviour at high scan speeds could be found in the ohmic drop distortion of the potential felt by the HMDE. When a new potential is required between the reference and working electrodes, some time is needed to charge the HMDE capacitor (C_d) throught the uncompensated cell resistance (R_u). This time depends on several variables, such as cell design, electrode area and solution composition. When the step time of the potential scan is lower than the product R_uC_d, the real potential on the electrode is lower than that applied. The ohmic drop produces a lower scan rate than the programmed value, an increase in peak width and a shift of the peak potential towards negative direction, as observed. The voltammogram is obtained with applied potentials that are higher than the real values. With square-wave modulation, this ohmic drop also affects each potential pulse at high scan speeds. As these pulses are very high (50 mV), the real potential achieved is only a small fraction of that. The result is very close potentials at the top and bottom of the pulses and the zinc reduction waves are therefore similar. Their subtraction produces a signal without the zinc peak.

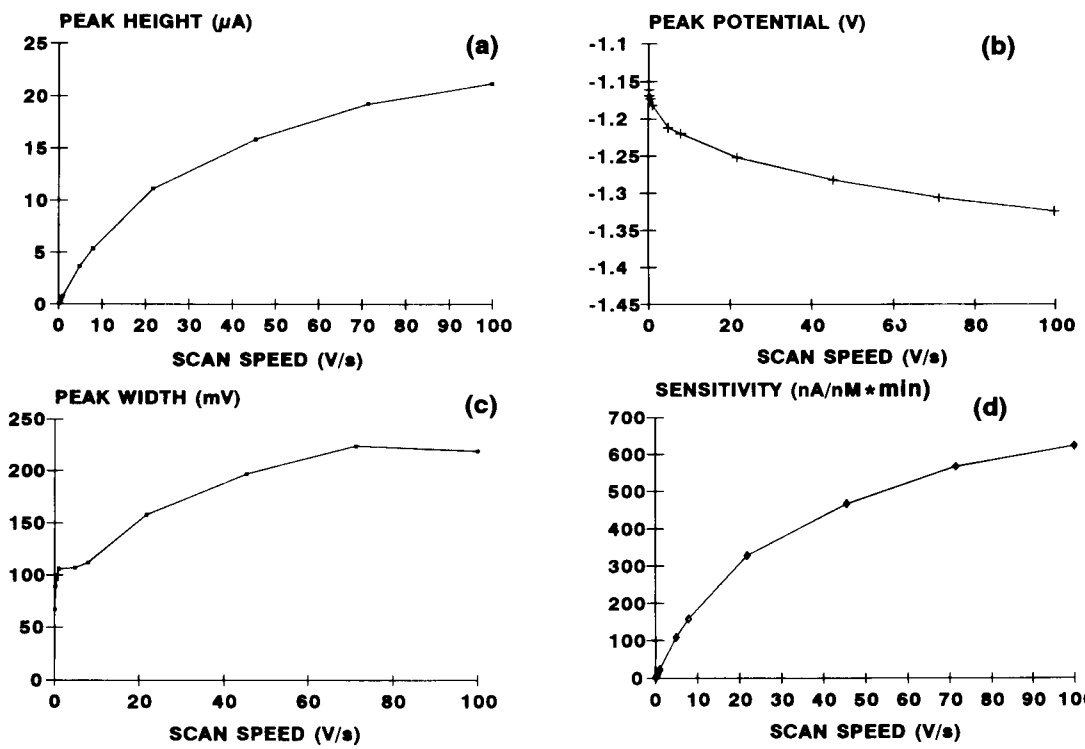

Fig. 3. Peak potential, peak width, peak height and sensitivity ratio versus potential scan speed for zinc from curves in Fig. 2.

The above experimental features do not perturb the analytical determination when using high scan speed staircase modulation (Fig. 2). No errors are introduced by the potential shift and peak width increase as these are constant at the same scan rate and cell conditions. Metal determination is done using an internal standard, which ensures reproducible conditions for peak quantification. At the same time, high scan speed staircase modulation produces high sensitivities and shorter analysis times. Further, determinations in the presence of oxygen or stirred solutions are feasible using this technique.

Oxygenated solutions

Purging is a time-consuming operation with the potential risk of contamination of the sample. It is especially inconvenient on-board an oceanographic research vessel, where gas facilities are not always available. Rapid cathodic stripping voltammetric determination of zinc was tested on oxygenated sea-water solutions and showed good results when discriminating the oxygen wave. This is irreversible and slower than metal reduction as a molecular rearrangement step is needed. However, the wave still appears even at very high scan speeds but the metal-to-oxygen reduction current ratio is now very high, both currents being in the same range. This improvement in the relationship between zinc and oxygen reduction currents makes it possible to determine zinc in the presence of oxygen directly on the baseline or by background subtraction. The blank could be obtained by a scan without any deposition time or by scanning the buffered solution with a deposition time but without PDC. Good results were obtained using both procedures.

Figure 4 shows results for the determination of zinc in the presence of oxygen at standard and high scan speeds. Figure 4a represents a slow scan speed (83 mV s^{-1}) with oxygen in the sample. The difficulty in obtaining the peak height is obvious as the oxygen reduction currents are masking the zinc peak. Figure 4b represents the same sample under the same conditions but after purging the solution, making the determination of the zinc possible. When the scan speed is raised to 8.3 V s^{-1} without purging (Fig. 4c), the

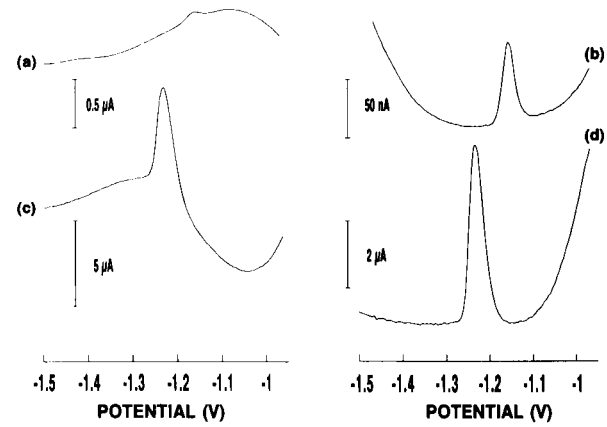

Fig. 4. Staircase wave adsorptive cathodic stripping voltammetry of coastal sea water containing 34 nM Zn. Conditions as in Fig. 1. (a) Unpurged solution using low scan speed (83 mV s^{-1}); (b) 10-min purged solution using low scan speed (83 mV s^{-1}); (c) unpurged solution using high scan speed (8.3 V s^{-1}); (d) curve after background subtraction.

zinc peak is now clear. It is very easy to evaluate the peak height directly using the background oxygen wave or eliminating it by a blank (Fig. 4d). This procedure is useless at conventional scan speeds as the differences between the oxygen and zinc currents are higher and the zinc currents are closer to the noise level.

Turbulent conditions

Usually the voltammetric determination of zinc is strongly affected by turbulence or vibration of the solution during the scan. This problem arises especially when determinations are carried out on-board an oceanographic vessel. Figure 5 shows the effect of stirring the solution at different scan speeds on the determination of the zinc. Figure 5a for a low scan speed is drastically perturbed by the motion of the solution. The noise introduced alters the curve completely and no peak is determinable. This can be achieved when a suitable quiescent time is used before and during the scan (Fig. 5b).

The scenario is considerably improved at high scan speeds, where peaks are unaffected by the stirring motion. Figure 5c–f obtained with the stirrer activated during the scan, show no significant noise perturbation. Scan speeds over 5 V s^{-1} in stirred solutions give analogous results to those

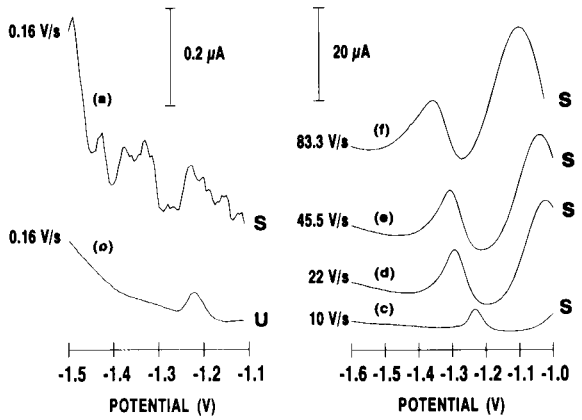

Fig. 5. Staircase wave adsorptive cathodic stripping voltammetry of coastal sea water containing 42 nM Zn. Conditions as in Fig. 1. Curves labelled S were obtained with stirring at 700 rpm during the scanning whereas those labelled U were obtained under quiescent conditions. (a, b) Low scan speed; (c–f) scan speeds as shown.

obtained by the standard procedure in quiescent conditions. A possible explanation for this insensitivity could be that the zinc reduction currents are increased by almost two orders of magnitude whereas the noise amplitude due to turbulence is not affected by the scan speed. In addition, the whole scan is now carried out within a few milliseconds and the high band noise does not affect the result.

Procedure for total zinc determination in oxygenated and stirred solutions

The features described in the presence of oxygen and turbulent conditions make the rapid adsorptive cathodic stripping voltammetric determination of zinc a very rapid and sensitive procedure for field analysis. A standard routine method is proposed for these conditions. A 10-ml aliquot of the acidified and UV-irradiated sample is pipetted into the voltammetric cell. The cell potential is set to -1.3 V and a new mercury drop is made. The deposition period involves stirring at -1.3 V for 1 min. The potential is then shifted to -0.9 V for 5 s before starting the scan in the negative direction. The scan is made using staircase modulation with a scan rate of 25 V s^{-1} and a pulse height of 5 mV. A zinc peak appears at ca. -1.27 V. A background correction is made by subtraction of the curve obtained without any deposition time at the first potential step (-1.3 V). The standard additions procedure is used to determine that peak height. Potentiostats with a very low time constant are required for this procedure.

The accuracy of the method was tested on NASS-4 open ocean sea-water reference material (National Research Council, Canada) in stirred and unpurged solutions. Figure 6a shows the curve obtained before background subtraction. The low concentration of zinc makes the direct detection of the peak on the oxygen wave difficult. After the background correction a clear peak appears (Fig. 6b) that is not perturbed by the state of the solution. The standard additions graph was linear over the range 0–60 nM ($r = 0.999$, $n = 4$). The concentration obtained (2.0 ± 0.1 nM) is in good agreement with the certified value (1.77 ± 0.27 nM), attesting to the accuracy of the measurement. The deposition time could also be increased if the concentration of the sample were too low or a larger peak were needed. The total analysis time for this sample was less than 6 min.

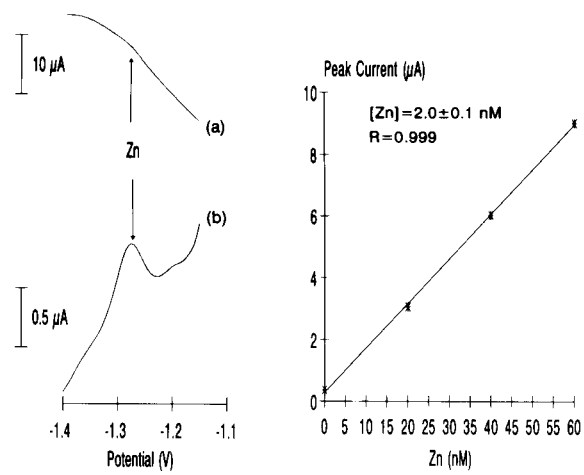

Fig. 6. Staircase wave adsorptive cathodic stripping voltammetry of NASS-4 open ocean sea water reference materials. PDC concentration, 1×10^{-3} M; BES, 0.01; scan rate, 25 V s^{-1}; deposition time, 60 s at -1.3 V; stripping, 5 s at -0.9 V. The solution was unpurged and stirred during accumulation and scanning. (a) Voltammogram of unpurged and stirred solution (during deposition and scanning); (b) scan after background subtraction.

Conclusions

It has been shown that a high scan speed combined with computerized instrumentation can achieve improvements over the traditional method of zinc determination by stripping voltammetry. The sensitivity is increased because the electroactive adsorbed material is reduced in a shorter time, producing higher faradaic currents. A compromise between the increase in faradaic and capacitance currents sets the best scan speed range (10–25 V s^{-1}). The determination of zinc in the presence of oxygen is successfully carried out by background subtraction. This is possible with a high scan speed because the oxygen and metal complex waves are now of the same order. The noise from turbulence is also avoided because fast scanning is insensitive to vibrations. The method described is especially convenient for on-board oceanographic cruises where the advantages outlined are particularly relevant. The total measuring time is also notably decreased.

REFERENCES

1 P.M. Saager, H.J.W. Debaar and R.J. Howland, Deep-Sea Res. A Oceanogr. Res., 39 (1992) 9.
2 C.M.G. van den Berg, P.J.M. Buckley, Z.Q. Huang and M. Nimmo, Estuarine Coastal Shelf Res., 22 (1986) 479.
3 A.M. Shiller and E. Boyle, Nature, 317 (1985) 49.
4 C.M.G. van den Berg and S. Dharmvanij, Limnol. Oceanogr., 29 (1984) 1025.
5 C.M.G. van den Berg, Mar. Chem., 16 (1985) 121.
6 C.M.G. van den Berg, Talanta, 31 (1984) 1069.
7 K. Kremling, Mar. Chem., 13 (1983) 87.
8 R.M. Moore, Geochim. Cosmochim. Acta, 45 (1981) 2475.
9 B. Svensmark and J. Larsen, Talanta, 35 (1988) 953.
10 C.A. Johnson, Geochim. Cosmochim. Acta, 50 (1986) 2433.
11 K.W. Bruland, Sci. Lett., 47 (1980) 176.
12 K.W. Bruland in J.P. Riley and R. Chester (Eds.), Chemical Oceanography, Vol. 8, Academic Press, London, 1983, p. 157.
13 J.R. Donat and K.W. Bruland, Mar. Chem., 28 (1990) 301.
14 L. Renman, D. Jagner and R. Berglund, Anal. Chim. Acta, 188 (1986) 137.
15 A.M. Bond, H.B. Greenhill, I.D. Heritage and J.B. Reust, Anal. Chim. Acta, 165 (1984) 209.
16 M.P. Newton and C.M.G. van den Berg, Anal. Chim. Acta, 199 (1987) 59.
17 J.J. Hernández-Brito, P. Cardona-Castellano, J. Perez-Peña and M.D. Gelado-Caballero, Electroanalysis, 2 (1990) 401.

Analytica Chimica Acta, 284 (1993) 413–418
Elsevier Science Publishers B.V., Amsterdam

Polarographic behaviour and determination of 1-(4′-bromophenyl)-3,3-dimethyltriazene

Ljubiša M. Ignjatović

Faculty of Physical Chemistry, University of Belgrade, P.O. Box 137, 11001 Belgrade (Yugoslavia)

Jiří Barek and Jiří Zima

Department of Analytical Chemistry, Charles University, 128 40 Prague 2 (Czech Republic)

Dragan A. Marković

Faculty of Physical Chemistry, University of Belgrade, P.O. Box 137, 11001 Belgrade (Yugoslavia)

(Received 30th June 1993)

Abstract

A study was made of the polarographic behaviour of the genotoxic substance 1-(4′-bromophenyl)-3,3-dimethyltriazene and optimum conditions were found for its determination by tast polarography and differential-pulse polarography at a static mercury drop electrode in the concentration range 1×10^{-4}–1×10^{-7} mol dm^{-3}. The results indicate that the method can be used at pH between 4.5 and 6.0 for the identification and determination of the investigated substance, which is protonated without decomposition in this pH range. It was established that for the reduction of the N=N group four electrons are required and the resulting products are 4-bromoaniline and dimethylhydrazine.

Keywords: Polarography; Bromophenyldimethyltriazene; Triazenes

The derivatives of 1-phenyl-3,3-dimethyltriazene are genotoxic substances, presumably acting via an alkylation mechanism [1]. At the same time, this type of substance exhibits carcinostatic properties [2]. In this connection, detailed studies have been carried out on its acute toxicity [3], metabolism [4] and protolytic splitting mechanism [5]. These substances can be determined by direct ultraviolet spectrophotometry [6] or visible spectrophotometry after the protolysis of triazene and subsequent coupling of the diazonium compound formed with *N*-ethyl-1-naphthylamine [7].

Although triazenes can be readily reduced electrochemically, little attention has so far been devoted to their polarographic determination. Direct current polarography has been used to study 1-phenyl-3,3-dimethyltriazene [8] and some its 2′-, 3′- and 4′-derivatives [7]. The use of this technique is limited to concentrations above 1×10^{-4} mol dm^{-3}. More sensitive techniques, such as differential-pulse polarography [9] and adsorptive stripping voltammetry [10,11] have been used for the determination of some triazene derivatives with limits of determination of about 1×10^{-7} and 2×10^{-11} mol dm^{-3}, respectively.

Correspondence to: Lj.M. Ignjatović, Faculty of Physical Chemistry, University of Belgrade, P.O. Box 137, 11001 Belgrade (Yugoslavia).

SSDI 0003-2670(93)E0485-P

In this work, an attempt was made to improve the sensitivity of determination of 1-(4′-bromophenyl)-3,3-dimethyltriazene by tast and differential-pulse polarography (DPP) at a static mercury drop electrode (SMDE). The mechanism of the polarographic reduction of the tested substance was also investigated.

EXPERIMENTAL

Chemicals

A stock standard solution of 1-(4′-bromophenyl)-3,3-dimethyltriazene in methanol (1×10^{-3} mol dm^{-3}) was prepared by dissolving a precisely weighed amount of the substance in freshly redistilled solvent. The tested substance was synthetized in the Research Institute for Organic Synthesis, Pardubice-Rybitvi, Czech Republic. A more dilute solution (1×10^{-4} mol dm^{-3}) was prepared by precise dilution of the stock standard solution, and both were stored in the dark. Britton–Robinson buffers were prepared in the usual way, i.e., by mixing a solution containing 0.04 mol dm^{-3} orthophosphoric acid, 0.04 mol dm^{-3} acetic acid and 0.04 mol dm^{-3} boric acid with the appropriate volume of 0.2 mol dm^{-3} sodium hydroxide solution. All chemicals used were of analytical-reagent grade (Merck). Water was doubly distilled in a quartz apparatus.

Apparatus

Polarographic measurements were carried out on a PA 4 polarographic analyser with an SMDE 1 static mercury drop electrode (both from Laboratorní Přístroje, Prague). The capillary employed had a diameter of 0.136 mm and the maximum drop size was used, obtained by opening the electromagnetic valve for 160 ms. A saturated calomel electrode (SCE) was used, to which all the potential values are related, along with a platinum auxiliary electrode. The measurements were performed at a polarization rate of 5 mV s^{-1} and an SMDE drop time of 1 s. A modulation amplitude of -100 mV was employed in DPP.

Constant-potential coulometric (CPC) measurements were performed using a PAR 173 potentiostat with a PAR 179 digital coulometer. The mercury pool was used as the cathode, with a saturated calomel reference electrode and platinum gauze counter electrode. The cathodic and anodic compartments were separated by sintered glass.

Spectrophotometric measurements were carried out on a Varian Cary 17D UV–visible spectrophotometer in 1-cm quartz cuvettes.

Procedure

Mixed Britton–Robinson buffer–methanol medium was used as the supporting electrolyte in order to ensure the solubility of the investigated substance. The actual pH of the Britton–Robinson buffer–methanol mixture (1 + 1) was measured with a combined pH electrode calibrated using acetate, borate and phosphate buffers in 50% methanol [12].

A 20-ml aliquot of an appropriate supporting electrolyte solutions was placed in a polarographic cell and the required amounts of the stock solution of the tested substance were added. Dissolved oxygen was removed from the polarographed solutions by bubbling with nitrogen, which was purified by passing it through a solution of chromium(II) ions in dilute hydrochloric acid over zinc amalgam. Prior to entering the polarographic cell, nitrogen was passed through a pre-bubbler containing a methanol–water mixture in the same ratio as in the tested solution.

Calibration graphs were measured in triplicate and evaluated by the least-squares linear regression method. The determination limit was calculated as ten times the standard deviation for ten determinations of the analyte at a concentration corresponding to the lowest value on the appropriate calibration straight line [13].

In the coulometric determination of the number of electrons exchanged, 20 ml of the supporting electrolyte were placed in the coulometric cell and bubbled with nitrogen, with simultaneous initiation of pre-electrolysis at a selected constant potential. After about 20 min, when the residual current value had decreased below 0.1 mA and no longer changed, the circuit parameters were adjusted for automatic residual current compensation. An aliquot of the stock solution of the

tested substance was then added and reduction was carried out at a constant potential with constant stirring and bubbling with nitrogen. The electrolysis was terminated when the current had decreased to the residual value and the charge passed was determined by electronic integration. The reduction was also followed spectrophotometrically and polarographically by removing an aliquot of the solution from the coulometric cell at preselected intervals and measuring its tast polarographic curve and UV spectrum. The samples were taken prior to commencing the coulometric reduction and after reduction of 20, 40, 60, 80 and 100% of the studied triazene.

All measurements were carried out at laboratory temperature (20 ± 1°C).

RESULTS AND DISCUSSION

Effect of pH on the polarographic behaviour of 1-(4'-bromophenyl)-3,3-dimethyltriazene

It can be seen from Fig. 1 that tast polarography of the tested substance yields a single wave. The half-wave potential of this wave shifts to more negative values with increasing pH and this dependence has an asymptotic character. At pH > 5.5 the polarographic wave decreases and at pH > 11 it completely disappears. In solution at pH < 5 the wave decreases slightly with time. The

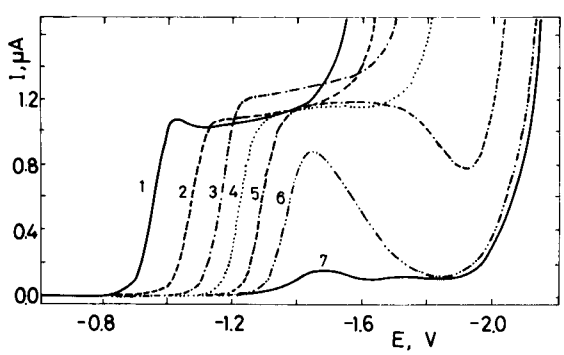

Fig. 1. Tast polarograms of 1-(4'-bromophenyl)-3,3-dimethyltriazene (1×10^{-4} mol dm^{-3}) in mixed Britton–Robinson buffer–methanol (1 + 1) medium at pH values of (1) 2.95, (2) 4.10, (3) 5.10, (4) 5.90, (5) 7.10, (6) 8.80 and (7) 10.25.

observed decrease, which is connected with the protolytic splitting of the tested substance [5], is virtually absent at pH > 5.

Assuming that protolytic decomposition in a buffered medium is a first-order reaction, the following equation can be used:

$$\ln I_l = \ln I_0 - kt$$

where I_0 is the wave height at the beginning of the reaction of protolysis, I_l the wave height at time t and k the first-order rate constant.

The linear dependence of ln I_l on time, which has been established, indicates that the reaction is pseudo-monomolecular in its behaviour. The rate constant, calculated as the negative value of the slope of the mentioned straight line, is equal to $(1.82 \pm 0.05)\times10^{-2}$ min^{-1} at pH 2.90 and $(3.4 \pm 0.5)\times10^{-3}$ min^{-1} at pH 4.10.

The atypical tast polarograms obtained in the pH region 7–9 are connected with the presence of methanol and its effect on the preliminary protonation reaction. The fact that the slope of the $E_{1/2}$ vs. pH dependence does not correspond to the relationship $dE_{1/2}/dpH = -mRT/\alpha n_a F$ indicates [14] that a substance adsorbed on the electrode surface undergoes the preliminary protonation reaction. As the methanol content increases, the rate of this preliminary reaction decreases both because of the decreased protonation rate constant and also because of the decreased adsorption of the tested triazene. The observed decrease in the limiting current in the region around −1.8 V at pH > 7 is probably connected with a decrease in the rate of surface protonation as a consequence of desorption of the substance at a much more negative potential than that of the electrocapillary maximum, where maximum adsorption of uncharged molecules of the investigated substance can be expected.

Figure 2 shows the effect of pH on the DP polarograms at the SMDE. It can be seen that the pH of the medium has the same type of effect on the height and peak position as in tast polarography.

It follows from logarithmic analysis of the tast polarograms that the electrode process is irreversible in the pH range 3–8. This was also confirmed by cyclic voltammetry [15] at a hanging

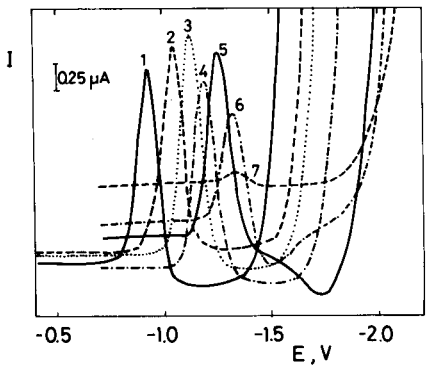

Fig. 2. DP polarograms of 1-(4′-bromophenyl)-3,3-dimethyltriazene (1×10^{-4} mol dm^{-3}) in mixed Britton–Robinson buffer–methanol (1 + 1) medium at pH values of (1) 2.95, (2) 4.10, (3) 5.10, (4) 5.90, (5) 7.10, (6) 8.80 and (7) 10.25.

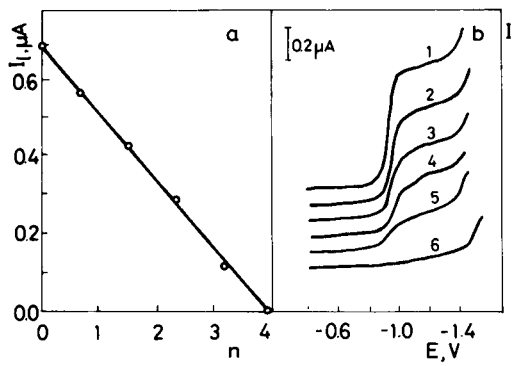

Fig. 3. Tast polarographic study of the reduction of 1-(4′-bromophenyl)-3,3-dimethyltriazene (1×10^{-4} mol dm^{-3}) by constant-potential coulometry at −1.400 V in Britton–Robinson buffer–methanol (1 + 1) medium at pH 5.10. (a) Dependence of the limiting current of the tested substance on the charge passed recalculated to the number of electrons, n, per molecule of reduced substance. (b) Tast polarograms of the electrolysed solution after passage of charge corresponding to n = (1) 0, (2) 0.8, (3) 1.6, (4) 2.4, (5) 3.2 and (6) 4.0.

mercury drop electrode: no anodic peak was observed in the pH range 2–10 at polarization rates from 5 to 200 mV s^{-1}. At pH 5.10 the peak position, E_p, shifts to more negative values with increasing rate of polarization, confirming the irreversible character of the electrode process. At the same pH value, a linear dependence between the wave height and square root of the mercury reservoir height in d.c. polarography, and between the peak potential and square root of the polarization rate in cyclic voltammetry, has been established. These dependences indicate that the electrode process is diffusion controlled.

It was found by coulometry at a constant potential of −1.400 V, corresponding to the limiting current of the studied substance at pH 5.10, that a total of four electrons are exchanged. It can be seen from the tast polarographic study of the electrolyzed solution (Fig. 3b) that the polarographically active group disappears, indicating that the product formed is not polarographically active in the studied potential range. It follows from the spectrophotometric study of the electrolysed solution (Fig. 4b) that it involves reduction of the chromophore, i.e., the triazene group. The dependence of the absorbance at 315 nm (Fig. 4a) on the charge transferred recalculated to the number of electrons exchanged per molecule (n) intersects the abscissa at the value of 4.0 electrons. An analogous result followed from the study of the reduction by tast polarography (Fig. 3a).

It is known [8] that unsubstituted 1-phenyl-3,3-dimethyltriazene undergoes a four-electron reduction giving aniline as the product. In order to identify the reduction product of the investi-

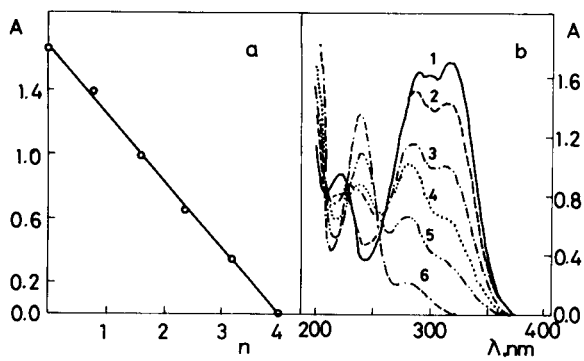

Fig. 4. Spectrophotometric study of the reduction of 1-(4′-bromophenyl)-3,3-dimethyltriazene by constant-potential coulometry at −1.400 V in Britton–Robinson buffer–methanol (1 + 1) medium at pH 5.10. (a) Dependence of the absorbance at 315 nm on the charge passed recalculated to the number of electrons, n, per molecule of reduced substance. (b) UV spectra of the electrolysed solution after passage of charge corresponding to n = (1) 0, (2) 0.8, (3) 1.6, (4) 2.4, (5) 3.2 and (6) 4.0.

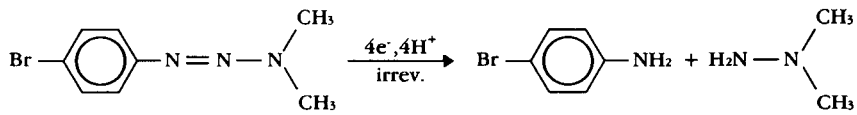

Fig. 5. Electrode reduction of 1-(4′-bromophenyl)-3,3-dimethyltriazene.

gated bromo derivative, the polarographic behaviour of 4-bromoaniline was studied. It follows from the polarographic measurements that 4-bromoaniline has no polarographic wave in the mixed Britton–Robinson buffer–methanol (1 + 1) medium at pH 5.10. At the same time, the UV spectrum of the 1-(4′-bromophenyl)-3,3-dimethyltriazene coulometric reduction product is the same as that of 4-bromoaniline.

It can be assumed on the basis of the above observations and on the basis of analogy with the polarographic behaviour of unsubstituted 1-phenyl-3,3-dimethyltriazene [8] that the tested substance is reduced according to the scheme shown in Fig. 5.

It can be assumed that the first reduction step yields the anion radical, which is immediately stabilized in acidic medium by accepting a readily available proton, resulting in the dependence of the half-wave potential on pH. In contrast, in alkaline medium, this anion radical is stabilized by a proton removed from a water molecule, because of a low concentration of free hydronium ions, so that the half-wave potential of the tested substance is independent of pH in this region.

Polarographic determination of 1-(4′-bromophenyl)-3,3-dimethyltriazene

For analytical purposes, the optimum supporting electrolyte was established to be Britton–Robinson buffer–methanol mixture at pH 5.10, in which the tested substance is sufficiently stable and the polarographic waves or peaks are well developed and readily evaluated. Using a mixture containing 50% (v/v) methanol, linear calibration plots were obtained for the tast polarographic and DPP determinations at the SMDE in the concentration range 1×10^{-6}–1×10^{-4} mol dm^{-3}. The DPP peak height was evaluated relative to the line connecting the minima on both sides.

It is preferable to carry out DPP and tast polarographic determinations in a mixture of five-fold-diluted Britton–Robinson buffer–methanol (9 + 1) at pH 5.10. As the concentration of the aqueous Britton–Robinson buffer decreases, the

TABLE 1

Parameters of the calibration graphs with slope A and intercept B and limits of determination (LOD) for 1-(4′-bromophenyl)-3,3-dimethyltriazene

Polarographic method	Concentration (mol dm^{-3})	$A/S(A)$ (mA dm^3 mol^{-1})	$B/S(B)$ (nA)	$S_{I,C}$ (nA)	r	LOD (mol dm^{-3})
Tast [a]	$(1–10) \times 10^{-5}$	10.6/0.1	13/3	3.4	0.9999	
Tast [a]	$(1–10) \times 10^{-6}$	11.2/05	2/1	3.3	0.9967	1×10^{-6}
Tast [b]	$(1–10) \times 10^{-6}$	13.9/0.2	5/1	1.6	0.9995	
Tast [b]	$(1–10) \times 10^{-7}$	23.3/0.9	1.8/0.6	0.6	0.9975	1×10^{-7}
DPP [a]	$(1–10) \times 10^{-5}$	18.5/0.2	−42/10	14.7	0.9998	
DPP [a]	$(1–10) \times 10^{-6}$	18.3/0.1	1.6/0.7	0.7	0.9999	2×10^{-7}
DPP [b]	$(1–10) \times 10^{-6}$	32.0/0.2	−5/1	1.3	0.9999	
DPP [b]	$(1–10) \times 10^{-7}$	33.3/0.2	−1.2/0.2	0.2	0.9999	5×10^{-8}

[a] Britton–Robinson buffer–methanol (1 + 1) medium, pH 5.10. [b] Fivefold diluted Britton–Robinson buffer–methanol (9 + 1) medium, pH 5.10.

residual current corresponding to impurities in the chemicals used for its preparation also decreases, leading to a smoother supporting electrolyte curve. A decrease in the methanol content in the polarographed solution leads to a shift in the half-wave and peak potential to more positive values (the difference in the E_p value in 50% methanol and 10% methanol at constant pH 5.10 is 70 mV) and increases the reversibility of the electrode process, reflected in an increase in the peak and wave height and thus also in the sensitivity of the determination. The use of the cited medium as the supporting electrolyte permits tast polarographic and DPP determinations of the tested substance in the concentration range 1×10^{-7}–10×10^{-7} mol dm^{-3}.

The parameters of the calibration straight lines: the slope A and its standard deviation $S(A)$, the intercept B and its standard deviation $S(B)$, the deviation of the experimental points from the calculated straight line, $S_{I,C}$, and the correlation coefficient, r, with the calculated limits of determination, LOD, for the above-described polarographic measurements are given in Table 1.

REFERENCES

1 J.H. Burchenal and S.K. Carter, Cancer (Philadelphia), 30 (1972) 1636.
2 F.A. Schmidt and D.J. Hutchinson, Cancer Res., 34 (1974) 1917.
3 V. Rambousek, V. Zvěřina and M. Matrka, Cesk. Farm., 27 (1978) 384.
4 V. Rambousek, V. Zvěřina and M. Matrka, Cesk. Farm., 27 (1978) 438.
5 M. Matrka, V. Rambousek and V. Zvěřina, Cesk. Farm., 27 (1978) 346.
6 R.J. Le Fevre and T.H. Liddicoet, J. Chem. Soc., (1951) 2743.
7 M. Matrka, V. Rambousek, L. Držkova and V. Zvěřina, Cesk. Farm., 27 (1978) 299.
8 G. Kazemifard, F. Moattar and J. Reisch, Acta Pharm. Yugosl., 28 (1978) 151.
9 V. Mejstřik, Z. Ságner, L. Držková and F. Krampera, Cesk. Farm., 34 (1985) 51.
10 J. Barek, S. Toubar and J. Zima, Collect. Czech. Chem. Commun., 56 (1991) 2073.
11 J. Barek and A.G. Fogg, Analyst, 117 (1992) 751.
12 M. Paabo, R.A. Robinson and R.G. Bates, J. Am. Chem. Soc., 87 (1965) 415.
13 K. Beyermann, Organic Trace Analysis, Ellis Horwood, Chichester, 1984, p. 45.
14 S.G. Mairanovskii, Talanta, 12 (1965) 1299.
15 R. Greef, R. Pat, L.M. Peter, D. Pletcher and J. Robinson, Instrumental Methods in Electrochemistry, Ellis Horwood, Chichester, 1985, p. 178.

Analytica Chimica Acta, 284 (1993) 419–433
Elsevier Science Publishers B.V., Amsterdam

Determination of the fat, protein and lactose content of milk using Fourier transform infrared spectrometry

H.J. Luinge, E. Hop and E.T.G. Lutz

Analytical Molecular Spectrometry, Utrecht University, P.O. Box 80083, 3508 TB Utrecht (Netherlands)

J.A. van Hemert

Milk Control Station "West-Nederland", Gouda (Netherlands)

E.A.M. de Jong

Netherlands Institute for Dairy Research (NIZO), Ede (Netherlands)

(Received 27th May 1993)

Abstract

In this paper the quantitative in-line determination of the composition of milk using Fourier transform infrared spectrometry is described. The fat, protein and lactose content are predicted of which the former two are compared with Röse-Gottlieb and Kjeldahl reference values respectively. Fat, protein and lactose are also determined using a MultiSpec infrared filter instrument. Calibration techniques such as classical and inverse least squares regression, principal component regression and partial least squares regression are applied and the results are compared. All methods appear to perform comparably with respect to prediction error and are equivalent to the conventional filter based method.

Keywords: Infrared spectrometry; Fats; Lactose; Proteins; Milk; Fourier transform

Milk is mainly composed of water (85.5–88.7%, w/w), fat (2.4–5.5%, w/w), protein (2.3–4.4%, w/w), lactose (3.8–5.3%, w/w), mineral substances (0.53–0.80%, w/w) and organic acids (0.13–0.22%, w/w) [1]. In the Netherlands milk is paid for according to fat and protein content. Furthermore, processing of milk into dairy products requires information on the components present. Thirdly, knowledge of the composition of milk is important from a viewpoint of quality control.

Goulden [2] outlined the basic principles of the application of infrared (IR) spectrometry for the analysis of milk. Currently, milk is analysed routinely with respect to fat, protein and lactose content using dedicated infrared filter instruments. Interlaboratory studies and evaluations of various instruments have been reported [3–6].

An infrared spectrum of milk ratioed against water as background is depicted in Fig. 1. Usually, the fat content is determined from absorbances at approximately 2854 cm^{-1} (CH_2 symmetric stretching) and 1746 cm^{-1} (C=O stretching). Protein is measured at 1548 cm^{-1} (amide II), and lactose at 1041 cm^{-1} (C–O stretching). Furthermore, spectral regions close to the absorbing regions are used in order to correct for background absorption and scattering. The bandwidth of the filters used is approximately 30 cm^{-1}. The concentration of the components is calcu-

Correspondence to: H.J. Luinge, Analytical Molecular Spectrometry, Utrecht University, P.O. Box 80083, 3508 TB Utrecht (Netherlands).

SSDI 0003-2670(93)E0457-I

lated from the absorbances using multiple linear regression models. Usually, initial predicted values are further corrected by using so-called intercorrection factors. The parameters in the models and the intercorrection factors are set by calibrating absorbances with potentiometers to conform with reference methods [7].

The infrared filter method has the advantage of being fast, accurate and robust, which makes it well suited for large-scale monitoring of fat, protein and lactose in raw farm tank milk. There are, however, several drawbacks. Filter instruments do not allow the analysis of other components (e.g., urea, citrate, phosphate). Furthermore, outlier detection can be difficult due to the fact that only small spectral regions are measured. This also prevents the application of advanced regression techniques such as partial least squares or principal component regression. The advantages of such methods to milk analysis have been demonstrated in the field of near-infrared spectrometry [8,9].

In order to alleviate the drawbacks mentioned the possibility of applying Fourier Transform mid-infrared spectrometry to the analysis of milk has been investigated. Initially, spectral windows corresponding with the filter regions in filter instruments were selected from the spectra. With the resulting data inverse least-squares (ILS) regression models for fat, protein and lactose were constructed and validated. Subsequently, full spectrum methods such as classical least-squares (CLS), principal component (PCR) and partial least squares (PLS) regression were applied and results were compared.

Preliminary investigations [10–12] have already shown that results comparable with those obtained from filter instruments are feasible. Van

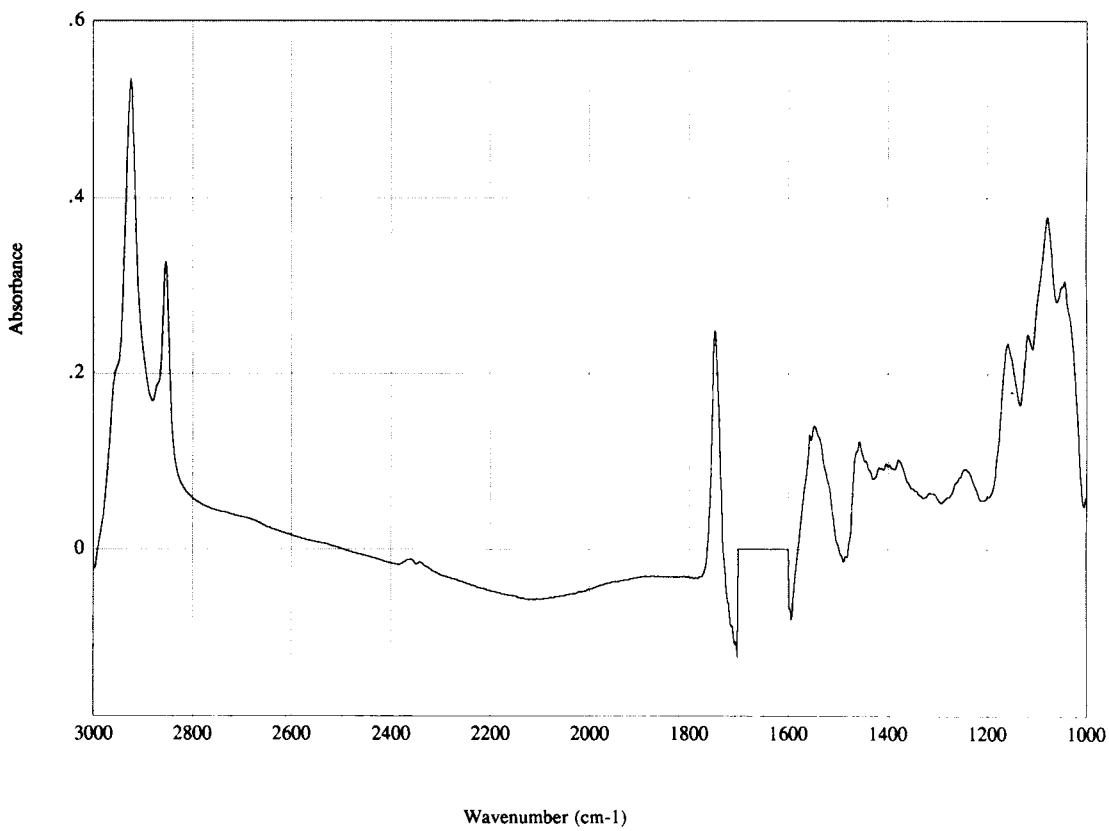

Fig. 1. Infrared spectrum of milk ratioed against water as background.

TABLE 1

Statistics for total, calibration and validation set expressed in %, w/w

	Total set (n = 55)		Calibration set (n = 20)		Validation set (n = 35)	
	Average	Standard deviation	Average	Standard deviation	Average	Standard deviation
Fat	4.63	0.28	4.64	0.35	4.63	0.23
Protein	3.46	0.15	3.49	0.20	3.45	0.12
Lactose	4.48	0.10	4.46	0.12	4.48	0.09

de Voort et al. [11] based their conclusions on a rather small set of artificial samples from commercial calibration powders. Lanher [12] presents a more elaborate investigation covering the analysis of various dairy products. With respect to the analysis of major components in milk, he applies ILS, PCR and PLS for the prediction of fat and protein.

In this paper a systematic investigation on the determination of fat, protein and lactose using several multivariate regression techniques is presented. Use is made of a representative set of farm tank milk samples measured in-line with an FT-IR and a filter instrument. In a subsequent paper the effects of seasonal variations in the composition of milk on the calibration models will be addressed.

THEORY

CLS regression is based on the assumption that the overall absorption of a sample can be regarded as a linear summation of absorptions of the components in the sample. In formula:

$$A_j = k_{0j} + \sum_{i=1}^{l} c_i k_{ij}$$

where c_i stands for the concentration of component i, A_j for the absorbance at wavenumber j, and k_{ij} for the product of the optical pathlength and the absorption coefficient corresponding with component i and wavenumber j. The number of components present is given by l. Background absorptions can be accounted for by including an intercept k_{0j}. For m samples the equation can be rewritten in matrix notation as:

$$\mathbf{A} = \mathbf{CK}$$

Here $\mathbf{A}$ is an $m \times n$ absorption matrix with m spectra (rows) consisting of n wavenumbers. $\mathbf{C}$ is an $m \times l$ concentration matrix and $\mathbf{K}$ an $l \times n$ matrix. During calibration samples with known contents are used to calculate matrix $\mathbf{K}$ according to:

$$\mathbf{K} = (\mathbf{C}^{\mathrm{T}}\mathbf{C})^{-1}\mathbf{C}^{\mathrm{T}}\mathbf{A}.$$

TABLE 2

Validation results of all models compared with reference methods.

	Filter-IR		CLS		ILS		PCR		PLS	
	MD [a]	SDD [b]	MD	SDD	MD	SDD	MD	SDD	MD	SDD
Fat	−0.003	0.031	0.001	0.025	0.013	0.029	0.002	0.025	0.004	0.024
Protein	−0.012	0.037	−0.008	0.041	0.003	0.039	0.001	0.036	0.001	0.035
Lactose [c]	–	–	−0.017	0.032	−0.005	0.025	−0.006	0.027	−0.005	0.029

[a] MD = Mean difference with the reference data (in %, w/w). [b] SDD = Standard deviation of the differences with the reference method (in %, w/w). [c] Values for lactose are calculated using filter-IR data as reference.

$\mathbf{C}^T$ is the transposed matrix of **C** (i.e., rows and columns interchanged). Matrix **K** gives a least-squares approximation of the spectra of the pure components.

In the prediction stage **C** is calculated from **A** and **K**:

$$\mathbf{C} = \mathbf{A}\mathbf{K}^T(\mathbf{K}\mathbf{K}^T)^{-1}$$

The calculations require two matrix inversions of matrices with dimensions equal to the number of components ($l \times l$). In case two or more components are highly correlated, problems may arise as the determinant of the matrices equals zero (collinearity). For CLS it is obligatory that the concentrations of all components contributing to the overall spectrum are known. Furthermore, the number of wavelengths and samples both have to be equal to or exceed the number of components. Hence, the method can be used as a full-spectrum method.

When applying ILS regression, also known as multiple linear regression (MLR), use is made of the fact that Beer's law can be rewritten into the following equation:

$$c_i = p_{i0} + \sum_{j=1}^{n} A_j p_{ij}$$

where p_{ij} stands for a proportionality constant corresponding with component i and wavenumber j and p_{i0} represents an intercept. When samples with different composition are available one can write in matrix notation:

$$\mathbf{C} = \mathbf{A}\mathbf{P}$$

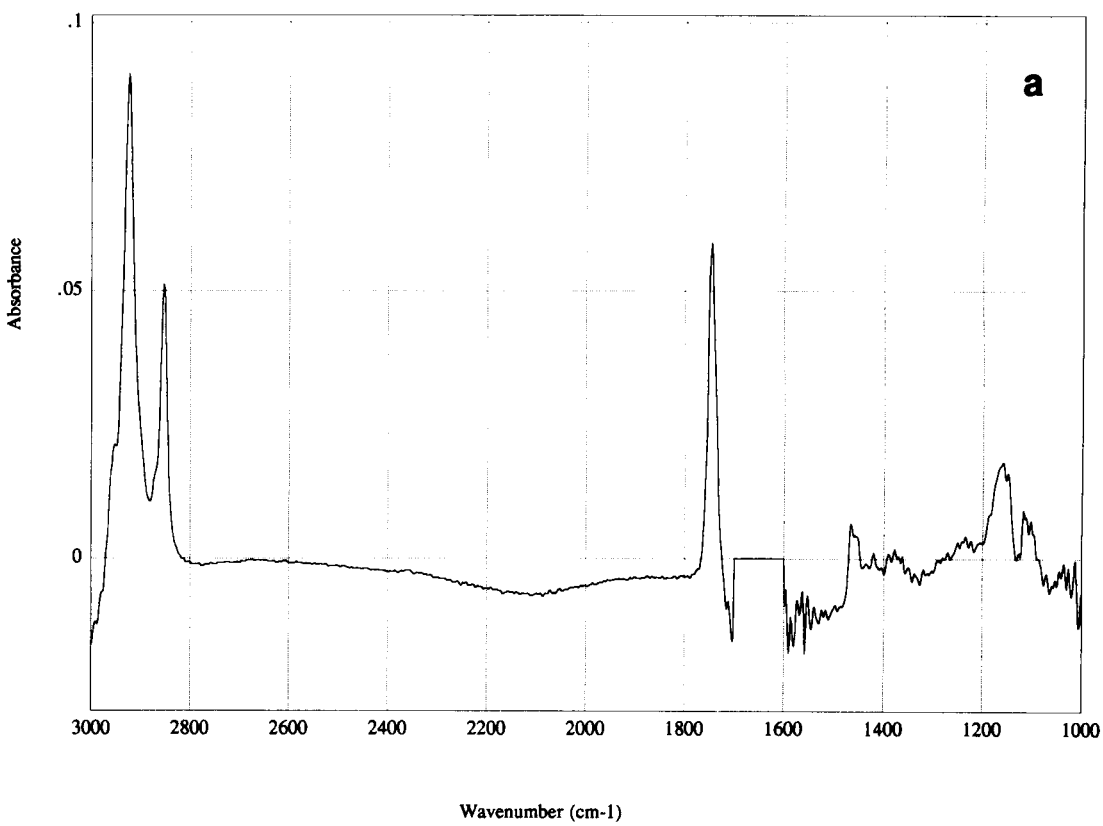

Fig. 2. Infrared spectra of (a) fat, (b) protein and (c) lactose obtained from CLS regression.

Again, **C** is an $m \times l$ concentration matrix, **A** an $m \times n$ absorption matrix, and **P** an $n \times l$ matrix. During calibration **P** is solved as:

$$\mathbf{P} = (\mathbf{A}^T\mathbf{A})^{-1}\mathbf{A}^T\mathbf{C}$$

For prediction of unknown contents the original calibration equation can be used. Hence, only one matrix inversion is required for ILS. In order to be able to calculate the inverse, the number of wavelengths should be equal to or less than the number of samples. In contrast to CLS, application of ILS to full spectra is hampered by the large number of samples required.

A reduction of the number of variables (i.e., wavelengths) can be obtained by principal component analysis, where new variables are constructed as linear combinations of the original ones. PCR and PLS both apply this principle. The data matrix **A** is decomposed into two matrices **T** and **B** as:

$$\mathbf{A} = \mathbf{TB}$$

where **B** is an $h \times n$ matrix representing a set of h principal component loading spectra and **T** is an $m \times h$ matrix containing the corresponding scores. Data reduction is achieved by using only k principal components with $k < n$. Subsequently, PCR uses the reduced matrix **T**′ instead of the original data matrix **A** in the regression equation used for ILS.

PLS regression is performed similarly to PCR with the exception that in PLS concentration information is used during the decomposition process. A more elaborate discussion of the techniques mentioned is beyond the scope of this

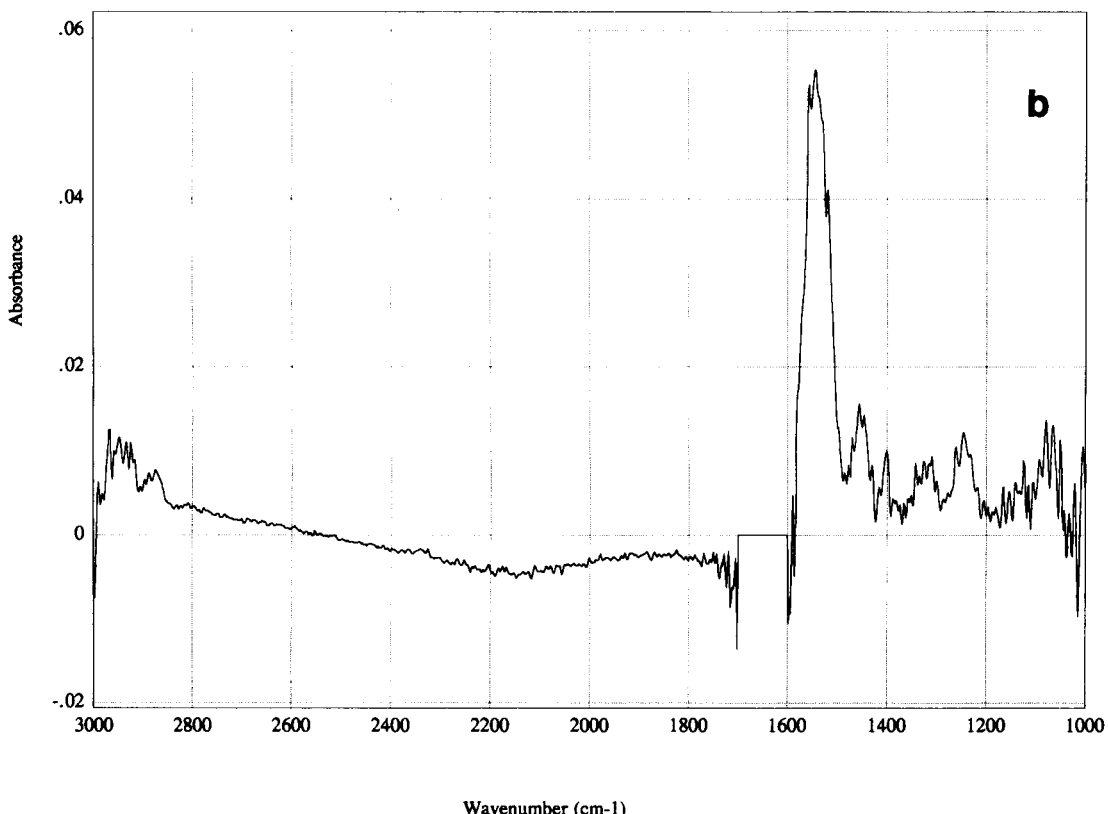

Fig. 2 (continued).

paper. However, an excellent overview is given by Haaland and Thomas [13].

In order to compare the results of the different calibration models, use is made of the root-mean-square error of estimation (RMSEE), which is defined as:

$$\text{RMSEE} = \sqrt{\sum_{i=1}^{m} (c_i - \hat{c}_i)^2 / [m - (f+1)]}$$

Here m stands for the number of samples in the calibration set, c_i is the concentration of sample i, $\hat{c}_i$ is the predicted concentration, and f is the number of factors used in the calibration model. In order to assess the quality of the predictions obtained from the validation set, the mean difference between the reference and infrared data (MD) and the standard deviation of the differences (SDD) will be used, where the difference is defined as the reference minus the infrared value.

EXPERIMENTAL

A set of 55 raw mixed tank milk samples, collected from the South-Holland area during wintertime, was analysed. Infrared spectra were recorded between 3000 and 1000 cm^{-1} on a Perkin-Elmer 1600 FT-IR spectrometer by averaging 4 scans with a resolution of 8 cm^{-1} (data point resolution: 2 cm^{-1}). Demineralised water was used as background. The region between 1700 and 1600 cm^{-1} contained much noise due to strong water absorptions and was zeroed therefore. The sample compartment was equipped with

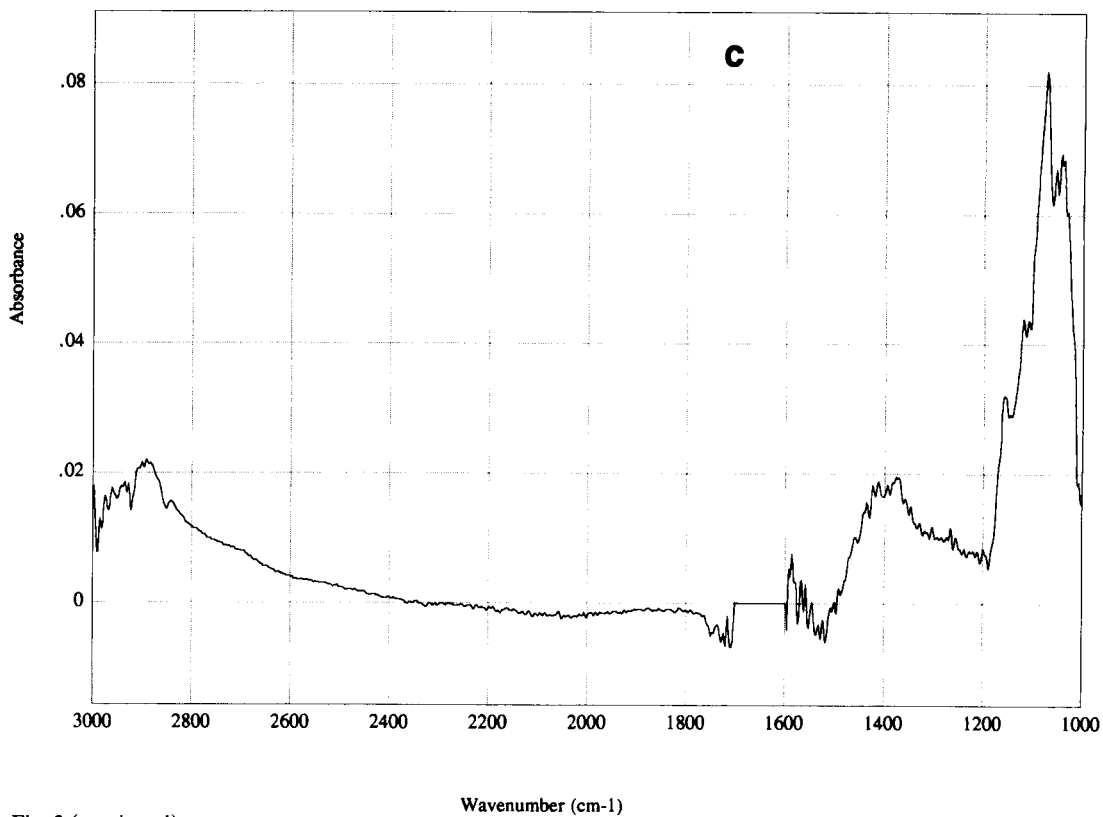

Fig. 2 (continued).

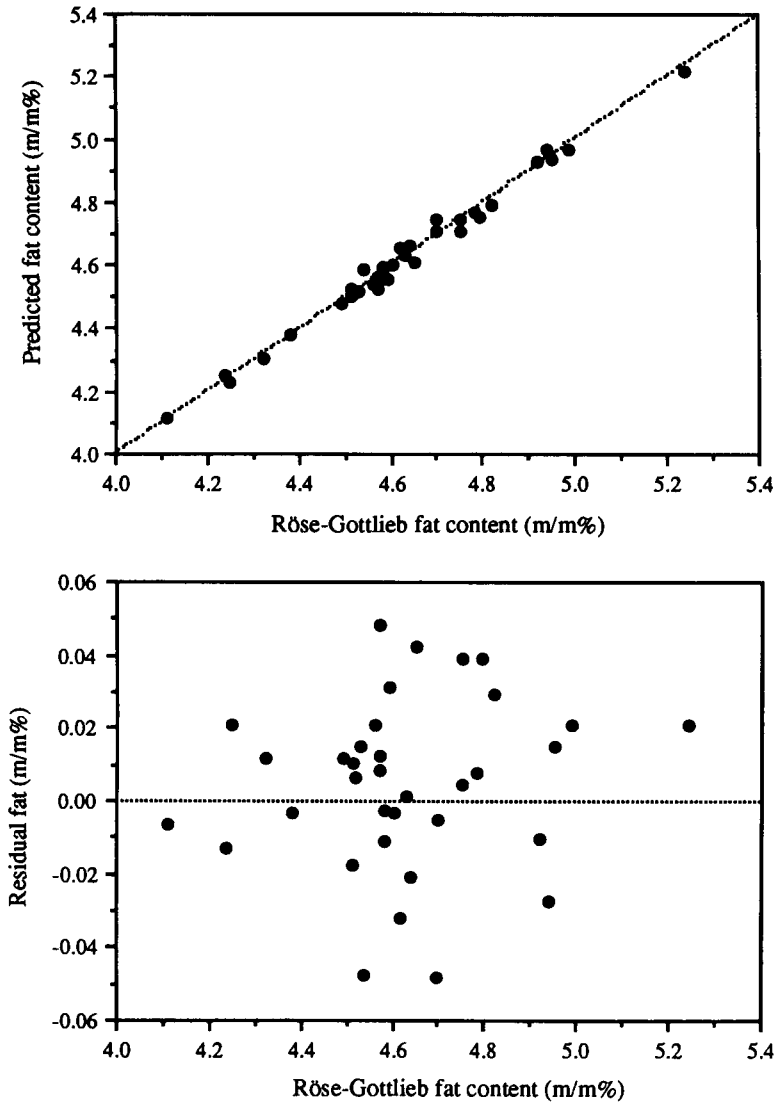

Fig. 3. Plots of (top) predicted versus Röse-Gottlieb fat content using a 2-factor PLS model and (bottom) residual (reference minus predicted) versus reference fat content.

a temperature stabilised (40.0 ± 0.1°C) CaF_2 cell with an optical pathlength of 40 μm. Prior to cell injection samples were heated to 45°C and homogenised with a two-step homogeniser (Delta Instruments) at pressures of approximately 17 and 8.5 MPa.

Also the fat, protein and lactose contents of the samples were determined with an infrared filter instrument (MultiSpec MAK2), which was calibrated according to routine procedures. Reference values for fat and protein were obtained from Röse-Gottlieb [14] and Kjeldahl ($N \times 6.38$) [15] analyses respectively. The fat content ranged from 3.88 to 5.27%, the protein content from 3.07 to 3.77% and the lactose content from 4.24 to 4.67%. Detailed statistics are shown in Table 1. There is a weak correlation between the fat and protein content ($r = 0.57$), whereas lactose is nei-

ther correlated with fat ($r = 0.03$) nor with protein ($r = -0.04$).

For ILS regression use was made of the integrated areas of spectral regions corresponding with the bandpass of the filters in the filter instrument.

RESULTS AND DISCUSSION

Selection of the calibration set

The total set of 55 samples was divided into a calibration and a validation set according to a procedure based on the method described by Isaksson and Næs [16]: (1) principal component analysis was applied to all spectra; (2) the scores of the samples on the five most important principal components (explaining 99% of the total variance in the spectra) were used in a K-means cluster analysis [17] that was performed to yield an arbitrary number of 20 clusters; (3) in order to compose a calibration set, from each cluster a sample was taken randomly with the only restriction that the samples with the extreme fat, protein and lactose contents had to be included; (4) the remaining 35 samples composed the validation set. The clusters had sizes ranging from 1 (5 clusters) to 8 (1 cluster) samples; the average size was 2.8 samples per cluster. For calibration and validation set the statistics in Table 1 were calculated.

Filter-infrared versus reference data

Comparison of the Röse-Gottlieb and the infrared filter data for fat showed that the mean difference (MD) for the samples in the validation set was -0.003% with a standard deviation (SDD) of 0.031%. For protein an MD of -0.012% was

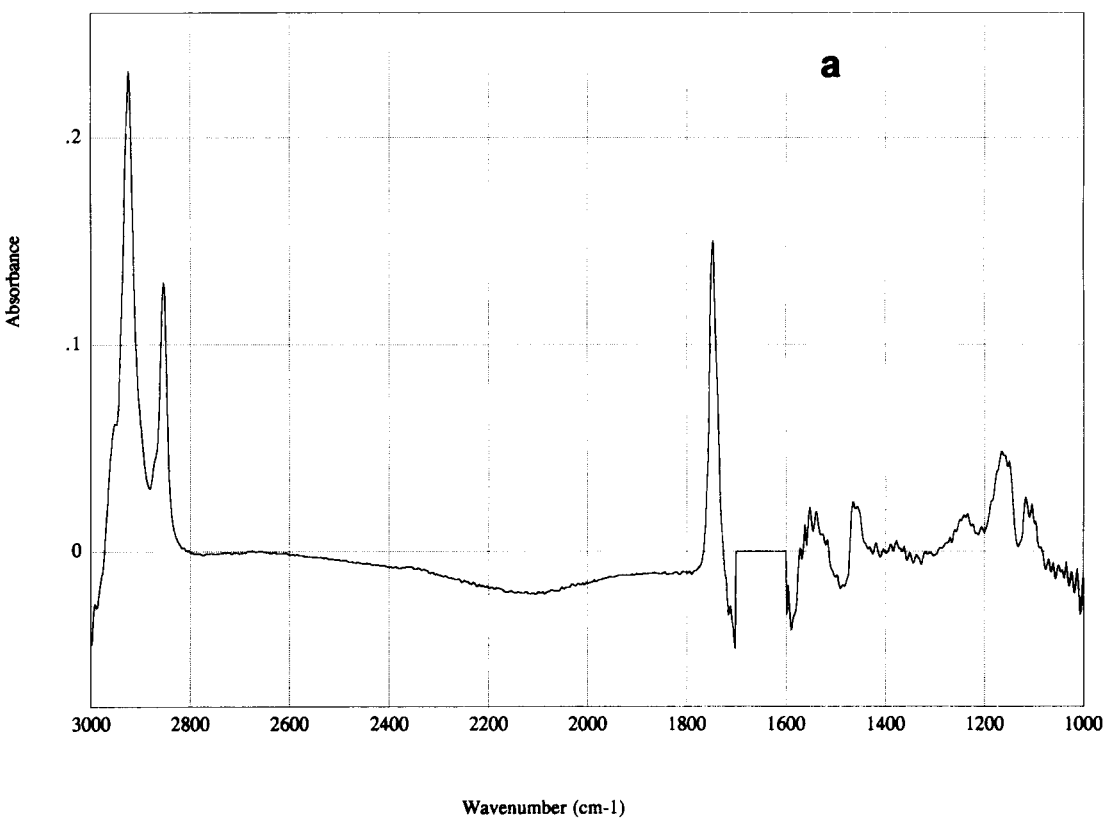

Fig. 4. Loading spectra of (a) first and (b) second PLS factor of fat model.

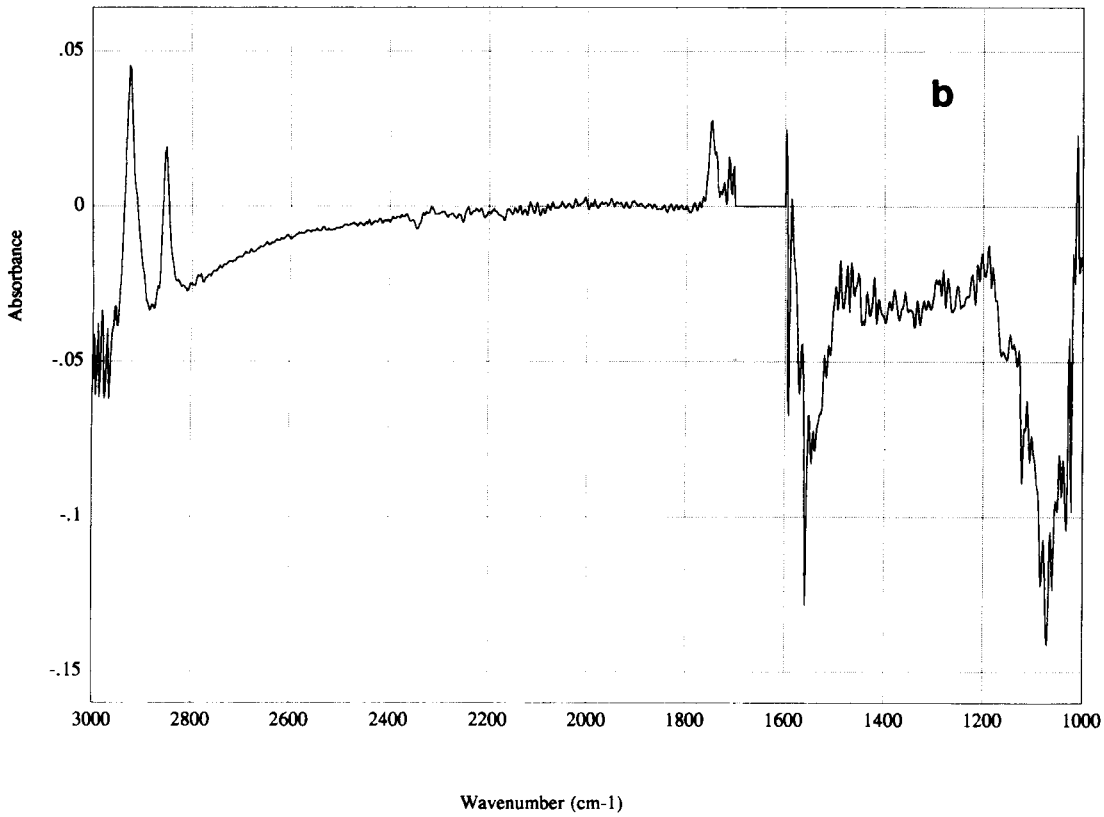

Fig. 4 (continued).

found when comparing the Kjeldahl and filter data. Apparently, the filter instrument gave values which were significantly too high (level of significance: 0.069%). The SDD was found to be 0.037%. At the time, for lactose only filter-infrared data were available.

The mean and the standard deviation of the difference between reference and instrumental results obtained from the analysis of m samples of milk should be $\leq 0.14/\sqrt{m}$ and $\leq 0.07\%$, respectively [18]. Both fat and protein infrared determinations meet these requirements (Table 2).

Classical least-squares regression

Since the main constituents of milk are water, fat, protein and lactose and measurements are corrected for the solvent, samples can – as a first approximation – be regarded as three-component mixtures. CLS regression was applied to the spectra in the calibration set using the Röse-Gottlieb, Kjeldahl and filter-infrared data for fat, protein and lactose respectively. The resulting **K**-matrix contained the least-squares estimates of the pure fat, protein and lactose spectra as shown in Fig. 2.

The fat absorptions corresponding with the asymmetric and symmetric CH_2 stretching at 2922 and 2852 cm^{-1} respectively, the C=O stretching of the triglycerides at 1746 cm^{-1} and the CH_2 deformation at 1466 cm^{-1} are clearly visible in Fig. 2a. (Intensities are 0.090, 0.051, 0.059 and 0.007 a.u. per % fat respectively). The absorption of ester C–O stretching vibrations appears around 1160 cm^{-1} (0.018 a.u. per % fat).

In Fig. 2b the spectrum of protein is displayed. The amide I band (C=O stretching) at 1670–1630 cm^{-1} is blocked by the strong absorption of water. As this region is zeroed the band is not

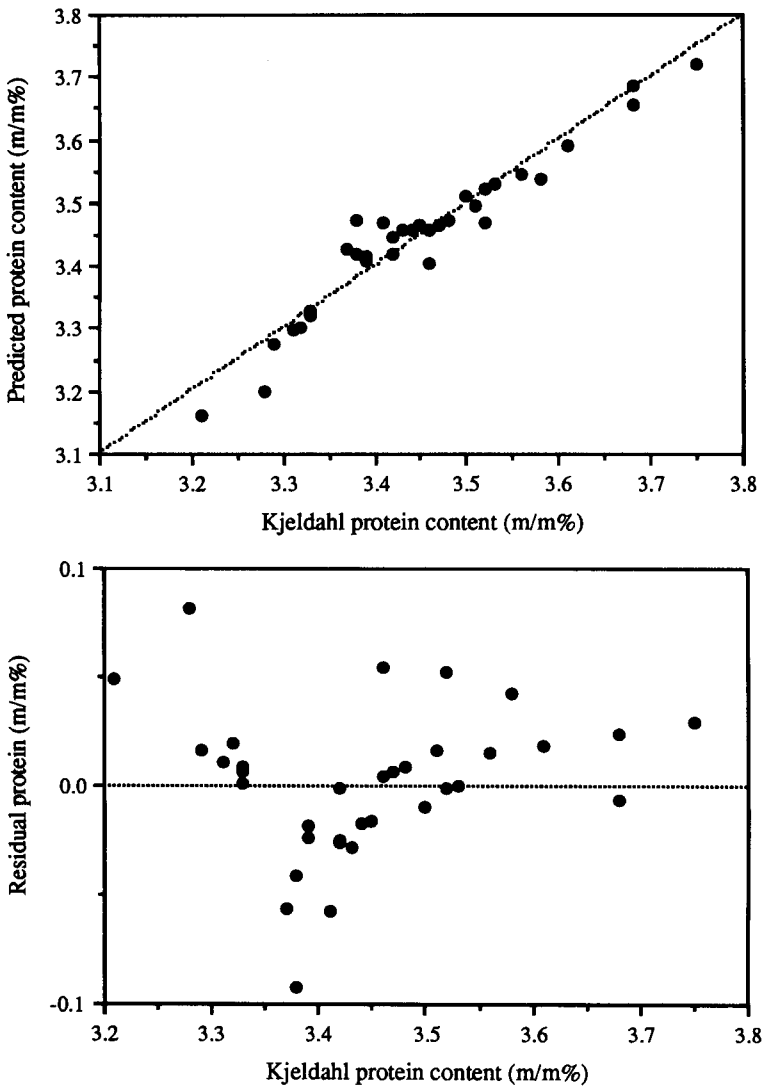

Fig. 5. Plots of (top) predicted versus Kjeldahl protein content using a 4-factor PLS model and (bottom) residual (reference minus predicted) versus reference protein content.

visible. The amide II band however appears intensely at 1544 cm^{-1} (0.055 a.u. per % protein).

The lactose spectrum is shown in Fig. 2c. Strong absorptions (C–O stretching) appear in the region 1100–1000 cm^{-1} with a maximum at 1074 cm^{-1} (0.082 a.u. per % lactose) and around 1400 cm^{-1} (C–O–H in plane deformation, approximately 0.018 a.u. per % lactose). Furthermore, overtones and combination bands give rise to an increasing baseline from 2500 cm^{-1} upward.

Reproduction of the original spectra gave an average root-mean-square-error of 0.002 a.u. which corresponds with the average noise level in the spectra. Hence, it appears that the assumption of a three-component mixture is reasonably valid. It should be noted that actually the noise in the spectra is heteroscedastic, i.e., it differs for

different wavenumbers. Hence, applying a weighted regression technique may further improve the predicted results.

Prediction of the calibration set values using the **K**-matrix gave an RMSEE of 0.027, 0.038 and 0.033% for fat, protein and lactose respectively. Fitting the spectra in the **K**-matrix on the validation data resulted in an SDD of 0.025, 0.041 and 0.032%. The mean difference for fat and protein were 0.001 and −0.008%. For lactose a small but significant bias of −0.017% was found (level of significance: 0.003%).

Inverse least-squares regression

ILS regression was performed using spectral regions corresponding with those of the filters in the filter instrument. By deleting regions contributing insignificantly to the model of a particular component, optimum models were obtained. In the fat model both the CH_2 and the C=O stretching region are present. Furthermore, one reference region appears to be sufficient to correct for baseline contributions. The protein model contains the amide II region and a baseline correction embodied by a reference region. Lactose can be predicted by using its characteristic absorption regions between 1100 and 1000 cm^{-1} and a reference region.

For fat, protein and lactose prediction of the contents in the samples of the calibration set yielded RMSEE values of 0.017, 0.035 and 0.027% respectively. For the validation set correspondingly SDD values of 0.029, 0.039 and 0.025% were calculated. The mean differences amounted to 0.013, 0.003 and −0.005%. The SDD values for fat and protein correspond well with the re-

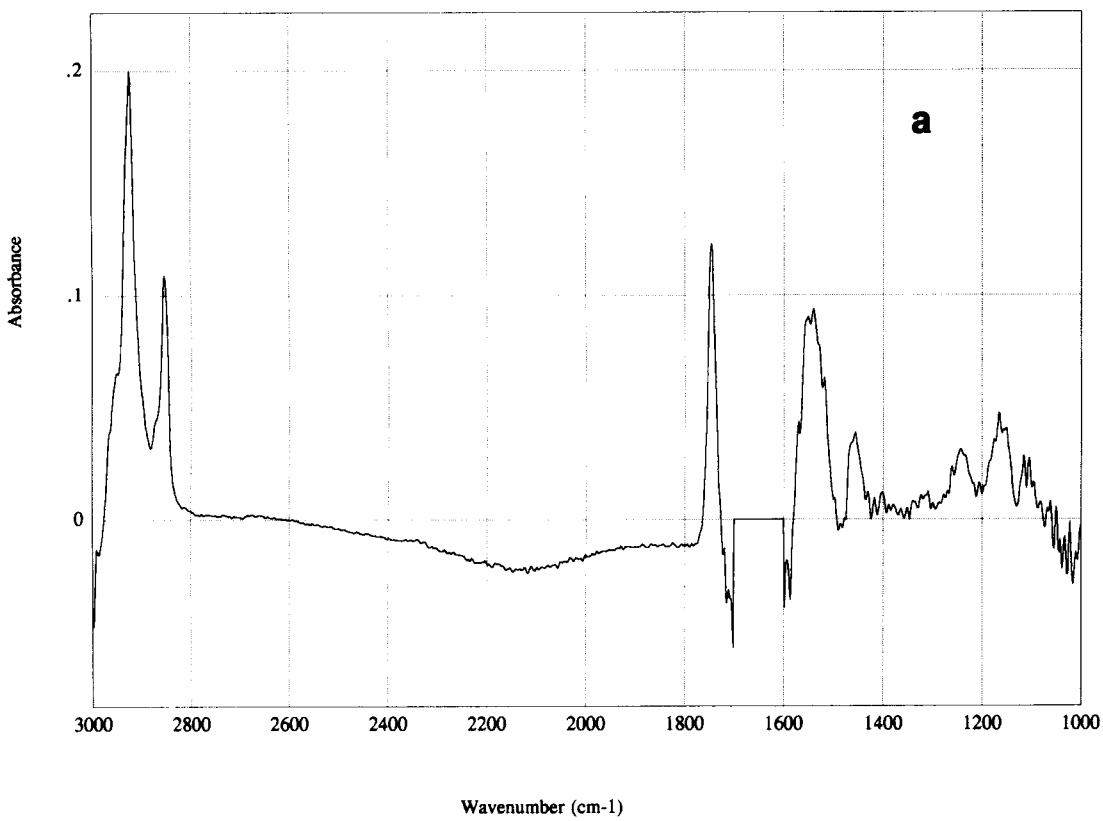

Fig. 6. Loading spectra of (a) first and (b) second PLS factor of protein model.

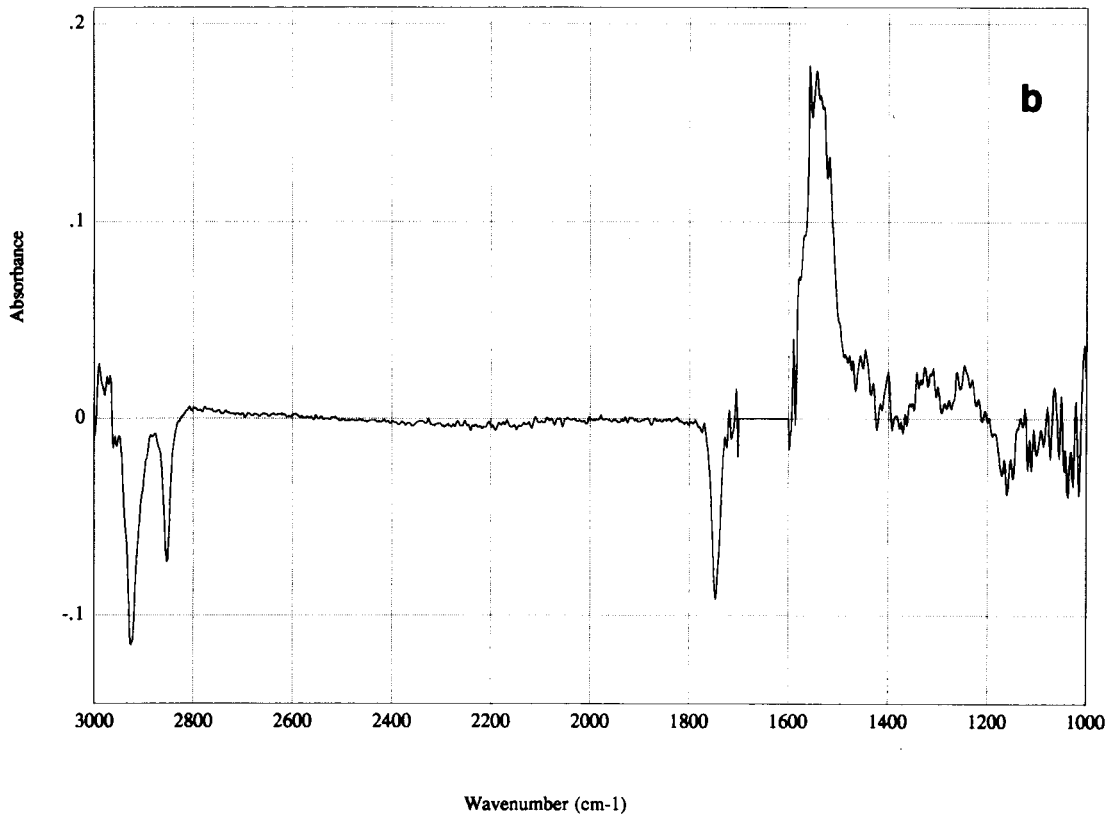

Fig. 6 (continued).

sults obtained from the filter instrument. For fat, however, a small but significant bias was found (level of significance: 0.013%).

Principal component regression

PCR applied to the samples of the calibration set with fat as dependent variable resulted in a 3-factor model with an RMSEE of 0.028%. Application of the resulting model to the validation samples yielded an MD of 0.002% and an SDD of 0.025%. For protein a 4-factor model was found with an RMSEE of 0.037%. The validation set yielded MD = 0.001% and SDD = 0.036%. Lactose, finally could be predicted optimally using a 2-factor model. The corresponding RMSEE and MD and SDD values were 0.031, −0.006 and 0.027%.

Partial least-squares regression

PLS regression yielded a two-factor model for fat giving an RMSEE of 0.027% for the calibration set and an MD and SDD of 0.004 and 0.024% for the validation set. In Fig. 3a the predicted fat contents are plotted against the reference values. Inspection of the residuals (i.e., reference minus predicted fat content, Fig. 3b) revealed that there was no significant correlation between the residuals and the fat content (r = 0.125).

The first loading spectrum of fat (Fig. 4a) clearly shows the absorptions corresponding with the CH_2 and C=O stretching of the triglycerides at 2922 and 2852 cm^{-1} and at 1745 cm^{-1} respectively. The absorption of the CH_2 deformation appears at 1466 cm^{-1} and of ester linkages around

1164 cm^{-1}. The second loading spectrum (Fig. 4b) reveals contributions of unmodelled fat (3000–2800 and 1745 cm^{-1}), protein (around 1550 cm^{-1}) and lactose (around 1070 cm^{-1}) variations. As was stated earlier, the curved baseline from 2500 cm^{-1} upward appears to be related to the presence of lactose. Subtraction of two spectra of samples with different composition but equal lactose content confirmed this by yielding a straight baseline.

PLS regression resulted in a 4-factor model for protein with RMSEE = 0.024%. Prediction of the validation set yielded MD = 0.001 and SDD = 0.035%. There was no concentration dependency of the residuals ($r = 0.102$, Fig. 5). In Fig. 6 the first two loading spectra are shown. The first

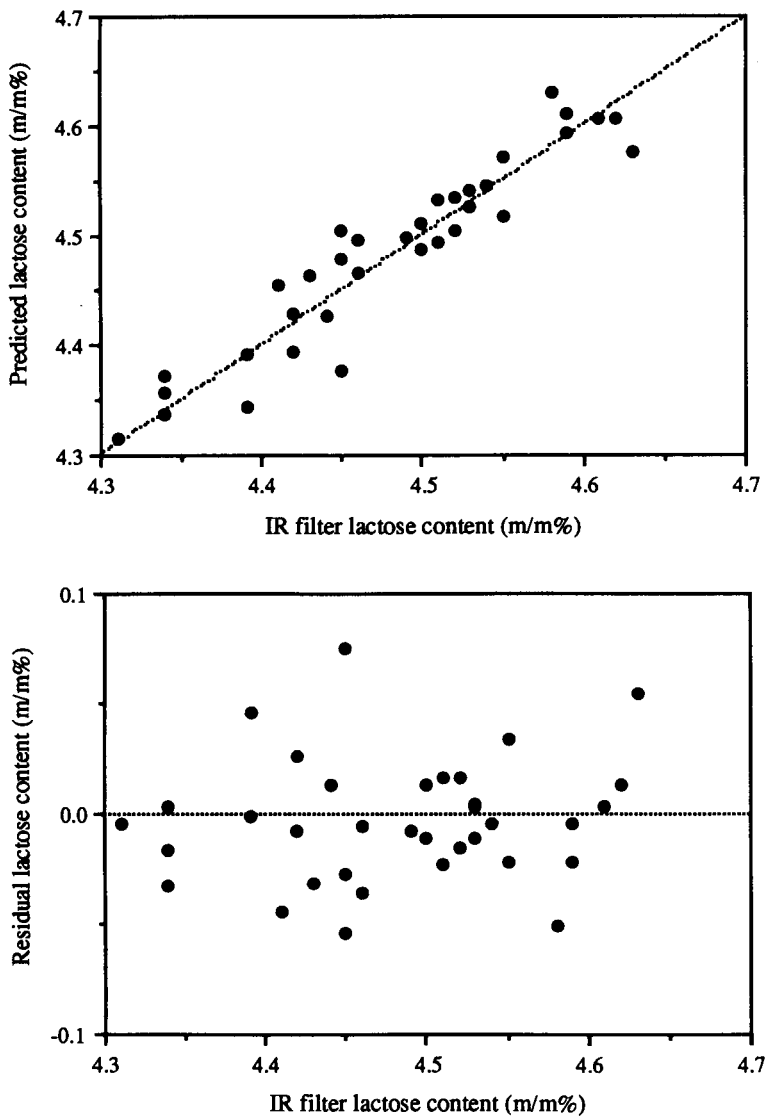

Fig. 7. Plots of (top) predicted versus infrared filter lactose content using a 4-factor PLS model and (bottom) residual (reference minus predicted) versus reference lactose content.

loading spectrum looks very similar to the corresponding one of fat. Obviously, the main variation in the spectra is due to the variation in fat content. However, an intensive amide II band around 1550 cm^{-1} is also clearly present. In the second loading spectrum the model is corrected for the fat contribution of the first loadings and again the band at 1550 cm^{-1} is visible.

PLS regression on lactose resulted in a 4-factor model with RMSEE = 0.021%. The validation set values were predicted with MD = −0.005 and SDD = 0.029%. There was no concentration dependency of the residuals ($r = 0.123$, Fig. 7). As is shown in Fig. 8 the first loading spectrum of lactose clearly shows the importance of the C–O stretching region for this component. Due to the major variation of fat and protein in the samples characteristic triglyceride and peptide bands are also visible. The second loading spectrum corrects the model for the fat and protein contributions from the first factor.

Conclusion

Comparison of the SDD values of the reference minus FT-IR and reference minus filter-IR data reveals no significant differences (at the 1% level) for any of the four multivariate methods. Furthermore, for none of the components a significant difference between the multivariate methods was found. For fat and lactose a significant bias was found when using ILS and CLS, respectively. However, all approaches give values that are within the limits imposed by the IDF standard for mid-infrared instruments [18].

Data acquisition, data transfer from the spectrometer to the PC and subsequent mathematical computations require approximately 10–15 s per spectrum. Hence, it can be concluded that Fourier

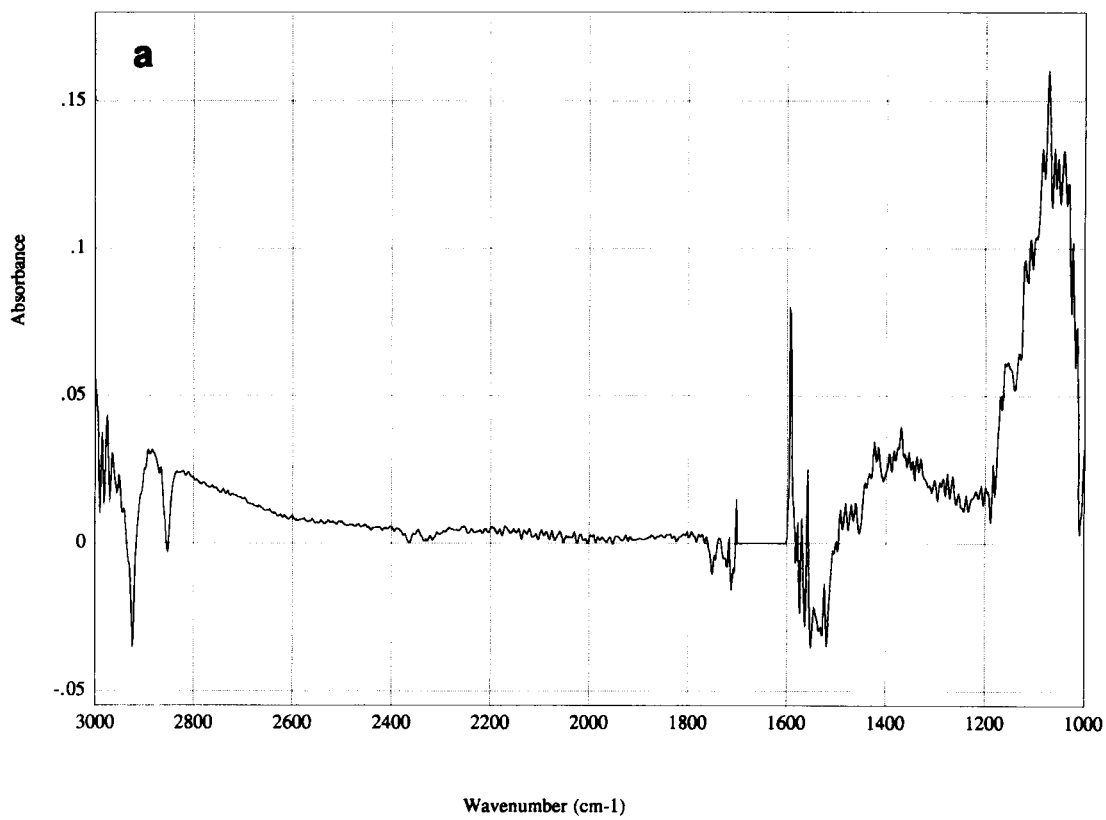

Fig. 8. Loading spectra of (a) first and (b) second PLS factor of lactose model.

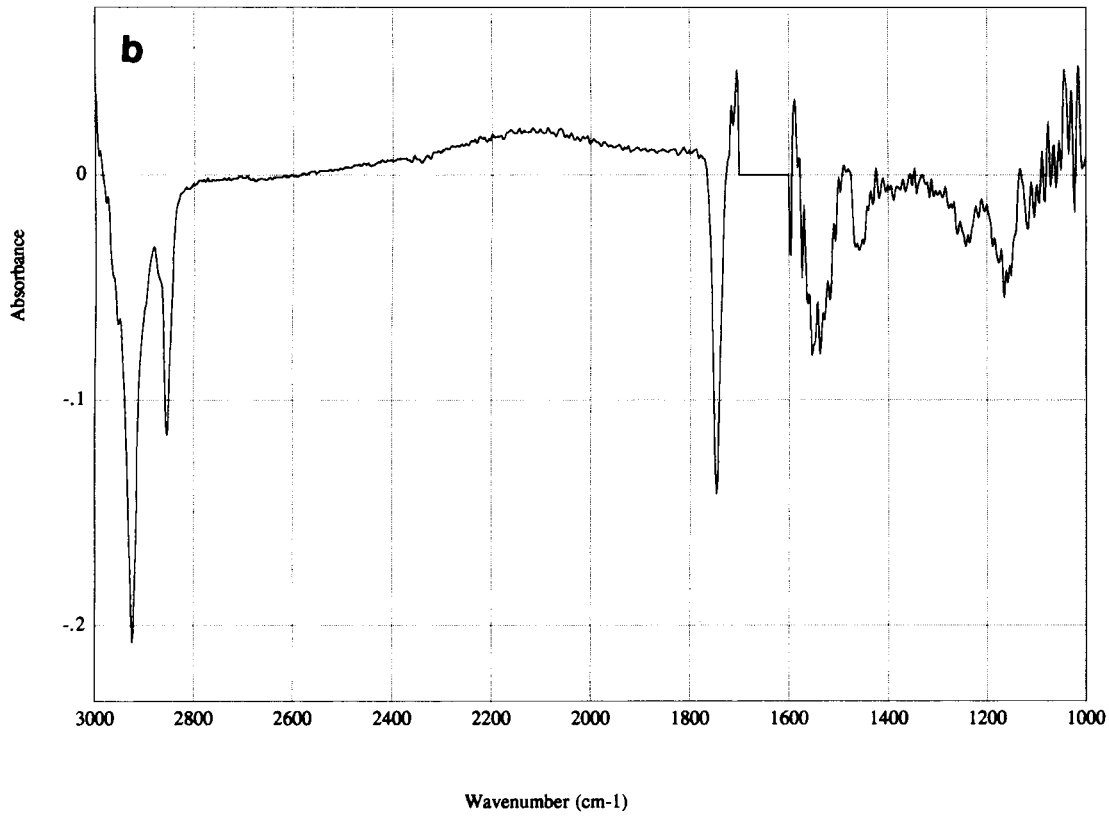

Fig. 8 (continued).

transform infrared spectrometry is well suited for the in-line analysis of fat, protein and lactose in milk samples.

Future investigations will be focused on the effect of seasonal variations in the composition of milk on the reliability of the FT-IR method.

REFERENCES

1 P. Walstra and R. Jenness, Dairy Chemistry and Physics, Wiley, New York, 1984.
2 J.D.S. Goulden, J. Dairy Res., 50 (1964) 273.
3 M.F. Kerkhof Mogot, J. Koops, R. Neeter, K.J. Slangen, H. van Hemert, O. Kooyman and H. Wooldrik, Neth. Milk Dairy J., 36 (1982) 195.
4 L.O. Sjaunja and I. Andersson, Acta Agric. Scand., 35 (1985) 345.
5 F.R. van de Voort, S. Kermasha, J.P. Smith, B.L. Mills and K.F. Ng-Kwai-Hang, J. Dairy Sci., 70 (1987) 1515.
6 D.A. Biggs and D.A. McKenna, J. Assoc. Off. Anal. Chem., 72 (1989) 724.
7 D.A. Biggs, G. Johnsson and L.O. Sjaunja, Bull. Int. Dairy Fed., 208 (1987) 21.
8 P. Robert, D. Bertrand, M.F. Devaux and A. Grappin, Anal. Chem., 59 (1987) 2187.
9 R.T. Carl, Nicolet FT-IR Spectral Lines, March, 1989, p. 15.
10 H.J. Luinge, E. Hop, E.T.G. Lutz, J.H. van der Maas, A. Holstra, J.A. van Hemert, J. Koops, H. Wooldrik, E.A.M. de Jong and G. Ellen, SPIE, Vol. 1575 (1991) 505.
11 F.R. van de Voort, J. Sedman, G. Emo and A.A. Ismail, J. Assoc. Off. Anal. Chem., 75 (1992) 780.
12 B.S. Lanher, Thesis, Université de Bourgogne, 1991.
13 D.M. Haaland and E.V. Thomas, Anal. Chem., 60 (1988) 1193.
14 International Dairy Federation, IDF Standard 1C, 1987.
15 International Dairy Federation, IDF Standard 20A, 1986.
16 T. Isaksson and T. Næs, Appl. Spectrosc., 44 (1990) 1152.
17 J.A. Hartigan, Clustering Algorithms, Wiley, New York, 1975.
18 International Dairy Federation, IDF Standard 141, 1988.

Analytica Chimica Acta, 284 (1993) 435–443
Elsevier Science Publishers B.V., Amsterdam

Expert system for the voltammetric determination of trace metals

Part III. Methods for determining mercury, selenium and vanadium

M. Esteban and C. Ariño

Departament de Química Analítica, Universitat de Barcelona, Av. Diagonal 647, 08028 Barcelona (Spain)

I. Ruisánchez, M.S. Larrechi and F.X. Rius

Departament de Química, Universitat Rovira i Virgili (Tarragona), Pl. Imperial Tàrraco 1, 43005 Tarragona (Spain)

(Received 11th December 1992; revised manuscript received 20th April 1993)

Abstract

A previously described expert system for the voltammetric determination of Cu, Zn, Cd, Pb, In, Ni, Co and Tl is enhanced and improved by means of the addition of methods for Hg, V and Se (optionally also Te). Special attention is paid to the determination of V, inside a wide concentration range, in different types of samples. The system guides the user in the choice of sample treatment and the most appropriate voltammetric procedure for the identification and the quantification of the trace metals. The techniques implemented are differential pulse polarography, anodic stripping voltammetry, cathodic stripping voltammetry and adsorptive stripping voltammetry, using mercury drop electrodes and a gold electrode (for the determination of Hg). For the identification and resolution of overlapping peaks (Cd and In), the system may call two external programs, written in turboBasic. Quantification is carried out by means of the multiple standard addition method, and the quality of the calibration plot is tested by several statistical validation tests. The expert system is developed using KES (knowledge engineering system).

Keywords: Voltammetry; Expert system; Mercury; Selenium; Vanadium; Trace metals; Chemometrics

Expert systems are powerful tools, within the domain of artificial intelligence, which use knowledge and operate according to the rules of reasoning of an expert, in order to guide a non-expert user. Such systems have already been applied in several branches of analytical chemistry, especially liquid chromatography [1], liquid–liquid extraction [2], spectrophotometry [3,4] and AAS [5]. In the electrochemical field, only one expert system for the automatic elucidation of electrode reaction mechanisms has been presented [6].

Recently, an expert system was described for the voltammetric determination of Cu, Zn, Cd, Pb, In, Ni, Co and Tl [7]. The expert system was developed using KES (knowledge engineering system) [8]. The system is based on versatile and powerful voltammetric methods developed during recent years, some of them becoming definitive routine methods [9,10].

At the moment, electroanalytical techniques (especially stripping voltammetry) form the basis of well-tested routine methods for toxic metal

Correspondence to: M. Esteban, Departament de Química Analítica, Facultat de Química, Universitat de Barcelona, Av. Diagonal 647, 08028 Barcelona (Spain).

SSDI 0003-2670(93)E0455-G

analysis in environmental surveillance, food control and occupational medicine, toxicology and hygiene [9].

Toxic trace metals are a class of environmental pollutants which require particular attention in the various compartments of the environment [9]. To this group of pollutants belong a priori toxic metals such as Hg, Cd and Pb, as well as those trace metals which essentially act below their respective threshold levels for man and mammals and display progressively toxic actions above their thresholds, e.g., Se, V, Cu, Zn, Co, etc. Furthermore, some of these metals can be used to determine the origin and quality of some type of sample. This is the case, for instance, for vanadium and nickel in petroleum [11,12].

This paper outlines the part of an expert system devoted to the voltammetric methods for the determination of Hg, V and Se. This part represents an enhancement and improvement of a previously described expert system devoted to a lower number of trace metals. The global expert system concerns the determination of Cu, Zn, Cd, Pb, In, Ni, Co, Tl, Hg, V and Se, at trace levels, by voltammetric means. It is based on the production of rules, which allow us to represent knowledge by means of conditional statements of the form IF ... and ... THEN ... and .... They support the strategies to be followed by the user in order to identify and quantify the above mentioned trace metals voltammetrically.

THE EXPERT SYSTEM

The expert shell KES [8] was used for the development of the present expert system. KES provides useful means for designing an effective user interface for the expert system.

The global architecture of the expert system is as described in previous papers [7], but with an enhancement in size, because of the wider possibilities considered here.

The present knowledge base deals with sample treatment, voltammetric procedure, identification and resolution of signals, and quantitative determination. The knowledge implemented is based on well-known procedures. The knowledge base has been enlarged, with respect to that of the previous simpler expert system [7], to include data on Hg, V and Se.

The sample treatment part is similar to that already proposed [7], but additional information is given about the mineralization of petroleum before determining vanadium and nickel. More detailed information on this subject is given in Fig. 4.

The choice of the technique is mainly determined by the concentration of the analyte. In this system, usual techniques in trace and ultratrace analysis such as differential pulse polarography (DPP), differential pulse anodic stripping voltammetry (DPASV), differential pulse cathodic stripping voltammetry (DPCSV) and differential pulse adsorptive stripping voltammetry (DPAdSV) have been considered. The choice of the electrode, although it is also related to the concentration level to be reached, is linked to the reproducibility. Because of the well-known difficulties associated with the use of some solid electrodes, especially the rotating thin mercury film electrode (TMFE), only mercury drop electrodes, dropping mercury electrode (DME) or static mercury drop electrode (SMDE), and the gold electrode are considered. However, the attention of the user is drawn to the unreliability of results obtained by non-experts using the gold electrode.

Similarly to previous parts of this expert system [7], in all cases, after the recording of the voltammograms, the expert system reports the information needed to identify the peaks and to detect the presence of anomalous features by means of the values of the peak widths at half-height. Further, the quantification of such peaks is by means of the external program COOKS 2 [7]. Quantification is carried out by means of the multiple standard addition method, and the quality of the calibration plot is tested by several statistical validation tests.

Mercury

The expert system recommends a voltammetric method for the simultaneous determination of Hg and Cu down to the ng l^{-1} range [13,14]. The method has proved to be reliable for Hg levels

above 100 ng l^{-1} (0.1 ppb), and it has been succesfully applied to natural waters and wines [13] and biomatrices [14].

The method is based on DPASV at a rotating gold electrode. A medium exchange to $HClO_4$ plus HCl is required subsequent to the cathodic accumulation stage before stripping. Figure 1 shows the information given by the expert system to the user. Because of the difficulties inherent to solid electrodes, a procedure for the preparation of the Au electrode is given. Obviously, the experimental conditions and the main instrumental parameters are reported.

For concentration levels below 100 ng l^{-1}, the expert system cites original papers in the literature or, better, recommends the assistence of an expert since the involved voltammetric methods required for this concentration level are beyond the scope of an expert system.

Selenium

For the determination of Se at levels above 200 ng l^{-1} (0.2 ppb), the expert system considers two possibilities, referred to as "first method" [15] and "second method" [16], both based on DPCSV onto a HMDE (Fig. 2). The expert system especially recommends the "first method" because, subsequently to the simultaneous determination of Cu, Cd, Pb and Zn by DPASV (see Part I, Ref. 7), Se can be determined in the same solution by DPCSV. For this trace metalloid, the electrochemical preconcentration is achieved by formation of an HgSe layer on the HMDE due to the anodic oxidation of mercury. Subsequently, the HgSe bound Hg(II) is again reduced during the cathodic scan and Se^{2-} is released into the solution. This method has been applied successfully in the analysis of atmospheric pollutants [9,15] at Se levels above 200 ng l^{-1} (0.2 ppb).

The second method is based on the formation of a layer of Cu_2Se, as well as Cu_4Te if Te is present. The method is substantially free of interferences and enables also the single determination of Se and Te in the presence of a 10^4-fold excess of the corresponding concomitant element.

An alternative method can be used for determining Se levels in the range 0.08–8 ppb [17]. Figure 3 shows the information given about the method, which is based on the use of a catalytic wave by means of DPP, using DME or SMDE.

If the user has no estimation about the approximate concentration of Se, the expert system recommends either "first method" or "second method".

Vanadium

For the determination of vanadium(V), the expert system considers four possibilities (Fig. 4). If an estimate of the concentration is available, and it is within the range 0.5–50 ppm, a method is recommended based on DPP onto DME or SMDE (Option 1). Two procedures are described for the sample treatment, both being successfully applied to the determination of V and Ni in petroleum [11,12].

For concentration levels within the 50–0.5 ppm range (Option 2), the expert system sends the users to further Options 3 or 4, by means of a simple operation of dilution. Figure 5 shows the information given by the expert system about the methods referred to as Option 3 and Option 4. Both methods are based on differential pulse adsorptive stripping voltammetry (DPAdSV) on an HMDE, and their detection limits are at the picomolar (sub-ppt) level.

The method described in Option 3 is performed in NH_4OH–PIPES buffer medium (pH 7.8) containing catechol [18]. The method recommended in Option 4 has been reported very recently for ultratrace measurements [19], and it is based on the interfacial accumulation of the vanadium–cupferron complex onto HMDE, followed by the catalytic reduction of the adsorbed complex in the presence of bromate. The dual amplification effect associated with these accumulation and catalytic processes results in a very low detection limit (0.25 ppt).

If no previous knowledge of the approximate concentration of V is available, the expert system recommends a preliminary test by means of the method described in Option 3.

Conclusions

The present expert system may be very useful for non-expert users in the electroanalytical field. It is based on well-tested methods, and special

Figure 1. Example of an interactive session with the expert system. Determination of Hg by using Differential Pulse Anodic Stripping Voltammetry (DPASV) onto the Rotating Gold Electrode.

Which of the following cations are to be determined?
1. Cu Zn Cd Pb
2. Ni Co
3. Tl
4. Se
5. Hg
6. V
7. others

=? **5**

Do you know the approximate metal-ion concentration?
1. yes
2. no

=? **1**

Which is the concentration range of Hg in the sample?
1. if [Hg] > 100 ng/l (0.1 ppb.)
2. if [Hg] < 100 ng/l (0.1 ppb.)

Note: The choice of the method depends on the concentration levels. The method corresponding to option 1, allows us the determination of Hg and Cu in the same run by common DPASV. The method has been successfully applied to natural waters, wines and biomatrices. In the last case a previous digestion of the sample with HNO3/HClO4, followed by UV irradiation, is recommended.

(Enter a number)
=? **1**

You should use Differential Pulse Anodic Stripping Voltammetry (DPASV) onto the Rotating Gold Electrode.

Preparation of the gold Electrode:
The surface of the gold electrode is first brushed with emery paper and subsequently polished with diamond paste of gradually decreasing grain size (7, 3, 0.7 μm) until a mirror like surface was attained. Fresh electrodes are activated electrochemically in 0.1 M $HClO_4$ containing 2.5 E-3 M HCl by successive polarization to -0.25 V and +1.7 V vs an Ag/AgCl electrode several times for 20 s.

The medium conditions are:
Before the stripping step and subsequent to the cathodic accumulation stage, the application of the method always requires a change of the medium composition to 0.1 M $HClO_4$ containing 2.5 E-3M HCl . This method allows us the simultaneous detection and/or determination of Hg and Cu.The surface of the gold electrode must be previously prepared.

The optimal instrumental conditions are:

E_r = Ag/AgCl or Standard Calomel Electrode (SCE). Ew = Au.
E_{aux} = Pt or glassy carbon.
E_{pe} = -0.2 V, t_{pe} = 5 - 10 min, w = 3000 rpm.
pulse = 50 mV. (in general, between 10 and 100 mV.)
v = 10 mV/s, tpulse = 30 - 100 ms, Ei = -0.2 V, Ef = +0.8 V.

attention is paid to standard methods. Techniques with very low detection limits are recommended, such as DPP, DPASV, DPCSV and DPAdSV. Mercury drop electrodes are mainly used because of their reproducibility. Only one solid electrode is taken into account: an Au electrode for the determination of Hg (optionally also Cu).

Which is the concentration range of Hg in the sample?
1. if [Hg] > 100 ng/l (0.1 ppb.)
2. if [Hg] < 100 ng/l (0.1 ppb.)

(Enter a number)
=? **2**

This expert system addresses the user to the original references quoted in the literature and/or to a human expert since the required methods are beyond the scope of the expert system. For more information enter the command: display attach Mercury of kb.

Figure 2. Determination of Se by using Differential Pulse Cathodic Stripping Voltammetry (DPCSV) onto the Hanging Mercury Drop Electrode (HMDE).

Which is the concentration range of the cation Se ?
1. if [Se] > 0.2 ppb.
2. if 0.08 ppb < [Se] < 8 ppb.

(Enter a number)
=? **1**

You should use Differential Pulse Cathodic Stripping Voltammetry (DPCSV) onto the Hanging Mercury Drop Electrode (HMDE).

Note: Two methods are available, both with 0.2 ppb determination limits and the instrumental conditions are the same. The first method is recommended if you are interested in determining also Cu, Pb, Cd and Zn. The second method is especially recommended if you are interested in simultaneous determination of Se and Te, in the concentration ranges 0.2 - 20 ppb and 0.2 - 50 ppb respectively.

First method:

The medium conditions are: A solution, free of organic compounds and surfactant, at pH = 2. This determination can be done after the anodic stripping of Cu, Zn, Cd and Pb.

The optimal instrumental conditions are:

E_r = Ag/AgCl or standard calomel electrode (SCE). E_w = HMDE.
E_{aux} = Pt or glassy carbon.
pulse = 50 mV, v = 10 mV/s, tpulse = 30 - 100 ms.
E_{pe} = -0.2 V, t_{pe} = 1-5 min, E_f = -0.7 V

Second method:

The medium conditions are: A solution, 0.5 M $(NH_4)_2SO_4$ + 4 E-3 M EDTA + 1 ppm $CuCl_2$ + 0.1 M H_2SO_4, at pH = 4.5.

The optimal instrumental conditions are:

E_r = Ag/AgCl or standard calomel electrode (SCE). E_w = HMDE.
E_{aux} = Pt or glassy carbon.
pulse = 50 mV, v = 10 mV/s, t_{pulse} = 30 - 100 ms.
E_{pe} = -0.4 V, t_{pe} = 1min, E_f = -1.2 V

If you are interested in examining bibliographical references, enter: display attach Selenium of kb

Figure 3. Determination of Se by using Differential Pulse Polarography (DPP) onto the Dropping Mercury Electrode (DME) or the Static Mercury Drop Electrode (SMDE).

Which is the concentration range of the cation Se ?

1. if [Se] > 0.2 ppb.
2. if 0.08 ppb < [Se] < 8 ppb.

(Enter a number)
=? **2**

You should use Differential Pulse Polarography (DPP) onto the Dropping Mercury Electrode (DME) or the Static Mercury Drop Electrode (SMDE).

The medium conditions are:

10 ml of the sample (previously treated), 2 ml Na_2SO_3 1.3 M, 2ml KIO_3 0.2 M, 5 ml NH_3-NH_4Cl buffer (pH=9), 2 ml EDTA 5% and 2 ml gelatin sol (0.1%)

The optimal instrumental conditions are:

E_r = Ag/AgCl or Standard Calomel Electrode (SCE). E_w = DME or SMDE.
E_{aux} = Pt or glassy carbon.
pulse = 50 mV. (in general between 10 and 100 mV.)
v = 10 mV/s, t_{pulse} = 30 - 100 ms.
E_i = -0.5 V, E_f = -0.9 V

Notes: The choice of the method depends on the concentration levels. If [Se] > 0.2 ppb, the expert system will recommend the application of the "first method" described in that section.
If you are interested in determining also Cu,Pb,Cd and Zn by means of DPASV, you can determine Se, in the same sample solution, after determining the above mentioned heavy metals. This possibility is also described in the first method of the choice 1. If you are interested in the simultaneous determination of Se and Te, in the concentration ranges 0.2-20 ppb and 0.2-50 ppb, respectively, the expert system will recommend the second method of the choice 1.

If you are interested in examining bibliographical references, enter: display attach Selenium of kb

Figure 4. Determination of V by using Differential Pulse Polarography (DPP) onto the Dropping Mercury Electrode (DME) or the Static Mercury Drop Electrode (SMDE).

Which is the concentration range of V(V) in the sample?

1. if 1.0E-5 M (0.5 ppm) < [V] < 1.0E-3 M (50 ppm)
2. if 1.0E-6 M (50 ppb) < [V] < 1.0E-5 M (0.5 ppm)
3. if 3.0E-10 M (15 ppt) < [V] < 1.0E-6 M (50 ppb)
4. if 1.0E-10 M (5 ppt) < [V] < 2.0E-9 M (100 ppt)

(The choice of the technique is mainly determined by the concentration of the analyte; the method corresponding to the option 1 allows the determination of Vanadium and Nickel in the same sample).

(Enter a number)
= ? 1

You should use Differential Pulse Polarography (DPP) onto the Dropping Mercury Electrode (DME) or the Static Mercury Drop Electrode (SMDE).

The medium conditions are:

The determination should be carried out in 0.01 M NH_3 - 0.01M NH_4Cl medium (pH = 8-9.). This method allows us the determination of Ni and V simultaneously. For such a case two possibilities have been described (Reference Vanadium). In the first one , Ni and V are measured in the same run, while in the second one, Ni is measured in the first run, subsequently EDTA is added to the solution, and finally V is measured.

Note: These methods have been successfully applied to petroleum containing 0.5 to 50 ppm of Vanadium and Nickel. In such a case the sample treatment should be as follows. Petroleum is first evaporated on a hot plate and then decarbonized in a muffle furnace at 600°C. Residues are treated with H_2SO_4 suprapur, taken to dryness, and redissolved in 10 ml 0.1M HCl. After quantitative transfer to a glass-stoppered cylinder, water and ammonium buffer was added, as described above . Chaumary recommends a first extraction with CCl_4 before the evaporation , followed by a filtration, treatment with anhydrous Na2SO4 and solvent evaporation in a rotavapor.

The instrumental parameters are:

E_r = Ag/AgCl or Standard Calomel Electrode. E_w = DME or SMDE.
E_{aux} = Pt or glassy carbon.
pulse = 50 mV (in general between 10 and 100 mV)
t_{drop} = 1 s, v = 10 mV/s, t_{pulse} = 30 - 100 ms.
E_i = -0.1 V, E_f = -0.8 V.
If you are interested in examining bibliographical references, enter: display attach Vanadium kb

Which is the concentration range of V(V) in the sample?

1. if 1.0E-5 M (0.5 ppm) < [V] < 1.0E-3 M (50 ppm)
2. if 1.0E-6 M (50 ppb) < [V] < 1.0E-5 M (0.5 ppm)
3. if 3.0E-10 M (15 ppt) < [V] < 1.0E-6 M (50 ppb)
4. if 1.0E-10 M (5 ppt) < [V] < 2.0E-9 M (100 ppt)

(Enter a number)
= ? **2**

You should dilute properly in order to apply option 3 or 4.

Figure 5. Determination of V by using Differential Pulse Adsorptive Stripping Voltammetry (DPAdSV) onto the Hanging Mercury Drop Electrode (HMDE).

Which is the concentration range of V(V) in the sample?

1. if 1.0E-5 M (0.5 ppm) < [V] < 1.0E-3 M (50 ppm)
2. if 1.0E-6 M (50 ppb) < [V] < 1.0E-5 M (0.5 ppm)
3. if 3.0E-10 M (15 ppt) < [V] < 1.0E-6 M (50 ppb)
4. if 1.0E-10 M (5 ppt) < [V] < 2.0E-9 M (100 ppt)

(Enter a number)
=? **3**

You should use Differential Pulse Adsorptive Stripping Voltammetry (DPAdSV) onto the Hanging Mercury Drop Electrode (HMDE).

The medium conditions are:

The determination should be carried out as follows: the sample, free of organic matter and surfactans, is adjusted to pH = 7.8 ± 0.4 by addition of NH_4OH. 100μl of 1M. PIPES buffer (PIPES = piperazine-N,N'-bis-2-ethane sulphonic acid monosodium salt) are added to 10 ml of the sample solution (pH = 7.8) and after passing N_2 for 6 min., 20 μl of 0.1 M catechol is added. According to the original reference Al(III), Si(IV), Mo(VI), As(V), all at 1.0E-7 M level, and Se(VI), Cr(VI), Cd(II), Ga(III), Te(VI) and Co(II) at 1.0E-8 M do not interfere.

The instrumental parameters are:

E_r = Ag/AgCl or Standard Calomel Electrode. E_w = HMDE.
E_{aux} = Pt or glassy carbon.
pulse = 50 mV, v = 10 mV/s, t_{pulse} = 30 - 100 ms.
E_{pe} = -0.1 V, E_f = -1.0 V.
t_{pe} = 1 - 15 min, t_r = 30 s.

If you are interested in examining bibliographical references, enter: display attach Vanadium kb

Which is the concentration range of V(V) in the sample?

1. if 1.0E-5 M (0.5 ppm) < [V] < 1.0E-3 M (50 ppm)
2. if 1.0E-6 M (50 ppb) < [V] < 1.0E-5 M (0.5 ppm)
3. if 3.0E-10 M (15 ppt) < [V] < 1.0E-6 M (50 ppb)
4. if 1.0E-10 M (5 ppt) < [V] < 2.0E-9 M (100 ppt)

(Enter a number)
=? **4**

You should use Differential Pulse Adsorptive Stripping Voltammetry (DPAdSV) onto the Hanging Mercury Drop Electrode (HMDE).

The medium conditions are:

The determination should be carried out in 2.0 E-5M. cupferron and 6.0E-3M. sodium bromate

The instrumental parameters are:

E_r = Ag/AgCl or Standard Calomel Electrode. E_w = HMDE.
E_{aux} = Pt or glassy carbon.
pulse = 50 mV, v = 10 mV/s, t_{pulse} = 30 - 100 ms.
E_{pe} = +0.1 V, E_f = -0.5 V.
t_{pe} = 90 s, t_r = 15 s.

If you are interested in examining bibliographical references, enter: display attach Vanadium kb

Economic support from the Spanish Ministry of Education and Science is acknowledged (DGICYT projects No. BP90-0453 and BP90-0821).

REFERENCES

1 J.A. van Leeuwen, B.G.M. Vandeginste, G. Kateman, M. Mulholland and A. Cleland, Anal. Chim. Acta, 228 (1990) 145.
2 M. Moors and D.L. Massart, Trends Anal. Chem., 9 (1990) 164.
3 K. Janssen and P. van Espen, Anal. Chim. Acta, 191 (1986) 169.
4 J. Smeyers-Verbeke, M.R. Detaevernier and D.L. Massart, Anal. Chim. Acta, 191 (1986) 181.
5 W.R. Browett, T.A. Cox and M.J. Stillman, in B.A. Hohne and T.H. Pierce (Eds.), Expert Systems Applications in Chemistry, ACS Symposium Series, Vol. 408, Washington, 1989, p. 210.
6 M. Pałys, M. Bos and W.E. van der Linden, Anal. Chim. Acta., 231 (1990) 59; 248 (1991) 429.
7 M. Esteban, I. Ruisánchez, M.S. Larrechi and F.X. Rius, Anal. Chim. Acta, 268 (1992) 95, 107; Trends Anal. Chem., 11 (1992) 135.
8 KES, PS Version 2.4, Software Architecture and Engineering Inc., Arlington, VA, USA, 1990.
9 H.W. Nürnberg, Sci. Total Environ., 37 (1984) 9; Pure Appl. Chem., 54 (1982) 253; Anal. Chim. Acta, 164 (1984) 1.
10 Deutsche Norm: DIN 38 406, Teil 16, March 1988.
11 D.D. Gilbert, Anal. Chem., 37 (1965) 1102.
12 Ch. Chaumery, Ann. Fals. Exp. Chim., 78 (1985) 161.
13 L. Sipos, J. Golimowski, P. Valenta and H.W. Nürnberg, Fresenius' Z. Anal. Chem., 298 (1979) 1.
14 R. Ahmed, P. Valenta and H.W. Nürnberg, Mikrochim. Acta I, (1981) 171.
15 V.D. Nguyen, P. Valenta and H.W. Nürnberg, Sci. Total Environ., 12 (1979) 151.
16 G. Henze, P. Monks, G. Tölg, F. Umland and E. Weissling, Fresenius' Z. Anal. Chem., 295 (1979) 1.
17 H. Taijun, Z. Zhengxing, D. Shanshi and Z. Yu, Talanta, 39 (1992) 1277.
18 The determination of Trace Metals in Marine and Other Waters by Voltammetry or AAS, HMSO, London, 1988.
19 J. Wang, B. Tian and J. Lu, Talanta, 39 (1992) 1273.

Analytica Chimica Acta, 284 (1993) 445–451
Elsevier Science Publishers B.V., Amsterdam

Qualitative and quantitative analyses of synthetic pigments in foods by using the branch and bound algorithm

Wei Zeng, Ping Wang, Huizhen Zhang and Shenyang Tong

Department of Chemistry, Peking University, Beijing 100871 (China)

(Received 11th June 1993; revised manuscript received 6th August 1993)

Abstract

Synthetic pigments in food can be simultaneously analysed qualitatively and quantitatively by using a spectrophotometric method combined with the branch and bound algorithm. This method does not require a preseparation of the pigments and the relative error for each component in mixed samples was less than 5%. Candy, jelly and soft drinks were analysed satisfactorily.

Keywords: UV–Visible spectrophotometry; Branch and bound algorithm; Food dyes; Foods; Pigments

Pigments are important food additives, and because natural pigments are expensive and it is difficult to stain and mix ideal colours, they are often replaced with synthetic pigments.

Synthetic pigments normally contain azo and aromatic ring structures. Pigments and their metabolic products in the body can be carcinogenic and can cause diarrhoea and deformation [1], so the components and contents of synthetic pigments in food are strictly limited in most countries and their determination in food is also receiving increasing attention.

Analyses of pigments usually proceed in two steps: first, preseparation of each pigment from the food by thin-layer chromatography [2], followed by quantitative analysis. These processes are complex and inconvenient, especially for large numbers of samples, and discoloration and hydrolysis in the first step may cause large errors (the relative error is often more than 10%). In recent years, dual-wavelength [3] and derivative spectrophotometry [4,5] have been used in determining mixing pigments also. However, in general, these methods are only suitable for the analysis of two-component mixtures. For multi-component mixtures, the determination errors increase rapidly with the number of components.

With the rapid development of chemometrics, methods such as factor analysis [6] and multiple linear regression [7] have been introduced for the determination of mixed pigments. These methods be used for the analysis of three- or multi-component systems, but with all of these methods one must know in advance the numbers and species of pigments in the food so that a corresponding training set of mixtures with known concentrations or corresponding absorptivity matrices of the pure components can be used. It is therefore troublesome to use these methods, so their practical use is greatly limited.

The aim of this study was to find a method that is simple, rapid, accurate and applicable to the analysis of mixed pigment systems. To solve

Correspondence to: W. Zeng, Department of Chemistry, Peking University, Beijing 100871 (China).

SSDI 0003-2670(93)E0478-P

this problem and to overcome the weaknesses in the above methods, the best subset selection method based on the branch and bound algorithm [8] was combined with a spectrophotometric method for the determination of pigments. This method has been used previously in chemical analysis [9,10]. Using this method, one only needs to analyse the absorption spectrum of one mixed sample, and then one can simultaneously evaluate which pigments are present and what their contents are. Using this method, one does not need to know the numbers and species of pigments in food in advance or to preseparate each pigment. Hence it is simple, rapid, accurate and suitable for the analysis of large numbers of samples. In this paper, the determination of pigments in candy, jelly and soft drink is described. All the results were satisfactory.

THEORY AND METHOD

According to the Lambert–Beer law, the general mathematical model of multi-component spectrophotometry is expressed as follows:

$$A = C_1E_1 + C_2E_2 + \cdots + C_mE_m + e$$

where A is the absorbance vector of mixtures at different wavelengths, E_i is the absorptivity vector of possibly present components i at different wavelengths, e is the error vector, which is a Gaussian distribution error of zero mean and uniform variance, C_i is the concentration of component i in the mixture (if a certain component is not present, its concentration is zero) and m is the number of possibly present components.

The branch and bound algorithm is based on the fundamental inequality

$$RSS(\mathrm{A}) \leqslant RSS(\mathrm{B})$$

where A is any set of independent variables and B is a subset of A. In other words, it is impossible to reduce the residual sum of squares (RSS) for a regression by deleting variables from that regression. The use of this inequality to restrict the number of subsets evaluated in a search for the best subset regression is illustrated by the five-variable inverse tree diagram in Fig. 1. The subset regression is computed by pivoting variables out of the regression from the top of the tree. The RSS for a node is obviously a lower bound for the RSS of its offspring. Hence, if we arrive at the node .2345, say, and had already computed one-, two- and three-variable regressions with RSS smaller than that for .2345, then one could ignore the fourteen descendents of .2345.

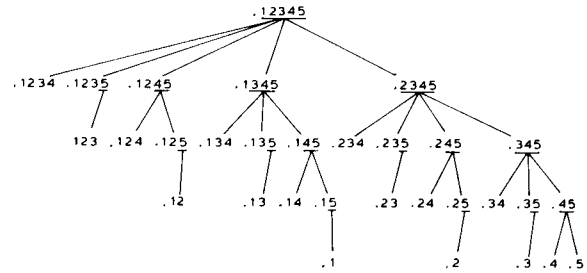

Fig. 1. Inverse tree.

In order to evaluate the importance of the variables and eliminate the effects of dimension and range of values, the data are autoscaled to zero mean and uniform variance by subtracting from each variable the mean and by dividing by the standard deviation.

In order to calculate effectively, a semi-sweep operator [11] is used.

Three common criteria (R^2, RMS_q and Cp) are used for determining the best subset (see Ref. 12).

EXPERIMENTAL

Instrumentation

Absorption spectra of the sample solution in 1.0-cm cuvettes were recorded every 4 nm in the range 360–680 nm on a Shimadzu UV-265 spectrophotometer. The program was written in TURBO PASCAL and run on an IBM PC-XT computer.

Preparation of standard solutions and mixed samples

Amaranth [FD&C Red 2, Colour Index (CI) 16185], Ponceau 4R (FD&C Red 1, CI 16255), Tartrazine (Tartar Yellow, CI 19140), Sunset Yellow FCF (FD&C Yellow 6, CI 15985), Indigo Carmine (FD&C Blue 2, CI 73015) and Brilliant

TABLE 1

Analytical results for mixed samples

No.	Concentration [a] ($mg\ l^{-1}$)						Analytical result ($mg\ l^{-1}$) and relative error (%)					
	A	B	C	D	E	F	A	B	C	D	E	F
1	0	14.46	0	0	0	18.31	0	14.46 ≪ 1%	0	0	0	18.38 < 1%
2	8.59	0	0	0	0	9.15	8.50 1%	0	0	0	0	9.27 1%
3	8.59	7.24	0	0	0	0	8.54 < 1%	7.16 1%	0	0	0	0
4	0	0	15.20	0	0	18.31	0	0	15.17 < 1%	0	0	18.45 < 1%
5	0	21.70	22.80	0	0	0	0	21.92 1%	23.02 1%	0	0	0
6	0	0	0	20.60	20.16	0	0	0	0	19.92 3%	20.28 < 1%	0
7	0	0	19.00	0	20.16	0	0	0	19.11 < 1%	0	20.26 < 1%	0
8	0	0	0	20.60	0	11.44	0	0	0	20.94 2%	0	11.67 2%
9	0	25.31	0	0	23.52	0	0	25.27 < 1%	0	0	23.36 1%	0
10	4.30	0	0	0	16.80	0	4.23 2%	0	0	0	17.15 2%	0
11	0	18.08	0	16.48	0	0	0	17.71 2%	0	16.58 < 1%	0	0
12	8.81	0	30.40	0	0	0	8.82 ≪ 1%	0	30.33 < 1%	0	0	0
13	8.59	0	7.60	0	0	0	8.56 < 1%	0	7.48 2%	0	0	0
14	8.59	0	0	8.24	0	0	8.58 ≪ 1%	0	0	8.21 < 1%	0	0
15	8.59	18.08	0	0	0	22.88	8.47 1%	18.11 ≪ 1%	0	0	0	23.07 1%
16	0	10.85	11.40	0	0	13.73	0 1%	10.95 2%	11.68	0	0	13.69 < 1%
17	8.59	18.08	19.00	0	0	0	8.53 < 1%	18.12 < 1%	19.27 1%	0	0	0
18	8.59	0	15.20	0	0	18.31	8.46 1%	0	15.04 1%	0	0	18.52 1%
19	4.30	25.31	0	0	16.80	0	4.37 2%	25.37 < 1%	0	0	17.33 3%	0
20	0	18.08	0	0	20.16	18.31	0	18.01 < 1%	0	0	19.57 3%	17.76 3%
21	4.30	0	0	0	11.96	22.88	4.26 1%	0	0	0	11.51 4%	22.68 1%
22	4.30	0	19.00	0	16.80	0	4.26 1%	0 ≪ 1%	19.01 < 1%	0	16.71	0
23	4.30	0	0	28.84	13.44	0	4.14 4%	0	0	28.84 ≪ 1%	13.41 < 1%	0
24	0	18.08	19.00	0	16.80	0	0	18.21 < 1%	19.13 < 1%	0	17.28 3%	0
25	0	0	19.00	20.60	23.52	0	0	0	18.31 4%	20.52 < 1%	23.41 < 1%	0
26	0	10.85	0	16.48	0	13.73	0	10.86 ≪ 1%	0	16.77 2%	0	13.62 < 1%

(Continued on p. 448)

TABLE 1 (continued)

No.	Concentration [a] (mg l^{-1})						Analytical result (mg l^{-1}) and relative error (%)					
	A	B	C	D	E	F	A	B	C	D	E	F
27	8.59	0	0	20.60	0	13.73	8.56 ≪1%	0	0	20.72 <1%	0	13.54 1%
28	0	0	0	16.48	13.44	18.31	0	0	0	16.65 1%	13.83 3%	18.44 <1%
29	8.59	18.08	0	16.48	0	0	8.54 <1%	18.08 ≪1%	0	16.79 2%	0	0
30	0	18.08	0	16.48	16.80	0	0	17.95 <1%	0	16.92 3%	17.15 2%	0
31	8.59	0	0	0	3.36	4.58	8.64 <1%	0	0	0	3.54 5%	4.73 3%
32	4.30	0	19.00	0	13.44	13.73	4.31 ≪1%	0	19.19 1%	0	13.47 <1%	13.57 1%
33	0	0	11.40	12.36	16.80	13.73	0	0	10.79 5%	12.36 ≪1%	16.77 <1%	14.31 4%
34	4.30	0	0	16.48	13.44	18.31	4.43 3%	0	0	16.47 ≪1%	13.27 1%	18.51 1%
35	6.45	0	11.40	12.36	0	13.73	6.45 ≪1%	0	11.76 3%	12.91 4%	0	12.97 5%
36	6.45	7.24	11.40	8.24	0	9.16	6.45 ≪1%	7.24 ≪1%	11.50 <1%	8.57 4%	0	8.99 2%
37	6.45	0	11.40	12.36	10.08	13.73	6.51 1%	0	11.57 1%	12.58 2%	10.05 <1%	13.37 3%
38	4.30	7.24	11.40	8.24	13.44	9.16	4.41 3%	7.41 2%	11.50 <1%	8.29 <1%	13.49 <1%	9.43 3%

[a] Added species A, B, C, D, E and F are Brilliant Blue CFCF, Tartrazine, Amaranth, Sunset Yellow FCF, Indigo Carmine and Ponceau 4R, respectively.

Blue CFCF (FD&C Blue 1, CI 42090) are food pigments for commercial use and were obtained from Shanghai Dye Chemical Institute. All pigments were weighed accurately and dissolved in deionized water and used to prepare mixed samples. According to Table 1, mixed samples were prepared by transferring accurately different kinds of pigments and adding 2 ml of 20% citric acid–sodium citrate buffer solution.

Pretreatment of foods

Candy. The candy was ground with a mortar and pestle, weighed accurately, dissolved in a certain volume of deionized water, gently warmed to dissolve completely and then 4–5 drops of HCl (6 mol l^{-1}) and 0.5 g of polyamide adsorbent were added. The mixture was stirred vigorously for polyamide to adsorb all pigments in solution. After filtration using a G3 glass filter, the adsorbent was washed in the following sequence on the filter: first with 30 ml of deionized water at 80°C several times, second with 10 ml of propanone, third with 300 ml of deionized water at 70°C several times and finally with 5% NaOH solution several times to desorb all pigments and obtain an alkaline solution of mixed pigments. To this solution 6 mol l^{-1} HCl was added dropwise until neutrality, then the solution was transferred into a 25-ml volumetric flask, 2 ml of 20% citric acid–sodium citrate buffer solution were added and the mixture was diluted to volume with deionized water.

Soft drink. The sample was transferred accurately, boiled and stirred continuously to remove carbon dioxide. Subsequent treatments were the same as above.

Jelly. The sample was weighed accurately, 20 ml of deionized water and 2 ml of 6 mol l^{-1} HCl were added and the mixture was warmed in a water-bath at 90°C with stirring to dissolve com-

pletely. After the solution had cooled, 5% NaOH solution was added dropwisely until the pH was 6.0, then 0.5 ml of 10.6% $K_4[Fe(CN)_6]$, 0.5 ml of 22% $Zn(OAc)_2$ and 5 ml of 95% ethanol were added separately and mixed completely in each step. After having been filtered and washed several times with deionized water, the filtrate was transferred to a 25-ml volumetric flask, then 2 ml of 20% citric acid–sodium citrate buffer solution were added and the solution was diluted to volume with deionized water.

Preparation of samples for the standard addition method. Candy and jelly were weighed accurately and warmed to dissolve with deionized water. Soft drink was transfered accurately. To all of the solutions accurate amounts of the appropriate pigments were then added. Subsequent treatments were the same as above.

TABLE 2

Analytical results for synthetic pigments in foods

Food	Colour	Addition [a] ($mg\ l^{-1}$)			Analytical result ($mg\ l^{-1}$)			Recovery (%)			Content ($mg\ kg^{-1}$)		
Candy	Red	F			F			F			F		
		0			9.24								
		9.15			18.21			98			11.55		
		B			B			B			B		
	Yellow	0			12.82								
		11.57			24.25			99			16.03		
		B		A	B		A	B		A	B		A
	Green	0		0	7.78		1.81						
		7.25		2.14	15.73		3.91	110		98	5.56		1.29
		A		C	A		C	A		C	A		C
	Purple	0		0	1.99		16.06						
		2.14		15.2	4.01		30.47	95		95	2.26		18.25
		A	B	F	A	B	F	A	B	F	A	B	F
	Blue	0	0	0	9.09	0.714	6.27						
		8.56	0.723	6.41	17.33	1.40	12.84	96	95	103	6.49	0.51	4.48
		A	B	F	A	B	F	A	B	F	A	B	F
	Brown	0	0	0	2.63	0.936	25.33						
		2.57	0.723	9.15	5.13	1.732	34.40	97	110	99	4.38	1.56	42.21
Jelly	Yellow	B			B			B			B		
		0			16.76								
		14.46			30.03			92			27.94		
		F			F			F			F		
	Red	0			16.54								
		13.73			30.24			100			20.67		
		B		A	B		A	B		A	B		A
	Green	0		0	14.96		1.43						
		13.02		1.28	28.85		2.80	107		107	23.37		2.23
		F		B	F		B	F		B	F		B
	Orange	0		0	5.15		15.29						
		4.58		9.40	10.37		24.14	114		94	4.95		14.70
Soft drink	Yellow	B			B			B					
		0			16.63								
		10.85			27.59			101					
		B	D	F	B	D	F	B	D	F			
	Orange	0	0	0	1.85	3.25	2.19						
		1.45	2.47	1.83	3.22	5.97	3.94	95	110	96			

[a] Added species A–F as in Table 1.

RESULTS AND DISCUSSIONS

Study of mixed samples

In China, there are only six kinds of synthetic pigments that are permitted for use in food. From Fig. 2, it can be seen that the absorption spectra of these six pigments are so similar that they greatly overlap and cannot be analysed separately. However, by using the branch and bound algorithm, one can determine the contents of the components of mixed pigments simultaneously without separation. To establish the analytical capability and reliability of the branch and bound algorithm, mixed samples with 1–6 components in all combinations were analysed. The results indicate that the species in the mixtures selected by the program were exactly as those mixed in advance, the species were neither mis-selected nor failed to be selected, and the relative error for each component in the mixed samples was less than 5%, which is in the range of relative errors of many spectrophotometric methods. In Fig. 3, curve 1 is for a mixed sample with six components (No. 38 in Table 1), and curve 2 is for a mixed sample with five components (No. 36 in Table 1). It can be seen that their absorption spectra are very similar, but both qualitative and quantitative results can be accurately obtained by analysing the two absorption spectra separately with the branch and bound algorithm.

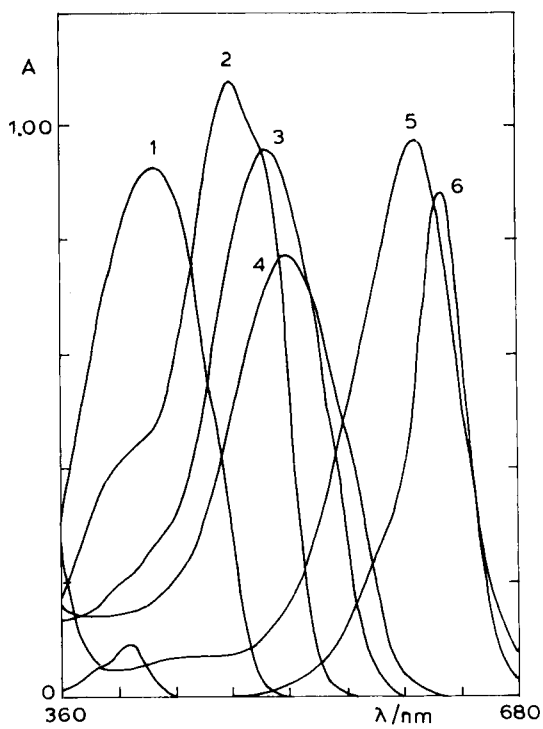

Fig. 2. Spectra of synthetic pigments. 1 = Tartrazine; 2 = Sunset Yellow FCF; 3 = Ponceau 4R; 4 = Amaranth; 5 = Indigo Carmine; 6 = Brilliant Blue CFCF.

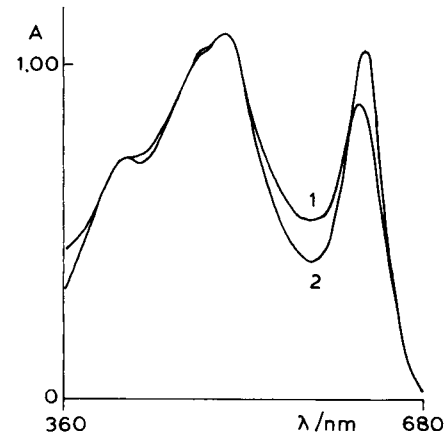

Fig. 3. Spectra of mixed samples: Curve 1 is for No. 36 in Table 1 and and curve 2 is for No. 38 in Table 1.

Determination of synthetic pigments in foods

About ten samples of three kinds of foods were analysed and the results are given in Table 2. To confirm the reliability of the food pretreatments, the standard addition method was also used, certain amounts of pigments being added accurately to the food samples before they were treated. The recoveries were close to 100%. The results show that the proposed method of food pretreatment is reliable.

Conclusion

The use of the branch and bound algorithm and a spectrophotometric method to determine the species and contents of synthetic pigments in food overcomes the weaknesses of other methods. This method does not require a preseparation of each pigment or a knowledge of the species and numbers of pigments in the food in advance. It only requires the measurement of the absorption spectrum of a mixed sample, then one

can simultaneously obtain the numbers, species and contents of all the pigments present in the food sample. It is simple, rapid and accurate and suitable for the analysis of large numbers of mixed samples.

This work was supported by the National Natural Science Foundation of China.

REFERENCES

1 T.-J. Ma and G.-F. Yang, New Edition Handbook of Food Additives, Agriculture Publishing House, Beijing, 1989, pp. 320–328.
2 H. Declercq and D.L. Massart, J. Chromatogr., 93 (1974) 243.
3 C.-R. Pan, Chin. J. Anal. Chem., 11 (1983) 218.
4 D.M. Marmion, Handbook of US Colorants for Foods, Drugs, and Cosmetics, Wiley, New York, 2nd edn., 1983, p. 36.
5 Y.-T. Chen and Z.-L. Zhuo, Chin. J. Anal. Chem. 16 (1988) 9.
6 T.-H. Li, C.-D. Wang and Z.-C. Gu, J. Tongji Univ., Nat. Sci. Ed., 18 (1990) 109.
7 Z.-M. Zhang, D.-X. Huang, G.-X. Mai and H. Sui, J. Shandong Univ., Nat. Sci. Ed., 24 (1989) 123.
8 G.M. Furnival and R.W. Wilson, Technometrics, 16 (1974) 499.
9 Y.-Z. Liang, Y.-L. Xie and R.-Q. Yu, Acta Chim. Sin., 48 (1990) 472.
10 W. Zeng, M.-H. Tu, K.-A. Li and S.-Y. Tong, Anal. Chim. Acta, 280 (1993) 173.
11 M.R. Schatzoff, S. Fienberg and R. Tsao, Technometrics, 10 (1968) 769.
12 J.D. Hwang and J.D. Winefordner, Prog. Anal. Spectrosc., 11 (1988) 209.

Analytica Chimica Acta, 284 (1993) 453–459
Elsevier Science Publishers B.V., Amsterdam

Sequential kinetic thermometric determination of the activity of peroxidase and catalase using catechol as substrate and inhibitor for their reaction with hydrogen peroxide

R. Forteza, E. Gómez, J.M. Estela and V. Cerdà

Department of Chemistry, Faculty of Sciences, University of the Balearic Islands, E-07071 Palma de Mallorca (Spain)

(Received 14th May 1993; revised manuscript received 30th July 1993)

Abstract

A kinetic thermometric method was developed for the determination of peroxidase by its catalytic effect on the oxidation of catechol by hydrogen peroxide. The proposed method allows the determination of peroxidase activity over the range 0.05–0.3 I.U. with an R.S.D. of 2.3%. The method was applied to the determination of peroxidase activity in prespiked matrices of animal origin (rat muscle and liver homogenates). The determination of the activity of peroxidase added to rat liver was found to be subject to a matrix effect that was corrected for by using an appropriate matrix-to-substrate concentration ratio. As catalase is thermometrically active at the same pH as peroxidase in its reaction with hydrogen peroxide and behaves similarly towards catechol when bound to a rat liver matrix, a procedure was developed for the sequential thermometric determination of the activity of both enzymes using catechol as substrate for peroxidase and inhibitor for catalase.

Keywords: Enzymatic methods; Kinetic methods; Thermometric methods; Catalase; Enzyme activity; Peroxidase

Horseradish peroxidase (EC 1.11.1.7) is an iron–porphyrin enzyme that catalyses the oxidation of a variety of electron donors by hydrogen peroxide [1;2]. The enzyme is also sufficiently stable so that its aqueous solutions can be stored at 5°C for over 1 year with no significant decrease in activity [3].

Peroxidase is primarily used as a secondary reagent for analytical purposes, usually in combination with a chromogenic donor for the determination of substrates that yield hydrogen peroxide in the main enzymatic reaction [4]. In immobilized form, peroxidase has been used for the determination of uric acid in a coupled reaction with uricase [5] and of L-phenylalanine in the presence of L-amino acid oxidase [6]. Also, various inorganic ions have been determined via their inhibitory effect on peroxidase activity [7].

Peroxidase is an enzyme of major analytical importance; current methods for measuring its activity are typically based on monitoring changes in the absorbance of a chromogenic donor (usually *o*-dianisidine, pyrogallol or guaiacol [4–10]). Biamperostatic [11] and potentiostatic [12] methods have also been used for this purpose.

Catalase activity can also be determined by using a variety of methods, among which that reported by Von Euler and Josephson [13], which employs H_2O_2 as substrate and measures unre-

Correspondence to: V. Cerdà, Department of Chemistry, Faculty of Sciences, University of the Balearic Islands, E-07071 Palma de Mallorca (Spain).

SSDI 0003-2670(93)E0464-I

acted permanganate, is worthy of special note. Also, Jolles [14] determined unreacted H_2O_2 by addition of KI and ammonium molybdate, followed by titration with thiosulphate ion. This method is applicable to homogenates, with which the permanganate method performs poorly owing to the reduction of MnO_4^- by material in the homogenate. Feinstein [15] developed a method that uses perborate instead of H_2O_2. Walker [16] determined catalase activity polarographically.

The advantages of using enthalpimetric or calorimetric procedures for enzyme assays have been discussed elsewhere [17–20]. The most salient feature of such procedures is their reliance on a intrinsic property of all chemical reactions, viz., the enthalpy of reaction. Accordingly, the main enzymatic reaction can be monitored without the need for a complex coupling procedure. As an example, an enthalpimetric method for measuring horseradish peroxidase activity [12] based on the enzyme-catalysed oxidation of iodide ion by hydrogen peroxide allows the determination of peroxidase activity in the range 2–79 I.U. with an R.S.D. of 3%.

This paper reports a kinetic thermometric method for the determination of horseradish peroxidase activity based on the enzymatic–catalytic oxidation of catechol by hydrogen peroxide. The method was used for animal homogenates and in the presence of beef liver catalase. Because catalase could not be removed from the peroxide-active fraction, whilst preserving peroxidase activity, the accurate determination of peroxidase activity was difficult [21]. The presence of peroxidase was routinely shown by means of the guaiacol reaction. It was found that the activity of beef liver catalase was inhibited in the presence of catechol, which allowed a routine procedure to be developed for the sequential determination of peroxidase and catalase activity in the absence and presence of an adequate amount of catechol.

EXPERIMENTAL

Apparatus

The temperature-monitoring system used consisted of a highly responsive thermometric thermistor with a nominal resistance of 100 kΩ at 25°C, a Wheatstone bridge furnished with a stabilized power supply and an x–t recorder with a sensitivity of 0.015°C mV^{-1} on a full scale of 2–5 mV (25 cm) that was operated at a speed of 1 cm min^{-1} in the determinations of peroxidase and catalase activity by the initial-rate method, i.e., by measuring dT/dt tangents (T = temperature, t = time) along the initial linear portions of the kinetic thermometric curves. In using the direct injection enthalpimetric method to determine catalase activity, the recorder full scale spanned 20 mV and a chart speed of 2 cm min^{-1} was used. The thermometric set-up employed has been described in detail elsewhere [22]. Hydrogen peroxide was placed in the thermometric cell with the aid of a syringe after thermal equilibrium had been reached. A paddle stirrer actuated by a synchronous motor was used to ensure thorough mixing of the reactants.

A Hewlett-Packard HP 8452A diode-array spectrophotometer furnished with quartz cuvettes of 1 cm path length was also used. The software needed to acquire and process spectra and kinetic curves at each point along the curves was developed by the authors.

Reagents

The solutions used in the experiments included the following: 1% catechol, prepared from commercially available reagent (Sigma, St. Louis, MO) in distilled water immediately prior to use in order to avoid autoxidation; 30% and 0.15% hydrogen peroxide, prepared from Probus analytical-reagent grade chemical; 0.1 M potassium phosphate buffer (pH 7); horseradish peroxidase (POD, EC 1.11.1.7), from Boehringer (Mannheim) (batch No. 12003025-50; ca. 200 I.U. mg^{-1} lyophilizate, 25°C; guaiacol and hydrogen peroxide as substrates); Beef liver catalase (EC 1.11.1.6), from Boehringer (batch No. 13457929-26; ca. 65 000 I.U. mg^{-1} suspension, 25°C; hydrogen peroxide as substrate); stock peroxidase solution in 3.2 M ammonium sulphate; and stock catalase solution in distilled, deionized water.

The first three and the distilled water used were kept in the laboratory where thermometric measurements were made, which was ther-

mostated at 22 ± 1°C. The enzyme solutions were stored at 4°C.

Spectrophotometric determination of peroxidase activity

In a spectrophotometric quartz cuvette of 1-cm path length and 4-ml capacity, place 3 ml of 0.1 M phosphate buffer (pH 7.0), 50 μl of 0.22% catechol, 50 μl of enzyme solution with an activity between 0.05 and 0.4 I.U. and 40 μl of 0.03% H_2O_2 solution. Ten seconds after the hydrogen peroxide is added, record the change in the absorbance at 388 nm as a function of time for 2 min. Finally, calculate activities from the slopes of the initial linear portions of the kinetic curves obtained.

Thermometric determinations

Kinetic determination of peroxidase activity. In a 75-ml polystyrene cuvette place 10 ml of 0.1 M phosphate buffer (pH 7.0), 10 ml of 1% catechol solution and the sample volume required to give a peroxidase activity between 0.05 and 0.3 I.U. and dilute to 49 ml with deionized water. As soon as thermal equilibrium has been reached, used a syringe to inject 1 ml of 0.15% H_2O_2 solution into the cuvette and record the temperature change as a function of time. Finally, calculate activities from the slopes of the initial straight portions of the kinetic curves.

Sequential determination of peroxidase and catalase activity. Mixtures containing catalase and peroxidase are first analysed for catalase activity by direct injection enthalpimetry in the absence of catechol. For this purpose, fill a polystyrene cuvette with a sample volume providing a catalase activity of 20–100 I.U. and 10 ml of 0.1 M phosphate buffer (pH 7.0) plus the volume of deionized water needed to make the volume up to 49 ml. As soon as thermal equilibrium has been reached, inject 1 ml of 30% H_2O_2 solution into the cuvette and record the kinetic thermometric curves for the reaction between catalase and hydrogen peroxide, from which activities are related to the overall temperature rise produced.

The peroxidase activity is determined in the presence of catechol as in the kinetic determination, with the constraint that the catalase activity must be lower than 260 I.U.

Preparation of matrices of animal origin

Animal matrices were obtained from 130-day-old female Wistar rats weighing 250–270 g which were killed by cervical dislocation. Rat liver and muscle homogenates were prepared in a Potter–Elvehjem vessel by using 15% of 0.1 M phosphate buffer (pH 7.0). The homogenates were subsequently centrifuged at 17000 *g* at 5°C for 10 min.

RESULTS AND DISCUSSION

Optimization of experimental conditions for kinetic thermometric determination of peroxidase activity

The influence of parameters such as pH, substrate and H_2O_2 concentrations and enzyme activity on the reaction kinetics was investigated. The pH was arbitrarily adjusted to 7.0 with 0.1 M phosphate buffer, which is one of the most commonly employed buffers in the determination of peroxidase using substrates similar to catechol [23]. Figures 1 and 2 show the effect of the hydrogen peroxide and catechol concentration,

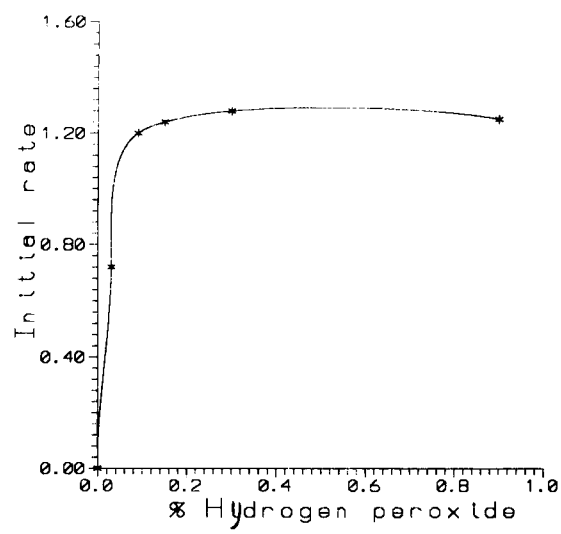

Fig. 1. Influence of H_2O_2 concentration on the initial rate in the kinetic thermometric determination of peroxidase activity using catechol as substrate. Sensitivity = 2 mV full-scale; chart speed = 1 cm min^{-1}; [catechol] = 0.04%; 0.25 I.U. peroxidase; pH = 7; V_f = 50 ml.

respectively, on the slopes of the thermometric curves. As can be seen, typical saturation curves with portions where the kinetics can be assumed to be of pseudo-zero order in substrate and H_2O_2 were obtained. In view of the results, 10 ml of 1% catechol with injection of 1 ml of 0.15% H_2O_2 were selected to implement the proposed method. It is worth noting that volumes of 1% catechol solution above 15 ml in the final volume (50 ml) yielded poor results owing to the presence of a sharply curved initial segment on the kinetic curves that precluded correct determination of the limits of the linear portion; this effect can be ascribed to the instability of the catechol solution arising from its rapid autoxidation at the working pH and temperature.

Under the chosen operational conditions, the initial rate and peroxidase activity were found to be linearly related over the range 0.05–0.3 I.U. ($dT/dt = 0.0210A_{POD} - 0.0001$, $r^2 = 0.9965$, $n = 4$, where A_{POD} is peroxidase activity in I.U. and dT/dt is in °C min^{-1}) with R.S.D. = 2.3% ($n = 4$, for 0.2 I.U.).

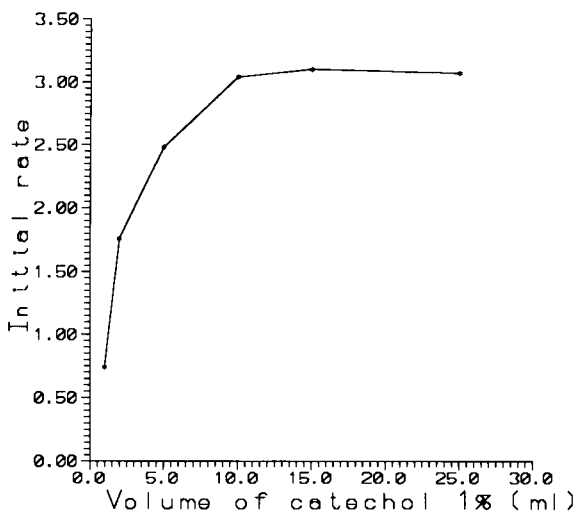

Fig. 2. Influence of catechol concentration on the initial rate in the kinetic thermometric determination of peroxidase activity using catechol as substrate. Sensitivity = 2 mV full-scale; chart speed = 1 cm min^{-1}; 0.13 I.U. peroxidase; pH = 7; V_f = 50 ml; $[H_2O_2]$ = 0.15% (1 ml).

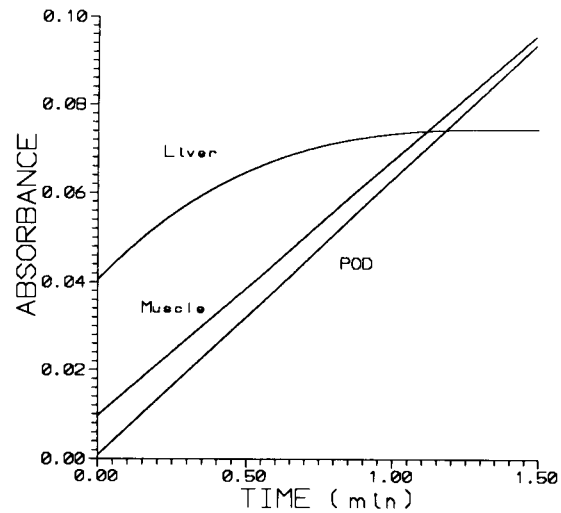

Fig. 3. Kinetic spectrophotometric curves obtained from spiked animal homogenates and a peroxidase standard of the same activity (0.2 I.U.) using catechol as substrate under the conditions described under Experimental.

Study of the applicability of the proposed kinetic thermometric procedure for the determination of the peroxidase added to animal homogenates

Application of the proposed spectrophotometric method to rat muscle and liver homogenates revealed inadequate peroxidase activity to be determined spectrophotometrically. Consequently, peroxidase was added to the homogenates in order to check whether the recoveries obtained in the spectrophotometric determinations were consistent with the added activities. The slopes of the respective kinetic curves obtained in the presence and absence of matrix were used as the recovery-related parameter. The recoveries obtained in both matrices using 20 μl of homogenate were all higher than 100%. However, as can be seen from Fig. 3, which shows the kinetic spectrophotometric curves obtained from a peroxidase standard and the spiked samples, the rat liver sample yielded a kinetic curve that reached saturation more quickly than did those of the peroxidase standard and the rat muscle matrix. This suggests that the liver matrix removes some of the hydrogen peroxide from the medium, so saturation of the kinetic curve occurs sooner. In any case, rat liver homogenates still allow peroxidase activity

to be determined provided that an adequate sample volume or a higher H_2O_2 concentration is used in order to ensure pseudo-zero-order kinetics in this last reactant.

A similar thermometric experiment revealed that the recoveries were correct for the rat muscle matrix although not exactly correct for the liver matrix when certain sample volumes were used. Further investigation of the liver matrix showed that injection of hydrogen peroxide caused an exothermic reaction that was completely inhibited by the presence of catechol. These findings, together with the spectrophotometric observations, appear to indicate that the liver matrix hosts an inhibition reaction whereby catechol is removed from the enzymatic action of the peroxidase in the medium, which may result in kinetics of order other than pseudo-zero in catechol. In addition, the catechol concentration may not be high enough to inhibit the reaction completely and the kinetics may not be pseudo-zero order with respect to H_2O_2. All this depends on the sample volume used. In summary, the kinetic process is influenced by the concentration ratios of matrix interferents, catechol, hydrogen peroxide and peroxidase. A combination of these effects resulted in incorrect recoveries.

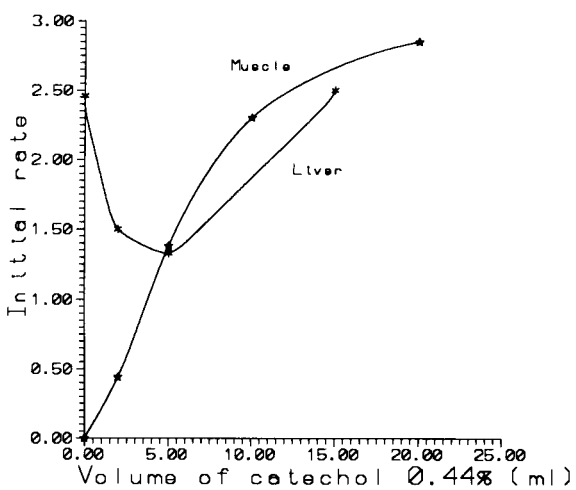

Fig. 4. Influence of catechol concentration on the initial rate of the kinetic thermometric curves obtained from animal homogenates (50 μl) spiked with 0.25 I.U. of peroxidase. Sensitivity = 2 mV full-scale; chart speed = 1 cm min^{-1}; pH = 7; V_f = 50 ml; $[H_2O_2]$ = 0.15% (1 ml).

In order to check the above assumptions, the experiments summarized in Fig. 4, which shows the tangents of the kinetic curves for the two peroxidase-spiked matrices as a function of the concentration of catechol (substrate), were carried out. As can be seen, whereas the muscle matrix behaved similarly to the peroxidase standard (Fig. 2), i.e., it yielded a typical saturation curve, the liver matrix conformed to the above-described deviant behaviour. Taking into account the previous reasoning and the fact that the catechol concentration in the medium should not exceed that in 15 ml of a 1% solution (for a final volume of 50 ml), homogenate volumes below 50 μl were chosen for the reasons given in describing the optimization of the experimental conditions. Such volumes always yielded 100% recoveries.

Study of the feasibility of the sequential kinetic thermometric determination of catalase and peroxidase activity

The interfering effect of the rat liver matrix led to a consideration of the potential presence of a catalase-like enzyme in the matrix. If this were indeed the case, the thermometric activity of catalase in its action on hydrogen peroxide could be exploited to develop a method for the sequential determination of peroxidase and catalase activity by monitoring the concentration of catechol, which would act as an inhibitor for catalase and a substrate for peroxidase.

Figure 5 shows the initial rates obtained thermometrically for a mixture of peroxidase and catalase as a function of the volume of catechol solution used. As can be seen, the graph is very similarly shaped to that obtained for the rat liver homogenate and, as expected, catalase activity was inhibited by controlling the catechol concentration. However, an experiment carried out to determine the extent of inhibition produced by catechol revealed that the effect on the overall temperature jump was much greater than that on the slope of the initial portion of the thermometric curve; in fact, inhibiting the enzyme action of 260 I.U. of catalase required the use of 5 ml of 1% catechol solution. The effect of adding various amounts of catalase (between 0 and 520 I.U.)

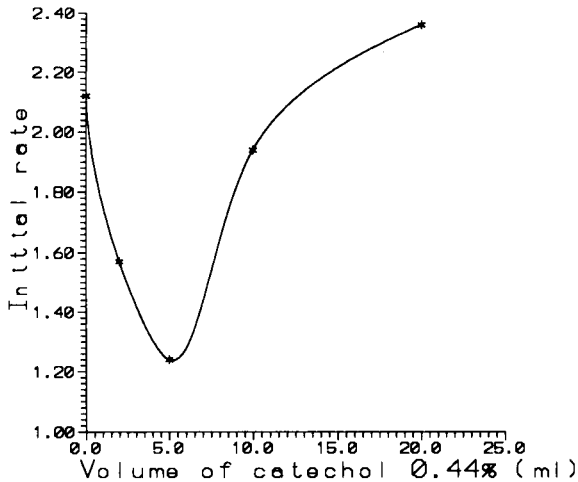

Fig. 5. Influence of catechol concentration on the initial rate of the kinetic thermometric curves obtained from a mixture of 0.10 I.U. peroxidase and 200 I.U. catalase. Sensitivity = 2 mV full-scale; chart speed = 1 cm min^{-1}; pH = 7; V_f = 50 ml; $[H_2O_2]$ = 0.15% (1 ml).

on the determination of peroxidase (0.25 I.U.) by the proposed kinetic thermometric method was also studied. Table 1 gives the initial rates found and the errors in each instance. As expected, addition of 130 I.U. resulted in an acceptably small error that was similar to the reproducibility of the method.

According to the above observations, implementation of the sequential thermometric method for the determination of catalase and peroxidase activity should first involve a determination of the catalase activity in the sample and then the selection of an adequate sample volume to ensure that its activity is fully inhibited by the action of catechol and hence that the peroxidase activity can be subsequently determined by using the proposed kinetic thermometric method.

The thermometric determination of catalase activity was approached in two ways. One involved carrying it out at the same pH and H_2O_2 concentration as in the peroxidase method. In this way, well defined kinetic curves are obtained with an initial linear portion that allows accurate calculation of the initial rate. Under these conditions, one can determine catalase activity over the range 40–260 I.U. However, the sensitivity of the method can be increased by increasing the hydrogen peroxide concentration, which also increases the initial rate. Thus, adding an adequate volume of 30% H_2O_2 solution allows a wider recorder scale (20 mV full-scale) to be used and hence lower catalase activities to be determined by calculating them from the overall temperature rise rather than the initial rate. The catalase activity was found to be linearly related to the temperature rise between 20 and 100 I.U. ($\Delta T = 0.00153 A_{CAT} + 0.0171$, $r^2 = 0.9897$, $n = 4$). Table 2 gives the results obtained in studying the reproducibility of the proposed method and its tolerance to various peroxidase activities, both of which are acceptable.

TABLE 1

Tolerance of the kinetic thermometric method for the determination of peroxidase activity to the presence of various catalase activities [a]

Sample composition	Initial rate (°C min^{-1}) [b]	Error (%)
0.26 I.U. peroxidase	0.00537 ± 0.00003	–
0.26 I.U. peroxidase + 130 I.U. catalase	0.00549 ± 0.00006	2.2
0.26 I.U. peroxidase + 260 I.U. catalase	0.00573 ± 0.00015	6.7
0.26 I.U. peroxidase + 520 I.U. catalase	0.00618 ± 0.00006	15

[a] Sensitivity = 5 mV full-scale; chart speed = 1 cm min^{-1}; pH = 7.0; [catechol] = 1% (10 ml); V_f = 50 ml; $[H_2O_2]$ = 0.15% (1 ml). [b] Mean ± S.D. (n = 3).

TABLE 2

Reproducibility and tolerance of the direct injection enthalpimetric method for the determination of catalase activity [a]

Sample composition	Δ [Temperature (°C)] [b]
20 I.U. catalase	0.0504 ± 0.0012
20 I.U. catalase + 0.30 I.U. peroxidase	0.0504 ± 0.0012
20 I.U. catalase + 1.22 I.U. peroxidase	0.0492 ± 0.0024
40 I.U. catalase	0.0804 ± 0.0036
40 I.U. catalase + 4.88 I.U. peroxidase	0.0780 ± 0.0024

[a] Sensitivity = 20 mV full-scale; chart speed = 2 cm min^{-1}; pH = 7.0; $[H_2O_2]$ = 30% (1 ml). [b] Mean ± S.D. (n = 3).

Conclusions

The results obtained in this work show the feasibility of determining peroxidase activity by using a kinetic thermometric method and catechol as substrate. Thermometric monitoring of the kinetics is preferable to other instrumental alternatives (e.g., spectrophotometry) as it allows the sequential determination of catalase activity by its reaction with hydrogen peroxide, which is inhibited in the presence of catechol, so the enzyme does not interfere with the thermometric determination of peroxidase.

The authors are grateful to the DGICyT (Spanish Council for Research in Science and Technology) for financial support granted for the realization of this work as part of Project PS89-0146.

REFERENCES

1 H. Theorell, in J.B. Summer and K. Myrback (Eds.), The Enzymes, Vol. 2 Pt. I, Academic, New York, 1951, p. 397.
2 B. Chance, in J.B. Summer and K. Myrback (Eds.), The Enzymes, Vol. 2 Pt. I, Academic, New York, 1951, p. 428.
3 Worthington Enzyme Manual, Worthington Biochemical, Freehold, NJ, 1977, p. 67.
4 G.G. Guilbault, Enzymatic Methods of Analysis, Pergamon, Oxford, 1970.
5 S.W. Kiang, J.W. Kuan and G.G. Guilbault, Clin. Chem., 22 (1976) 1378.
6 G. Guilbault and G. Nagy, Anal. Lett., 6 (1973) 301.
7 G.C. Guilbault, P. Brignac and M. Zimmer, Anal. Chem., 40 (1968) 190.
8 J. Putter, in H.U. Bergmeyer (Ed.), Methods of Enzymatic Analysis, Vol. 2, Academic, New York, 1974, p. 685.
9 J. Putter, Habilitationsarbeit, Universität Bonn, Bonn, 1964.
10 Peroxidase Assay Data Sheet, Sigma, St. Louis, MO, 1993.
11 S. Pantel and H. Weisz, Anal. Chim. Acta, 89 (1977) 47.
12 J.K. Grime and K.R. Lockhart, Anal. Chim. Acta, 106 (1979) 251.
13 H. von Euler and K. Josephson, Justus Liebigs Ann. Chem., 452 (1927) 158.
14 A. Jolles, Münch. Med. Wochenschr., 51 (1904) 2083.
15 R.N. Feinstein, J. Biol. Chem., 180 (1949) 1197.
16 B.S. Walker, Proc. Fed. Am. Soc. Exp. Biol., 1 (1942) 140.
17 C.D. McGlothlin and J. Jordan, Anal. Chem., 47 (1975) 1479.
18 C.D. McGlothlin, J.K. Grime and J. Jordan, presented at the Symposium on New Approaches to the Routine Determination of Serum Enzymes, American Chemical Society, New York, April 1976, paper No. 71.
19 K. Levin, Clin. Chem., 23 (1977) 929.
20 C. Spink and I. Wadso, Methods Biochem. Anal., 23 (1976) 1.
21 S.P. Colowick and N.O. Kaplan, Methods Enzymol., 2 (1955) 792.
22 R. Forteza and V. Cerdà, Anal. Chem., 58 (1986) 453.
23 H.U. Bergmeyer, Methods of Enzymatic Analysis, Verlag Chemie, Weinheim, 3rd edn., 1983, p. 267.

Calendar of forthcoming meetings

★ *indicates new or amended entry*

★ ***January 16–21, 1994***
Ventura, CA, USA
Gordon Research Conference on Electrochemistry. *Contact:* Gordon Research Conferences, Gordon Research Center, University of Rhode Island, Kingston, RI 02881-0801, USA.

January 25–28, 1994
San Diego, CA, USA
3rd International Symposium on Automation, Robotics and Artificial Intelligence applied to Analytical Chemistry and Laboratory Medicine. *Contact:* SCITEC, av. de Provence 20, 1000 Lausanne 20, Switzerland. Tel.: +41 21 624 1533; Fax: +41 21 624 1549.

January 31–February 3, 1994
San Diego, CA, USA
HPCE '94. 6th International Symposium on High Performance Capillary Electrophoresis. *Contact:* Shirley Schlessinger, HPCE '94 Symposium Manager, 400 East Randolph Street, Suite 1015, Chicago, IL 60601, USA. Tel.: +1 312 527-2011.

February 13–16, 1994
San Francisco, CA, USA
2nd International Glycobiology Symposium: Current Analytical Methods. *Contact:* Paddy Batchelder, P.O. Box 370, Pleasanton, CA, USA. Tel.: +1 510 426-9601; Fax: +1 510 846-2242.

★ ***February 15–19, 1994***
Salt Lake City, UT, USA
2nd Conference on Optical Probes of Conjugated Polymers and Fullerenes. *Contact:* Conferences & Institutes, University of Utah, 2174 Annex Building, Salt Lake City, UT 84112, USA. Tel.: +1 801 581-5809; Fax: +1 801 581-3165.

February 21–25, 1994
Prague, Czech Republic
International Symposium and Exhibition on Fibre Optic Sensors and Environmental Monitoring. *Contact:* Direct Communications GmbH, Att. Ms. Karin Burger, Xantener Strasse 22, D-1000 Berlin 15, Germany. Tel.: +49 30-8815047; Fax: +49 30-8822028; Telex: 181 479 speco d.

February 22–25, 1994
Antwerp, Belgium
HTC 3. Third International Symposium on Hyphenated Techniques in Chromatography. *Contact:* Royal Flemish Chemical Society (KVCV), Working Party on Chromatography, c/o Dr. R. Smits, BASF Antwerpen N.V., Central Laboratory, Scheldelaan, B-2040 Antwerp, Belgium. Tel.: +32 3 568 2831; Fax: +32 3 568 3250; Telex: 31047 basant b. *(Further details published in Vol. 268, No. 2).*

February 23–25, 1994
Antwerp, Belgium
Workshops and short courses to precede HTC 3, Third International Symposium on Hyphenated Techniques in Chromatography. *Contact:* Royal Flemish Chemical Society (KVCV), Working Party on Chromatography, c/o Dr. R. Smits, BASF Antwerpen N.V., Central Laboratory, Scheldelaan, B-2040 Antwerp, Belgium. Tel.: +32 3 568 2831; Fax: +32 3 568 3250; Telex: 31047 basant b.

February 28–March 4, 1994
Chicago, IL, USA
PITTCON '94. Pittsburgh Conference on Analytical Chemistry and Applied Spectroscopy. *Contact:* Pittsburgh Conference, Suite 332, 300 Penn Center Blvd., Pittsburgh, PA 15235-9962, USA.

March 27–30, 1994
Galveston, TX, USA
International Federation of Automatic Control (IFAC) Symposium on Modeling and Control in Biomedical Systems. *Contact:* IFAC Biomedical Symposium, University of Texas Medical Branch, Box 55176, Galveston, TX 77555-5176, USA. Tel.: +1 409 770-6628 or 770-6605; Fax: +1 409 770-6825.

April 10–13, 1994
Mandelieu La Napoule, France
ANATECH 94. 4th International Symposium on Analytical Techniques for Industrial Process Control. *Contact:* ANATECH 94 Secretariat, Elsevier Advanced Technology, Mayfield House, 256 Banbury Road, Oxford OX2 7DH, UK. Tel.: +44 865 512242; Fax: +44 865 310981.

★ ***April 12–15, 1994***
Liverpool, UK
The Royal Society of Chemistry Annual Chemical Congress. RSC 94. *Contact:* Dr. John F. Gibson, Secretary (Scientific), The Royal Society of Chemistry, Burlington House, London W1V 0BN, UK. Tel.: +44 71 437-8656; Fax: +44 71 437-8883.

★ ***April 18–22, 1994***
Lorne, Australia
6th International Conference on Near Infrared Spectroscopy. *Contact:* NIR-94, Peter Flinn, Pastoral and Veterinary Institute, Mt. Napier Road, Private Bag 105, Hamilton, Victoria 3300, Australia. Tel.: +61 55 730-915; Fax: +61 55 711-523.

April 19–22, 1994
Munich, Germany
ANALYTICA 94. 14th International Trade Fair for Biochemical and Instrumental Analysis with International Conference. *Contact:* Bernhard Schauder, ANALYTICA Press Office, Münchener Messe- und Ausstellungs-Gesellschaft mbh, Messegelénde, Postfach 12 10 09, D-8000 Munich 12, Germany. Tel.: +49 89-51070; Fax: +49 89-5107506; Telex: 5212086 ameg d.

April 19–21, 1994
Manchester, UK
CHEMSPEC EUROPE 94. Exhibition (April 20–21) and Symposium (April 19–20). *Contact:* Jane Malcolm-Coe, PR

& Publicity Manager, FMJ International Publications Ltd., Queensway House, 2 Queensway, Redhill, Surrey RH1 1QS, UK. Tel.: +44 737 768611; Fax: +44 737 761685.

May 8-13, 1994
Minneapolis, MN, USA
HPLC '94. 18th International Symposium on High Performance Liquid Chromatography. *Contact:* Janet E. Cunningham, Barr Enterprises, P.O. Box 279, Walkersville, MD 21793, USA. Tel.: (301) 898-3772; Fax: (301) 898-5596.

★ ***May 16–19, 1994***
Ottawa, Ont., Canada
24th International Symposium on Environmental Analytical Chemistry. *Contact:* Dr. M. Malaiyandi, CAEC, Chemistry Department, Carleton University, Ottawa, Ont., Canada K1S 5B6; Fax: +1 613 788-3749; or Dr. J.F. Lawrence, Food Research Division, Banting Research Centre, Health and Welfare Canada, Ottawa, Ont., Canada K1A 0L2; Fax: +1 613 941-4775.

May 22–26, 1994
Venice, Italy
ESEAC '94. 5th European Conference of Electroanalysis. *Contact:* Prof. Salvatore Daniele, Department of Physical Chemistry, The University of Venice, Calle Larga S. Marta 2137, I-30123 Venice, Italy. Tel. +39 41 5298503; Fax: +39 41 5298594.

★ ***May 29–June 3, 1994***
Chicago, IL, USA
42nd ASMS Conference on Mass Spectrometry and Allied Topics. *Contact:* Judith A. Sjoberg, ASMS, 815 Don Caspar, Santa Fe, NM 87501, USA. Tel.: +1 505 989-4517; Fax: +1 505 989-1073.

May 30–June 1, 1994
Bergen, Norway
SSIR 94. Scandinavian Symposium on Infrared and Raman Spectroscopy. *Contact*: Dr. Alfred A. Christy, Department of Chemistry, Allegt. 41, University of Bergen, N-5007 Norway. Tel.: +47 55 213363; Fax: +47 55 329058); or Laila Kyrkjebø, Department of Chemistry, University of Bergen. Tel.: +47 55 213342.

May 30–June 3, 1994
Nagoya, Japan
Pyrolysis 94. 11th International Symposium on Analytical and Applied Pyrolysis. *Contact:* Dr. H. Ohtani, Department of Applied Chemistry, Nagoya University, Nagoya 464-01, Japan. Tel.: +81 52-7815111, ext. 4664/3560; Fax: +81 52-7814895.

★ ***May 31–June 3, 1994***
Bruges, Belgium
Second International Symposium on Hormone and Veterinary Drug Residue Analysis. *Contact:* Prof. C. van Peteghem, Symposium Chairman, Faculty of Pharmaceutical Sciences, University of Ghent, Harelbekestraat 72, B-9000 Ghent, Belgium. Tel.: +32 9-221 8951 ext. 235; Fax: +32 9-220 5243.

June 1–3, 1994
New Orleans, LA, USA
Biosensors '94. 3rd World Congress on Biosensors. *Contact:* Kay Russell, Elsevier Advanced Technology, Mayfield House, 256 Banbury Road, Oxford OX2 7DH, UK. Tel.: +44 865 512242; Fax: +44 865 310981.

June 5–7, 1994
Bruges, Belgium
VIth International Symposium on Luminescence Spectrometry in Biomedical Analysis — Detection Techniques and Applications in Chromatography and Capillary Electrophoresis. *Contact:* Prof. Dr. Willy R.G. Baeyens, Symposium Chairman, University of Ghent, Pharmaceutical Institute, Dept. of Pharmaceutical Analysis, Lab. of Drug Quality Control, Harelbekestraat 72, B-9000 Ghent, Belgium. Tel.: +32 9-2214175; Fax: +32 9-2218951.

June 8–11, 1994
Toledo, Spain
Flow Analysis VI. 6th International Conference on Flow Analysis. *Contact:* M. Valcarcel or M.D. Luque de Castro, Flow Analysis VI, Departmento de Química Analítica, Facultad de Ciencias, E-14004 Córdoba, Spain. Tel.: +34 57 218616; Fax: +34 57 218606.

★ ***June 12–15, 1994***
Washington, DC, USA
1994 PREP Symposium and Exhibit. International Symposium on Preparative Chromatography. *Contact:* 1994 PREP Symposium Manager, c/o Barr Enterprises, 10120 Kelly Road, P.O. Box 279, Walkersville, MD 21793, USA. Tel.: +1 301 898-3772; Fax: +1 301 898-5596.

June 13–15, 1994
Lund, Sweden
FFF'94. 4th International Symposium on Field-Flow Fractionation. *Contact:* The Swedish Chemical Society, The Analytical Section, Wallingatan 24, 3tr, S-11124 Stockholm, Sweden. Fax: +46 46104525.

June 19–24, 1994
Bournemouth, UK
20th International Symposium on Chromatography. *Contact:* The Executive Secretary, Chromatographic Society, Suite 4, Clarendon Chambers, 32 Clarendon Street, Nottingham NG1 5JD, UK. Tel.: +44 603-500596; Fax: +44 602-500614.

June 20–22, 1994
Valladolid, Spain
ESOPS-11. 11th European Symposium on Polymer Spectroscopy. *Contact:* J.M. Pastor, ESOPS-11, Física de la Materia Condensada, Facultad de Ciencias, Universidad de Valladolid, 47005 Valladolid, Spain. Tel.: +34 83 423194; Fax: +34 83 423192 or 423013.

★ ***June 20–23, 1994***
Ringe, NH, USA
2nd Oxford Conference on Spectroscopy. *Contact:* Dr. Art Springsteen, Labsphere Inc., P.O. Box 70, North Sutton, NH 03260, USA. Tel.: +1 603 927-4266; or Dr. C. Burgess, Glaxo Manufacturing Servies, Harmire Road, Barnard Castle, Co. Durham, DL12 8DT, UK. Tel. +44 833-692490; Fax: +44 833-692774.

June 28–29, 1994
Singapore
CHEMSPEC ASIA 94. Exhibition and Conference. *Contact:* Jane Malcolm-Coe, PR & Publicity Manager, FMJ International Publications Ltd., Queensway House, 2 Queensway, Redhill, Surrey RH1 1QS, UK. Tel.: +44 737 768611; Fax: +44 737 761685.

★ ***July 10–15, 1994***
Merseburg, Germany
16th International Symposium on the Organic Chemistry of Sulfur. *Contact:*

Dr. Schukat, Department of Chemistry, Martin Luther University Halle-Wittenberg, Geusaer Straße, D-06217 Merseburg, Germany. Tel.: +49 3461/462086; Fax: +49 3461/462370.

July 11–14, 1994
Norwich, UK
Spectroscopy Across the Spectrum IV: Techniques and Applications of Analytical Spectroscopy. *Contact:* Dr. D.L. Andrews, Hon. Secretary, Spectroscopy Across the Spectrum IV, School of Chemical Sciences, University of East Anglia, Norwich NR4 7TJ, UK.

July 20–22, 1994
Hull, UK
7th Biennial National Atomic Spectroscopy Symposium. *Contact:* Dr. Steve Haswell, School of Chemistry, University of Hull, Hull HU6 7RX, UK. Tel: +44 482-465469.

July 31–August 5, 1994
Ottawa, Ont., Canada
8th International Symposium on Molecular Recognition and Inclusion. *Contact:* Mrs. Hguette Morin-Dumais, 8th ISMRI, Steacie Institute for Molecular Sciences, National Research Council Canada, Room 1157, 100 Sussex Drive, Ottawa, Ont., Canada K1A 0R6. Tel.: +1 613 990-0936; Fax: +1 613 954-5242; E-mail: ismri@ned1.sims.nrc.ca.

July 1994
Maastricht, The Netherlands
International Chemometrics Research Meeting. *Contact:* Laboratory for Analytical Chemistry, Faculty of Science, Catholic University of Nijmegen, Toernooiveld 1, 6525 ED Nijmegen, The Netherlands.

August 2–6, 1994
Changchun, P.R. China
The Second Changchun International Symposium on Analytical Chemistry (CISAC). *Contact:* Prof. Qinhan Jin, Department of Chemistry, Jilin University, Changchun 130023, P.R. China. Tel.: 0431-822331, ext. 2433; Fax: 0431-823907.

August 22–26, 1994
Hong Kong
ICORS '94. XIV International Conference on Raman Spectroscopy. *Contact:* Prof. Nai-Teng Yu, ICORS '94, c/o Department of Chemistry, The Hong Kong University of Science and Technology, Clear Water Bay, Kowloon, Hong Kong.

August 23–26, 1994
Guildford, UK
QSA-8. International Conference on Quantitative Suface Analysis: Techniques and Applications. *Contact:* Doreen Tilbrook, Division of Materials Metrology, National Physical Laboratory, Teddington, Middlesex TW11 0LW, UK.

September 11–16, 1994
Essen, Germany
EUCMOS XXII. XXII European Congress on Molecular Spectroscopy. *Contact:* Congress Secretariat, Gesellschaft Deutscher Chemiker, Abt. Tagungen, P.O. Box 900440, W-6000 Frankfurt 90, Germany. Tel.: +49 69 7917-366; Fax +49 69 7917-475; Telex 4 170 497 gdch d. *(Further details published in Vol. 272, No. 2).*

★ ***September 12–14, 1994***
Paris, France
Workshop on Biosensors and Biological Techniques in Environmental Analysis. *Contact:* Prof. M.-C. Hennion, ESPCI, Lab. Chimi Analytique, 10 rue Vauquelin, 75005 Paris, France.

★ ***September 12–17, 1994***
Madrid, Spain
Frontiers in Analytical Chemistry: Surface and Interface Analysis. A course organized with the ERASMUS Network "Analytical Chemistry". *Contact:* Prof. Dr. A. Sanz-Medel, Universidad di Oviedo, Quimica Fisica e Analitica, E-33006, Oviedo, Spain. Tel.: +34 8 510-3474; Fax: +34 8 50-3480.

September 18–22, 1994
Chambéry, Savoy, France
14th International CODATA Conference. Data and Knowledge in a Changing World: The Quest for a Healthier Environment. *Contact:* Prof. J.-E. Dubois, ITODYS, Université Paris 7, 1 rue Guy de la Brosse, 75005 Paris, France. Fax: +33 1 42881466. E-mail: codata@paris7.jussieu.fr (Internet).

September 21–23, 1994
Stockholm, Sweden
5th International Symposium on Pharmaceutical and Biomedical Analysis: *Contact:* Swedish Academy of Pharmaceutical Sciences, P.O. Box 1136, S-111 81 Stockholm, Sweden. Tel.: +46 8 245085; Fax: +46 8 205511.

September 22–24, 1994
Constanta, Romania
12th Conference on Analytical Chemistry. *Contact:* Dr. Gabirel-Lucian Radu, Romanian Society of Analytical Chemistry, 13 Blvd. Carol I, Sector 3, 70346 Bucharest, Romania.

October 3–7, 1994
St. Peterburg, Russia
ISCMS '94. International Symposium: Chromatography and Mass Spectrometry in Environmental Analysis. *Contact:* ISCMS '94, Dr. Alexander Rodin, State Institute of Applied Chemistry, Dobrolubov Ave. 14, 197198, St. Petersburg, Russia. Tel.: +7 812 2389786; Fax: +7 812 2338989; Telex: 121345 ptb sigma.

October 17–19, 1994
Strasbourg, France
3rd International Symposium on Supercritical Fluids: Thermodynamics, Physico-chemical Properties, Technology and Applications. *Contact:* ISASF, Mle. Brionne, ENSIC, P.O. Box 451, F-54001 Nancy Cedex, France. Tel.: +33 83175003; Fax: +33 83350811.

November 9–11, 1994
Montreux, Switzerland
11th Montreux Symposium on Liquid Chromatography–Mass Spectrometry (LC/MS; SFC/MS; CE/MS; MS/MS). *Contact:* M. Frei-Häusler, Postfach 46,

Announcements are included free of charge. Information on planned events should be sent well in advance [preferably 6 months or more] to: ACA Newsbrief, Elsevier Science Publishers P.O. Box 330, 1000 AH Amsterdam, The Netherlands Fax: (+31) 20 5862 845

CH-4123 Allschwil 2, Switzerland. Tel.: +41 61-4812789; Fax: +41 61-4820805.

★ ***November 21–22, 1994***
Enschede, The Netherlands
μTAS'94. Workshop on Micro Total Analysis Systems. *Contact:* Dr. Albert van den Berg, University of Twente, MESA Research Institute, P.O. Box 217, 7500 AE Enschede, The Netherlands. Tel. +31 53 892 691; Fax: +31 53 309 547.

March 6–10, 1995
Jülich, Germany
6th International Hans Wolfgang Nürnberg Memorial Symposium on Metal Compounds in Environment and Life, 6: Analysis, Speciation and Specimen Banking. *Contact:* Dr. H.W. Dürbeck, Institute of Applied Physical Chemistry, Research Center, Jülich (KFA), P.O. Box 1913, D-5170 Jülich, Germany.

★ ***June 5–8, 1995***
Singapore
Fifth Symposium on Our Environment and First Asia-Pacific Workshop on Pesticides. *Contact:* The Secretariat, 5th Symposium on Our Environment, c/o Department of Chemistry, National University of Singapore, Kent Ridge, Rep. Singapore 0511. Fax: +65 779-1691.

July 9–15, 1995
Hull, UK
SAC 95. *Contact:* Analytical Division, The Royal Society of Chemistry, Burlington House, Piccadilly, London W1V 0BN, UK. Tel.: +44 71 437-8656; Fax: +44 71 734-1227.

August 27–September 1, 1995
Leipzig, Germany
CSI XXIX. Colloquium Spectroscopicum Internationale XXIX. *Contact:* Gesellschaft Deutscher Chemiker, Abt. Tagungen, P.O. Box 90 04 40, D-60444 Frankfurt/ Main, Germany.

August 27–September 1, 1995
Budapest, Hungary
10th International Conference on Fourier Transform Spectroscopy. *Contact:* Mrs. Klára Láng/Mr. Attila Varga, Conference Office, Roland Eötvös Physical Society, P.O. Box 433, H-1371 Budapest, Hungary. Tel./Fax: +36 1 201-8682.

★ ***September 4–5, 1995***
Paris, France
Sample Handling of Pesticides in the Aquatic Environment. Short course preceding the 5th Workshop on Chemistry and Fate of Modern Pesticide. *Contact:* Prof. M.-C. Hennion, ESPCI, Lab. Chimi Analytique, 10 rue Vauquelin, 75005 Paris, France.

★ ***September 6–8, 1995***
Paris, France
5th Workshop on Chemistry and Fate of Modern Pesticides. *Contact:* Prof. M.-C. Hennion, ESPCI, Lab. Chimi Analytique, 10 rue Vauquelin, 75005 Paris, France.

September 12–15, 1995
Leuven, Belgium
5th International Symposium on Drug Analysis. *Contact:* Prof. J. Hoogmartens, Drug Analysis '95, Institute of Pharmaceutical Sciences, Van Evenstraat 4, B-3000 Leuven, Belgium. Tel.: +32 16 283440; Fax: +32 16 283448.

Announcements of meetings

SSIR 94. SCANDINAVIAN SYMPOSIUM ON INFRARED AND RAMAN SPECTROSCOPY, BERGEN, NORWAY, MAY 30–JUNE 1, 1994

The First Scandinavian Symposium on Infrared/Raman Spectroscopy will be held in the Science building at the University of Bergen. It will cover all fundamental aspects, instrumental developments and applications in (mid and near) infrared/Raman spectroscopy and new sampling techniques such as diffuse reflectance, internal and external reflectance, specular reflectance, photo acoustic etc. The symposium will also cover hyphenated techniques such as GC–IR, LC–IR, GC/MS–IR, SFC–IR and infrared microspectroscopy. Furthermore, spectral interpretation and neural networks and chemometric techniques in spectral data handling and interpretation are also subjects of interest.

Scientific Program
The scientific program includes invited lectures, keynote lectures and contributed papers (oral and poster). The language of the Symposium is English.

Publication
The proceedings of the Symposium will be published in a special volume of *Vibrational Spectroscopy*. The papers will pass through the normal refereeing procedure before acceptance.

For further information, please contact: Dr. Alfred A. Christy, De-

partment of Chemistry, Allegt. 41, University of Bergen, N-5007 Norway. Tel.: +47 5 213363 (after 9 Sept. 1993: +47 55 213363); Fax: +47 5 329058 (after 9 Sept. 1993: +47 55 329058); or Laila Kyrkjebø, Department of Chemistry, University of Bergen. Tel.: +47 5 213342 (after 9 Sept. 1993: +47 55 213342).

WORKSHOP ON BIOSENSORS AND BIOLOGICAL TECHNIQUES IN ENVIRONMENTAL ANALYSIS, PARIS, FRANCE, SEPTEMBER 12–14, 1994

Rapid advances have been observed in the use of biosensors, immunochemical methods and other biological techniques as new tools for environmental analysis. The workshop will be an opportunity for scientists dedicated to analytical environmental chemistry, and often working in different areas, to discuss together some special topics of common interest such as:

— immunological techniques (immunoassays, use of immunosorbents for the sample pretreatment, preconcentration and clean-up, and coupling with chromatographic techniques, immunosensors, antibody production...)
— enzymatic techniques (enzymatic sensors, enzymatic reactors, inhibition...)
— polymerase chain reaction (PCR) technology, DNA probes
— biosensors based on plant, animal and human tissue (whole cells, cell organelles...)
— microbial systems
— bioanalytical detection techniques (receptor-based biosensors, use of membrane proteins...)
— other biosensors
— validation of results

The workshop will take place in the Ecole Supérieure de Physique et de Chimie Industrielles, well situated in the heart of the old Latin Quarter in Paris.

For further details contact: Prof. M.-C. Hennion, ESPCI, Lab. Chimi Analytique, 10 rue Vauquelin, 75005 Paris, France.

FRONTIERS IN ANALYTICAL CHEMISTRY: SURFACE AND INTERFACE ANALYSIS, A COURSE ORGANIZED WITHIN THE ERASMUS NETWORK "ANALYTICAL CHEMISTRY", MADRID, SPAIN, SEPTEMBER 12–17, 1994

The course is sponsored by the Working Party of Analytical Chemistry of the Federation of European Chemical Societies. It is an introductory course on the major techniques for surface and interface analysis and their applications in chemistry and physics, particularly for solving problems in materials and environmental sciences. The subjects will be:

— Electron probe techniques: EPMA and SEM, AEM (including EDX, EELS), AES. Lecturers: F. Adams and P. van Espen (UIA Antwerp)
— Ion probe techniques: SIMS (dynamic and static), RBS and ISS, ERD, NRA. Lecturer: M. Grasserbauer (TU Wien)
— Photon probe techniques: XPS and UPS (lecturer from UIA Antwerp), laser-based MS (M. Grasserbauer), IR and Raman (R. Kellner, TU Wien)
— Field probe techniques: AFM and STM. Lecturer: G. Friedbacher (TU Wien)
— Combined use of techniques for problem solving, e.g. high performance materials (H. Ortner, Darmstadt), microelectronics (M. Grasserbauer), environmental sciences (F. Adams).

For information, registration and application for stipends contact: Prof. Dr. A. Sanz-Medel, Universidad di Oviedo, Quimica Fisica e Analitica, E-33006, Oviedo, Spain. Tel.: +34 8 510-3474; Fax: +34 8 510 3480.

μTAS '94. WORKSHOP ON MICRO TOTAL ANALYSIS SYSTEMS, ENSCHEDE, THE NETHERLANDS, NOVEMBER 21 AND 22, 1994

The Research Intitute MESA from the University of Twente is organizing this workshop. Its aim is to present the newest developments in the fields of (silicon-based) micro liquid handling, sample treatment and detection of (bio)chemical parameters, for medical diagnostics, process control, automotive and environmental applications. The organizers are Prof. P. Bergveld and Dr. A. van den Berg.

For further details contact: Dr. Albert van den Berg, University of Twente, MESA Research Institute, P.O. Box 217, 7500 AE Enschede, The Netherlands. Tel. +31 53 892 691; Fax: +31 53 309 547.

ANABIOTEC 94

5th International Symposium on Analytical Techniques, Systems & Strategies in Biotechnology

---

31 October — 2 November 1994

Minneapolis Hilton & Towers, USA

Learn of the new instruments and techniques for analytical chemistry
Improve monitoring of industrial scale processes
Update your strategies for clinical diagnosis
Meet international colleagues and contacts

The analytical chemistry of complex matrices involving species of a biological origin is a rapidly developing research frontier.

ANABIOTEC 94 — consisting of plenary sessions, selected original papers, posters and an exhibition — will address the wide array of research issues involved in this field. This symposium is the ideal forum for information exchange between the fields of analytical chemistry, biochemistry, clinical chemistry and biotechnology: you need to be there!

For further information send a copy of this advert, complete with your address details to:

Anabiotec 94 Conference Secretariat, Elsevier Science Ltd,
PO Box 150, Kidlington, Oxford OX5 1AS, UK.
Tel: +44 (0) 865 512242
Fax: +44 (0) 865 310981

PUBLICATION SCHEDULE FOR 1994

	S'93	O'93	N'93	D'93	J	F	M	A	M			
Analytica Chimica Acta	281/1 281/2 281/3	282/1 282/2 282/3	283/1 283/2	283/3 284/1 284/2	284/3 285/1–2 285/3	286/1 286/2 286/3	287/1–2 287/3 288/1	288/2 288/3 289/1	289/2–3 290/1 290/2			
Vibrational Spectroscopy		6/1			6/2		6/3		7/1			

INFORMATION FOR AUTHORS

Detailed "Instructions to Authors" for *Analytica Chimica Acta* was published in Volume 256, No. 2, pp. 373–376. Free reprints of the "Instructions to Authors" of *Analytica Chimica Acta* and *Vibrational Spectroscopy* are available from the Editors or from: Elsevier Science Publishers B.V., P.O. Box 330, 1000 AH Amsterdam, The Netherlands. Telefax: (+31-20) 5862845.

Manuscripts. The language of the journal is English. English linguistic improvement is provided as part of the normal editorial processing. Authors should submit three copies of the manuscript in clear double-spaced typing on one side of the paper only. *Vibrational Spectroscopy* also accepts papers in English only.

Rapid publication letters. *Letters* are short papers that describe innovative research. Criteria for letters are novelty, quality, significance, urgency and brevity. Submission data: max. of 2 printed pages (incl. Figs., Tables, Abstr., Refs.); short abstract (e.g., 3 lines); *no* proofs will be sent to the authors; submission on floppy disc; *no* revision will be possible.

Abstract. All papers and reviews begin with an Abstract (50–250 words) which should comprise a factual account of the contents of the paper, with emphasis on new information.

Figures. Figures should be prepared in black waterproof drawing ink on drawing or tracing paper of the same size as that on which the manuscript is typed. One original (or sharp glossy print) and two photostat (or other) copies are required. Attention should be given to line thickness, lettering (which should be kept to a minimum) and spacing on axes of graphs, to ensure suitability for reduction in size on printing. Axes of a graph should be clearly labelled, along the axes, outside the graph itself. All figures should be numbered with Arabic numerals, and require descriptive legends which should be typed on a separate sheet of paper. Simple straight-line graphs are not acceptable, because they can readily be described in the text by means of an equation or a sentence. Claims of linearity should be supported by regression data that include slope, intercept, standard deviations of the slope and intercept, standard error and the number of data points; correlation coefficients are optional.

Photographs should be glossy prints and be as rich in contrast as possible; colour photographs cannot be accepted. Line diagrams are generally preferred to photographs of equipment. Computer outputs for reproduction as figures must be good quality on blank paper, and should preferably be submitted as glossy prints.

Nomenclature, abbreviations and symbols. In general, the recommendations of IUPAC should be followed, and attention should be given to the recommendations of the Analytical Chemistry Division in the journal *Pure and Applied Chemistry* (see also *IUPAC Compendium of Analytical Nomenclature, Definitive Rules*, 1987).

References. The references should be collected at the end of the paper, numbered in the order of their appearance in the text (*not* alphabetically) and typed on a separate sheet.

Reprints. Fifty reprints will be supplied free of charge. Additional reprints (minimum 100) can be ordered. An order form containing price quotations will be sent to the authors together with the proofs of their article.

Papers dealing with vibrational spectroscopy should be sent to: Dr J.G. Grasselli, 150 Greentree Road, Chagrin Falls, OH 44022, U.S.A. Telefax: (+1-216) 2473360 (Americas, Canada, Australia and New Zealand) or Dr J.H. van der Maas, Department of Analytical Molecular Spectrometry, Faculty of Chemistry, University of Utrecht, P.O. Box 80083, 3508 TB Utrecht, The Netherlands. Telefax: (+31-30) 518219 (all other countries).

0003-2670/93/$06.00

This issue is printed on acid-free paper.

PRINTED IN THE NETHERLANDS

Announcement from the Publisher

Elsevier Science Publishers encourages submission of articles on floppy disk.

All manuscripts may now be submitted on computer disk, with the eventual aim of reducing production times still further.

- The preferred storage medium is a 5¼ or 3½ inch disk in MS-DOS format, although other systems are welcome, e.g. Macintosh.
- After **final acceptance**, your disk plus one final, printed and exactly matching version (as a printout) should be submitted together to the editor. **It is important that the file on disk and the printout are identical.** Both will then be forwarded by the editor to Elsevier.
- Illustrations should be provided in the usual manner.
- Please follow the general instructions on style/arrangement and, in particular, the reference style of this journal as given in 'Instructions to Authors'.
- Please label the disk with your name, the software & hardware used and the name of the file to be processed.

Contact the Publisher for further information:

Elsevier Science Publishers
Analytica Chimica Acta
P.O. Box 330
1000 AH Amsterdam, The Netherlands
Phone: (+31-20) 5862 791 Fax: (+31-20) 5862 459

ELSEVIER SCIENCE PUBLISHERS

711\414\140\079\03

0003-2670(19931230)284:2;1-8